National Library of Canada
Acquisitions and Bibliographic Services Branch
395 Wellington Street
Ottawa, Ontario
K1A 0N4

Bibliothèque nationale du Canada
Direction des acquisitions et des services bibliographiques
395, rue Wellington
Ottawa (Ontario)
K1A 0N4

Your file Votre référence

Our file Notre référence

NOTICE

The quality of this microform is heavily dependent upon the quality of the original thesis submitted for microfilming. Every effort has been made to ensure the highest quality of reproduction possible.

If pages are missing, contact the university which granted the degree.

Some pages may have indistinct print especially if the original pages were typed with a poor typewriter ribbon or if the university sent us an inferior photocopy.

Reproduction in full or in part of this microform is governed by the Canadian Copyright Act, R.S.C. 1970, c. C-30, and subsequent amendments.

AVIS

La qualité de cette microforme dépend grandement de la qualité de la thèse soumise au microfilmage. Nous avons tout fait pour assurer une qualité supérieure de reproduction.

S'il manque des pages, veuillez communiquer avec l'université qui a conféré le grade.

La qualité d'impression de certaines pages peut laisser à désirer, surtout si les pages originales ont été dactylographiées à l'aide d'un ruban usé ou si l'université nous a fait parvenir une photocopie de qualité inférieure.

La reproduction, même partielle, de cette microforme est soumise à la Loi canadienne sur le droit d'auteur, SRC 1970, c. C-30, et ses amendements subséquents.

Canada

OPTIMAIZATION OF SURFACE/SUBSURFACE FLOW FOR AN ARID WADI-RESERVOIR SYSTEM

Walid Saleh

A Thesis

in

The Department

of

Civil Engineering

Presented in Partial Fulfillment of the Requirements

for the Degree of Doctor of Philosophy at

Concordia University

Montréal, Québec, Canada

May, 1994

ISBN 0-315-97620-9

Canada

ABSTRACT

OPTIMAIZATION OF SURFACE/SUBSURFACE FLOW FOR AN ARID WADI-RESERVOIR SYSTEM

Walid Saleh, Ph.D.
Concordia University, 1994

Arid and semi-arid lands suffer from scarce water conditions. Rainfall occurs over brief intervals and has an erratic behavior producing short intensive floods. If intermittent surface water floods are optimally managed they may help respond to the increasing demands for water in arid countries. One of the appropriate uses of such water is the recharge of ground water aquifer systems. Underground storage represents a cost-free augmentation of surface storage. Also, water stored in the underground can be used to cover a part of the increasing need arising from rapidly expanding urbanization, as well as industrial and agricultural demands.

An optimization procedure employing dynamic programming is presented for obtaining optimal water recharge from a network of reservoirs in an arid watershed. The final solution yields an optimal releases and storages from the study's reservoir network. The optimization procedure takes into account evaporation losses while meeting the irrigation demands of two selected crops (wheat, and barley). The objective function was formulated to give maximum infiltration. The procedure employed produces more or less uniform infiltration by maximizing the minimum infiltration volume. That is, during drought periods, a "hedging rule" places high penalty on large deficits than on small ones. Its main function is to increase infiltration during periods of low flow.

Since wadis are not gauged to provide records of flow, monthly as well as weekly inflows were generated using a watershed model. The model provided an assessment of flood wave movement through the dry wadi and the flood occurrence of some rainfall events.

The overall optimization approach has a simulation process nested in the optimization procedure. A generalized numerical infiltration simulation component based on the control volume method was integrated into the optimization procedure for the simulation of ground water flow. It helps evaluate the soil moisture redistribution and the horizontal and vertical wetting front corresponding to optimal conditions.

The optimization procedure was carried out for a system of farming reservoirs in the Muwagar watershed south east of Amman, Jordan. The study area consisted of a 74 km^2 watershed with three existing reservoirs and several irrigated agriculture lots. The results obtained correspond to an optimal release and storage policies, for one, and three reservoirs on monthly as well as weekly basis, and for five reservoirs on a monthly basis only. The ground water recharge model using the optimal storage and release policies showed a substantial increase in the horizantal wetting front in comparison with the present situation.

CLAIM OF ORIGINALITY

To the best of the author's knowledge, the following contributions are original:

- The optimization procedure combining an incremental dynamic programming method along with both surface and control volume subsurface flow simulations. The overall optimization procedure represents a complete hydrologic cycle, from rainfall, overland flow, optimization of recharge, to the simulation of subsurface flow.

- The implicit approach used to simulate and optimize deterministically the problem of surface/subsurface flow interaction in arid zones.

- The application of the simulation components and incremental dynamic programming to multi-reservoir management in arid zones. Component analyses are used to simulate the surface flow and the subsurface flow under the optimal condition. These also, reduce the computation effort and address the dynamic behavior of the surface/subsurface flow pattern.

- The development of the control-volume simulation component for the subsurface flow in arid zones. Comparision against finite element methods proved the superiority of the control volume method in terms of reducing computation time and increasing accuracy.

ACKNOWLEDGMENT

I take this opportunity to express my sincere appreciation to my thesis advisor, Dr. Semaan Sarraf, for his indispensable support and helpful guidance which brought about the realization of this thesis.

Further thanks go to the people at the International Development Research Center (IDRC), Scholarships and Awards Division, for their financial support which was made available through the Young Canadian Researchers Awards.

I would also like to acknowledge the assistance of the staff of the Water and Environmental Research and Study Center, University of Jordan, namely, Dr.M. Shatanawi, (Director), Dr. Elias Salameh, and Dr. Auni Taimeh, for providing assistance in collecting the field data necessary to carry out this work.

Beyond this, I wish to express my heartfelt gratitude to my wife, Sana Hawamdeh, for her moral support as well as her enduring understanding. Also, special thanks goes to my sisters Rasmia and Lina for their support. My love goes to my son, Khalid, who lightens my heart again after the loss of my two brothers, Mohammed & Khalid.

Finally, I would like to thank Ms. Carol Plathan for editing the manuscript.

This thesis is dedicated to my mother, wife and son, for their love, patience, and support.

TABLE OF CONTENTS

LIST OF FIGURES

LIST OF TABLES

LIST OF SYMBOLS

$\overline{S}_{max}$: vector of maximum allowable reservoir storage

$\overline{S}_{min}$: vector of minimum allowable reservoir storage

$\overline{INFW}_t$: vector of monthly/weekly inflow

$\overline{DEM}_t$: vector of monthly/weekly irrigation demand

$\overline{EVAP}_t$: vector of monthly/weekly evaporation rate

$\overline{QINF}_t$: vector of monthly/weekly infiltration rate

$\varnothing_t$: a function that relates the reservoir storage to its surface area

Ω_t: a function that relates reservoir storage to the projection of reservoir bottom area

$\overline{S}_t$: vector of reservoir storage at the beginning of the monthly/weekly time period t

$\overline{U}_t$: Vector of reservoir release during the monthly/weekly time period t

W: total yield (m^3)

α_t: water monthly use coefficient (related to each crop)

$\dot{a}$: penalty coefficient =0.001-0.007.

$L(\psi)$: Quasilinear Differential Operator

ψ : Pressure Head

ψ^0: Pressure Head at Old Time Value

ψ^1: Pressure Head at New Time Value

ψ_P^0: Pressure Head at The Center of The Control Volume at Old Time Value

ψ_E^0: Pressure Head at The East Face of The Control Volume at Old Time Value

ψ_W^0: Pressure Head at The West Face of The Control Volume at Old Time Value

ψ_N^0: Pressure Head at The North Face of The Control Volume at Old Time Value

ψ_S^0: Pressure Head at The South Face of The Control Volume at Old Time Value

ψ_P^1: Pressure Head at The Center of The Control Volume at New Time Value

ψ_E^1: Pressure Head at The East Face of The Control Volume at New Time Value

ψ_{W^1}: Pressure Head at The West Face of The Control Volume at New Time Value

ψ_{N^1}: Pressure Head at The North Face of The Control Volume at New Time Value

ψ_{S^1}: Pressure Head at The South Face of The Control Volume at New Time Value

P : Point At The Center of The Control Volume

E : Point At The East Face of The Control Volume

W : Point At The West Face of The Control Volume

N : Point At The North Face of The Control Volume

S : Point At The South Face of The Control Volume

e : The Interface Placed Midway Between P and E

w : The Interface Placed Midway Between P and W

n : The Interface Placed Midway Between P and N

s : The Interface Placed Midway Between P and S

ψ_r : Residual Pressure Head

ψ_a : Air Pressure Head

ψ_L : Minimum Pressure Head

K_{ij} : The Saturated Hydraulic Conductivity Tensor

Ksx : The Saturated Hydraulic Conductivity in x direction

Ksz : The Saturated Hydraulic Conductivity in z direction

krw : Relative Permeability, $0 \leq krw \leq 1$

Sw : Water Saturation Degree

Swr : Residual Water Saturation Degree

Se : Effective (normalized) Water Saturation Degree

ϕ : Water Porosity

ρ : Water Density

g : Gravitational Acceleration

μ : Water Viscosity

Q : Volumetric Rate Via Source (or Sink) Per Unit Volume of The Porous Medium

Qc : The Constant Part of The Linearized Source Term

Qp : The Variable Part of The Linearized Source Term

x_i, x_j : Cartesian Coordinates Representing The Horizontal And Vertical Directions x and z respectively

Ss : Specific Storage

C : Coefficient of Vertical Formation Compressibility

B : Water Compressibility Coefficient

$G(\psi)$: Is The Overall Storage Coefficient

t : Elapsed Time

Δt : Time Derivative

Δx : x-Dimension of The Control Volume

Δz : z-Dimension of The Control Volume

Γx : Diffusion Term in x-Direction

Γz : Diffusion Term in z-Direction

$(\Gamma x)e$: Diffusion Term in x-Direction at The East Interface of The Control Volume

$(\Gamma x)w$: Diffusion Term in x-Direction at The West Interface of The Control Volume

$(\Gamma z)n$: Diffusion Term in z-Direction at The North Interface of The Control Volume

$(\Gamma z)s$: Diffusion Term in z-Direction at The South Interface of The Control Volume

f : Weighting Factor between 0 and 1

$(\delta x)_e$: Distance From The Control Volume Center To The East Node

$(\delta x)_w$: Distance From The Control Volume Center To The West Node

$(\delta x)_n$: Distance From The Control Volume Center To The North Node

$(\delta x)_s$: Distance From The Control Volume Center To The South Node

a_E : East Node Coefficient

a_W : West Node Coefficient

a_N: North Node Coefficient

a_S : South Node Coefficient

a_P : Coefficient at Center of The Control Volume

b : Integration Coefficient

A, g, d: Empirical Parameters

b': Root Effectiveness function

CHAPTER I

INTRODUCTION

1.1 SCOPE OF THE PROBLEM

Water is used for many purposes such as irrigation, hydropower, navigation, pollution abatement, etc. Unlike other natural resources, water is renewable through the hydrologic cycle. The availability of water and its temporal and spatial distribution are, however, governed by climactic factors over which man has little control. The natural availability of water is often not in agreement with the demand by human societies. Control of water has been practiced since the early days of civilization. Water control includes primarily the construction of regulation facilities in the form of storage and diversions. For many developing countries, water resources development projects have been and will continue to be important components of their national infrastructure development.

In countries suffering from desertification such as Jordan, surface/subsurface water interaction plays an important role in combating this phenomena and in the agriculture development of the area. Also, the use of natural aquifers to store water in arid regions eliminates the disadvantages associated with surface storage, such as evaporation, pollution, siltation, and health hazards. The existing ecological systems of these regions are fragile and prone to degradation. They are exposed to further degradation unless new systems are introduced which allow sustainable development.

The storage of water in arid and semi-arid regions is a major limiting factor in the development of sound economic and social structures. In these regions, where groundwater is often the only source, almost any development of aquifers constitutes overdraft conditions. The erratic nature of precipitation in arid countries exerts a profound

influence upon the accumulation and replenishment of groundwater. Natural recharge, on the average, is likely to be insignificant because of several factors:

1- For most of the year, rainfall is relatively small compared with potential evaporation;

2- Storm intensity frequently exceeds the infiltration capacity of the ground surface resulting in over land flow;

3- The unsaturated zone tends to dry out and may therefore absorb a significant volume of infiltrating water;

4- A semi-permeable crust may form in the unsaturated zone comprising the sediments that impede infiltration.

During occasional floods, infiltration through beds of ephemeral wadis (wadi is a reach that water flow occurs only during rainy season) is the major source of aquifer recharge. These ephemeral wadis flow only as a result of surface runoff generated by rainfall of high intensity and short duration. The wadis will often carry large volumes of water during a flood lasting a few hours, days or exceptionally, weeks. Artificial recharge in these regions can play an important management role in conserving water and avoiding depletion of the existing aquifers. Utilization of excess runoff to increase groundwater recharge from emphemeral wadis can contribute significantly to the establishment and maintenance of adequate water supplies. Increases in recharge amounts may help enhance water quality and may also lead to expansion of agricultural development. Recognition of these adverse conditions stresses the need for optimum utilization of available water.

1.1.1 Surface/Subsurface Water Interchange

Although water resources development has often been based on the predominant use of either surface water or groundwater, it must be emphasized that each of these components has far-reaching effects on the other. Surface water flows are sustained by ground water resources, and groundwater is replenished by infiltration derived from precipitation on the earth's surface. Coordinated development and management of the combined resources are critical. Linkage between surface water and ground water should be investigated in all regional studies so that any adverse effects can be noted and opportunities for joint management understood.

Underground reservoirs are often extensive and can serve to store water for a multitude of uses. If withdrawals from these reservoirs consistently exceed recharge, mining occurs and ultimate depletion of the resource results. By properly coordinating the use of surface water and groundwater supplies, optimum regional water resource development seems likely to be assured.

When infiltration is practised by spreading water over soils in basins and ditches or by flooding, the amount of water entering the aquifer depends on three factors: a) the infiltration rate, b) the percolation rate, and c) the capacity for horizontal water movement.

a) The infiltration rate, also called the entry, intake or acceptance rate, is the rate at which water is picked up by the soil. At the beginning of spreading operations and assuming a homogeneous aquifer up to ground surface, the infiltration rate is equal to the percolation rate mentioned above. At the point of entry into the aquifer, however, clogging occurs by the deposition of particles carried by the water in suspension or in solution, by algal growth, colloidal swelling and soil dispersion, microbial activity, and other factors. This clogging seals pore openings and increases entry resistance. With the same water level

in the spreading basins, the entry velocity diminishes and is, after some time, only a fraction of its original value.

b) The percolation rate is that at which the water is able to move downward through the soil. After trapped air has been removed, the percolation rate is constant, depending on the flow pattern and the coefficient of permeability in the vertical direction. With aeolian formations, the coefficients of permeability are about the same in all directions, but with fluviatile and marine deposits, the vertical coefficient may be a few to many times smaller than the horizontal one.

c) The capacity for horizontal water movement depends on the flow pattern and the coefficient of transmissivity of the aquifer below the groundwater table.

For water management in arid areas, infiltration is an important factor for many purposes for it improves water quality. Also, storage of excess water from wet periods for subsequent use in dry ones and preserves surplus water as the main aims. Besides this, the quality of river water to be used for public supplies may be improved by artificial infiltration, removing various impurities by filtration and reducing water-quality variations by dispersion inside the aquifer.

In rural areas, rain-water falling to the ground either percolates downward to the groundwater table or flows away above or directly below the ground surface to drainage ditches, the ratio between both discharges depending on the permeability of the soil and the slope of the ground surface. In water-scarce areas where loss of water by evapo-transpiration must be avoided at all costs, spreading basins may now be constructed to hasten the percolation process so as to augment groundwater supplies as much as possible.

1.1.2 Artificial Ground Water Recharge

This technique incorporates a manmade transfer of water from the surface into the underground to be stored there and extracted during later stages. This process is equivalent to surface storage in dams but with different techniques and results.

Evaporation losses are reduced tremendously when water is stored in the underground, hence, under prevailing semi-arid climatic conditions, more water is saved. Underground storage saves water from direct pollution. Also, infiltration of surface water to the ground and flow in the underground is accompanied by numerous chemo-physical reactions which generally result in water purification. In spite of the difficulties and theoretical and technical problems incurred during artificially recharging water to the underground, such techniques guarantee more reliable amounts and qualities of water.

One of the most common ground water recharge practices is the use of spreading basins. This is the passage of surface water through the non-saturated zone of the soil and geological strata to the saturated part of the underlying aquifer. Infiltration expresses the essential vertical movement of water through the non-saturated zone. The downward movement of the water is governed by a variety of factors: the vertical permeability of the soil; the presence of gases in the non-saturated zone; the presence or absence of limiting layers with small vertical permeability; and the changes which affect soil structure during infiltration, changes caused by physical or chemical bacteriological influences. When new spreading-basins are put into operation, infiltration rates decrease initially, and then increase after the first hours or first days of operation. The changes later become less predictable; in most cases a decrease in infiltration rates is observed once again, which may then eventually level out, and often seem to continue indefinitely. Sometimes, a second temporally and smaller increase of infiltration rates may again be observed. After the spreading-ground dries, the cycle repeats itself, although generally at a lower level.

However, saturation very rarely reaches deeper than the uppermost layer of the profile. Several methods are commonly used in measuring infiltration rates. The method which gives the most relevant results for spreading grounds is in-situ testing and this should be employed whenever possible.

Spreading-basins must be selected or constructed with relatively more or less flat bottom that is to be covered evenly by small quantities of water. If the ground selected for spreading operations slopes too much, the amount of earth-moving required for the construction of the basins is, in most cases, a major economic limiting factor. An accumulation of silt can be alleviated by using part of the basins for settling. One advantage of basins, especially if the water-supply stems from intermittent streams, is the hold-over storage they provide. Basins must be operated intermittently in order to allow infiltration capacities to be reconstituted by drying.

1.2 LITERATURE REVIEW

The prediction of the movement of water in arid soils is a difficult problem whose difficulty is enhanced the drier the soil, the net effect of which is to cause a wide range of water transport properties, such as permeability, which makes calculations difficult. Nevertheless, an accurate evaluation of surface/subsurface flow conditions is important in the planning, design and operation of land development projects. The most practical and effective means of achieving an optimal strategy is by using mathematical modeling of a water system in relation to rainfall quantities, evaporation, irrigation demand, and infiltration of the surface water.

Mathematical modeling is the most frequently used system engineering technique for planning and analysis of large-scale problems. Mathemetical models permit the evaluation of economic and physical consequences of planned or alternative water systems,

changes in operating and allocation policies, and for different assumptions of inflows, costs, and social impositions. For the purpose of the present work which requires surface and subsurface simulation, two type of models, namely simulation and optimization, are reviewed here.

1.2.1 Simulation Models

Mathematical simulation models are descriptive models which attempt to represent the essential physical and operational characteristics of real systems. They are useful in predicting responses to varying inputs and in providing scenarios of proposed changes or modification to a system. Simulation models can accurately represent complex interactions between system components, whether they are linear, nonlinear, convex or non convex. Their flexibility make them widely accepted for many water resources modeling applications.

Mathematical models have been developed to simulate rainfall-runoff in a watershed. Others have been developed to simulate the subsurface flow mainly to predict soil moisture redistribution due to surface water infiltration.

1.2.1.1 Watershed Models

Many short-term rainfall-runoff models are classified as event simulation models as contrasted with sequential or continuous models. Such an event simulation model allows greater flexibility for the use of distributed parameters and shorter time increments.

Rainfall-runoff processes are recognized by most event simulation models. Most of the U.S. Federal Agency Single-Event Models have a specific computation technique for

losses, unit hydrographs, river routing, reservoir routing, and base flow. These models include, the following:

a) U.S. Geological Survey Rainfall-Runoff Model. This model is classified as an event simulation model because its calibration is based on short term records of rainfall, evaporation, and discharges during a few documented floods [Warren, 1989]. Carrigan calibrated the USGS model to be used in evaluating short stream flow records and calculating peak flow rates for natural drainage basin [Carrigan, 1973]. The model monitors the daily moisture content of the subbasin soil and can be used as a continuous stream flow simulation model.

b) Computer program for project Formulation Hydrology (TR-20) of the U.S. Department of Agriculture Soil Conservation Service, 1973, is recognized as an engineer-oriented rather than a computer oriented package [Warren, 1989]. The TR-20 was designed to use soil and land-use information to determine runoff hydrographs for known storms and to perform reservoir and channel routing.

c) Other programs are also of similar simulation capability such as the problem-oriented computer language for Hydrologic Modelling (HYMO), [Williams, 1973] and the Storm Water Management Model (SWMM), of the U. S. Environmental Protection Agency, 1977.

d) Among single event models, the Hydrologic Engineering Center Flood Hydrograph Model is the most widely used [Warren, 1989]. The model consists of a calling program and six subroutines. Two of these subroutines determine the optimal unit hydrograph, loss rate, or wadi flow routing parameters by matching recorded and

simulated hydrograph values in comparison to other event-simulation models. The model is relatively compact and able to execute a variety of computational procedures in a single computer run.

The above models have been used to simulate variety of cases. For example, of the earlier use, in June 1963, the Oak Creek watershed experienced a severe flood-producing storm in a 6 hr period. Average excess rain depths over each of the nine subareas ranged from 1.0 in (25.4 mm) to 7.8 in (198.0 mm). The total watershed area was 258 sq. miles (668.2 km^2). Using a single run of the model the storm hydrograph was simulated at important locations in the watershed, and the peak flow was also evaluated. The model gave a fair representation of the storm characteristics which were used in the design of a reservoir in that area [U. S. Army Corps of Engineers, 1985]. David, P. et. al., 1980, used the Hydrologic Engineering Center Model to optimize the appropriate Muskigum Hydrologic routing coefficients to obtain a best fit with the method of characteristics exact solution. Cheng-Kang T., et al, 1987, also used the above model to determine the hydrographs to design a regional storm water detention basin network.

These models however, can only be used effectively if they have been thoroughly and properly calibrated to closely reflect the behavior of the watershed. For a single event storm the criteria are based on the degree of agreement in the measured and predicted hydrographs such as the peak flow rates, runoff volumes, and the sum of squared residuals. For example, several works (Duan et al., 1992) used the sum of squares of the differences between the measured and predicted hydrographes, while others (e.g., Liong et al., 1991) used the peak flows and the runoff volumes. Automatic procedures would require optimization routines to be connected to the model.

1.2.1.2 Subsurface Simulation Models

Many models have been developed to solve the subsurface flow equation (the modified Richard's equation). These models however, are distinguished by their means of deriving the discretization of differential equations or in the type of numerical methods used. The most commonly used numerical methods are the finite difference (FDM) and finite element method (FEM). In the applications of these methods, proper discretization schemes for FDM are necessary while physically realistic shape functions and weighting functions for FEM are required. Without these the resulting discretization equations may lead to unstable solutions. Also, as an alternative method, the control-volume method, formulates the discretized algebraic equations based on physical conservation principles.

In the finite element method and in most weighted residual methods, the assumed variation of pressure head (ψ) consisting of the grid point values and the interpolation functions (or profiles) between the grid points is taken as the approximate solution. In the finite difference method, only the grid points values of (ψ) are considered to constitute the solution, without any reference as to how (ψ) varies between the grid points. The control volume approach has the appearance of the finite difference, but it employes many features of the finite element. In the control volume method, the interpolation formulas or the profiles are regarded as auxiliary relations needed to evaluate the required integrals in the formulation. Once the discretization equations are derived, the profile assumption can be forgotten. This point view permits complete freedom of choice in employing different profile assumptions for integrating different terms in the differential equation.

The fundamental to the theory of groundwater motion (Darcy's Law) is macroscopic concept. Hubbert [1940] shows that in order to derive the macroscopic concept, attention on a scale change of several orders of magnitude without abusing the

kinematics properties of the flow system should be sought. In most natural groundwater systems, the velocity of motion is so small that the kinetic energy component can, in fact, be safely neglected.

Buckingham's capillary potential and Hubbert's fluid potential assumes that groundwater is in a constant state of motion, obeying Newtonian laws. Simply, the fluid potential at a point in the flow region is the amount of mechanical energy stored in a unit mass of the fluid.

The fundamentals for a unified treatment of transient subsurface flow in variably saturated porous media was introduced first by Buckingham [1907]. His work is referred to as the capillary potential concept. Hubbert [1940], developed the concept of the fluid potential, which with Darcy's law represents the base of almost all recent analysis of isothermal flow of liquids in porous media

Two theories exist that describe flow through saturated-unsaturated porous media. One theory admits a fundamental difference between flow in the unsaturated zone and flow in the saturated zone. In this theory, water in the unsaturated zone is assumed to have relative compressibility, while water in the saturated zone is assumed to be incompressible. It is assumed that positive changes in pressure correspond to increases in moisture content anywhere in the unsaturated zone, but in the saturated region the moisture content is assumed to be constant, independent of changes in pressure. The propagation of pore water pressure should suddenly change at the boundary between saturated and unsaturated soil. By accepting the existence of this discontinuity postulated in this theory, the transient saturated-unsaturated interface constitutes an internal moving boundary.

An alternate theory proposes that the flow exhibits sufficient continuity so that it is mathematically unnecessary to differentiate between the saturated and unsaturated zones. Freeze [1969] terms this the physical and mathematical continuity between the saturated flow system and flow in the unsaturated zone.

The difference between the two theories can be viewed in terms of the moisture characteristic. The moving boundary theory purports that the curve relating moisture content and pressure head exhibits a first-order discontinuity (a discontinuity in the first derivative) at saturation whereas the continuous flow theory suggests that no discontinuity exists.

Problems concerning modelling water flow in variably saturated porous media have been studied intensively for over two decades. These problems are difficult to solve for cases involving highly nonlinear soil moisture characteristics and atmospheric boundary conditions associated with seepage faces, infiltration, and evaporation.

Freeze [1971] was the first to present finite-difference model and used it to investigate saturated-unsaturated transient flow in nonhomogeneous, isotropic aquifers. His model was formulated using an implicit Picard iterative procedure with a vertical line successive overrelaxation matrix solution scheme. Although this scheme can accommodate a large number of nodal unknowns, it has serious limitations in handling cases involving steady state flow with seepage faces and/or evaporation and infiltration [Huyakorn, 1984].

Since then, there have been a limited number of studies on variably saturated flow simulation and related model development. Among these are studies by Segol [1977], Frind and Verg [1978], Reisenauer et al. [1982], Davis and Segol [1985], and Huyakorn

[1986]. Two modelling approaches were used in these studies. The first approach [Reisenauer et al., 1982] was formulated using the integrated finite-difference method (IFDM) with a mixed explicit-implicit Picard iterative procedure and a matrix inversion or a point successive relaxation scheme [Narasimhan and Witherspoon, 1976]. This approach permits the use of an irregular mesh to provide a more efficient representation of a region with complex geometry than the conventional finite-difference approach. However, nodal connections and nodal area data are required to calculate mass fluxes. The coordinates, connections, and areas must satisfy certain orthogonality constraints to ensure mass conservation. These constraints make it difficult, if not impossible, to model general curvilinear shapes. Difficulty in obtaining nonoscillatory steady state solution without time stepping has been reported [Kincaid et al., 1984, pp.3-37]. Also, potential problems exist in using mixed explicit-implicit time stepping with a point successive relaxation solution scheme for problems involving highly nonlinear soil properties and seepage faces.

.

The second approach (presented by Segol [1977], and Frind and Verge [1978]) was based on the Galerkin finite-element method in conjunction with a fully implicit Picard iterative procedure and a direct matrix solver. This approach is more flexible than the IFD approach in fitting curvilinear shapes. However, its potential usefulness is limited by excessive core storage and central processing unit (CPU) time required by the direct matrix solution procedure, even for problems involving a few thousand nodes.

Huyakorn [1986] developed a Galerkin finite-element model in conjunction with a fully implicit Picard algorithm for both rectangular and triangular prism elements. The slice successive overrelaxation scheme that permits a fairly large number of nodal unknowns was used. Tsakiris [1991], presented a Finite Volume model. The method is based on the finite difference method with boundary fitted coordinates.

However, numerical diffculties can arise sometimes, especially under heterogeneous conditions, for infiltration into initially dry soils, or for coarser materials that are characterized by sharp wetting fronts. Studies that have examined the accuracy of various numerical techniques pertinent to the one-dimensional unsaturated flow which include Haverkamp et al., (1977), and Van Genuchten (1982). Haverkamp et al., indicated that solutions obtained by using implicit (FDM) with implicit or explicit evaluation of hydraulic properties are the most accurate. By comparison of several numerical solutions, van Genuchten concluded that Hermitian (FEM) with a four- or five-point Lobatto integration scheme was the most accurate.

More recently, Celia et al., (1987) and Milly (1988), reported mass balance problems in the pressure-based form of the Richard's equation. By analyzing the accuracy of numerical solutions of the different forms of the Richard's equation, Celia et al., (1990), concluded that the solution of the pressure-based form is generally inaccurate and conserves mass poorly. They also indicated that the mixed form conserves mass; accuracy, however, is not automatically guaranteed. Finally, they showed that treatment of the time derivative is a critical factor in obtaining accurate results. Studies have demonstrated also that the head-based form of the Richards equation is inaccurate for infiltration into very dry soils [e.g., Kirkland et al., 1992]. Recent studies have improved on the efficiency of various numerical solutions. Some of the new advances are related to pressure head transformation, implicit time iteration, and interblock parameter estimation [e.g., Ross and Bristow, 1990]. For example Zaidel and Russ (1992), introduced an estimate of finite difference interblock conductivity that allowed the use of a coarse spatial mesh. Gottardi and Venutelli (1992), introduced a moving finite-element method that allowed the use of coarse mesh in which grid points are moved along the wetting front , thereby allowing a smallar number of nodes without sacrificing numerical accuracy. The method has

limitations regarding applicability to layered systems and use under time-varying boundary conditions.

The errors in the solutions obtained by Celia et al., (1990) are seemingly associated not only with the form of the equation solved, but to a greater extent with the choices of mesh sizes, especially those for the time step. Although the mass-conserving solutions presented in that publication are more accurate that those obtained by the pressure-based form, they are still characterized by a numerical dispersion or overshooting, problems that can be resolved only through adjusting the temporal and spatial increments. Hence, the pressure-based form of the Richards equation, and other forms as well, can provide accurate and mass-conserving solutions, provided care is taken in designing the spatial and temporal mesh. El-Kadi and Ling (1993) concluded that their finite difference solution of a transformed form of the Richards equation, the same difficulties are shared as are associated with other forms.

All of the above applications, however, have either been on small hypothetical systems or else rely on certain simplified conditions. Relatively little is known about whether these analyses are practical for real basins under real conditions. The general transient case requires either a top boundary at the ground surface and the inclusion of the unsaturated zone or a movable top boundary at the water table, either of which alternative may lead to difficulties in practical problems. Implicit in all these analyses is the acceptance of the second of the theories given above, the continuous flow theory.

In the control-volume however, a nonuniform (power grid) grid spacing can be used with the computation domain discretized into non-overlapping control volumes. Computation nodes are placed at the control volumes centroids which eliminates the need

for a special discretization equation for the near-boundary control volumes and boundary-conditions are directly applied at the boundary faces. A fine grid was employed at all boundaries where the pressure head (ψ) varies abruptly, and a coarse grid where (ψ) varies rather gently. The discretization equations, which are non-linear and coupled, are solved by an iterative procedure.

The most attractive feature of the control volume formulation is that the integral conservation of quantities such as mass, pressure, and species is exactly satisfied over any group of control volumes and, ultimately, over the whole computation domain. Since this characteristic pertains to any number of grid points, a coarse grid solution exhibits exact integral balance.

1.2.2 Optimization Models

Simulation models, however, may not yield an optimal solution, since this depends upon a particular set of system variables chosen by the analyst. The best answer obtained after repeated experimentation cannot be guaranteed to be optimum. Repeated experimentation (simulation runs) to determine the best management plan for the subsurface system can be quite time consuming and expensive.

Optimization models, on the other hand, are prescriptive models aimed at identifying the "optimum" solution on a specified index of performance (the objective value) and meeting all the relevant constraints. Examples of optimization techniques commonly used in water resources systems engineering are linear programming, dynamic programming, optimal control theory, stochastic programming, and nonlinear programming, etc.

Many optimization techniques have been developed over the last two decades to solve the problem of optimal operation of a multi-reservoir system. Among the most common techniques are, linear programming, dynamic programming, successive linear programming, the feasible direction method, and optimal control theory.

Dynamic programming (DP) is one of the most widely used optimization technique in reservoir operation studies. The major breakthrough in dynamic programming was, however, due to Bellman's (1957) work in developing what is now known as discrete dynamic programming. Bellman defined dynamic programming as "the theory of multistage decision processes". The advantage of dynamic programming over other methods such as linear programming is that the problem is solved one stage at a time. The computation burden therefore increases linearly with the number of stages whereas in the linear and nonlinear programming methods, it varies with the square of the number of stage. The greatest advantage of Dynamic Programming, however, is that there is no restriction of any kind on the type and form of the objective function.

Although standard Dynamic Programming can be formulated either in the continuous or discrete form, the latter is more popularly used for most applications is in water resources systems for the reason of simplicity. In discrete dynamic programming, the computation burden is dependent on the number and discretization of the state variable. For a system with (n) state variables and (m) levels of discretization in each state variable there are (m^n) combinations that have to be explicitly evaluated at each stage of analysis. The computation burden of Dynamic Programming therefore increases exponentially with the number of reservoirs (state variable). Bellman (1957) referred to this characteristic as the "curse of dimensionally" which is the greatest weakness of Dynamic Programming. Even with the largest computer available, the maximum number of state variables that can be

accommodated is less than 10. Efforts have, been focused on ways to reduce the computation burden and/or circumventing the dimensionally problem.

Incremental dynamic programming (IDP) is an alternative to avoid the dimensionality problem of (DP). Incremental dynamic programming (IDP) was the results of the works of Larson (1968), Hall (1969) and Heidari (1971). Heidari labeled this technique as discrete differential dynamic programming and demonstrated its successful application on a simple, hypothetical four-reservoir system with a linear objective function. IDP, as it is more commonly known, starts with an aimed state trajectory and searches over a corridor of states defined by one discretization above and below the trial solution. If a neighboring trajectory results in an improved objective value, the initial trajectory is replaced and the iterative procedure is continued. After an "all interior" solution is obtained, the corridor width is reduced and the procedure is repeated. In this way, the optimum solution is progressively refined until final convergence. The computation burden and memory requirement of IDP is a function of (3^n) where n is the number of state variables. IDP is therefore not immune to the curse of dimensionally and can at best handles five to six reservoirs or state variables. Discrete dynamic programming is a powerful optimization approach to solving a wide variety of problems in many fields and is well suited to microcomputer applications.

The use of dynamic programming for the analysis of reservoir design and operation has three important advantages compared to linear programming. The first and most important is the ability of dynamic programming to easily handle non-linear objective functions and constraints such as those involving squared shortages, evaporation, infiltration and hydropower. The second advantage is that it is relatively easy to solve a dynamic programming problem for many months or periods. The third advantage is that constraints decrease the computational burden of dynamic programming. In linear

programming, constraints actually limit the number of options that must be evaluated. The more constraints, the fewer the options to evaluate, and the smaller the resultant problem.

1.2.3 Conjunctive Use of Simulation/Optimization Models

To simulate the subsurface flow by optimization alone would be practically infeasible, since the governing surface/subsurface flow equations are highly non-linear and involve many parameters that have to be evaluated. Also, subsurface flow is uncontrollable in nature, that is, there is no controllabie component entering into or coming out of the underground storage. From a watershed, the underground flow depends on the surface storage controlled by making decisions concerning its water release. A promising approach would be to develop an optimization model which could incorporate a simulation scheme. Such an optimization model could be very helpful in determining the conjuctive use of surface/subsurface water by determining an optimal recharge rate and its reflection on the subsurface moisture redistributions.

The choice of optimization model for the present system is highly dependent on the conjunctive use of optimization and simulation methods. When applied conjectively, both techniques expected to achieve the desired results. The optimization model was first used to screen through the large number of feasible alternatives to arrive at an optimal preferred solution which may then be used thorough the ground water simulation component.

Jacoby and Lanucks (1972) used a such approach on the study of the Delaware River basin and reported favorable results. Fontane (1982) developed a methodology based on simulation and optimization modeling, the essential characteristic of which was to screen a combination of any two reservoirs into a single equivalent reservoir. Supangat (1985) presented a combined optimization simulation approach to determine storage strategies for a

range of possible future water or energy demands. The use of the simulation model was to find the best relation between yield and storage of each reservoir and also to refine possible configurations before they are optimized. Labadie et al., (1988) used this technique for the optimization of in-system storage urban stormwater in combined sewer systems for reducing pollution from untreated overflows.

Mathematical optimization techniques in conjunction with simulation models have been used to design pump-and-treat ground water reclamation schemes. Yet, the choice of optimization techniques is limited to the mathematical form of a typical ground water remedation problem. Optimization of remediation, with its coupled ground water flow and contaminant transport equations, requires handling a system of nonlinear equations. The dimension of this nonlinear optimization problem is typically large, and the convexity of the problem cannot be guaranteed. Several examples reported in the literature [e.g., Yazicigil et al., 1987] use the embedding technique as a mechanism for coupling the simulation model of a particular ground water system with an optimization model. The model enables the determination of optimal allocation of wells in different aquifers and their pumping rates. More recent models were also developed using mathematical optimization techniques for the optimization of ground water remediation [e.g., Ahlfeld, 1990; Chang et al., 1992; Culver and Shoemaker, 1992]. Other models include Culver and Shoemaker, (1993), Karatzas and Pinder, (1993), and Brimberg et al., (1993). Implicit in these studies is their limitation to deep aquifers were there is no interaction with the surface water.

In the area of stream-aquifer interaction, Taylor (1970) demonstrated a study with a simple and small problem using the linear programming technique. Morel-Seytoux and Daly (1975) derived a method to compute response coefficients for stream-aquifer systems which they called a "discrete kernal generator." The method involved solving the system of

simultaneous linear equations in addition to the aquifer simulation. However, as it was pointed out later by Morel-Seytoux (1975a), this method was limited to aquifers in which drawdowns had small effects on transmissivity. Later, Illangaserkare and Morel-Seytoux (1982) coupled two discrete kernel (matrix response) approaches for an isolated aquifer and isolated stream to derive combined influence (response) coefficients using a linear relationship of the stream-aquifer interaction. Also Morel-Sytoux et al., (1990) developed an analytical model to predict the recharge rate from an ephemeral stream after a fully saturating wetting front reached the shallow water table. However, these studies, do not address an optimal analysis of the surface/subsurface flow. Also, they were based on a simplified analytical solution and do not address the dynamics of the problem.

1.3 STUDY OBJECTIVES

The present research deals with the optimization of ground water recharge from a wadi-reservoir sytem in arid lands. Mathematical optimization techniques in conjunction with surface/subsurface flow simulation are used. Such an optimization model aims at determining the conjuctive use of surface/subsurface water by determining optimal recharge volumes and their reflection on subsurface moisture redistributions. Usually, the local wadis are un-gagged and therefore, watershed analysis is necessary to project planning, design and in the development of arid lands. The analysis was designed to simulate the surface runoff responses of a watershed to precipitation by representing the arid wadi basin as an interconnected system of hydrologic components. Each component models an aspect of the precipitation-runoff process within a portion of the basin, commonly referred to as a sub basin. The analysis is based on the hydrologic routing technique with consideration given to arid or semi arid land. The computations of the event runoff hydrographs take into account major loss rate components of land depression, evaporation, and base flow. Runoff hydrographs are routed by the wadi storage method. Reservoir routing is done using the spillway and low-level outlet conditions.

The simulation of the subsurface flow is based on the control-volume method. It is developed to simulate ground water recharge under optimized conditions and to compare the results with existing ones. Of particular interest, is to obtain a better understanding of the water pressure head distribution and the moisture content redistributions due to an infiltration profile in a semi-arid to arid lands. It is also of interest to find ways to utilize infiltrated water in agricultural practices. The model is based on the general subsurface continuity equation with its upper boundary at the ground surface.

The present optimization methodology attempts to represent the essential physical and operational characteristics of a reservoir system. It is also useful in predicting responses to varying inputs and in providing scenarios of proposed changes or modification to a system. The model can accurately represent the complex interactions between system components, whether they are linear, nonlinear, convex or non convex.

The combined use of the optimization and the control volume simulation techniques for the present system is highly dependent on the specifics of the problem, such as the number of reservoirs, soil type, and ecological system of the area. For the problem at hand, there are merits in the conjunctive use of optimization and simulation models. The optimization model is first used to screen through the large number of feasible alternatives to arrive at an optimal preferred solution which was subsequently used thorough ground water simulations. Such an approach combines the best features of the two methods and hence can be highly advantageous for application on large, complex systems.

In developing the present model the following assumptions are made:

- The hydrological parameters used in the model are assumed to reflect the temporal as well as spatial averages within a subbasin.
- The rainfall, evaporation and infiltration rates are assumed to be uniform over each sub

basin.

- The wadi bed slope and water surface slope are assumed to be equal and therefore, the acceleration effect is negligible.
- The overall soil storage coefficient $G(\psi)$ is invariant in time.
- Soil-specific storage (S_s) is assumed to be constant in time in the saturated flow zone and zero in the unsaturated flow zone.

The objective of this study is to address the dynamic behavior of the surface/subsurface flow in arid lands. In the model developed here, incremental dynamic programming is combined with a surface flow model and a control-volume subsurface flow simulation to determine an optimal control of surface/subsurface water based on a time-varying infiltration rate from an arid wadi-reservoir system.

The specific objectives of the present research are:

1. To develop a well designed and tested optimization procedure for water recharge which complies with a numerical surface/subsurface transport model capable of simulating the complex phenomena of surface/subsurface water development in arid lands;
2. To test and calibrate the optimization procedure as well as various simulation components against field conditions;
3. To analyze and optimize the infiltration process from an existing reservoir system at the Muwaqar project.

CHAPTER II
PROBLEM FORMULATION AND THEORETICAL DEVELOPMENT

2.1 DESCRIPTION OF THE PROBLEM

In semiarid regions (Areas reciving rainfall less than 200 mm/year), conjunctive use of surface/subsurface water storage is often sought to offset deficits in the dry seasons and to enable storage and recharge of excess water during wet seasons. An important feature of aquifers is their ablity to meet demands during periods having long cyclic variations in surface runoff.

Efficient management of ground water recharge systems calls for a set of hierarchical decisions concerning every specific levels of operation. Surface reservoirs appear to be a dominant component of almost every important ground water recharge system. The reservoir operation for maximizing ground water recharge is regarded as one of the most important aspects of the storage and release policy, since the system performance depends, to a large extent, on the way the reservoirs are operated.

An overall hydrologic system may be seen as two subsystems, a surface subsystem and underground one, which are physically interelated in such a manner that water can flow from one subsystem to the other. In arid lands, the surface subsystem consists of a watershed area interconnected by a wadi-network that collects the runoff due to rainfall events from the higher elevated portion of the watershed to the lower elevated portion downstream of the main wadi. A reservoirs network can be constructed to impound the wadi runoff at desired locations in the watershed. The optimization of reservoirs location and size is out of the scope of this study.

The surface subsystem also consists of planned irrigated agricultural lots at desired locations in the watershed. These lots can be irrigated by pumping water from the reservoirs. Therefore, the physical parameters of the surface subsystem are the precipitations represented by precipitation events, land surface runoff, wadi routing, reservoir routing, and land surface interception/infiltration.

In order to evaluate the above parameters, the wadi basin can be modeled as an interconnected group of subareas. This is based on the assumption that the hydrologic processes can be represented by model parameters which reflect average conditions within a subarea. If such averages are inappropriate for a given subarea then it would be necessary to consider smaller subareas within which average parameters do apply. Model parameters represent temporal as well as spatial averages. Thus the time interval to be used should be small enough such that averages over the computation interval are applicable. Other important parameters such as evaporation losses, irrigation demands, and infiltration from the reservoir network are also incorporated into the surface subsystem, and explained later.

In addition to the information concerning the components of surface flow and atmospheric events, a description of the complex hydrologic system also requires that the behavior of the underground subsystem be mathematically defined in such a way that it describes the response of the underground subsystem to the infiltration from the surface subsystem. An accurate mathematical representation of the underground subsystem available appears to be highly complex and somewhat burdensome to compute within an optimization model. Keeping in mind that the continuity conditions of the underground subsystem must be satisfied and also that the recharge to the underground aquifer is a non-negative time function value.

The flow components of both the underground and surface subsystems change simu. aneously with time. Depending upon their mutual relationships, various hydraulic conditions can be found. These conditions will determine whether the exchange flow, will be either positive (into the underground) or negative (out of the underground). This study is restricted to the flow directed from the surface subsystem into the underground subsystem, so that the underground water content increases with time. Therefore, the problem at hand is to optimize the flow that is directed from the surface subsystem to the underground one. This flow is called recharge/infiltration of the surface water from a surface reservoir network to the underground subsystem.

The system depicted in Fig.(2.1) {see Appendix A} can be thought of as a body of surface water representing the surface subsystem, while the underground subsystem consists of porous geological formations which depend upon the hydraulic conditions of the system, it can be filled either with water or air.

In the above system, it is necessary to distinguish between the system operated under optimal and non-optimal conditions. The hydrologic system dealt with in this research consists of a wadi network and man-made surface reservoirs. Optimal operation of a water storage reservoir to maximize infiltration is based on some optimal policy of water storage and release. Finding the optimal policy requires a compatible optimization model that incorporates the hydrologic behavior of the surface flow as well as the underground flow conditions. The optimal policy is based on an evaluation of maximizing recharge resulting from a release-storage policy in successive time intervals, meeting the demands of various agricultural activities and taking into account the evaporation losses.

Reservoir optimization in many cases utilizes the year as the time increment. This treatment is only satisfactory for large surface reservoirs where the total annual inflow

represents a relatively small fraction of the reservoir capacity. This approach may result in significant errors in optimal policy when applied to small or medium size reservoirs. The possible errors may be accentuated by large seasonal variations of flows and/or demand, such as irrigation, and hydropower generation, etc. In addition, the optimal use of coupled surface and underground storage requires evaluation of the optimal policy over a finer grid of time increments than a year.

2.2 MATHEMATICAL FORMULATION

Theoretical development and problem formulation will be based on a hypothetical multireservoir system operated for maximization of recharge over a time horizon of a T period representing the rainy season with simulated inflows and initial reservoir content, S_1. Let us consider N reservoirs with no restriction on their layout configuration. That is, reservoirs can be in series or parallel. Fig.(2.2) {see Appendix A} shows a typical reservoir system for which the present problem formulation is applicable.

2.2.1 Optimization Procedure

Since in arid zones flow records are usually not available, a deterministic optimization procedure is considered with the following objective function structure in terms of Max(min) infiltration as follows:

$$F = \underset{\overline{S_{t+1}}}{\text{MAX}} \left\{ \text{MIN } \overline{\text{QINF}_t} \left\{ \varnothing_t \left(\overline{S_t} \right) \right\} \right\} \tag{2.1}$$

Subject to the following constraints:

$$\overline{U_t} = \overline{S_t} - \overline{S_{t+1}} + \overline{\text{INFW}_t} - \overline{\text{DEM}_t} - \overline{\text{EVAP}_t}\, \Omega_t \left(\overline{S_t} \right) - \overline{\text{QINF}_t} \left\{ \varnothing_t \left(\overline{S_t} \right) \right\} \tag{2.2}$$

$$\overline{S}_{min} \le \overline{S}_{t+1} \le \overline{S}_{max} \tag{2.3}$$

$$\overline{U}_{min} \le \overline{U}_{t+1} \le \overline{U}_{max} \tag{2.4}$$

where:

$\overline{U}_{max}$: vector of maximum allowable reservoir release;

$\overline{U}_{min}$: vector of mimimum allowable reservoir release;

$\overline{S}_{max}$: vector of maximum allowable reservoir storage;

$\overline{S}_{min}$: vector of minimum allowable reservoir storage;

$\overline{INFW}_t$: vector of monthly/weekly inflow;

$\overline{DEM}_t$: vector of monthly/weekly irrigation demand;

$\overline{EVAP}_t$: vector of monthly/weekly evaporation rate;

$\overline{QINF}_t$: vector of monthly/weekly infiltration rate;

$\varnothing_t$: a function that relates the reservoir storage to its surface area;

Ω_t: a function that relates reservoir storage to the projection of reservoir bottom area;

$\overline{S}_t$: vector of reservoir storage (state variable) at the beginning of the monthly/weekly time period t;

$\overline{U}_t$: vector of reservoir release (decision variable) during the monthly/weekly time period t.

For multireservoir systems, S, U, INFW, are vectors of dimension N, where N is the number of reservoirs. In the more general case, the dimension of decision or control variable U need not be the same as the state variable S. Although the routing of the inflow from upstream to downstream reservoirs is taken into account by the watershed simulation component, in the optimization procedure it is assumed that there is no time lag or attenuation of flows between reservoirs. This assumption is justified since the times of travel of flow between reservoirs are small compared to the time discretization of the study.

Eq. (2.2) is commonly known as the state equation derived from the consideration of mass balance at all storage and non-storage nodes in the system. The evaporation losses

are considered dependent on the reservoir surface areas, where the infiltration is considered as a function of the projection of the surface area. The average surface area of the reservoir however is:

$$\varnothing_t(S_t) = \frac{(A(S_t) + A(S_{t+1}))}{2} \qquad (2.5)$$

where $A(S_t)$ is the reservoir surface area at storage level S_t, taken from elevation-area-capacity data for the reservoir site. Crop water demands were calculated based on the requirement of wheat and barley cultivated in 10 irrigated hectares of semi-arid to arid lands. The relation used to calculate the irrigation demand is given as follows (Doorenbos, and Puritt, 1984):

$$V_t = \frac{10}{E_p} \sum_{t=1}^{T} \frac{(A\,ET_{crop} - P_e - G_e)}{1\text{-}LR} \qquad (2.6)$$

where;

V_t : volume of water needed for irrigation (m^3/period);

Ep: the water distribution efficiency in the field;

ET_{crop}: crop water requirement (mm/period);

P_e : effective rainfall (mm);

G_e : ground water contribution (= 0.0 mm);

LR : leaching requirements (in tenthes);

A : size of the irrigated area (ha).

Effective rainfall (P_e) is the amount of rainfall that is intercepted by plant foliage. The contribution from groundwater (G_e) is determined by the depth of the ground water table below the root zone, the capillary properties of the soil and the soil water content in the root zone. Other than net irrigation requirments, water is needed for leaching

acumulated salts from root zone and to compensate for water losses during conveyance and application. This amount of water is called the leaching requirment (LR).

The objective function (F) of Eq.(2.1), for the multireservoir recharge systems is typically multi-dimensional, nonlinear, and separable in time. A pertinent feature of the above optimization problem is the dimension or size of the problem. For a system with N reservoirs and T time period, the number of state and decision variables totals 2NT. There are NT equality constraints and 4NT inequality constraints of the type described by variable bounds. Hence, even with moderate values of N and T, the resulting optimization problem can be large and its solution may not be simple.

For the infiltration optimization problem defined by Eqs. (2.1-2.4), a sequential decision nature is evident in the objective function and the state dynamic equation. The state variables in this problem are reservoir storage and the decision or control variables refer to reservoir releases. For multireservoir systems of moderate size (more than three reservoirs), standard multidimensional dynamic programming is computationally difficult but this is well within the capability of incremental dynamic programming.

The above objective function is nonlinear in the form of backward dynamic programming. Backward dynamic programming was chosen since it is more practical in water resources systems than forward dynamic programming (Labadie, 1990). This implies that optimal infiltration on the final state S_{t+1} is included in $F_t(S_t,U_t)$.

The procedure employed produces more or less uniform infiltration by maximizing the minimum infiltration volume. That is, during drought periods, a "hedging rule" places high penalty on large deficits than on small ones. Its main function is to meet the demand (maximizing infiltration) during periods of critical flow. This procedure makes the planning

and operation of the reservoir system more flexible. The basic idea behind using a critical low-flow period to find an operating rule is that if an operating rule performs well during a critical period, then it can be assumed that it will also perform well during more normal periods.

The hedging rule is implemented by defining what is called a buffer storage level "S_{buffer}" in each reservoir. This level must lie between S_{min} and S_{max}. If storage at the beginning of any time period t, S_t, happened to be above this level, then the release U_t is tolerated for that time period. However, if storage volume S_t happened to be below S_{buffer}, then U_t is minimized.

However, optimization of infiltration, with its coupled subsurface flow equations, requires handling of a system of nonlinear equations. The dimension of this nonlinear optimization problem would typically be large, and the convexity of the problem should be guaranteed. In the optimization model developed here, incremental dynamic programming is performed in conjunction with a control-volume underground flow simulation component to determine the optimal surface water infiltration and its reflection on the underground subsystem.

2.2.2 Surface Flow Simulation

In this section, a mathematical rainfall-runoff simulation is presented to evaluate the surface runoff for precipitation events. In this simulation component, precipitation excess is computed by subtracting infiltration and detention losses based on a soil water infiltration rate function. The resulting rainfall excesses are then routed by the kinematic wave techniques to the outlet of the subbasin. The kinematic wave rainfall excess-to-runoff transformation allows for the uniform distribution of the surface runoff over each subbasin.

In the evaluation of surface flow, land surface interception, depression storage and infiltration are referred to as precipitation losses. Interception and depression storage are intended to represent the surface storage of water grass, local depressions in the ground surface, cracks, and in the surface area where water is not free to move as overland flow. Infiltration represents the movement of water to areas beneath the land surface. Two important factors should be noted about the precipitation loss computation. First, precipitation which does not contribute to the runoff process is considered to be a loss, and second, it does not provide for soil moisture or surface storage recovery.

2.2.2.1 Watershed Input Data Preperation

In this investigation, the wadi basin was subdivided into an interconnected system of wadi network components, using topographic maps and other geographic information Fig. (2.1). These were developed as follows:

1) The watershed boundary of the study wadi is delineated first from a topographic map. Supplementary information, such as dwelling drainage maps, was used for accurate representation.

2) Segmentation of the basin into a number of subbasins determines the number and types of wadi network components to be used in the analysis. Two factors impact on the basin segmentation:

   - First, the actual project development and objectives were used to define the sub areas of interest in the basin.
   - Second, the hydrometeorological processes such as average precipitation, and infiltration rates as well as basin characteristics such as watershed slope, channel length and slope, impacts on the number and location of subbasins. The assumption of uniform precipitation and infiltration rates over a subbasin, becomes less accurate as the subbasin becomes larger. Each subbasin is

intended to represent an area of the watershed which, on the average, has the same hydraulic/hydrologic properties.

3) Each subbasin was represented by a combination of components, such as subbasin runoff, wadi routing, reservoir, diversion and other components.

4) The subbasins and their components are linked together to represent the connectivity of the wadi basin.

2.2.2.2 Simulation Procedures

The subbasin land surface runoff component, such as in subbasins SUB.1, and SUB.2 in Fig. (2.1) is used to represent the movement of runoff over the land surface and in wadi channels. The input to this component is taken in the form of an event precipitation hyetograph.

In the present study, precipitation excess is computed by subtracting infiltration and detention losses based on a soil water infiltration rate function. The rainfall and infiltration are assumed to be uniform over the subbasin. The resulting rainfall excesses are then routed by the unit hydrograph technique to the outlet of the subbasin producing a single runoff hydrograph. The unit hydrograph technique produces a runoff hydrograph at the lowest wadi point in the subbasin.

The wadi routing component is used to represent flood wave movement in the wadi. The input to the component is taken as wadi hydrograph resulting from individual or combined routed contributions of subbasin runoff, wadi routings, or diversions.

The use of the reservoir component is similar to that of the wadi routing component described above. The reservoir component is used to represent the storage-outflow characteristics of a reservoir. Reservoir outflow is solely a function of storage (or surface water elevation) in the reservoir and not dependent on the wadi controls. The storage indication method of routing a hydrograph through a reservoir is also called the Modified Pulse Method [Warren, 1989]. A flood wave passing through a storage reservoir is both delayed and attenuated as it enters and spreads over the pool surface, water stored in the reservoir is gradually released as flow over spillway. Storage values for various pool

elevations in the reservoir were determined from computations of confined volumes measured from topographic maps.

In the kinematic wave interpretation of the equations of motion, it is assumed that the bed slope and water surface slope are equal and acceleration effects are negligible. A basic requirement for the application of continuous kinematic wave theory to a wadi routing is that the boundary forces in the wadi should approximate the gravity forces. Thus flow at any point in the channel can be computed from Manning's formula. Also, the momentum equation is reduced to a functional relation between area and discharge, the movement of a flood wave is described solely by the continuity equation.

2.2.3 Subsurface Flow Formulations

In addition to the information concerning the components of surface flow and atmospheric events, a description of the complex hydrologic system also requires that the behavior of the underground subsystem be represented in a mathematically sound form.

The theoretical basis of the subsurface flow in a natural environment is affected by many factors, such as the configuration of the soil texture, hydrogeological, hydrological, and hydraulic conditions. There are a large number of parameters usually required for subsurface flow computations. By assuming that the soil-air phase is insignificant, the water flow can be described by Richards equation (Richard, 1931):

$$L(\psi)=\frac{\partial}{\partial x}\left[\frac{k_{ij}k_{rw}(\psi)\rho^2 g}{\mu}\left(\frac{\partial \psi}{\partial x_j}+\frac{\partial x_2}{\partial x_i}\right)\right]=\rho\phi\frac{\partial S}{\partial t}+S\frac{\partial(\rho n)}{\partial t}+Q \qquad (2.7)$$

Where:

(i,j =1,2): summation indices;

$L(\psi)$: quasilinear differential operator;

ψ : pressure head;

$k_{ij} = K_{ij}\,\mu/\rho g$: is the saturated soil permeability;

S : water saturation degree;

k_r : relative permeability, $0 \le K_r \le 1$;

ϕ : water porosity;

ρ : water density;

g : gravitational acceleration;

μ : water viscosity;

Q : volumetric rate via sources (or sink) per unit volume of the porous medium.

x_i, x_j : Cartesian coordinates representing the horizontal (as direction related to the problem at hand as well) and vertical directions, x and z respectively.

Equation (2.7) describes both saturated-unsaturated flow conditions. By applying the chain rule, $\frac{\partial s}{\partial t}$ becomes;

$$\frac{\partial s}{\partial t} = \frac{\partial s}{\partial \psi}\frac{\partial \psi}{\partial t} = \frac{c}{\phi}\frac{\partial \psi}{\partial t} \tag{2.8}$$

Where:

$C(\psi) = \phi \frac{\partial Sw}{\partial \psi}$: is the soil specific moisture capacity. By substituting Eq.(2.8) for $\frac{\partial s}{\partial t}$ in Eq.(2.7) and rearranging Eq. (2.7) it becomes;

$$L(\psi) = \frac{\partial}{\partial x}\left[\rho K_{ij} k_r(\psi)\left(\frac{\partial \psi}{\partial x_j} + \frac{\partial x_2}{\partial x_i}\right)\right] = \rho\left[C(\psi) + S_w(\psi) Ss\right]\frac{\partial(\psi)}{\partial t} + Q \tag{2.9}$$

By taking

$$G(\psi) = C(\psi) + S_w(\psi)S_s \tag{2.10}$$

$$L(\psi)=\frac{\partial}{\partial x}\left[K_{ij}k_r(\psi)\left(\frac{\partial \psi}{\partial x_j}+\frac{\partial x_2}{\partial x_i}\right)\right]= G(\psi)\frac{\partial \psi}{\partial t} + Q \tag{2.11}$$

Where:

K_{ij} : saturated hydraulic conductivity tensor;

S_S : specific storage = ρg (ac + n b)

a : coefficient of vertical formation compressibility;

b : water compressibility coefficient;

By taking a' = a ρ g and b' = b ρ g then,

$$S_S=(a'c+b'n) \tag{2.12}$$

$G(\psi)$: overall storage coefficient

t : elapsed time;

S_W : water saturation.

Therefore, the final form of the diffusion partial differential equation with respect to its principal coordinates becomes:

$$L(\psi)=\frac{\partial}{\partial x}\left[K_{sx}\, k_{rw}(\psi)\frac{\partial \psi}{\partial x}\right] +\frac{\partial}{\partial z}\left[K_{sz}\, k_{rw}(\psi)\left(\frac{\partial \psi}{\partial z}+1\right)\right]= G(\psi)\frac{\partial \psi}{\partial t} + Q \tag{2.13}$$

where, K_{sx}, K_{sz} are the saturated hydraulic conductivity in x, and z-directions, respectively. For the purpose of convenience in this work, the term $G(\psi)$ is assumed to be invariant in time.

In this solution, the specific storage, S_s, is defined as the volume of water released from storage per unit volume of saturated soil due to a unit decrease in pressure head ψ. It is assumed to be constant with time in saturated flow regions and zero in unsaturated flow regions, because in these regions storage is controlled much more by moisture content than by compressibility effects. In many situations the latter effects are small even in the saturated zone and S_s can be set equal to zero (Neuman, 1983). The saturated hydraulic conductivity Ksx, and Ksz in horizontal and vertical directions, respectively, varies only in space and not in time. Following standard practice, pressure head, ψ, is positive in saturated zones and negative in unsaturated zones (ψ is zero at the pheratic surface).

The dependent variables are the pressure head ψ and the water saturation, Sw. These variables are related by a nonlinear relationship which depends on the soil type. The relative hydraulic permeability is also a nonlinear function of the pressure head.

CHAPTER III
NUMERICAL PROCEDURES

3.1 BASIC CONCEPT

The overall solution procedure is based on the optimal control algorithm, which is comprised of the incremental dynamic programming optimization model combined with two simulation components and performs an interface between them to reach an optimal solution. The first simulation component consists of a hydrologic routing based on the kinematic wave equation. The second simulation component represents the underground subsystem which is based on the control volume method. Fig. (3.1) {see Appendix A} shows the flow chart of the optimal control model. The hydrologic simulation component is necessary in the evaluation of the watershed runoff due to a rainfall event. It provides an assessment of flood wave movement through the wadi, and the flood occurrence of several rainfall events. This analysis is used to simulate the surface runoff responses of the watershed to several precipitation events by representing the wadi basin as an interconnected system of hydrologic components. Each component models an aspect of the precipitation runoff process within a portion of the watershed.

The computation of the event runoff hydrographs takes into account major loss rate components of land depression, evaporation and base flow. Runoff hydrographs are routed by the wadi storage method. Reservoir routing is done using the spillway and low level outlet conditions.

The optimization model is responsible for guiding the solution according to the objective function (optimal recharge) using information regarding the routed inflows to each reservoir calculated by the hydrologic simulation component of the system for each month based on analyzing each rainfall event. The optimization model run results in optimal

recharge and the corresponding storage policies, which can then be converted to a water head and inflow to be used as input data for the control volume simulation component.

The underground simulation component is responsible for implementing the optimal policies given by the optimization model for analyzing the subsurface flow conditions. Of particular interest is to obtain a better understanding of water pressure head distribution and the moisture content redistributions due to the optimal infiltration profile in a semi-arid land. The moisture content profile is an important factor in adopting an irrigation scheme.

In summary, the optimal control algorithm strengths are that:

- Considers the entire system of surface/subsurface flow interaction;
- Uses an efficient optimization technique based on IDP theory, which interacts with the hydrologic as well as the control volume simulation components;
- User-friendly, since it only requires input that is necessary for the hydrologic simulation to generate inflow required for the over all optimization algorithm;
- Has moderate computation requirements.

3.2 OPTIMIZATION PROCEDURE AND COMPUTATION

In the dynamic programming procedure, constraints (Eqs.(2.3&2.4)) on the reservoir storages and releases (state and decision variables) have simple upper and lower bounds. A sequential decision nature is evident in the optimization of a recharge objective function (Eq. 2.1) and in the state dynamics equation (Eq. 2.2). The state variables in this problem are the reservoir storages (S_t) and the decision or control variables refer to reservoir releases (U_t). Stage in the present problem is denoted by time. Note that initial reservoir storage (state, S_t) can actually have a range of values rather than just a single

known value. As a first step in the solution, it is important to define a recursive optimal return function, $F_t(S_t)$ as follows:

$$F_t(S_t) = \underset{S_{t+1}}{\text{Max}} \left[\text{Min}\{ f_t(S_t,S_{t+1},U_t)+F_{t+1}(S_{t+1})\}\right] \quad (3.1)$$

for t= 1, ...T and

$$F_{T+1}(S_{t+1})=\Phi(S_{T+1}) \quad (3.2)$$

where $f_t(S_t,S_{t+1},U_t)$ is an incremental benefit function (incremental recharge volume in this case from one state to another) of the state variable S_{t+1} (reservoir storage) and the decision variable (reservoir release); $\Phi(S_{T+1})$ is the terminal volume of water left in storage at the end of the study period. The above equations (Eq. 3.1 and 3.2) are subject to the constraint sets defined in Eqs. 2.2 to 2.4. The above formulation (which is in an invertible form) is usually adopted for multi-dimensional problems.

The recursive optimal equations [(3.1) and (3.2)] are true of any stage (time). With the value of the terminal value function, $F_{T+1}(S_{t+1})$ known (zero in most cases), it is possible to solve recursively for $F_T(S_t)$, t= T, ..., 1 as a series of single-stage (time) optimization problems. At each stage (time), the optimal return function is calculated for all feasible discretizations of the state variables (reservoir storage) and the results together with the corresponding optimal decisions variables (reservoir release) are stored for subsequent use. When the last stage (optimal reservoir storage) is reached, the optimal storage value, $F^*_1(S_1)$ is identified together with optimal reservoir release (U^*_1). A trace back is then carried out to determine the optimum values of U^*_t and S^*_{t+1} for all stages (i.e. t= 1, ...,T). Therefore, the solution sequence of the recursive equation is as follows:

$$F_{I,T} \text{----} F_{I-1,T-1} \text{----} F_{1,1} \text{------} U_{1,1}^* \text{--------} U_{2,2}^* \text{-----} U_{I,T}^*$$

The objective function (optimal recharge in this case), has no more an upper bound exponential function but a discrete function. This procedure is based on the principle that "no matter in what state or what stage one may be, in order for a policy to be optimal, one must proceed from that state and stage in an optimal manner." Bellman (1957).

The computation burden of the above solution procedure, is therefore dependent on the number of reservoir storages (state variables) and the level of discretization. Incremental dynamic programming reduces the computation burden of standard dynamic programming by defining a corridor centered on an initial guess of the state (reservoir storages) trajectories, thus limiting the number of discretizations in each state variable (reservoir storage) to at most three (Labadie, 1988). The process can be summarized as follows:

1. Start with an initial guess of reservoir release (decison variables);

2. Determine the corresponding state trajectories using Eq. (2.2)

3. Define a corridor on the state space using an initial corridor width of ΔS;

4. Solve the above multidimensional dynamic programming with restricted state-space in the usual manner. Determine the revised optimum solution for the state variables;

5. Check whether the solution from Step 3 is all interior (i.e., no state variable lies on the boundary of corridor). If this is true, the solution is optimal with respect to the discretization, ΔS. To refine this solution, ΔS may be reduced (a process known as splicing) and the above procedure repeated from Step 3.

The solution is terminated when ΔS has been spliced to the desired level of accuracy;

6. If the solution from Step 3 is not entirely interior, develop a new corridor centered on the revised state trajectories and repeat the entire procedure from Step 3 while maintaining the same corridor width (ΔS).

A uniform discretization interval (DELS) is selected for the reservoir storage (state variable, S_t). The reservoir release (decision variable, U_t), was discretized into increments (DELU). The optimization was performed over the reservoir state of storage at time t+1 (S_{t+1}) in increments of DELS. However, the resulting reservoir release (decision variable, U_t) was rounded off according to the increments DELU value scince it has little effect on the solution procedure.

Selection of the reservoir state of storage discretization interval (DELS) is extremely important since it affects execution time, computer storage requirements, and solution accuracy. It was found by experience in solving such problems (Labadie, 1988), that the value of the reservoir storage increment, (DELS), and its bounds should be selected such that:

$$(S_{max}-S_{min})/DELS \leq 101 \qquad (3.3)$$

Then, the optimization of recharge problem is first solved using the coarse increments of reservoir storage increment, (DELSI). Thereafter, a "splicing" option was used whereby the initial "coarse" interval of reservoir storage increment (DELSI) is refined to reach a final desired interval DELSF < DELSI . The selected real-valued parameter (SPLICE > 1) such that after a complete solution over all stages, a tightened "corridor"

(Fig.(3.2)) {see Appendix A} is defined around the current solution and a new interval of reservoir state of storage increment (DELS) is selected at iteration k by:

$$DELS^{(k)} = DELS^{(k-1)}/SPLICE \tag{3.4}$$

until

$$DELS^{(k)} \leq DELSF, \text{ where } DELS^{(0)} = DELSI \tag{3.5}$$

where:

DELSF: represents the final reservoir storage interval.

Once the optimum recharge volume is found, the range of options to be considered is reduced to an area about the optimum policy just found. This process is repeated until the desired accuracy is obtained. The feasible corridor region in the reservoir storage was controlled by the integer parameter SMULT ≥ 1. That is, for iteration k, the reservoir storages (states S_t) are constrained to lie within:

$$\max [S_t^{(k-1)} - SMULT^* DELS, S_{min}] < S_t$$
$$\leq \min [S_t^{(k-1)} + SMULT^* DELS, S_{max}] \tag{3.6}$$

where $S_t^{(k-1)}$ is the solution of the reservoir state of storage computed at the previous iteration. A new solution S_t^* (t = 1, ..., T) is then obtained and it is set to:

$$S_t^{(k)} = S_t^* \ (t = 1, ..., T) \tag{3.7}$$

If solution $S_t^{(k)}$ occurs on any portion of the boundary of the corridor, then splicing is not performed for the next iteration since the solution has converged to the optimimum recharge value. If the reservoir storage solution occurs completely within the interior of the corridor of all optimization time (stages), then reservoir storage increment (DELS) can be further reduced. If the optimal objective recharge value at iteration k is a repeat of that at the

previous solution, then it is assumed that convergence to a discrete local optimum occurred. Otherwise, a new corridor defined as (SMULT) increments of $DELS^{(k)}$ is specified and the process repeated. If it is suspected that a saddle point or "flat spot" has been encountered, rather than a true local optimum, a tie-breaking option is introduced which should result in the solution process continuation. The splicing option was then used, whereby once convergence occurred for a current reservoir storage increment (DELS), a refined (DELS) is computed by Eq.(3.4) and the process repeated. It should be noted that the splicing option is only advantageous when open loop optimal policies are sought.

The objective function (optimal recharge) for each stage (time) is computed in a subroutine called OBJECT. In the normal backward solution mode, stage (time) t represents the actual evolutionary process of the system. In this case, and since the final desired reservoir storage is known, the state transformation equation Eq.(2.2) is formulated in the subroutine STATE in an inverted form, where it was solved for the reservoir release (decision variable U_t).

Optimization is performed over all discrete reservoir release U_t (or reservoir storage S_{t+1}) to assure attaining discrete global optima. The procedure has the capability of storing only feasible states for the next stage in the calculations.

After each time (stage), the following are stored for subsequent calculations: $F_t(S_t)$, and $S^*_{t+1}(S_t)$. Since $F_t(S_t)$ will be immediately used in the stage t-1 calculations, it is always stored in the main memory. The optimal policies $U_t^*(S_t)$ target states $S^*_{t+1}(S_t)$ are only used during "trace back" after all stages have been computed, so these policies are performed from known S_1 using the stored optimal policies and target reservoir storage (states).

Since the objective function is defined in terms of an exponential function which is non-convex, reaching a global optimum solution may not be guaranteed. However, by optimizing recharge using the present objective function, the goal is to obtain a better operation policy which improves the system performance towards the optimal solution. In general, IDP cannot guarantee a global optimum solution. However, if a good initial guess is available, and with a judicious choice of corridor width and splicing factor, the technique can have a high probability of converging to a good local optimum if not the global solution. It is therefore important that the user experiment with different initial solutions, corridor widths and splicing factors.

3.3 SOLUTION OF THE SUBSURFACE FLOW EQUATIONS

3.3.1 Discretization Equation

The discretization equation is now derived by integrating Eq.(2.13) over the control volume (Fig. 3.3a) {see Appendix A} and over the time interval from t to t+Δt. For the grid point P, points E and W (denoting east, and west) are its x-direction neighbors, while N, and S (denoting north, and south) are the z-direction neighbors. Since time is a one-way coordinate, we obtain the solution by marching in time from a given initial distribution of pressure head. Thus, in a typical time step the task is this: given the grid-point values of ψ at time t, find the values of ψ at time t+Δt. The given values of ψ at time t are denoted as ψ_P^0, ψ_E^0, ψ_W^0, ψ_N^0, and ψ_S^0, and the unknown values of ψ at time t+Δt as ψ_P^1, ψ_E^1, ψ_W^1, ψ_N^1, and ψ_S^1. Thus, the unsteady term of Eq. (2.13) becomes;

$$G(\psi)\int_w^e\int_n^s\int_t^{t+\Delta t}\frac{\partial\psi}{\partial t}\,dt*\,dx*\,dz = G(\psi)*\Delta x*\Delta z*(\psi_P^1-\psi_P^0) \qquad (3.8)$$

where: n is placed at the center of the interface between P and N; s is placed at the center of the interface between P and S; e is placed at the center of the interface between P and E, and w is placed at the center of the interface between P and W.

Where the order of the integrations is chosen according to the nature of each term in the equation. For the representation of the term $\frac{\partial \psi}{\partial t}$, it is assumed that the grid-point value of ψ prevails throughout the control volume.

By taking:

$\Gamma_x = K_{sx}\, k_{rw}$, $\Gamma_z = K_{sz}\, k_{rw}$, then;

$$\int_t^{t+\Delta t}\int_n^s\int_w^e (G_x)\frac{\partial \psi}{\partial x}\, dt^*\, dz + \int_t^{t+\Delta t}\int_w^e\int_s^n (G_z)\left(\frac{\partial \psi}{\partial z}+1\right) dt^*\, dx = \left[(G_x)_e \frac{(\psi_e - \psi_p)}{(\delta x)e}\right.$$

$$\left.(G_x)_w \frac{(\psi_p - \psi_w)}{(\delta x)w}\right]^* \Delta t^* \Delta z + \left\{\left[(G_z)_n \frac{(\psi_n - \psi_p)}{(\delta z)n} + (G_z)_n\right] - \left[(G_z)_s \frac{(\psi_p - \psi_s)}{(\delta z)s} + (G_z)_s\right]\right\}^* \Delta t^* \Delta x + (Q_c + Q_p^* \psi_p)^* \Delta t^* \Delta x^* \Delta z \qquad (3.9)$$

At this point, an assumption about ψ_P, ψ_E, ψ_W, ψ_N and ψ_S changes in time from t to t+Δt is needed. A generalized assumption can be proposed as follows:

$$\int_t^{t+\Delta t} \psi_p\, dt = \left[f\, \psi_p^1 + (1-f)\, \psi_p^o\right]^* \Delta t \qquad (3.10)$$

where f is a weighting factor between 0 and 1. In the present case, a fully implicit scheme (f=1) is adopted. Using similar formulas for ψ_E, ψ_W, ψ_N, ψ_S, and by dropping the superscript 1, and replacing each term in Eq.(3.10), the following equation can be obtained;

$$a_P \psi_P = a_E \psi_E + a_W \psi_W + a_N \psi_N + a_S \psi_S + b \tag{3.11}$$

where:

$$a_E = \frac{((\Gamma_x)_e * \Delta z)}{(\delta x)e} ;$$

$$a_W = \frac{((\Gamma_x)_w * \Delta z)}{(\delta x)w} ;$$

$$a_N = \frac{((\Gamma_z)_n * \Delta x)}{(\delta z)n} ;$$

$$a_S = \frac{((\Gamma_z)_s * \Delta x)}{(\delta z)s} ;$$

$$a_P^0 = \frac{(G(\psi) * \Delta x * \Delta z)}{\Delta t} ;$$

$$b = (Qc * \Delta x * \Delta z) + a_P^0 \psi_P^0 + [(\Gamma_z)_n - (\Gamma_z)_s];$$

$$a_P = a_E + a_W + a_N + a_S + a_P^0 + Q_p * \Delta x * \Delta z \tag{3.12}$$

where the product of ($\Delta x * \Delta z * 1$) is the volume of the control volume.

At this point, it is interesting to examine the physical significance of the various coefficients in the discretization equation. The neighbor coefficients a_E, a_W, a_N, and a_S represent the conductance between the point P and the corresponding neighbor. The term $a_P^0 \psi_P^0$ is the internal water pressure (divide by Δt) contained in the control volume at time

t. The constant term b consists of the internal pressure and the rate of pressure generation in the control volume resulting from Q_c. The center-point coefficient a_P is the sum of all neighbor coefficients (including a_P^0, which is the coefficient of the "time neighbor" ψ_P^0) and contains a contribution from the linearized source term.

3.3.2 Solution Procedure

It should be noted that, while constructing the discretization equation, we cast it into a linear form. However, it is useful to consider the derivation of the equation and its solution as two distinct operations, and there is no need for the choices in one to influence the other. In the computer program, the two operations are conveniently performed in separate sections, and either section can be independently modified when desired. The solution of the discretization equation is obtained by the Tridiagonal-Matrix Algorithm (TDMA). Direct methods (i.e., those requiring no iteration) for solving the algebraic equation arising in multi-dimensional problems are much more complicated and require rather large amounts of computer storage and time.

The alternative, then, is that iterative methods for the solution of algebraic equation be used. These start from a guessed field of ψ, and use the algebraic equation in some manner to obtain an improved field. Successive repetitions of the algorithm finally lead to a solution that is sufficiently close to the correct solution of the algebraic equation. On the other hand, a non-linear situation usually arises in the calculation of the soil hydraulic properties. The relative hydraulic conductivity for example, depends on ψ, and the source term is also dependant on ψ. Then, the coefficients in the discretization equation will themselves depend on ψ. This is being handled by iterations.

The process involves the following steps in the computer program:

1- The program starts with a guess or estimate for the values of ψ at all grid points.

2- From these guessed ψ's the program calculates tentative values of the coefficients in the discretization equation.

3- It then solves the nominally linear set of algebraic equation to get new values of ψ.

4- With these ψ's as a better guesses, the program returns to step 2 and repeats the process until further integration ceases to produce any significant changes in the values of ψ.

The final unchanging state is called the convergence of the iterations, which is actually the correct solution of the nonlinear equation. Iterative methods usually require very small additional storage in the computer, and they are especially attractive for handling nonlinearities. In a nonlinear problem, it is not necessary or wise to take the solution of the algebraic equation to final convergence for a fixed set of coefficient values (Patanker, 1980). With a given set of these values, a few iterations of the equation-solving algorithm are sufficient before updating the coefficients. It seems that, in general, there should be a certain balance between the effort required to calculate the coefficients and that spent on solving the equations. Once the coefficients are calculated, sufficient iterations must be performed to extract substantial benefit from the coefficients, but it is unwise to spend an excessive amount of effort on solving equations that are based on only tentative coefficients.

3.3.3 Interface Conductivity

In Eq. (3.12), the interface conductivity $(\Gamma_x)_e$, has been used to represent the value of conductivity (Γ_x), pertaining at the control- volume face e (Fig. 3.3b). Similarly, $(\Gamma_x)_w$, $(\Gamma_z)_n$, and $(\Gamma_z)_s$ refers to the interface, w, n, and s, respectively. Since the conductivity (Γ) is a function of the principle coordinates x and z, it is desirable to know the value of (Γ) only at the grid points, W, P, E, N, and S are readily available. The hydraulic conductivity

of all faces has therefore, been represented by a harmonic mean of all point values rather than the arithmetic mean, i.e;

$$\Gamma_e = \frac{1}{\left[\frac{1-\vartheta_e}{\Gamma_P} + \frac{\vartheta_e}{\Gamma_E}\right]} \tag{3.13}$$

where;

$$\vartheta_e = \frac{(\delta_x)e+}{(\delta_x)e}$$

However, for the case where the interfaces are placed midway between grid points $\vartheta_e = 0.5$ and Eq.(3.13) becomes:

$$(\Gamma x)_e = \frac{2\,\Gamma_P * \Gamma_E}{\Gamma_P + \Gamma_E} \tag{3.14}$$

This approach leads to an accurate representation of conductivity at the interface especially when an abrupt change in the conductivity is evident. The harmonic mean approach leads to a correct interface water flux value.

3.3.4 Source Term Linearization

The source term Q is a function of the pore water pressure (ψ), which can be expressed in a linearized form given by:

$$Q = Q_c + Q_P \psi_P \tag{3.15}$$

where: Q_C is a constant term of the source, while Q_P is a function of ψ_P representing the value of the source term at the center of the control volume. In the computation process, and during each iteration cycle required by the nonlinear behavior of the equation, Q_P would be recalculated from the newly iterative values of ψ. This linearization of the source term Q, necessitates a null or negative Q_P, [Patanker, 1980].

In the upper soil layer and in the plants root zone, the sink term in the continuity equation was linearized by Neuman, and Davis (1983), as follows:

$$Q= \Gamma(\psi-\psi_r)b' \tag{3.16}$$

where:

ψ_r = is the pressure head in the root zone, and

b'= root effectiveness function.

Eq. (3.16) can be seen as a particular form of Eq.(3.15), and has been tested in the present model.

3.3.5 Initial And Boundary Conditions

To solve Eq.(3.12), it is necessary to know the initial conditions within the flow region. The initial conditions consist of a description of the spatial distribution of the dependent variable ψ, at some time that is referenced as zero (t=0). Considering the integral over a control-volume in the flow equation, at any instant of time $t_o = 0$, there is an initial distribution of ψ_o within the flow region bounded by a boundary node. The initial distribution of ψ for this node takes on the trivial form:

$$\psi(x_i,t=0)= \psi_o(x_i) \tag{3.17}$$

Where:

ψ_o is a prescribed function of x_i.

At such an impermeable boundary, the diffusion flux of ψ normal to the boundary surface is specified.

In addition to these boundary types, and along the atmospheric boundary, a complex combination of boundary conditions can exist. At the soil-air interface, water may leave the system through evaporation or enter the system through infiltration. Although the potential rate of evaporation is controlled by atmospheric conditions, evaporation from soil is also dependent on the moisture content of the soil. I.e., the actual rate of evaporation may be limited by the ability of the soil to transmit water upward from below. In a similar manner, the potential rate of infiltration may be greater than the rate at which the soil can transmit water downward and away from the boundary, e.g., during a rainfall event, the precipitation rate may exceed the infiltration capacity and ponding or runoff may occur. In both cases, the potential flux at the boundary is controlled by external conditions while the actual flux depends on antecedent soil moisture conditions.

A priori prediction of the exact boundary condition to specify under the above conditions is not possible. In this work, the solution is obtained by maximizing the absolute value of the flux (while maintaining the appropriate sign) subject to the following requirements (Hanks, et al., 1969):

$$|V_i n_i| \leq E_s^* \tag{3.18}$$

and

$$\psi_L \leq \psi \leq 0 \tag{3.19}$$

where:

E_s^* : prescribed potential surface flux,

ψ_L : minimum allowed pressure head at the soil surface.

V_i: potential surface flux= $K_{ijk_{rw}}(\frac{\partial \psi}{\partial x_j}+\frac{\partial x_2}{\partial x_i})$ (3.21)

Both of these quantities are a function of time. It should be noted that the potential surface flux may be positive (for infiltration) or negative (for evaporation). Methods for calculating E_s^* and ψ_L are discussed by Feddes et al. (1974).

At nodes along prescribed flux boundaries, the values of Q are computed by multiplying Darcy's velocity Vi by Δx. At internal nodes which do not act as sources or sink, the value of Q is equal to zero. Internal nodes that act as sources and sinks have values of Q equal to the known fluid generation or extraction rate. Nodes in the root zones are treated as regular interior nodes (Q=0) as far as Q is concerned.

Evaporation and infiltration boundaries are simulated by applying either prescribed head or prescribed flux boundaries depending on whether or not Eq.(3.18) is satisfied. During the first iteration of any time step, such nodes are treated as prescribed flux boundaries with flux equal to some fraction of the specified potential flux. If the computed pressure head satisfies Eq.(3.19), the absolute value of the flux at the node is increased by an amount calculated according to:

$\frac{|\psi_L|}{|\psi_n|}$ in the case of an evaporation boundary; (3.21)

$\frac{|\psi_L|}{|\psi_L - \psi_n|}$ in the case of an infiltration boundary. (3.22)

If, however, Eq.(3.19) is not satisfied, the boundary node becomes a prescribed head boundary during subsequent iteration with

$\psi = \psi_L$ for evaporation boundaries;

$\psi = 0$ for infiltration boundaries.

If during any stage of the computations, Eq.(3.19) is not satisfied, the calculated flux exceeds the specified potential flux, the node is assigned a flux equal to the potential value and is again treated as a prescribed flux boundary. The iterative process outlined above is continued until convergence is achieved at all nodes in the control volume finite network.

The inherent difficulty in treating seepage faces has been overcome in the present work owing to the ease with which prescribed pressure head and prescribed normal flux boundary conditions can be assigned at each node with the control volume method. Consider a given segment of the boundary along which a seepage face has chances to develop during any stage of the computation. During each iteration, the saturated part of this segment is treated as a prescribed pressure head boundary with ψ=0. At the same time, the unsaturated part is treated as a prescribed flux boundary with Q=0. The relative length of each part is continually adjusted during the iterative process until all calculated values of Q along the saturated part and all calculated values of ψ along the unsaturated part are negative, indicating that water is leaving the porous medium through the saturated part of the boundary.

CHAPTER IV

VALIDATION OF THE SUBSURFACE SIMULATION COMPONENT

4.1 ONE-DIMENSIONAL FLOW TESTING

4.1.1 Test Case I: One-Dimensional Horizontal Flow

The first test case concerns adsorption into a soil column with two ends subject to constant heads Fig. (4.1) {see Appendix A}. The main purpose of this test is to check the control volume solution with the corresponding regular Galerkin finite element solution of Huyakorn, et. al., (1984), and with the semi-analytical solution of Philip (1955, 1969). For the sake of convenience, linear constitutive relations of K_{rw} versus Sw, and Sw versus ψ were used. These relations and their values are as follows:

$$K_{rw} = \frac{(S_w - S_{wr})}{(1 - S_{wr})} \tag{4.1}$$

$$\frac{(\psi - \psi_a)}{(\psi_r - \psi_a)} = \frac{(1 - S_w)}{(1 - S_{wr})} \tag{4.2}$$

where:

S_{wr}: represents the residual soil moisture content= 0.333, ψ_r: is the initial water pressure head=-100 cm, and ψ_a: is the air pressure =0.0 cm. Uniform nodel spacing and time steps of $\Delta x = 1$ cm, and $\Delta t = 0.01$ day were used respectively.

To obtain the numerical solutions, the flow region was discretized using a uniform grid of 20 nodes spaced 1cm apart. The time discretization was performed in a simple manner using a constant value of Δt=0.01 day. The results of the present control volume simulation component are obtained by simulating the water saturation and pressure head

values on the nodes (at the centers of the control-volumes), whereas the results given by the SATURN code of Huyakorn et. al., (1984) correspond to the values at the element's centroids. Both solutions agree well with the semi-analytical solution.

To provide further assessment of the numerical results, a plot of pressure head profiles is presented in Fig.(4.2) {see Appendix A}. The results obtained from both methods are in good agreement. However, it should be noted that, in this case, which involved a transient solution of a mildly nonlinear problem, the SATURN code using the Newton-Raphson algorithm took approximately 3 to 4 iterations per time step to converge to the final solution within a head tolerance of $1x10^{-3}$ cm, where for the control volume solution, it took 3 iterations per time step to reach a head tolerance of $1x10^{-7}$cm.

The nonlinear flow equation converged satisfactory within three iterations. The iterative technique can be seen to have successful convergence capabilities. No swings in the values of the pressure head are noticeable. The use of underrelaxation helps in obtaining fast convergence.

4.1.2 Test Case II: Vertical Flow in a Multi-Layered Soil System.

The main purpose of this test is to evaluate the capabilities of the control volume method to handle problems involving a multi-layer porous media. It is also to compare the control volume solution with the corresponding regular finite element solution of Huyakorn et. al., (1984). This example focused on a situation concerning infiltration in a multilayered soil system as a site in a semi-arid environment. The flow model consists of four layers with a total depth of 700 m. These layers are: a sand layer which starts at the ground surface to a depth of 100 m, then followed by 40 m layer of silt, then 300 m layer of sand,

and the last layer which consists of 260 m of clay. The flow model is presented in Fig. (4.3) {see Appendix A}.

More specifically, the test evaluates the capability of the proposed method to handle a field problem involving moisture movement in desiccated soils with highly nonlinear constitutive relations. Finlayson (1977), stated that this type of problem is difficult to solve numerically because, under the stated conditions, the eigen-values of the coefficient matrix of the physical system are widely spread in magnitude. This depends on the degree of variation in the values of the effective hydraulic conductivity and the moisture capacity over the flow region. To study the transient response of the flow system, it was assumed that initially the flow system was in a steady state while receiving a recharge rate of 0.16 m/yr. Then the recharge rate was reduced to 0.006 m/yr, and the transient simulation was carried out over a period of 8.1 yrs. The soil moisture characteristics used were based on experimental data taken from Elzeftawy and Cartwright, (1983). For further discussion on the data, see Huyakorn, et. al., 1984.

The change in the values of relative permeability is up to six orders of magnitude. This is indicative of severely nonlinear flow condition from the numerical point view. To obtain the numerical results, the flow region was represented by a uniform grid consisting of 70 nodes. The initial condition of the transient flow case was derived by performing a steady state analysis using the recharge rate of 0.16 m/yr. Huyakorn (1984), performed the steady state solution using the Newton-Raphson algorithm, which took 10 iterations to converge to a head tolerance of $1x10^{-4}$ m (whereas his Picard algorithm did not converge for the steady state case). By using the control volume method along with the TDMA, the computation of the steady state case was performed with only 4 iterations to converge to a head tolerance of $1x10^{-6}$ m. Following the steady state analysis, a transient flow

computation was performed using the derived initial conditions and a recharge rate of 0.006 m/yr. The time step values were generated using the following algorithm :

$$\Delta t_1 = 1.141 \text{ yr}, \quad \Delta t_k = 1.4\, \Delta t_{k-1} \leq 500 \text{ yr.}, \text{ for } k=2,\ldots,8.1.$$

On the average, it took the SATURN code 8 iterations per time step to converge to a head tolerance 1×10^{-4} m, where, using the present control volume model, the transient simulation was completed in 3 iterations with a head tolerance of 1×10^{-8} m.

The present linearization practice can be seen to have produced a rapid convergence. This description of an adaptation of the present model to an unsteady problem shows that the extra effort needed to perform unsteady computations is quite small. Yet, it is possible to produce extensive pore water pressure field representations. The results of the transient flow analysis are presented in Fig.(4.4) {see Appendix A} which illustrates the pressure head profiles.

4.2 TWO-DIMENSIONAL FLOW TESTING

4.2.1 Test Case I: Flow in a Formation With Lenticular Deposits

This test is designed to check the developed model against a regular Galerkin finite element model of Huyakorn et. al., (1984). It consists of a two-dimensional simulation of steady state flow in an unsaturated zone above the water table. The flow field under consideration was reproduced after Huyakorn et al., (1984). The soil formation consists of alluvial sand deposits with a low permeability layer of clay and a layer of loam. The size of the flow field is 9.14 m wide and 15.2 m deep. The low permeability loam is 3 m in width and 6 m in depth. The clay layer is 3 m in width and 1.6 m in depth. The pheriatic line is

located at the bottom of the flow field. The schematic representation of the problem considered is shown in Fig. (4.5) {see Appendix A}. The difference in the saturated hydraulic conductivity between the fine and course materials is up to five orders of magnitude. In addition, each type of soil material has highly non-linear relative permeability and water saturation curves. These features are designed to test the capability of the numerical scheme to accommodate not only abrupt changes in gradients but also a wide range of values of effective conductivity. Huyakorn et al., (1984) used Picard and Newton-Raphson algorithms in the SATURN code to perform a one-stage steady state solution using a rectangular grid consisting of 135 elements. The constitutive relations for K_{rw} and S_w in terms of ψ were supplied to the SATURN code in a tabulated form. The initial pressure head was set to zero, and a linear interpolation of K_{rw} and S_w values was used to compute the element matrices.

The geometric configuration of the problem as well as the same number of elements used by Huyakorn et al., were reproduced in the present model. Also, the constitutive relations of K_{rw} and S_w used by Huyakorn et. al., were supplied to the code in simple analytical functions. Huyakorn, (1984) stated that a poor estimate of ψ but rather fast convergence to the final solution was obtained after 12 iterations within a head tolerance of 10^{-4} m. In this test, the final solution was obtained by the present model with only 8 iterations required to achieve convergence within a head tolerance of 10^{-7} m.

Comparisons of computed values of water saturation and pressure head are given in Fig. (4.6) and Fig. (4.7) {see Appendix A} which illustrate the effect of the low-permeability lenses on moisture and pressure head distributions. As shown, the presence of lenses of fine materials causes a substantial buildup of water saturation and abrupt changes in the pressure gradient at the interfaces of the different materials. These effects are known

as capillary perching, which is often encountered when a fine-grained layer overlies a coarser one. The figures also show good agreement between the Galerkin and control volume solutions. Some differences encountered are due to the manner in which the constitutive relations are introduced to the control-volume code. Also, the use of a nonuniform grid in the present model, compared to a uniform grid used by Huyakorn, may contributed to these differences.

4.2.2 Test Case II: Flow in Subsurface Drainage System

The second test case is based on a laboratory experiment performed by Duke (1973) and Hedstorm et al., (1983). The purpose of the research was to obtain a better understanding of the drainage of agricultural soils and to develop better design procedures for subsurface drainage systems. In the experiment on which this test case is based, a flume 1220 cm long, 122 cm deep and 5.1 cm thick was carefully packed with Poudre Sand. Poudre Sand was used since it is fairly uniform and its hydraulic properties have been well documented. The capillary pressure versus moisture content and relative conductivity versus moisture content relations are presented in simple analytical relations. The saturated hydraulic conductivity of Poudre Sand is 556.4 cm/day and its effective porosity is 0.348. This sand is isotropic and for the purposes of this case the specific storage is assumed to equal zero.

The experiment consisted of simulating a constant infiltration rate at the soil surface while maintaining a constant fluid level in a fully penetrating drainage channel at the ends of the flume. Although these experiments were conducted for several outflow fluid levels and a variety of infiltration rates, in the case selected for simulation the fluid level was held at the same elevation as the lower impermeable boundary of the flume and the infiltration rate was set at 10.35 cm/day.

A vertical cross-section of one half of the flow system under consideration is presented in Fig. (4.8) {see Appendix A}. Because the flow system is symmetrical about the center line between the two drainage ditches, the right boundary may be taken as impermeable and only one half of the system needs to be considered. For the purposes of the simulation, it was assumed that the system was initially in static equilibrium. The constant infiltration rate equal to 10.35 cm/day was assumed to begin at a time of zero days.

In the control volume as well as in the finite element mesh, small vertical element dimensions were used near the soil surface because the initial hydraulic gradients at these locations were large. Small element dimensions, both horizontally and vertically, were utilized near the drainage channel to allow the seepage face to develop realistically as the low system became saturated.

In the Neuman and Davis (1983) finite element mesh, larger horizontal element dimensions were used in the right portion of the mesh, where, in the present control-volume mesh, small horizontal as well as vertical dimensions were used along all boundaries. Total number of nodes used was 226.

Initially, small time steps were utilized in the computations. This was necessary to ensure convergence at small times since large hydraulic gradients exist near the soil surface. The time steps were lengthened as the computations progressed and the hydraulic gradients in the system became smaller.

A plot of pressure head versus height above the impermeable lower boundary is presented in Fig. (4.9) {see Appendix A}. The results of the simulation of the present control volume method are very similar to those predicted by Neuman and Davis, (1983) in the Galerkin finite element solution. The control volume method took three iterations per time step to achieve a head tolerance of 1×10^{-7} cm, whereas in Neuman and Davis, (1983) a head tolerance of 1 cm was achieved. Another advantage to this method is that the input data file of Neuman is very long and tedious, hereas in the control-volume method, there is practically no separate input data file. Instead it is easy to change and input the variables directly to the main program. This is a convenient and practical interactive way of simulation especially if different simulation conditions are at hand.

4.2.3 Test Case III: Flow in Subsurface Irrigation System

This test case is designed to evaluate the capabilities of the control-volume method in modelling multi-layer and non-isotropic conditions. It is also designed, to subject the method to cases involving water uptake by plant roots as well as to evaluate recharge rate to an underground aquifer. This problem illustrates the two-dimensional aspect of the flow in a multi-layered system: to utilize the soil evaporation and plant transpiration facilities provided by the present control-volume solution, and to compare its performance in comparison with the Galerkin finite element solution provided by Neuman and Davis, (1983).

Field data considered was reproduced after Neuman and Davis, (1983). The test case involves the study of the effects of subsurface irrigation on a potato field. The field consists of sixteen hectares of peaty soil, 1.4 m thick, underlaid by sandy soils to a depth of 10 m. The sand layer is separated from the underlying aquifer by 2.0 m of low

permeability sediments. Outside the field, the underlying aquifer is penetrated by wells which intermittently remove water from the aquifer.

In order to estimate the water losses which occur in the upper layers of the soil due to plant transpiration, soil evaporation, and the losses to lower aquifer, several unlined ditches, in which the water level is controlled across the field, were excavated.

Since the ditches are parallel to one another, the flow system is assumed to be symmetrical with respect to the center line of the field between two ditches and the center line of one of the ditches. Therefore, it is adequate to consider only half of the flow system bounded by two ditches. A vertical cross section of the flow system under consideration is shown in Fig. (4.10) {see Appendix A}. The depth of the water in the ditch is maintained at 74 cm, below the soil surface. Initially the water table in the field was located at the same level and a static equilibrium existed with the hydraulic heads. As illustrated in Fig. (4.10), the peat soil was divided into three distinct layers, B_1, B_2 and B_3, according to field investigations. Thus, five distinct soil layers, namely, three peat layers, a sandy soil, and a low conductivity layer confining the lower aquifer, are presented in the flow region. The relative hydraulic conductivity as a function of soil water content for each of the above materials was represented by an analytical relation constructed after Neuman and Davis (1983) input data file. The peat and sand layers are assumed to be non-isotropic, having horizontal conductivities 10 times as large as the vertical conductivity. The saturated vertical hydraulic conductivities are 1.4 cm/hr for peats B_1 and B_2 and 0.2 cm/hr for peat B_3 while the saturated vertical hydraulic conductivity of the sand is 0.27 cm/hr. The bottom confining layer is considered isotropic with a saturated conductivity of 0.044 cm/hr. Effective porosities of the five soil layers are 0.73, 0.93, 0.93, 0.36 and 0.52 in decending order from the soil surface down through the lowest layer. Specific storage was set at zero

for all the soils in the system. The only crop grown in the field is potatoes. The depth of the root zone is taken to be 40 cm with the top of the root zone at a depth of 5 cm. The root effectiveness function, b', is assumed to vary with depth and time (Neuman and Davis, 1983).

The symmetry condition implies that flow is not allowed to take place across the vertical boundary along the right and left sides of the flow region. The pressure head at the bottom of the system varies with time due to the extraction of water from the lower aquifer. Also, the maximum allowable rate of plant transpiration and soil evaporation is time dependent.

The flow field was meshed with 416 nodes in a nonuniform grid, pressure heads were specified at the nodes along the bottom of the low conductivity layer and along the saturated portion of the ditch. The total head at the nodes along the saturated portion of the ditch was held constant. At the nodes along the bottom of the system the total head varied with time. For the nodes at the soil surface, excluding the node at the top of the ditch, the rate of evaporation was maintained within the maximum allowable rate.

During the 24 hour simulation period, the time step (TSTEP) was increased gradually from its initial value of one hour by a factor of 1.2.

The cumulative volume of water leaving the soil surface via evapotranspiration and leakage into the underlying aquifer, as well as the water infiltration into the system from the ditch, are shown as functions of time in Fig. (4.11) {see Appendix A}.

In the lower portion of the sublayer, B_3 peat and in the sand, as well as in the low conductivity layer, the flow is directed downward the underlying aquifer. Near the soil surface in the B_1 peat and in the very top portion of the B2 peat, the flow is directed upward in response to evaporation at the soil surface. In the upper portion of the root zone, the flow is principally downward while in the lower root zone it is directed upward. This pattern is due to water extraction by the roots and converges to a particular soil level at which the rate of water uptake by the roots is maximum. Beneath the root zone, flow is also directed upward within the B_2 peat but another gradient divide is evident at approximately the interface between the B_2 and B_3 peats.

Fig. (4.12) {see Appendix A} shows the computed values of the pressure head up to 24 hours of the simulation time. A close agreement between the control volume method and the Galerkin finite element method is achieved. The slight discrepancy is largely due to the analytical approximation of soil properties data. It should be noted, however, that very small difference occurs within the saturation region where most of the flow is occuring.

In the control-volume method, it took five iterations per time step to reach a head tolerance of 10^{-8} cm. On the contrary, Neuman and Davis, (1983), stopped the simulation at a head tolerance of 1 cm only. Another advantage of the present code is the ease in assembling the data and in changing it at designed time steps.

CHAPTER V
FIELD WORK AND MEASUREMENTS

5.1 BACKGROUND

This chapter describes the field work and data collection nesessary to calibrate the optimization algorithm against field conditions. The need for such calibration is essential to validate the model to optimize a field problem in arid lands. Such testing is required not only to simulate the essential physical parameters related to a field case, but is rather to address the possibility to improve the performance of an existing system. Without this, the improvement as well as future expansion of any project would be lengthy and complicated process.

In 1985, the University of Jordan, Faculty of Agriculture, and the Water and Environmental Research and Study Center, started a major project aimed at developing agriculture production in areas suffering from desertification. One of the objectives of the project is to effectively utilize surface water for various agriculture activities. Small earth dams were constructed to impound surface runoff and store it behind these dams. Over the past few seasons, the project has accumulated significant data to support this hypothesis. Field observations indicate that approximately 900,000 cubic meters of water usually pass the project during a given season.

The main concept used to increase the amount of irrigation water is by manipulating high surface run-off which is considered characteristic of the area and the main source for irrigation water needed for various agricultural activities.

Surface run-off is manipulated in two ways:-

1. Direct: by the use of various water harvesting techniques. In these techniques, a certain area is used as a run-off area where water is collected and concentrated in a smaller area planted with special crops such as trees or field crops.
2. Indirect: by intercepting the run-off water behind earth dams. The stored water is then used for irrigation when needed.

The amount of precipitation on the average is about 150 mm/year. The soil type and low vegetation cover allow a large portion of the rain to flow as surface runoff towards the main wadi and its tributaries, causing short intensive floods.

A. Muwaqar, data collection and preparation was carried out in collaboration with the University of Jordan, Faculty of Agriculture, and Water and Environmental Research and Study Center. This data consists of continuous rainfall measurements, infiltration rates, evaporation rates, and drawdown of water levels behind the reservoirs. Infiltration measurements were made possible with the help of installed infiltrometers. Other parameters of the watershed such as wadi bed slope, cross sectional area, tributaries lengths, and runoff volumes from these tributaries were not available. For the purposes of the present study these parameters were evaluated partially by field measurements and/or by calculations. Soil parameters were also evaluated based on the soil type such as curve number (CN), as well as vegetative cover, and roughness, which are needed as an input to the model.

In addition to the existing meteorological installations that are equipped to measure rainfall rates, insolation, wind speed and directions, air temperature, and relative humidity, an evaporation tank was put into operation together with 3 rain gauges. The first is non-

automatic at 1 m height and covers a 200 cm^2 area, the second is an automatic gauge placed at a height of 1.2 m above the surface, also with a 200 cm^2 area and the third was at the ground level with an area of 400 cm^2.

5.2 ECOLOGICAL CHARACTERISTICS OF THE WATERSHED AREA

The ecological system of the Muwaqar area is characterized by long dry summers which extend from late April to November. The effective winter season is only three months long, with an average annual precipitation of 150 mm. The low permeability of the top soil layer and low vegetative cover allow a large portion of the rain to flow as surface runoff towards the wadis causing short intensive floods. More than 50 million cubic meters of water are flowing annually to the desert where they either evaporate or infiltrate (Salameh, and Wirth, 1989). This water is not only virtually unexploitable but also increases soil erosion. Therefore, this area is characterized by a low infiltration rate, high evaporation rate, low vegetative cover, and limiting water resources. The region suffers from several problems related to the prevailing ecosystem. These problems can be summarized as follows:

5.2.1 Climate

The present climate in the study area and its surroundings is classified as arid with an annual rainfall range of 100-200 mm. The rainfall season begins between late October to early November and ends towards late April or early May. Maximum rainfall occurs during January-February. The rainfall is basically irregular, sporadic and unpredictable. Therefore, heavy showers cause tremendous losses of water through surface runoff, thus decreasing the amount of water stored in the soil. High evaporation demands are caused by strong wind gusts and high temperatures, thus substantially lowering the water available for plant growth in comparison with the actual amount of rainfall. This phenomenon is responsible for the

thinning out of plant cover, causing further erosion and accelerating the rate of soil fertility degradation.

Sporadic heavy storms usually occur during April as a result of climatic instability (Khamassen). The mean maximum and minimum air temperatures during January are 13°C and 3°C, respectively, and the mean maximum and minimum temperatures during August are about 33°C and 17°C, respectively, and the mean annual air temperature is 17°C. Absolute maximum and minimum temperatures during the same months are 41°C and 3°C, respectively. The mean and annual relative humidity during August are 70% and 45%, respectively. The area is windy with a mean annual solar radiation of 550 cal/cm/day.

5.2.2 Topography

The general topography of the area is undulating with some isolated hilly areas. The general surface shape is rather linear with smooth rounded edges. This type of topography is ideal for sheet erosion where soil materials are transported from higher po' 's and re-deposited on the back slope positions. Coupled with the modification caused by soil moisture variation along the same slope, significant soil differences are produced within very short distances. Among the soil properties mostly affected is the soil depth which becomes substantially shallow, if slope gradient exceeds 5%. Deep soil profiles are observed on lower slope gradients. The distribution of the secondary carbonate is also dependent on the distribution of moisture and the extent of erosion along slope. The calcic horizon is absent or lies deeper than 100 cm in soils occurring at a slope of less than 2% and occurs at shallower depths when the slope is between 2-5%. If the slope exceeds 5%, the soil becomes very shallow and the a secondary carbonate layer is not formed.

5.3 DESCRIPTION Of CATCHMENT AREA AND DAMS SITES

Fig. (5.1) {see Appendix A} depicts the Muwaqar project-site. The catchment area has its highest point at 954 m above sea level in the North-West, which is also the water divide between the Azraq Basin in the East and the Dead Sea basin in the West. The three dams constructed by the Faculty of Agriculture as part of Muwaqar project are about 760 m above sea level [Salameh, and Wirth, 1989].

The catchment area has a dense drainage pattern of small tributary wadis with normally gentle sloping hills of less than 5 percent in between. The soil is normally uncovered except for some small bushes. Part of the catchment area is ploughed every year, but the crop can not develop full ripeness in normal years and grazing takes place in the spring. Roads, housing areas, and some small dwellings scattered over the whole Muwaqar watershed cover less than one percent of the catchment area. The paved road linking Amman with Azraq crosses the catchment areas with a length of approximately 10 km and a width of 15 m and may contribute a small measurable amount of surface water to the floods.

The soil type and the sparse vegetation cover allow a large portion of the precipitation water to flow as surface runoff towards the wadis, causing short intensive floods. The area is covered by limestones with thin intercalation of cherts. Both are highly fractured and are exposed at the bottom of the wadis.

The top layer of overburden consists mainly of silty-sand, sometimes mixed with gravel and boulders of limestone and chert. The thickness of the overburden reaches 1-2 m, but at steeper slopes it reaches only a few centimeters. Layers of gravel (limestones and

chert) within the silt occur mainly in the deeper portions of the wadi courses and are exposed at their concave flanks due to bank erosion.

The small dams are constructed without a core with materials from the surrounding area; they have a height of approximately 3 m above the wadi bed. The spillways have a width of about 10 m each and are made of concrete with the lowest point around 2 m above the wadi bed. Spillway surfaces are made of concrete which allows a rapid flow of water that can be measured easily by a float connected to an automatic recorder.

5.4 FIELD EXPERIMENTS AND MEASUREMENTS

Three small earth fill dams were constructed by the Faculty of Agriculture along wadi El-Maghayir, approximately 10 kms east of Muwaqar village, to impound flood waters and to store them for use during the dry season for irrigation purposes. These dams are designated by dam 1 lying upstream, dam 2 in the middle, and dam 3 lying downstream of dam 1 and dam 2 (Fig.(6.1)).

5.4.1 Dams Hydraulics

The water level in the reservoirs was measured using automatic recorder installed on these reservoirs. Dam 3 was measured against a fixed reference point using a hand-klinometer. The measurements started in December 1987 and continued into 1990.

During the dry season in 1987 the silt accumulated at the bottom of dams 1 and 3 was removed and both reservoirs were enlarged by removing part of the Quaternary deposits.

5.4.1.1 Dam 1

On December 12, 1987, the first dam was filled to the crest of the spillway, and no more water was received by it until December 20. During this time, the water level dropped by 1 m.

The average amount of evaporation measured in a standard pan-evaporation dish was 1.3 mm/day. According to the experience gained in Jordan, pan-evaporation is 1.25 to 1.3 of the actual evaporation from reservoirs (Salameh and Khawaj, 1984).

From December 12 to 20, 1987, the actual amount of evaporation would be 8 to 8.3 mm in 10 days. Related to the drop in the reservoir water level of 1 m, the amount of evaporation during December, January and even February, can be considered as negligible. The infiltration rate is calculated to be=14.4 x 10^{-5} cm/second.

During December 21 to 23, precipitation of the amounts of 2.5, 4 and 2.5 mm fell on the catchment area. This provided dam 1 with an amount of water which kept its level almost constant at a depth of 1 m, until December 25. After that the water level dropped from 1 m to 2.0 m during the time period December 25 to January 3, 1988, which means a drop of 100 cm in 9 days. The infiltration rate is calculated to be = 14.1 x 10^{-5} cm/second.

On Jan. 5, 1990, this dam was filled, 4 days later a drop in the water level of 10 cm was noticed. As mentioned earlier, evaporation during this time of the year is negligible (3.2 mm in 4 days). Hence, the infiltration rate is calculated to be 2.9 x 10^{-5} cm/s. After that this infiltration rate gradually decreases to 2.66 x 10^{-5} cm/s in the following few days. In the following weeks and until April 1990, the average infiltration rate reached a value of 1.2 x 10^{-5} cm/s, which coincides with the values obtained for the end of the rainy season from 1987 to 1989.

5.4.1.2 Dam 2

Dam 2 receives water which passes through dam 1 and small amounts from its local catchment area. Dam 2 water level dropped monotonously from December 9, as the dam was filled, to January 3rd. During this period of 25 days, a drop in water level of 0.75 m was measured. The amount of evaporation was around 25 mm. The infiltration rate is calculated to average = 3.35×10^{-5} cm/sec.

The infiltration rate of this reservoir bottom started with a value of 2.89×10^{-5} cm/s. The rate of infiltration decreased gradually to 2.8×10^{-5} cm/s within a few weeks and to 1.48×10^{-5} cm/s by the end of the season in April 1990.

During the year 1989, measurements were only possible until mid-February with the infiltration rate being as low as 2×10^{-5} cm/s; which coincides with the infiltrate rate at the same time period of 1987-1989. Hence, it can be expected that the infiltration rate at the end of the rainy season, 1989, would have been similar to that of 1990, (i.e., 1.4×10^{-5} cm/s).

5.4.1.3 Dam 3

Dam 3 showed the same pattern of water level decline as in the case of dam 2. The drop in water level was monotonous and equal to 2.25 m in 25 days. The average infiltration rate is calculated to be 10.14×10^{-5} cm/s which is 3 times the infiltration rate in dam 2 and 70% of that in dam 1.

As mentioned above, the silt accumulation in dams 1 and 3 was removed in the summer of 1987, which clearly illustrates the effects of siltation on the infiltration rates.

In the successive measurements on the three reservoirs, the time declined water levels in the three dams flatten with time. This indicates the effects of siltation on the

infiltration rate, although during these periods the evaporation rates gradually increase from 1mm/day in December and January to 7mm/day in May. Table (5.1) summarizes the information about the infiltration and evaporation obtained for the three dams during 1987-1990.

The drop in the infiltration rate in dam 1 from 14.2×10^{-5} cm/s in December 1987 to 6.98×10^{-5} cm/s in January and February 1988 and to 1.0×10^{-5} cm/s for the period from March to May 1988, clearly illustrates the importance of removing the silt accumulated at the reservoir bottoms in order to enhance infiltration.

For dam 1, the infiltration rate in May 1990, after silt accumulation is merely 7.4% of that in December 1989, where the silt was previously removed.

In the case of dam 2, the infiltration rate at the beginning of the season (December 1989) was 3.35×10^{-5} cm/s, which is three times that of dam 1 at the end of the season (May 1990). This clearly indicates that the silt accumulated during the summer in dam 2 has been exposed to strong drying and shrinking. This led to the formation of mud cracks, which, at the beginning of the rainy season 1989, led to higher infiltration rates than those prevailing at the end of the season in dam 1.

The accumulation of additional silt during 1990 in dam 2 lowered the infiltration rate from 3.35×10^{-5} cm/s in December 1989 to 1.078×10^{-5} cm/s in May 1990. The last figure is very close to that of dam 1 at the end of the season, May 1990. This would mean that the accumulated silt in one rainy season lowers the infiltration rate to a minimum which is considered as the limiting infiltration rate or the infiltration rate of silt itself.

Table (5.1): Infiltration and Evaporation Calculations For Dams 1, 2, and 3.

period	Time Period (days)			Average Evaporation cm/period				Drop in Water Level (cm)			Net Drop due Infiltration			Infiltration Rate (cm/Sec)x 10^{-5}		
Dam	1	2	3	mm/d	1	2	3	1	2	3	1	2	3	1	2	3
Dec. 87	9	25	25	1	0.8	2.6	2.6	100	72	2.25	99.17	72.4	222	14.2	3.35	10.1
Jan +Feb 88	5	8	11	1.6	0.8	1.3	1.8	31	17	62	-------	-------	60.0	6.98	2.26	6.33
Dec.88+ Jan.89	20	24	25	1	2	2.4	2.5	42	35	63	40	32.6	65	2.3	3.92	4.03
April + May 89	32	----	----	5.3	17	------	------	45	-------	-------	28	-------	-------	1.01	-------	-------
Jan. 90	----	20	----	1	------	2	------	-------	46	-------	-------	44	-------	-------	2.55	-------
Feb. 90	----	19	----	1.8	------	3.4	------	-------	37	-------	-------	33.53	-------	-------	2.01	-------
March 90	----	39	----	2.4	-----	9.3	-----	-----	73	-----	-----	63.4	-----	-----	1.30	-----
April 90	21	14	14	-----	-----	-----	-----	40	30	26	-----	-----	-----	1.30	1.74	1.82

In 1989, dam 1 starts with an infiltration rate of 2.3 x 10^{-5} cm/s during December and January. It decreases to 1.05 x 10^{-5} cm/s in February and March and further to 1.01 x 10^{-5} cm/s in April and May. This clearly illustrates that the limiting factor for the infiltration process is the accumulation of silt and the permeability of silt and not the underground rocks.

Dams 2 and 3 also show the same behavior; higher infiltration rates at the beginning of the rainy season asymptotically decreasing towards the end of the season to the infiltration rate of silt.

The higher rates at the beginning of the rainy season are caused by the higher secondary permeability of the silt as a result of drying and mud crack formation during the summer months.

The infiltration rate for reservoir 3 in 1990 started also with a value of 2.89 x 10^{-5} cm/s. In 1989, it started with a value of 3 x 10^{-5} cm/s, then the infiltration rate declined to an average value of 1.8 x 10^{-5} cm/s by the end of the season. Considering the infiltration rate values obtained in 1990 and comparing them for the three dams, the following can be concluded:

1. The infiltration rate at the beginning of the rainy season has a value of around 3 x 10^{-5} cm/s.

2. This infiltration rate decreases with time to values of 1.2 x 10^{-5}, 1.5 x 10^{-5} and 1.8 x 10^{-5} cm/s for dams 1, 2 and 3, respectively.

3. The relatively high infiltration rate at the beginning of the rainy season is the result of mud cracks which develop during the dry season.

4. The infiltration rates at the end of the rainy season reflect the permeability of the silt, which forms the limiting layer for infiltration. The infiltration rates of the gravel underlying the wadi bottom are, as indicated by the different tests, much higher than those after silt accumulation. During the experiments on basins, the infiltration rates at the beginning and end of the experiments ranged from 20×10^{-5} cm/s to 3×10^{-5} cm/s and 50×10^{-5} cm/s to 9×10^{-5} cm/s, respectively.

5. The increasing infiltration rate at the end of the season from dam 2 to dam 3 illustrates the effect of silt accumulation. Dam 1 receives most of the silt which precipitates at its bottom. Dam 2 receives only what flows over from dam 1, and dam 3 receives only what flows over from dam 2. This means that dam 3 water is the least silty and dam 2 is less silty than dam 1, which, as mentioned above, is reflected in their infiltration rates.

6. Seepage through the overburden around the three constructed earth dams was not observed downstream. This indicates that, the horizontal movement of the infiltrated water in the direction of the flow in the Wadi is negligible. In 1989, Salameh, and Wirth, based on their field observations, showed that the infiltrated water has seeped down through the silty-gravel layer to the B4-Aquifer, located 30 km to the east of Muwaqar. Also Agrar-and Hydrotechnik (1977), their field investigations support the former. This is due to the inclination of the soil strata and their altitude, which direct all seeping water to travel to the east to join the groundwater zone of Azraq aquifer 30 km away.

5.5 VOLUME OF INFILTRATION

Each dam was filled several times during every rainy season. The water collected during each filling either evaporated or infiltrated to the underground water or was pumped to be used for irrigation.

The amount of evaporated and infiltrated water depends on the surface areas of the reservoir lakes, therefore, depth-area curves, depth-volume lines were constructed for each dam (Figure 5.2, 5.3, and 5.4) {see Appendix A}.

The evaporation was measured in a standard evaporation pan. For the periods during which water was available in the dams the daily evaporation ranged from zero to 10 mm. During December, January and February, the amounts of average actual daily evaporation is less than 1 mm. In comparison to the average daily infiltration rate during the same months of 50-60 mm/day, the evaporation can be considered negligible.

The infiltration water amount during periods of water level decline in the reservoirs was measured as the difference in storage. From March onwards, the evaporation was subtracted from the same difference. During the periods where the dams were filled, (continuous inflow due to successive rain events) the infiltrated amounts were calculated using the infiltration rates obtained from the time-water level drop measurements carried out on the different dams.

The amounts of infiltration water in 1988 for dams 1, 2 and 3 was found to be 82,000, 25,770 and 59,800 m^3, respectively. The contributions of dams 1 and 3 were 3 and 2 times that of dam 2 because of silt removal during the previous summer of 1987.

The amounts of infiltration in 1990 for reservoirs 1, 2 and 3 was found to be 27,580, 21,800 and 23,000 m^3, respectively, with a total contribution to the underground of 72,680 m^3.

The decline in the infiltration amounts compared to those of 1989 for dams 1 and 3 are attributed to silt accumulation for the second year. However, dam 2 seems to have reached its optimal infiltration rate accounted for by the permeability of a relevant silt layer.

In 1989, the infiltrated amounts of water in the three dams were, somehow, compatible with the surface areas of their lakes; which are 16,042 m^2 , 12,377 m^2 and 14,817 m^2 for dams 1, 2 and 3, respectively.

5.6 FLOOD DATA

The three constructed dams lie, as mentioned earlier, successively along the same wadi within a distance of 1 km. The difference in the catchment areas of dams 1 and 2 does not exceed a few square kilometers, hence it is negligible for flood-rainfall evaluation of the total area of 70 km^2. Therefore, it is only necessary to measure the floods reaching one dam to elaborate on the runoff-precipitation ratios. Nevertheless, dams 1 and 2 were equipped with flood recorders.

The floods flowing through Wadi El-Maghayir were monitored during the rainy seasons of 1987 through 1990. In the first year, 1987, the dam bodies were several times partly destroyed due to the vehemence of floods and the improper construction of the dams. Therefore, the available data during this period proved to be unreliable.

The first flood of 1988/89 started on December 24, and ended on December 25. The amount of precipitation was 33 mm, or 2.05 MCM over the catchment, causing a total discharge of 302,560 m^3. The runoff-precipitation ratio was calculated to be 14.8%.

The second flood, on the 26 and 27 of December 1989, caused an amount of precipitation of 16 mm, equivalent to 1.02 MCM of water, resulted in a flood of 340,530 m^3 with a runoff-precipitation ratio of 33.3%. This is a high value compared to the first flood.

The third flood took place on the 21 and 22 of January 1990, was caused by an amount of precipitation of 24 mm, equivalent to 1.52 MCM of water. The runoff-precipitation ratio is 15.7%.

The fourth flood, on February 12 and 13, was the result of 16.0 mm of precipitation with a total amount of water of 1 MCM causing a runoff-precipitation ratio of 4.6%. During this rainy season, precipitation fell partly in the form of snow. The first flood, the last portion of the second flood and the fourth flood were mainly the result of snow precipitation. The runoff-precipitation ratios of snow events are relatively low. This can best be seen during the fourth flood which had a ratio of 4.5%.

The total amount of precipitation of which floods were measured in the rainy season 1988/89 was 120 mm. This precipitation on the catchment area produced a runoff amount of 950,000 m^3 over the spillway of the first dam and an infiltration of some 27,800 m^3. (Table (5.2))

The average yearly runoff-precipitation ratio is calculated to be 13.2%. The runoff-precipitation ratio of this rainy season was highly affected by snow precipitation. Since

Table (5.2): Runoff Precipitation Ratio For The Rainy Season 88-90.

Date	Amount of ppt (mm)	Discharge (m^3)	Storage to Fill Dam+ Infiltration	Amout of ppt Over the Cathment Area	Runoff ppt Ratio
24-26/12/88	33	$302x10^3$	$0.56x10^3$	$2.05x10^6$	14.8%
26-27/12/88	16.5	$340x10^3$	$0.53x10^3$	$1.02x10^6$	33%
21-22/1/89	24.5	$232x10^3$	$7.34x10^3$	$1.52x10^6$	15.7%
13.2.89	16.4	$40.9x10^3$	$4.85x10^3$	$1.00x10^6$	4.6%
12-19/2/90	17	$476x10^3$	----------	$1.24x10^6$	39.6%
12-14/3/90	23.4	$50.9x10^3$	----------	$1.64x10^6$	31%
2-3/4/90	14	$17.2x10^3$	----------	$0.98x10^6$	17%

snow accumulation allows the melting water to slowly infiltrate into the rocks resulting in lower surface runoffs.

5.6.1 Rainy Season 1989/1990

The first flood took place in the period from February 12 to February 19, but the rain giving rise to the flood commenced on February 14. The amount of precipitation was 17 mm with a total rainfall of 1.2 MCM resulting in the discharge of 475.000 m^3 of water. Hence the runoff-precipitation ratio is calculated to be 39.6% which is quite a high ratio indicating the intensity of precipitation event.

The second flood took place in the period from March 12 to 14 with a precipitation amount of 23.4 mm and a total water volume of 1.638 MCM, resulting in a discharge of 508,500 m^3 of water. The runoff-precipitation ratio was calculated to be 31%, which is less than that during the first flood.

The third flood took place in the period between April 1 and 3, with an amount of precipitation of 14 mm and a total water volume of 0.98 MCM, resulting in a discharge of 17,180 m^3 of water. The runoff-precipitation ratio was calculated to be 17%. This is the lowest ratio calculated for the three floods.

The decrease in the infiltration rate can be attributed, to the decrease in precipitation intensity, increase in temperature, and decrease in relative humidity of the air. The average air temperature and relative humidity in January and February has an average of 4.8 ^oC, 85%, whereas in April it reached 1.9 ^oC, 41.5%, respectively. This means that part of the precipitation falling during the higher temperature periods is immediately returned to the atmosphere by evaporation. During the cooler period it forms an overland flow resulting in higher runoff-precipitation ratios.

The average weighted runoff-precipitation ratio for 1990, taking into account all precipitation and runoff events, equals 22.3% Compared to average runoff precipitation ratios in Jordan of around 7%, indicating the importance of flood utilization in such areas, (Table (5.2)).

5.7 MUWAQAR SOIL HYDRAULIC RELATIONS

The soil hydraulic relations, namely, water effective saturation (Se), liquid saturation (Sw), and relative permeability (k_{rw}), were approximated by Cooley and Wesphal (1974) functions:

$$Se = 1 \qquad \text{for } \psi \geq \psi a \qquad (5.1)$$

$$Se = \frac{A}{A+(|\psi-\psi_a|)^b} \qquad \text{for } \psi \leq \psi a \qquad (5.2)$$

$$k_{rw}=(Se)^d \qquad (5.3)$$

where:

$$Se = \frac{(Sw-Swr)}{(1-Swr)} \qquad (5.4)$$

in which Se denotes the effective (normalized) saturation, ψ_a the air entry pressure, Swr the residual saturation, and A, b, and d, are empirical parameters. The values of these parameters are presented in Table (5.3a). The soil characteristics are presented in Table (5.3b).

TABLE (5.3a): Parameters Of Soil Relations At Muwaqar.

Material Type	A	b	d
Silt Sand	7.5	3.0	3.5

Silt Gravel	4.7	3.5	1.1
Silt Sand	7.5	3.0	3.5

5.3b): Soil Characteristics At Muwaqar.

Material Type	Saturated Hydraulic Conductivity K, m/day	Thickness B, m	Porosity n	Residual Saturation Swr
Silt Sand	7.31×10^{-3}	1.0	0.49	0.075
Silt Gravel	0.028	1.0	0.209	0.050
Silt Sand	7.31×10^{-3}	98.0	0.49	0.075

To obtain fairly realistic soil hydraulic relations at the Muwaqar project, it was necessary to obtain the above independent parameters. Of these parameters, the saturated moisture content is always available as it can be easily obtained experimentally. Also the residual moisture content may be measured experimentally, for example by determining the moisture content of a very dry soil. Unfortunately, the residual moisture content measurements are not always made routinely, and hence have to be estimated by extrapolating existing soil moisture retention data. In this study, the residual moisture content is defined as the moisture content for which the gradient of the moisture content-pressure becomes zero (excluding the region near the saturated moisture content which has also has a zero gradient). Also, the hydraulic conductivity will approach zero when the moisture content approaches the residual moisture content. From a practical point of view it seems sufficient to define the residual moisture content at some large negative value of the pressure head, e.g., at -10^{-6} cm.

The relationship of liquid saturation to pressure head is affected by pore size distribution of porous media, and it was shown that, based on the analysis of many different types of soil samples, the value of exponent b almost always lies between 2 and 4 (Brooks and Corey, 1966). A curve-fitting analysis was used to determine the values of the parameters presented in Table (5.3a).

CHAPTER VI
MODEL APPLICATION TO FIELD CASE PROBLEMS

6.1 OPERATION PERIOD SELECTION

In the present chapter, application of the recharge optimization model to a wadi-reservoir system at the Muwaqar area will be carried out. In addition to the three existing reservoir system in the Muwaqar area, the model will be applied to a proposed system of two reservoirs to be built at RED 30 and RED 40 (Fig. 6.1) {see Appendix B}. To obtain the optimal conditions of the proposed and the existing reservoirs, a comprehensive evaluation of the present three reservoirs and the proposed two reservoirs conditions is required. A schematic layout of the Muwaqar optimization reservoir layout is shown in Fig. (6.2) {see Appendix B}. The three existing reservoirs are shown in solid line triangles and the two planned ones are shown in dashed line triangles. As far as the optimization process is concerned, the problem at hand has the dimension of NT, in which N represents the number of reservoirs involved, and T is the operation period. An incremental dynamic programming study will be carried out for a time period of 7 months, representing the rainy season using two time increment scenarios. The first scenario is on a monthly basis, where as the second scenario on a weekly basis. The rainy season at Muwaqar begins in November and ends in May each year.

The choice of a 7-month study period rather than a year-round one, is based on a storage-yield study using linear programming techniques. The linear programming study was first carried out for a year-round period, then for 7 months over the rainy season. For the storage-yield evaluation, average monthly evaporation and infiltration rates were used. The irrigation demands were calculated using Eq. (2.6) based on a 10-hectars irrigated lot for two crops (wheat and barley), as practiced in the Muwaqar project.

The formulation of the linear programming for the 12/7 month periods is as follows:

The objective function for optimizing reservoir storage-yield is:

$$H = \text{Max}(W - \text{å}S) \tag{6.1}$$

Subject to:

$$S_{t+1} = S_t + INFW_t - EVAP_t - Ut - INFL_t - \alpha_t W \tag{6.2}$$

$S_1 = S_{13}$ ($S_1 = S_8$)/based on rainy season

$S_2 \leq S_{max}$

.

.

.

$S_7 / S_{12} \leq S_{max}$

where:

S_t: reservoir volume at the beginning of the month (m^3)

S_{t+1}: reservoir volume at the end of the month (m^3)

$INFW_t$: inflow into the reservoir (m^3)

$INFL_t$: infiltration volume (m^3)

$EVAP_t$: evaporation volume (m^3)

U_t: reservoir release (m^3)

W: total yield (m^3)

α_t: water monthly use coefficient (related to each crop)

å: penalty coefficient =0.001-0.007.

The initial storage in the reservoirs in the first period is represented by S_1, which is also used as the final storages S_{13}/S_8, for carryover into the next year of operation. Therefore, the constraint of $S_1 = S_{13}$ (S_8) is a necessary requirement so as to have a closed loop. The rest of the constraints, S_2, ..., S_{12} (S_7), were set to the maximum reservoir storage capacity which is in this case is set to 32,000 m^3. This is because the main objective is to maximize the storage-yield of the reservoirs over the period of interest.

Using the above linear programming formulations, the year-round yield was found to be about 30,000 m^3 for the three reservoirs, which corresponds to the max reservoir capacity. This small yield is due to the absence of rainfall during the summer time in the Muwaqar watershed. In addition, during this period, the water evaporation from the reservoirs is very high.

On the other hand, the 7-month reservoir yield was found to be 170,000 m^3. This value is somewhat closer to the value obtained in the year around yield after field observation. Therefore, the 7 month period was used to carry out the incremental dynamic programming model. Nontheless, the Muwaqar project is being operated for the rainy season, that is for a 7-month period. For the rest of the year activities are halted and the reservoirs are prepared for the coming season. This preperation includes the removal of the silt that accumulated during the winter season in order to increase the infiltration capacity for the coming year.

6.2 APPLICATION OF THE MODEL TO THE MUWAQAR PROJECT

Having selected the 7-month period as the operational basis, the overall incremental dynamic programming optimization procedure was formulated. In order to apply the model to the Muwaqar project, the optimization model requires a set of data which consists of the surface inflows, evaporation and infiltration rates. In order to obtain the surface inflow

data, the Muwaqar watershed was subdivided into a number of subbasin based on Geographic and Geological data (Fig. 6.1). The estimated wadi inflows, assuming a uniform precepitation rate over each subbasin, have been determined by kinematic wave wadi routing. In determining subbasin runoff by the kinematic wave method, three conceptual elements are used: flow planes, collector channels, and a main channel. The kinematic wave routing technique transforms rainfall excess into subbasin outflow to the main wadi that interconnects the whole watershed.

Other data required for the optimization model include physical characteristics of the Muwaqar reservoir system such as irrigation demands, infiltration and evaporation rates, guess of initial conditions and mathematical definitions of the recharge objective function and its constraints. The Muwaqar reservoir system characteristics data required by the optimization model include the upper and lower bounds on reservoir storages and releases. These are disscussed later in this chapter.

In order to carry out the optimization procedure, the surface reservoir geometry must be evaluated. Two components are of interest: 1) reservoir storage capacity, and 2) reservoir surface area. These two geometric components are defined from topographic maps and surveying data. The surface reservoir content is then described as a function of the reservoir water head measured for a given reference point. In this work, the surface area of the reservoir pool function was derived from elevation-area-storage curves of each reservoir as explained in Chapter 5, {see Figure 5.2, 5.3, and 5.4, Appendix A}. An exponential curve fitting procedure was used to convert these data into mathematical equations as follows:

$$\text{For reservoir No.1} \quad A=\frac{\log_{10}(S_t)-\log_{10}(1933.1)}{0.00006738} \tag{6.5}$$

For reservoir No.2 $$A=\frac{\log_{10}(S_t)-\log_{10}(989.51)}{0.000011265} \quad (6.6)$$

For reservoir No.3 $$A=\frac{\log_{10}(S_t)-\log_{10}(1594.2)}{0.000070403} \quad (6.7)$$

where; A= reservoir surface area; and S_t = reservoir storage at time t. These storage-surface area relationships are necessary to evaluate the evaporation volume for the period of optimization. The average area between two time steps was used in the calculations of the evaporation losses. The evaporation rate and the infiltration rate were measured at the field by evaporation pan and infiltrometer, respectively.

Since the water depth in the full reservoir is about 2m and the reservoir is of a regular shape, the projection of the surface area can be approximated to be the same as the surface area itself. Also, since the depth to the water table is large compared to the depth of water in the reservoir, the downward movement of the infiltrated water results from gravitational driving force only. These were necessary to identify the system under the general conditions.

The recharge objective function at hand requires the specification of the constraints set to complete the formulation of the optimization problem. For the Muwagar reservoir system, these constraints comprise state-dynamics equations and physical bounds on variables. They are therefore identical to the standard problem formulation described by Eqs. (2.1) to (2.4).

6.3 RAINFALL-RUNOFF SIMULATION

The section describes the simulation of the rainfall-runoff process as it occurs in the El-Maghayer Wadi basin. The components function of the model is based on simple

mathematical relationships intended to represent individual meteorological, hydrologic and hydraulic processes which comprise the precipitation-runoff process. These processes are separated into precipitation, interception/infiltration, transformation of precipitation excess to subbasin outflow, and flood hydrograph routing. In order to calibrate the surface simulation component, the subsequent sections discuss two different rainfall-runoff simulation cases. The first rainfall event has been simulated using the precipitation hyetograph shown in Fig. (6.3) {see appendix B}. This figure represents a rainfall event that took place on the 21st-22nd of January, 1990. The rainfall event started with a moderate intensity, then it intensified on the 5th hour and reached a maximum rate of precipitation of 4.5 mm/hr on the 14th hour. The rainfall had a very low intensity on the 19-21st hr, but increased on the 22nd and 23rd hour. This precipitation hyetograph was used as the input for the runoff calculations. The specified precipitation is assumed to be a basin average (i.e., uniformly distributed over the basin).

Fig. (6.4) {see Appendix B} shows the computed hydrograph, resulting from the simulation along with the observed hydrograph that was calculated using field data at dam 1. In Fig. (6.4), two flow peaks are present, the first is on the 23rd hour, and the second is on the 11th hour on the 23rd day of January, 1990. The first peak has an almost symmetrical bell shape. The two peaks represent the discharge flow at reservoir No. 1. Fig. (6.4) also shows a good agreement between the observed and computed hydrographs, for instance, the observed peak flow is 466 ft^3/s (13.2 m^3/s), where the computed peak flow was 472 ft^3/s (13.3 m^3/s), with a difference of 6 ft^3/s (0.17 m^3/s), and a 1.3 percent error. The present small discrepancy between the observed and the computed discharge flow is mostly due to the approximate nature of the field measurements. The basin schematic diagram of the simulation components is presented in Fig.(6.5) {see Appendix B}.

Table (6.1) shows a runoff summary, which gives the subbasin areas in square miles, station names, peak flow for each station, and an average flow for maximum operation for 6, 24, 72-hrs. This table also gives details of the routing process along the wadi. Five analysis stations are reported, RED 10, RED 20, RED 30, RED 40, and RED 50. The flow at RED 10 represents the combined flow of subbasin RED RI and RED RF, then the flow is routed through reach 10TO20 where it is combined at RED 20 with the discharges of RED RJ, RED RH, and RED RN subbasins. The discharge is routed through reach 20TO30 to RED 30, then through reach 30TO40 and 40TO50, and final discharge is calculated at reservoir No.1.

The second simulation represents a case of a rainfall-runoff and a routing of the flow at the spillway of dam 2 through dam 1. Fig. (6.6) {see Appendix B} depicts the hyetograph which was used as an input for the runoff calculations. The precipitation hyetograph represents a rainfall event that took place on the 24th-27th of February, 1990. The rainfall event started with a moderate intensity of about 2 mm/hr. However, some intensity fluctuations were present around the 14th-22nd, with the maximum intensity of up to 3.0 mm/hr on the 16th. From the 4th hour of the 27th, the rainfall intensity was weak till the 22nd hour, however, on the 22nd hour the intensity was at the maximum. This represents the erratic nature of rainfall at the Muwaqar site. The maximum rainfall intensity of 5.5 mm/hr took place on the 22nd hour of the 27th. of February, 1990. The basin schematic diagram of the simulation components is presented in Fig. (6.7) {see Appendix B}. The computed hydrograph is compared with the observed hydrograph in Fig. (6.8) {see Appendix B}. These hydrographs represent the overflow over the spillway of dam 2. Two peaks are present in Fig. (6.8) with the maximum on the 18th hour. The two peaks are not of a uniform bell shape as was the case in the first event. This is due to the erratic nature of the rainfall event at hand. From Fig. (6.8), a good agreement is observed, and it is clear that the calculated peak flow obtained is about 1025 ft^3/s (29 m^3/s), where, the

observed peak flow is about 1010 ft^3/s (28 m^3/s), with a difference of 15 ft^3/s (1 m^3/s), and an error percentage of 1.5%.

Table (6.2) presents a runoff summary of the second rainfall event. The table gives the basin areas in square miles, station names, peak flow in cubic feet per second, an average flow for maximum operation at 6, 24, and 72-hrs. The peak flow in each of the subbasins is higher than those in the first simulation run. Also the average flow for maximum operation is also higher than those reported in Table (6.1). This is due to the higher intensity in the second simulation run. The peak flow of RED RI and RED RF is combined at the analysis point RED 10. Then the combined flow is routed through reach 10TO20. Three subbasins (RED RJ, RED RH, and RED RN), along with the routed peak flow of RED RI and RED RF are combined at the analysis point RED 20. The combined flow was then routed through reach 20TO30, which was combined with the peak flow of RED RL and RED RM at the analysis point RED 30. At reservoir No. 1 the peak flow is the combined flow at the analysis point RED 40, which is routed through reach 40TO50. The peak flow discharge at reservoir No.2 is the combined flow of reservoir No.1 and subbasin RED 50.

TABLE (6.1) RUNOFF SUMMARY OF THE FLOW AT DAM1 ON 21st-22nd OF JANUARY 1990 (flow in cubic meter per hr.)

BASIN AREA Sq. Km	*STATION*	*PEAK FLOW*	*AVERAGE FLOW FOR MAX. OPERATION*		
			6 - hr	24 - hr	72 - hr
1.68	RED RI	0.65	0.34	0.17	0.17
1.97	RED RF	0.76	0.37	0.2	0.2
2 COMBINED	RED 10	1.39	0.7	0.34	0.34
ROUTED TO	10 TO 20	1.25	0.65	0.31	0.31
1.86	RED RJ	0.935	0.48	0.23	0.23
0.98	RED RH	0.6	0.31	0.14	0.14
1.89	RED RN	0.74	0.34	0.2	0.2
4 COMBINED	RED 20	3.45	1.67	0.877	0.877
ROUTED TO	20 TO 30	3.1	1.47	0.85	0.85
1.92	RED RL	0.96	0.45	0.25	0.25
5.0	RED RM	2.5	1.3	0.62	0.62
3 COMBINED	RED 30	6.43	3.34	1.6	1.6
ROUTED TO	30 TO 40	5.8	3.0	1.44	1.44
6.76	RED RQ	3.37	1.73	0.85	0.85
2 COMBINED	RED 40	8.97	4.67	2.26	2.26
ROUTED TO	40 TO 50	8.07	3.88	1.84	1.84
UNIT HYD	E.DAM1	13.36	6.5	3.3	3.3
2.5	RED 50	1.5	0.76	0.37	0.37
3 COMBINED	RED 50	14.58	7.3	3.6	3.6

TABLE (6.2) RUNOFF SUMMARY OF THE FLOW AT DAM 2 ON THE 24th-27th OF FEBRUARY 1990 (flow in cubic meter per hr.)

BASIN AREA sq. Km	*STATION*	*PEAK FLOW*	*AVERAGE FLOW FOR MAX. OPERATION*		
			6-hr	24-hr	72-hr
1.68	RED RI	1.53	0.76	0.45	0.45
1.97	RED RF	1.784	0.87	0.51	0.45
2 COMBINED	RED 10	3.3	1.67	0.85	0.85
ROUTED TO	10 TO 20	2.26	1.076	0.566	0.566
1.86	RED RJ	1.73	0.85	0.81	0.81
0.98	RED RH	0.96	0.48	0.28	0.28
1.89	RED RN	1.7	1.02	0.68	0.68
4 COMBINED	RED 20	6.5	3.2	1.56	1.56
ROUTED TO	20 TO 30	4.47	2.24	1.104	1.104
1.92	RED RL	1.755	0.85	0.48	0.48
5.0	RED RM	4.6	2.32	1.161	1.161
3 COMBINED	RED 30	10.6	5.24	2.66	2.66
ROUTED TO	30 TO40	7.45	3.68	1.87	1.87
6.76	RED RQ	6.23	3.0	1.56	1.56
2 COMBINED	RED 40	13.36	6.6	3.34	3.34
ROUTED TO	40 TO 50	9.4	4.64	2.35	2.35
UNIT HYD	E.DAM1	15.7	8.18	3.2	3.2
2.5	RED 50	2.35	1.1	0.51	0.51
3 COMBINED	RED 50	16.7	8.55	3.74	3.74
UNIT HYD	E.DAM2	29	14	7.25	7.25

6.4 SUBSURFACE FLOW SIMULATIONS UNDER NON-OPTIMIZED CONDITIONS

6.4.1 One-Dimensional Simulations

6.4.1.1 Case Study: Cumulative Inflow Simulation Under Reservoir No.1

The purpose of this case study is to investigate the cumulative inflow rate due to infiltration from a reservoir at Muwaqar. Also, the water pressure and soil moisture content responses to the infiltration are investigated. Different infiltration rates under the reservoir are considered. The water level in the reservoir was considered a function of rainfall quantity, infiltration rates and evaporation from the pond behind the reservoir spillway. The infiltration was assumed uniform over the whole bottom area of the reservoir through the silty-gravel layer.

Since the flow system under consideration consists of a vertical flow and the data was presented in terms of depths rather than volumes, it is convenient to model only a 1 m strip at the flow system at the reservoir bottom. Because the soil utilized in the experiments was initially very dry, a very fine element spacing was utilized near the soil water interface at the bottom of the reservoir where the greatest hydraulic gradient is expected. Also, this was adopted in the vicinity of the groundwater table. The flow region was discretized into 100 nodes starting at the soil surface. The initial conditions of the transient flow were derived by performing a steady state analysis.

The first reservoir was considered since it is the first to be filled, the closest to the agriculture field, and is parallel to an irrigation pond which is located on the right side of the reservoir at about 100 m next to the field that is used for experimental agricultural practices. The water is usually pumped from the first reservoir to the pond. At a later stage

this water is used for irrigation purposes after the settlment of the suspended load. The bottom of the reservoir consists of a silty gravel layer 1 m deep, followed by a layer of silty-sand with its lower boundary at the water table which is found at 100 m below ground surface [Taimeh, 1989]. The high permeable silty-gravel layer might lead to convergence difficulties unless the numerical solution scheme is designed to accommodate not only abrupt changes in the gradients of the constitutive relations but also a wide range of values of effective conductivity. A graphical representation of the conceptual flow model is shown in Fig. (6.9) {see Appendix B}. The vertical flow occurs as a result of infiltration at the bottom of the reservoir.

For the conditions that prevail only at reservoir No.1 simulation was carried out using the following procedure: the simulation period were from December to May, (1990), and they usually started when the reservoir was full (the water depth behind the spillway is 2.0 m), and the simulations stopped when the reservoir was empty. The first simulation was carried out for a period of 24 days. Then, the second simulation run took 30 days, starting with a full reservoir and ending at the time when it is empty. The initial conditions of this simulation period were the final results of the first one. The third simulation run was carried out for a period of 60 days, with the initial conditions being the final results of the second run. The infiltration ratios were 0.122 m/day, 0.06 m/day, and 0.03 m/day, for the first, second, and third runs, respectively. The conditions of these runs are presented in Table (6.3). Also, presented in this table are the infiltration rates of the three runs (24, 54, and 114 days) under the reservoir.

Table (6.3): Infiltration Rates For Time Period Of 24, 54, And 114 Days:

RUN NUMBER	INFILTRATION AT RESERVOIR NO. 1
NO.1 (UP TO 24 DAYS)	RATE = 0.122 m/day
NO.2 (UP TO 54 DAYS)	RATE = 0.06 m/day

NO.3 (UP TO 114 DAYS)	RATE = 0.03 m/day

The pressure head at the bottom of the unsaturated flow system is equal to zero at all times, because the infiltrated water does not particularly reach the groundwater table found at 100 m below ground surface.

For the purposes of the simulation, it was assumed that the unsaturated flow system was initially in static equilibrium. The infiltration rate that was used in the computation was taken as an average rate .

Since the present code does not require a separate data file for mesh generation, the initial and the prescribed pressure heads were easily specified at the designed nodes in the flow field. The nodes were numbered sequentially from bottom to top. The total number of nodes simulated were 100. Nodes at bottom of the reservoir were assigned a prescribed pressure head which is equal to the depth of ponded water. An initial pressure head of ψ equal to the node height above a reference line taken as groundwater table was assigned to all nodes except for the nodes at the bottom of the reservoir since they were treated as initial and boundary conditions.

The simulation was initially executed for one day. Subsequent simulations up to a final time of 24, 54, and 114 days were performed using the restart feature. Three iterations per time step were enough to reach a full convergence to a head tolerance of 1×10^{-10} m.

As expected, the solution can be seen to have converged well in three iterations. The final results show that the effect of law permeability reduces the rate of change in the

pressure head value in the silty-sand layer. Also, the pressure head distribution is at the residual value at greater depths.

Local pore water pressure in excess of the given boundary pressure are created by water-flux boundary condition. At the bottom of the reservoir boundary, the pressure head is quite high so as to transfer the prescribed water flux into the calculation domain.

The treatment of variable conductivity, nonlinear source term, and a variety of boundary conditions are presented. With this background, it should be possible to apply the present simulation component to a large number of unsteady conduction problems.

The water pressure head distributions for the first run (t= 0, 6, 12, 18, and 24 days), the second run (t= 24, 30, 36, 48, and 54 days), and the third run (t= 54, 66, 78, 94, and 114 days), are presented in Fig. (6.10), Fig. (6.11), and Fig. (6.12) {all Fig.s are shown in Appendix B}, respectively. In these figures, the curve shown in a solid line represents the initial pressure head conditions of each run. For example, the solid curve in Fig. (6.10) at t=0 days represents the initial pressure head conditions of the first run. Also, the solid line in Fig. (6.10) at t=24 days represents the initial pressure head conditions of the second run, and so forth. The pressure head profile at t=54 days shown in Fig. (6.11) represents the initial pressure head conditions of the third run. The pressure head at the nodes located close to the reservoir wadi bottom interface are positive. Although the pressure head is increasing with time due to the infiltration, the pressure head decreases with depth through the silty-sand layer.

The moisture content distribution for t= 54, 66, 78, 94, and 114 days is presented in Fig. (6.13) {see Appendix B}. In this figure, full saturation occurs under the reservoir and the moisture content decreases in the silty-sand layer. The curves start with a gentle

slope in the silty-gravel layer. However, in the low permeability layer of silty-sand, the moisture content profiles have a sharp drop. These abrupt changes in the moisture content are accounted for effectively in this control volume approach. This proves the effectiveness of the control volume method. Also from Fig. (6.13), the wetting front depth under the reservoirs is about 12.72 m. This is an indication that immediate recharge to the underlaying aquifer is not present. This is due to two factors: the quantity of the available water is small to travel the 100 m below the ground surface to reach the groundwater table; and the low permeability of the silty sand layer does not allow fast percolation of the infiltrated water. Therefore, direct recharge by means of injection wells is an attractive solution if the aquifer recharge is an important issue to the planners of Muwaqar project. However, methods to effectively utilize the infiltrated water have to be sought to obtain optimal management and operation of the Muwaqar project.

Fig. (6.14) {see Appendix B} presents a comparison of the cumulative inflow determined by the numerical simulation and the cumulative inflow as measured in the field. The simulated cumulative inflow closely matches the measured data.

6.4.2 Two-Dimensional Simulations

In this simulations, two test cases have been performed. The first aims at obtaining a better understanding of the horizontal movement in the wadi flow direction of the infiltrated water. The second examines the seepage in the horizontal direction perpendicular to the flow in the wadi.

6.4.2.1 Case Study I: Flow Simulation Along The Muwaqar Wadi

This test case is to simulate the infiltration from the three reservoirs which are situated in the unsaturated zone well above the water table. These reservoirs are inter-connected with wadi El-Maghayer, which is the main artery for runoff from the 74 km^2

watershed. They constitute a source of water that infiltrates into the subsurface soil layer. The unsaturated flow region is composed of a highly permeable silty gravel layer to a depth of 1 meter at the wadi bed, followed by a layer of a low permeable silty sand up to the groundwater table which is located at a depth of 100 meters [Taimeh, 1989].

For the purpose of the computations, the entire unsaturated flow region is discretized into (60 x 40) node points. The flow field extends from the center line of the first reservoir to the center line of the third reservoir (Fig. 6.15) {see Appendix B}. This covers a total horizontal distance of 1000 m with a relatively negligible wadi bed slope (less than 1%).

Since a mixed-boundaries system is at hand (different infiltration rates in the three reservoirs and in the two wadi segments that connects them), it is convenient to draw first the control-volume boundaries and let the grid-points follow as a consequence. The grid points are located such that, six were laid at the bottom of the first reservoir, eighteen were laid on the first segment of the wadi bed, twelve were laid at the bottom of the second reservoir, eighteen grid-points were laid at the second segment of the wadi-soil interface, and six grid-points at the bottom of the third reservoir were formed. The grid-points at the bottom of the three reservoirs were considered as constant Neuman flux points and were assigned an average infiltration rate per run. The grid-points on the wadi-bottom were specified as infiltration or evaporation nodes.

Three simulation runs were conducted, with a time period of 24, 30, and 60 days, respectively. These runs represent rainfall events where floods over the spillways of the dams usually occur. All runs started with a full reservoir (initial water height of 2 m). The varying infiltration rates used in these computer runs are presented in Table (6.4a, 6.4b, 6.4c), respectively. These rates were obtained from field measurements.

Table(6.4a):Infiltration Rates For Time Period Of 24 Days:

TIME	Time≤10 days	Time>10 days
Reservoir # 1	0.122 m/day	0.122 m/day
Wadi Segment #1	0.022 m/day	-8.64D-03 m/day
Reservoir #2	0.029 m/day	0.029 m/day
Wadi Segment #2	0.014 m/day	-8.64D-03 m/day
Reservoir #3	0.087 m/day	0.087 m/day

6.4b) Infiltration Rates For Time Period Of 30 Days:

TIME	Time≤10 days	Time>10 days
Reservoir # 1	0.06 m/day	0.06 m/day
Wadi Segment #1	0.017 m/day	-0.0144 m/day
Reservoir #2	0.02 m/day	0.02 m/day
Wadi Segment #2	0.017 m/day	-0.0144 m/day
Reservoir #3	0.055 m/day	0.055 m/day

6.4c) Infiltration Rates For Time Period Of 60 Days:

TIME	Time≤10 days	Time>10 days
Reservoir # 1	0.03 m/day	0.03 m/day
Wadi Segment #1	0.014 m/day	-0.04 m/day
Reservoir #2	0.0195 m/day	0.0195 m/day
Wadi Segment #2	0.014 m/day	-0.04 m/day
Reservoir #3	0.03 m/day	0.03 m/day

In this case study, it is assumed that flow does not take place across the vertical boundaries along the left and right sides of the flow region. The pressure head at the bottom of the computation field at the water table is taken equal to zero. The pressure head at the bottom of the reservoirs is taken as equivalent to the height of water behind the dam.

The time step was set to a one day period. The total simulation period of the three runs was 114 days. Four iterations per time step were found to be enough to reach a full convergence to a head tolerance of $1x10^{-7}$m.

Fast convergence along with accurate results were obtained. Unlike the Explicit scheme and Crank-Nicolson scheme, the fully implicit scheme used in this code does not impose any restrictions neither on the size of mesh elements nor on the time step. It is unconditionally stable for any mesh element size as well as any time step, this simulation component can be used as a predictor of the moisture content redistribution in an actual field to optimize and manage an irrigation system.

The present component does not require a separate input data file. The input data is easy to change as necessary before and/or after the restart procedure. Each run consists of simulating the unsaturated flow subjected to the infiltration rate measured at the soil surface. The water level in the reservoirs was introduced as a function of the infiltration, evaporation, and pumping rates. Each run was terminated when the water head in the reservoir attains zero meter and the following run starts when the reservoirs is full again.

The water pressure head for the first, second, and third run is presented in Fig. (6.16), Fig. (6.17), Fig. (6.18), Fig. (6.19), Fig. (6.20), Fig. (6.21), Fig. (6.22), Fig. (6.23), Fig. (6.24), Fig. (6.25), Fig. (6.26), Fig. (6.27), and Fig. (6.28) respectively {all Figs. are shown in Appendix B}. These figures represent simulation results for t= 0, 8, 10

24, 26, 32, 34, 44, 54, 62, 74, 94, and 114 days, respectively. The pressure head decreases from a positive value at the bottom of the reservoirs to a negative value in the silty-sand layer. Below 8.31 m from ground surface (wadi bed) the pore water pressure gradient becomes insignificant. Under the wadi bed the pore water pressure increases during the period of infiltration ($t \leq 10$ days) with a rate of change higher near the reservoir than further away. However, the pressure head below the wadi bed starts to decrease ($t \geq 10$ days) due to evaporation as shown in Fig. (6.27) and Fig. (6.28).

The moisture content distribution at time of 54 and 114 days of simulation is presented in Fig. (6.29), and Fig. (6.30) {both Fig.s are shown in Appendix B}. It is shown that, the moisture content is at full saturation and then decreases until it reaches the residual moisture content in the silty-sand layer. However, no significant changes in the moisture content were observed below the wadi bed due to the unavailability of surface water (limited to the flood water) and the negligible horizontal movement of the infiltrated water. In addition, the high rate of evaporation, and high hydraulic conductivity of the soil induce low soil moisture holding capacity.

Also from Fig. (6.30), the wetting front depth under the reservoirs was about 8.31 m. Compared to an observed value of 3.9 m, a slight horizontal movement of the infiltrated waters in the direction of the wadi flow is computed. This can be easily deduced from Fig. (6.17), Fig. (6.18), Fig. (6.19), and Fig. (6.20), representing pressure head variations along the depth from the ground surface. These figures also show that the horizontal movement of infiltrated water is limited to the nodes on the wadi bottom that are close to the reservoirs, and it gradually vanishes as the infiltration ceases. Also, these figures indicate that there is no significant change in the pressure head at the nodes located away from the reservoirs. Field observations also show that, the infiltrated water completely vanishes as

early as mid June where high evaporation takes place due to hot temperatures in summer time, and dry weather conditions, [Salameh, and Wirth, 1989].

The depth of the wetting front was determined in the present simulations by comparing the moisture content at the individual nodes. It was located at the midpoint between two adjacent nodes with the lower node moisture content is practically unchanged.

6.4.2.2 Case Study II: Flow Simulation Perpendicular To The Muwaqar Wadi

The second case study was performed to investigate the horizontal movements of the infiltrated water. Field observations show that there is subsurface water movement transversal to the wadi [Salameh and Wirth (1989)]. These also show that the infiltrated water has seeped down into the silty-gravel layer, then horizontally under the ground surface. This horizontal movement is due to the inclination of the soil strata that directs all seeping waters to travel to the east to join the nearby aquifer around Azraq, 30 km from El-Maghayer wadi.

This case test deals with a two-dimensional simulation of unsteady flow in the unsaturated zone above the water table. The flow field encompasses the first reservoir and 50 m (the midpoint between the first reservoir and an irrigation pond) strip of bare soil. The water pumped from the first reservoir is used for irrigation purposes after the settling of the suspended load in a nearby pond. The right side of the reservoir is considered, since the inclination of the unsaturated subsurface strata is in that direction. The bottom of the reservoir consists of a silty gravel layer to a depth of 1 m, followed by a deep layer of silty-sand. The bare soil strip consists of silty-sand layer at the surface and extends over a depth of 2 m. A silty-gravel layer of 1m thickness is found below followed by a silty-sand layer down to the water table. The high permeable silty-gravel layer constitutes some difficulties

in the simulation process unless the numerical scheme is designed to accommodate abrupt changes in the gradients of the soil conductivity. The schematic description of this case study is shown in Fig. (6.31) {see Appendix B}.

Infiltration rates considered under the reservoir were different from those along the strip of land. Nodes at the strip were specified as infiltration nodes during the rainfall, and as evaporation nodes thereafter. The water level in the reservoir was a function of rainfall quantity, infiltration rates and evaporation.

For this case study, three stage simulation runs (24, 30, and 60 days) were performed. each run starting with a full reservoir of 2 m water height. The conditions of these runs are presented in Table (6.5).

Table (6.5): Infiltration Rates For Time Period Of 24, 54, And 114 Days:

RUN NUMBER	RESERVOIR NO. 1	BARE SOIL SURFACE
NO.1(UPTO 24 DAYS)	RATE= 0.122 m/day	RATE=0.005 m/day
NO.2(UPTO 54 DAYS)	RATE = 0.06 m/day	RATE= -1.5D-3 m/day
NO.3(UPTO114 DAYS)	RATE = 0.03 m/day	RATE= -8.5D-3 m/day

Since the subsurface unsaturated flow system can be taken as symmetrical about the center line of the wadi, the right boundary is taken as impermeable, and therefore it is possible to consider half of the flow system only. Also, the flow is not allowed to take place across the vertical boundary below the bottom of the reservoir along the left side of the flow region. The pressure head at the bottom of the unsaturated flow system is equal to zero at all times, because the infiltrated water does not particularly reach the groundwater table found at 100 m below ground surface.

For the purposes of the simulation, it was assumed that the unsaturated flow system was initially in static equilibrium. The infiltration rate that was used in the computation was taken as an average rate.

Nodes at the soil surface are specified either as infiltration nodes during rainfall or otherwise at rainfall cession. The nodes are numbered sequentially from the bottom of the flow field to the top and from left to right along individual transverse lines. A mesh of (60 x40 = 2400) nodes is used. Nodes at the bottom of the reservoir were assigned a prescribed pressure head equivalent to the depth of ponded water. An initial pressure head of ψ equal to the node height above a reference line taken as groundwater table, was assigned to all nodes except for the nodes at the soil surface and those at the bottom of the reservoir, since they were treated as initial and boundary conditions.

The simulation was first conducted for one day. Subsequent simulations of up to a final time of 24, 54, and 114 days were performed using the restart feature. Three iterations per time step were sufficient to reach a full convergence to a head tolerance of $1x10^{-7}$ m.

The fast convergence of this model demonstrates the effectiveness and accuracy of the implemented control-volume method. The mesh is designed in such away that no extra treatment is necessary for the near-boundary control volume; the available boundary-condition data, such as given pressure head ψ or water flux, are directly used at the corresponding boundary.

The water pressure head for t= 0, 2, 10, 24, 26, 34, 54, 56, 62, 74, 94, and 114 days are shown in Fig. (6.32), Fig. (6.33), Fig. (6.34), Fig.(6.35), Fig. (6.36), Fig. (6.37), Fig. (6.38), Fig. (6.39), Fig. (6.40), Fig. (6.41), Fig. (6.42), and Fig. (6.43), respectively {all Figs. are shown in Appendix B}. Under the reservoir, the pressure head

starts with positive value in the silty-gravel layer, and decreases until it becomes negative in the silty-sand layer. For the bare soil, the pressure head increases (due to infiltration) at the top nodes (close to the ground surface), and decreases through the top silty-sand layer. However, in the silty-gravel layer, the pressure head increases again due to the horizontal movement of the infiltrated water from the reservoir Fig. (6.43). The rate of increase in the pressure head value is relatively higher at the nodes closer to the reservoir. Also shown in these figures is the decrease in the pressure head in the lower silty-sand layer. The effect of evaporation on the pressure head at the soil surface is evident in Fig. (6.43) where the pressure head decreases.

The higher pressure head values correspond to the silty-gravel layer. Obviously, a large water flux enters the coarse material which has reasonably high hydraulic conductivity. The pressure head values decrease is in the direction of the fine silty sand layer. This can be explained on the basis of the hydraulic permeability field. The water flow resistance offered by the fine material in the silty sand layer reduces water flux across the flow surface. A lack of water flux reduces the local pressure head in that region.

An overall effect of the fine silty sand layer on the flow direction is to increase water flux into the silty gravel layer causing the water to travel horizontally along that layer.

The moisture content distribution for t= 54, and 114 days is presented in Fig. (6.44), and Fig. (6.45), respectively {both Fig.s are shown in Appendix B}. In these figures full saturation occurs under the reservoir and the moisture content decreases in the silty-sand layer. There are no significant changes in the moisture content at the bare soil surface due to the low permeability of the silty-sand layer. However, the moisture content increases in the silty-gravel layer due to the horizontal movement of the infiltrated water from the reservoir. The high permeabilty of this layer direct the infiltrated water to travel

horizontally rather than vertically as it is the case in unsaturated porous media. Also, in this test case irregularities are implemented along with time-varying boundary conditions.

Fig. (6.45) also shows, the vertical wetting front is about 4.0 m, in close agreement with field observations [Salameh, and Wirth]. The difference between the simulated and observed value is 0.1 m represents an error of 1 percent. It is reasonable to assume that this difference corresponds to the computed value in case study I. The horizontal wetting front reached a distance of 11.19 m from the reservoir through the silty gravel layer. Conversely to the simulation case study I, the water is not subjected to high evaporation because the upper silty sand layer is of very low permeability. Thus, it works as a cover and prevents the infiltrated water from evaporating or percolating in to the ground water table.

6.5 OPTIMIZATION OF SURFACE FLOW SUBSYSTEM

6.5.1 Optimization Of The Muwaqar Reservoir System

6.5.1.1 Case Study- Reservoir No. 1

This case study involves the evaluation of the actual situation that prevails at reservoir no. 1 at Muwaqar project, Fig. (6.1). As is required by incremental dynamic programming, an initial corridor width and splicing factor must be specified. The value of the initial reservoir storage (state variable) discretization interval DELSI, is set at 3000 m^3, and the final desired interval DELSF is set at 100 m^3. The splicing factor is set to 2.0 and the order of accuracy for reservoir release (control variable) increment DELU is set at 100 m^3. Discretization of the reservoir release (DELU) does not directly affect the computational procedure (Labbadie, 1988), and therefore is set to a small value (100 m^3). The above corridor width represents about 10% of the reservoir storage capacity, and was obtained

using Eq. (3.3). The termination criteria is that an all "interior" solution has been reached and that the corridor width has been spliced to 1.

These initial reservoir storages (state trajectories) are represented by the static storage policy which represents the reservoir dead storage value. Deterministic optimization over the rainy season was carried for two time increment scenarios. The first was conducted using monthly time increments. The monthly-based deterministic optimization solution results in a set of an "optimal" release (decision trajectories), and "optimal' storage policy, that if employed would produce the optimal recharge volume. These results are summarized in Table (6.6), which includes the monthly reservoir storage along with monthly corresponding optimal recharge volumes and reservoir releases. The mean optimum objective recharge value of 3593.715 m^3 is attained.

The optimal release and storage trajectories obtained are plotted in Fig.(6.46) {see Appendix C}. As it can be seen in the figure, the highest release occurs in the second month since the reservoir storage is not allowed to exceed the initial storage (state trajectories). However, the release thereafter starts to decrease towards the third month where it reaches a value of 20,000 m^3. Meanwhile, the storage at the same month reaches its maximum 32,000 m^3 and continues for the rest of the season. Also from Fig.(6.46), the value of the reservoir release on the fourth month starts to pick up until it reaches a value of 26,000 m^3 and the reservoir storage stays at the maximum value of 32,000 m^3. This is an indication that at the fourth month the inflow to the reservoir is higher than that of the third month. However, the release starts to decrease thereafter until it reach a 0 m^3 value at the end of the rainy season. Fig.(6.47) {see Appendix C} shows the highest optimal objective recharge function value is obtained at the third month. However, the optimal recharge value starts to decrease even though the reservoir is still at full storage conditions. This is due to the hydraulic properties of the soil, where usually at the beginning of recharge period

Table (6.6): Optimal Storage, Release, and Optimal Recharge Volume For Reservoir No.1.

Date 89-90 Season	Optimal Storage (m^3)	Optimal Release (m^3)	Optimal Recharge Volume (m^3)
November	4000	652.62	4351.002
December	9000	192914.4	8345.077
January	32000	101068.9	10781.56
February	32000	127403.7	4688.894
March	32000	26703.07	4688.894
April	32000	16363.63	4688.894
May	32000	498.182	3593.715

allows a large volume of water to infiltrate, and after some time the recharge rate will decrease. This decrease is also a function of the siltation deposition at the bottom of the reservoir which seals the soil voids.

A second scenario was carried out using weekly time increments for the same initial storage discretization values (state trajectories) reported in the case of monthly based time increments. Also, the same deterministic optimization procedure was used. Results of the weekly deterministic optimization procedure are shown at Fig.(6.48) {see Appendix C}. This figure shows the optimal reservoir storage and release policies. The behavior of the weekly reservoir release as well as storage is very close to that of monthly basis with minor fluctuations in the storage trajectories. More specifically, the reservoir reached full storage value at the fifth week, keeping the release at about 0 m^3. However, on the eighth week, reservoir storage dropped to about 26,000 m^3, then it start to fluctuate about full conditions on the 18th week whereafter the storage was steadily full to the end the season. On the other hand, the release reached it highest value at the eighth week, where the irrigation demand was minimal. Then, the release was fluctuating between zero and 15,000 m^3 from week number 11 to 14, then it goes to zero on the week number 22 and continues thereafter. The optimal recharge objective function value is presented in Fig.(6.49) {see Appendix C}, where it reaches a maximum value of 2,700 m^3 from week number 5 untill week number 12, then decreases on the thirteenth week to a value of 1,200 m^3 and stays steady untill week number 24 , where it decreases towards week number 25 to a value of 900 m^3, and it goes steady to the end of the season.

6.5.1.2 Case Study - Three Reservoirs

This case study deals with the reservoirs No. 1, No. 2, and No. 3, of the Muwagar reservoir system (Fig.(6.1)). The three reservoirs have been operational since 1985. They were built without control gates and are filled and emptied several times during the wet

(rainy) season. An optimization study is sought to obtain an operational policy that produces maximum infiltration. It is aimed at keeping the reservoirs full as much as possible while satisfying irrigation demands and taking into account evaporation losses. The initial storage discretization interval for the first reservoir was set to the value used in the previous analysis. An initial storage (state variables) discretization interval (DELSI) of 2000.00 m^3 was used for the second and third reservoirs, where the final desired storage discretization interval (DELSF) of 100.00 m^3 was used for both reservoirs. The splicing factor and the order of accuracy for release (control variables) DELU are the same as in the reservoir No. 1 problem. Also, as in the previous optimization problem, two time increments were adopted, the first was on a monthly basis, while the second was on a weekly basis for the whole winter season. The results of the monthly as well as weekly based time increments were obtained using the deterministic optimization procedure explained earlier.

Table (6.7) summarizes the monthly optimization results in terms of the optimal release trajectories for each of the three reservoirs along with the optimal recharge objective volume. Table (6.8) illustrates the monthly reservoir storage required to obtain the optimal recharge volume. The mean optimal recharge volume for the three reservoir-system of 9409.75 m^3 is obtained over the rainy season.

The monthly optimal release policy obtained is plotted in Fig. (6.50) {see Appendix C}. In this figure, reservoir No.2, since it is located between reservoir No. 1 and No. 3, has the highest release volume, so as to pass the water to reservoir No.3. The release from reservoirs No.1 and No. 3 are very close to each other. However, the maximum release volume was attained on the second month, which reached a volume of 74,000 m^3 for the second reservoir and 69,000 m^3 for the first and the third reservoir. The high release volume on this month is due to high inflow into the reservoirs where their capacity is much

Table (6.7): Optimal Storage and Optimal Recharge For The Three Reservoirs .

Date 89-90 Season	Optimal Storage Reservoir No.1 (m^3)	Optimal Storage Reservoir No.2 (m^3)	Optimal Storage Reservoir No.3 (m^3)	Optimal Recharge Volume (m^3)
November	4000.0	2000.0	2000.0	10049.49
December	29937.5	4312.5	2062.5	21427.94
January	30062.5	20062.5	28062.5	28000.97
February	30062.5	20062.5	28062.5	12177.6
March	30062.5	20062.5	28062.5	12182.24
April	30062.5	20062.5	28062.5	12177.6
May	30062.5	20062.5	28062.5	9409.745

Table (6.8): Optimal Releases Trajectories For The Three Reservoirs.

Date 89-90 Season	Optimal Release Reseervoir No.1 (m^3)	Optimal Release Reservoir No.2 (m^3)	Optimal Release Reservoir No.3 (m^3)
November	18279.47	10479.72	11.388
December	683790.4	733722.1	691469.9
January	349326.9	373343.3	350667.1
February	421532.2	454732.2	435262.9
March	106682.7	109532.2	96380.9
April	66895.36	69920.82	60764.18
May	16116.7	8691.575	1668.052

less than the inflow volume. Then on the third month, second reservoir release dropped to 37,500 m^3. At the same time, the first and the third reservoirs release reached a volume of 35,000 m^3. The lower release volume here is to keep the reservoir at full condition since the inflow in this month is less than that on the third month. However, on the fourth month an increase in the three reservoirs release is noticed, where the second reservoir release reached a value of 45,000 m^3. Thereafter, the release of the three reservoirs starts to drop until it reaches 0 m^3 at the end of the season. The above reservoirs release policy is to satisfy the overall objectives, mainly to obtain an optimal recharge volume.

Fig. (6.51) {see Appendix C} shows the optimal storage profile required for each reservoir to achieve an optimal recharge volume. As a response to the release policy obtained in Fig.(6.50), reservoir No. 2 storage profile did not reach full condition. Reservoir No. 2 maximum storage attained was 20,000 m^3 on the third month and continued at this level to the end of the season. However, the storage in reservoirs No.1 and 3, reached the maximum storage target with a volume of 30,000 m^3 for each of them. The monthly optimal recharge for the three reservoirs combined is shown in Fig. (6.52) {see Appendix C}, with the highest value obtained on the third month which has a low irrigation demand and minimal evaporation losses.

The weekly based analyses were carried out using the same initial storage discretization intervals DELS (state trajectories) as in the monthly based one, along with the same deterministic optimization procedure. In this analysis, the reservoir storages as well as the release policies were different from that on a monthly basis. For example, Fig.(6.53) {see Appendix C} shows the optimal storage policies for the three reservoirs. In this figure, the storage in reservoir No. 1 is fluctuates between a full storage in the weeks where inflow occurs and to less than that otherwise. For instance, up to the fourth week, the first reservoir storage did not exceed its initial storage volume, and instead decided to

pass the flow to reservoirs No. 2, and No. 3, where they reached the maximum target storage to the end of the season. However, the storage in reservoir No. 1 increased slightly in the fifth week, then dropped back to the initial storage the eighth week. The storage in this reservoir reached the maximum target storage on the weeks were most of the flow occurs which are, weeks 9, 12, 15, 18, 22, 26, and 28. On the other hand, the storage fell short of the target value in the weeks where there was no inflow into the reservoirs, such as weeks 8, 10, 11, 13, 16, 17, 19, 21, 23, 24, and 25. However, in these weeks, the storage increased as time was progressing towards the end of the season.

The optimal release policy for the three reservoirs is shown in Fig. (6.54) {see Appendix C}. The release from the first reservoir started on the fourth week with value of about 50000 m^3, then the release reached almost 690,000 m^3 on the seventh week in an effort to fill the two reservoirs that lay behind it. Then the release reached 0 m^3 on the eighth, and ninth weeks, since there was no inflow to the reservoir. On the tenth week however, the release reached up to 330,000 m^3 to pass the flow to the two reservoirs behind. After the thirteenth week, where the release from reservoir No. 1 was about 400,000 m^3 the release from this reservoir was equal to zero towards the end of the season. The other two reservoirs (reservoir No. 2, and No. 3), had similar release policies, where most of the time they released part of the inflows that was beyond their storage capacities, with the highest release occurs on the eighth, eleventh, and fourteenth, week. The optimal recharge profile is presented in Fig.(6.55) {see Appendix C}, where it has reached maximum value of 7100 m^3 on the twelfth week, then it dropped on the thirteenth week and then continue somehow uniform towards the end of the rainy season. This behavior is similar to that on the monthly basis.

6.5.1.3 Case Study - Five Reservoirs

In this case study, two additional proposed reservoirs were analyzed together with existing three reservoirs. These reservoirs were located upstream of the existing reservoir No. 1 at the Muwaqar project, more specifically at RED30 and RED40 (See Fig. (6.1)). Since the two proposed reservoir sites are close to the site of reservoir No. 1, the site specifications such as soil type, slope, geological formation and configuration of the reservoirs are taken to be similar to the existing reservoir No. 1. Hence, similar elevation-area-storage curves were adopted for the planned two reservoirs. Also, same initial storage discretization interval DELSI, and the final desired interval DELSF were chosen the same as the variables for reservoir No. 1. Thereafter, the deterministic optimization procedure can be applied to the five reservoir problems to optimize the recharge by providing release and storage policies.

Table (6.9) summarizes the results obtained which represent the optimal release policy for each of the five reservoirs. Table (6.10) illustrates the reservoirs storage required to obtain the optimal recharge profile. Table (6.11) show the optimal recharge objective values. The mean optimal recharge objective value for the five reservoir system is 12280.7 m^3. The optimal release policies obtained are plotted in Fig. (6.56) {see Appendix C}. In this figure, the release policy of the first reservoir was the lowest among all reservoirs. The behavior of its release policy was to achieve the target storage which is equivalent to a capacity at 32,000 m^3. Therefore, at the beginning of the optimization period, the release of the first reservoir was increasing gradually until it reached a maximum value of 250,000 m^3 towards the fourth month, then it started to decrease towards the end of the optimization period were it reaches 0 m^3. This behavior of the first reservoir release policy is to allow more water to be stored in the reservoir and to keep it at full condition. The other four reservoirs adopted a similar release policy, where the highest release was in the second month. Then, the release of the rest of reservoirs (No.2, No.3, No. 4, and No. 5) starts to

Table (6.9): Optimal Storage Trajectories For Five Reservoirs.

Date 89-90 Season	Optimal Storage Reservoir No.1 (m^3)	Optimal Storage Reservoir No.2 (m^3)	Optimal Storage Reservoir No.3 (m^3)	Optimal Storage Reservoir No.4 (m^3)	Optimal Storage Reservoir No.5 (m^3)
November	4000.0	4000.0	4000.0	2000.0	2000.0
December	4400.0	4400.0	4000.0	2400.0	4000.0
January	20000.0	7200.0	4000.0	2400.0	2000.0
February	30000.0	32000.0	6800.0	2800.0	2000.0
March	32000.0	32000.0	32000.0	32000.0	32000.0
April	32000.0	32000.0	32000.0	24000.0	20000.0
May	32000.0	32000.0	32000.0	32000.0	32000.0

Table (6.10): Optimal Release Trajectories For Five Reservoirs.

Date 89-90 Season	Optimal Storage Reservoir No.1 (m^3)	Optimal Storage Reservoir No.2 (m^3)	Optimal Storage Reservoir No.3 (m^3)	Optimal Storage Reservoir No.4 (m^3)	Optimal Storage Reservoir No.5 (m^3)
November	25207.52	28674.04	15596.2	10642.38	0.0
December	40691.4	583871.1	571215.1	641343.7	631522.7
January	199596.1	273230.9	254994.9	284709.2	272477.0
February	252818.1	340219.5	297016.4	301347.19	254349.6
March	61252.07	80877.14	67580.21	77976.19	97643.6
April	38180.63	50117.25	41297.88	35313.71	0.0
May	9420.356	8612.313	0.0	7678.072	0.0

Table(6.11): Optimal Recharge Volume of Five reservoirs.

Date	Optimal Recharge Volume (m^3)
November	12680.67
December	16900.98
January	22742.13
February	16868.07
March	19983.14
April	19975.91
May	16862.36

decrease towards the end of the optimization period, where it reaches 0.0 m^3. Fig. (6.57) {see Appendix C} shows the optimal storage required for each reservoir to achieve the optimal recharge value. As expected, the first reservoir has the highest storage values, where it starts to fill up from the second month until it reaches full condition in the fourth month and continues to be full untill the end of the optimization period. The other reservoirs for the first four months were not filled up which means that the solution of this case did not reach a global optimal solution. This is due to the curse of dimensionality problem of DP. The optimal monthly objective values for the five reservoirs are shown in Fig. (6.58) {see Appendix C}.The maximum objective recharge was obtained on the third month where it reach a value of 23,000 m^3.

The results above give the final values of reservoirs state of storage and release at the end of the optimization period T. These results were obtained under the condition that the reservoirs storage (state) at the beginning of the given time period were at initial assumed values of storage and release. It should be noted that the final reservoir state, never violate these conditions.

6.6 SIMULATION OF THE SUBSURFACE FLOW SUBSYSTEM UNDER OPTIMIZED CONDITIONS.

The following section deals with simulation of the unsaturated subsurface flow pattern at the Muwaqar project site based on the optimized reservoir control, and to a comparison of these results with those of the non-optimized conditions.

As reported in Chapter 5, the reservoirs are situated on a silty gravel layer 1 m deep, followed by a layer of silty-sand which extends to the water table found at 100 m below ground surface [Taimeh, 1989]. The high permeable silty-gravel layer could lead to convergence difficulties unless the numerical solution scheme is designed to accommodate

not only abrupt changes in the gradients of the constitutive relations but also a wide range of values of effective conductivity. The subsurface flow occurs due to infiltration at the bottom of the reservoir system.

The simulations period was from November (1989) to May (1990) under the optimized contitions. The reservoir storages are as shown on Fig. (6.53) through the simulation period of 210 days compared to 114 days under the present conditions. The infiltration ratio used in the simulation is based on the mean optimal recharge profile shown in Fig.(6.52).

The pressure head at the bottom of the unsaturated flow system is set equal to zero at all times, because the infiltrated water does not reach the ground water table found at 100 m below ground surface.

For the purposes of the simulation using the present code, it was assumed that the unsaturated flow system was initially in static equilibrium. Also, since the present code does not require a separate data file for mesh generation, the initial and the prescribed pressure heads were easily specified at the designed nodes in the flow field. The nodes were numbered sequentially from bottom to top. Nodes at the bottom of the reservoir were assigned a prescribed pressure head which is equal to the depth of imponded water. An initial pressure head of ψ equal to the node height above a reference line taken as ground water table was assigned to all nodes except for the nodes at the bottom of the reservoir since they were treated as initial and boundary conditions.

Local pore water pressure in excess of the given boundary pressure are created by water-flux boundary conditions. At the bottom of the reservoir boundary, the pressure head is quite high so as to transfer the prescribed water flux into the calculation domain.

6.6.1 Optimized Two-Dimensional Simulations

The following case is to examine the seepage in the horizontal direction perpendicular to the flow in the wadi based on the optimized conditions. The case of seepage along the wadi flow direction was not considered, since it was shown before that the amount of seepage in the wadi flow direction is not significant and subjected to a high evaporation rate due to high permeability of the gravel layer. Also, this was in agreement with the field observation of Salameh and Wirth, (1989). Therefore, this case deals primarily with a two-dimensional simulation of unsteady flow in the unsaturated zone above the water table perpendicular to the wadi flow. The flow field encompasses the first reservoir and a 50 m (the midpoint between the first reservoir and an irrigation pond) strip of bare soil. The right side of the reservoir is considered, since the subsurface flow is in that direction which has been demonstrated by field and numerical results. The bottom of the reservoir consists of silty gravel layer to a depth of 1 m, followed by a deep layer of silty-sand. The bare soil strip consists of silty-sand layer at the surface and extends over a depth of 2 m. A silty-gravel layer of 1m thickness is found below followed by silty-sand layer down to the water table. The schematic description of this case study is shown in Fig. (6.31).

Infiltration rates considered under the reservoir were different from those along the strip of land. Nodes at the strip were specified as infiltration nodes during the rainfall, and as evaporation nodes thereafter. The water level in the reservoir was a function of rainfall quantity, infiltration rates and evaporation, and was kept full during the simulation based on the optimization results.

Since the subsurface unsaturated flow system can be taken as symmetrical about the center line of the wadi, the right boundary is taken as impermeable, and therefore it is possible to consider half of the flow system only. Also, the flow is not allowed to take

place across the vertical boundary below the bottom of the reservoir along the left side of the flow region. The pressure head at the bottom of the unsaturated flow system is equal to zero at all times, because the infiltrated water does not particularly reach the ground water table found at 100 m below ground surface.

The nodes are numbered sequentially from the bottom of the flow field to the top and from left to right along individual transverse lines. A mesh of (60 x40 = 2400) nodes is used. Nodes at the bottom of the reservoir were assigned a prescribed pressure head equivalent to the depth of ponded water. An initial pressure head of ψ equal to the node height above a reference line taken as the ground water table, was assigned to all nodes except for the nodes at the soil surface and those at the bottom of the reservoir, since they were treated as initial and boundary conditions.

The simulation was first conducted for one day. Subsequent simulations up to a final time of 210 days were performed using the restart feature. Three iterations per time step were sufficient to reach a full convergence to a head tolerance of $1x10^{-7}$ m.

The fast convergence of this model demonstrates the effectiveness and accuracy of the implemented control-volume method. The mesh is designed in such away that no extra treatment is necessary for the near-boundary control volume; the available boundary-condition data, such as given pressure head y or water flux, are directly used at the corresponding boundary.

The water pressure head for t= 24, 54, 114 and 210 days are shown in Fig.(6.59), Fig.(6.60), Fig.(6.61), and Fig.(6.62), respectively (see Appendix C). Under the reservoir, the pressure head starts with positive value in the silty-gravel layer, and decreases until it becomes negative in the silty-sand layer. For the bare soil, the pressure

head increases (due to infiltration and the effect of the horizontal movement of the infiltrated water from the reservoir) at the top nodes (close to the ground surface). However, in the silty-gravel layer, the pressure head increases again due to the horizontal movement of the infiltrated water from the reservoir (Fig. (6.62)). The rate of increase in the pressure head value is relatively higher at the nodes closer to the reservoir. Also shown in these figures is the decrease in the pressure head in the lower silty-sand layer.

The higher pressure head values correspond to the silty-gravel layer. Obviously, a large water flux enters the coarse material which has reasonably high hydraulic conductivity. The pressure head values decrease in the direction of the fine silty sand layer. This can be explained on the basis of the hydraulic permeability field. The water flow resistance offered by the fine material in the silty sand layer reduces water flux across the flow surface. A lack of water flux reduces the local pressure head in that region.

An overall effect of the fine silty sand layer on the flow direction is to increase water flux into the silty gravel layer causing the water to travel horizontally along that layer.

6.7 COMPARISION OF SUBSURFACE FLOW SIMULATION RESULTS FOR OPTIMIZED AND NON-OPTIMIZED CONDITIONS

The results obtained under the present optimized case are compared with those obtained from simulating the actual field conditions in the following:

The moisture content distribution for t= 54, 114, and 210 days is presented in Fig. (6.63), Fig.(6.64), and Fig. (6.65), respectively {see Appendix C}. In these figures, full saturation occurs under the reservoir and the moisture content decreases in the silty-sand layer. There are no significant changes in the moisture content at the bare soil surface which is due to the low permeability of the silty-sand layer. However, the moisture content

increases in the silty-gravel layer due to the horizontal movement of the infiltrated water from the reservoir. The high permeability of this layer directs the infiltrated water to travel horizontally rather than vertically as it is the case in unsaturated porous media. Also, in this test case irregularities are implemented along with time-varying boundary conditions.

Fig. (6.64) also shows the vertical wetting front is about 4.48 m, whereunder the actual situation for the same time the value was 3.01 m. The difference between the simulated and observed value is 1.47 m, which is due to the availability of the flux from the full reservoir. The horizontal wetting front reached a distance of 17.84 m from the reservoir through the silty gravel layer. Under the actual simulated conditions, the horizontal wetting front reached a distance of 11.69 m with a difference of 6.15 m for the same simulation period of 54 days. For the simulated time of 114 days, and under the present optimized conditions, the horizontal wetting front reached a distance of 25.49 m, and the vertical wetting front was 6.05 m, whereas the previous simulation the horizontal wetting front was 17.19 m, with a difference of 8.3 m. At the final time of 210 days of simulation, the horizontal wetting front reaches a distance of 32.5 m. However, under the actual situation no water is available for infiltration due to the present management scheme.

The results clearly illustrate the capability of the optimization algorithm in identifying improved operation policies for increasing the output performance of the Muwaqar reservoir recharging system.

The preceding results confirm that, for a reasonably good prediction of the subsurface subsystem flow based on the optimized infiltration from the surface subsystem is achived with only few surface flow parameters must be estimated. Further, since the surface flow parameters (surface runoff, and evaporation and infiltration volumes) simulation is accurately reflect the field conditions, acceptance of this part for the

otimization recharge problem is justified. The use of the present methodology can be used for either the natural or modified conditons of the hydrologic system.

CHAPTER VII

CONCLUSIONS AND RECOMMENDATIONS

An optimization procedure employing incremental dynamic programming is presented for obtaining the optimal water recharge from a network of reservoirs in arid areas. The final solution yields the optimal releases and storages from the study reservoir network. The optimization procedure takes into account the evaporation losses while meeting the irrigation demands of two selected crops (wheat, and barley). The optimization was carried out for systems consisting of one, three, and five reservoirs over the rainy season. Since wadis are not gauged to provide records of flow, monthly as well as weekly inflows were generated using a watershed analysis. The analysis provided an assessment of flood wave movement through the dry wadi and the flood occurrence of rainfall events.

The objective function was formulated to give the maximum infiltration. The procedure employed produces more or less uniform infiltration by maximizing the minimum infiltration volume. That is, during drought periods, a "hedging rule" places a high penalty on large deficits rather on small ones. Its main function is to meet the demand (maximizing infiltration) during periods of critical flow. A generalized numerical infiltration simulation component based on the control-volume method was integrated into the optimization procedure for the simulation of ground water flow. It helps to evaluate the soil moisture redistribution and the horizontal and vertical wetting front corresponding to optimal conditions.

Field data were conducted in collaboration with the University of Jordan, Faculty of Agriculture and the Water and Environmental Research and Study Center. The experimental

field study included measurements of the infiltrated water, evaporation rate, flood analysis, and mapping of the soil types and their hydraulic properties.

The watershed analysis is based on hydrologic routing techniques with emphasis on arid or semi arid land. This analysis is used to simulate the surface runoff responses of an arid watershed to precipitation by representing the wadi basin as an interconnected system of hydrologic components. Each component models an aspect of the precipitation-runoff process within a portion of the watershed.

The computation of the event runoff hydrograph takes into account major loss rate components of land depression, evaporation, and base flow. Runoff hydrographs are routed by the wadi storage method. Reservoir routing is done using the spillway and low-level outlet conditions.

The overall optimization approach has a simulation process nested in the optimization procedure. This component is based on the control-volume method used to evaluate the soil moisture redistribution and the horizantal and vertical wetting fronts corresponding to optimal condition. The control-volume approach is a well suited method for the prediction of water flow that involves the imposition of physical conservation principles on finite control volumes in the computation domain. They are, therefore, amenable to easy physical interpretation, and their solutions satisfy global conservation requirements, even for a coarse grid.

Line-by-line iterative procedures along with the tri-diagonal matrix algorithm were used to solve the continuity equation. The iterative procedure employed uses under-relaxation to enhance the convergence of the solution for strongly nonlinear equations. A

material balance formulation was included in the model to ensure an overall mass balance after completing each time step. This method accounts for hysteresis in the water content-pressure head relation.

Theoretical and field tests have been performed to demonstrate the effectiveness of the control-volume approach. These cases show that the method is capable of accommodating large variations in the hydraulic conductivity as well as highly nonlinear soil moisture characteristics.

The computation procedure was applied to the Muwagar research project near Amman, Jordan. The study area consisted of a 74 km^2 watershed with three existing reservoirs and several irrigated research lots. The results obtained correspond to the optimal release and storage policies, for one, three reservoirs on a monthly as well as weekly basis, and for five reservoirs on a monthly basis only. The ground water simulation component was employed using the optimal recharge policies and the results show a substantial increase in the horizantal wetting front in comparison with the present situation.

The model can be applied to a wide range of applications. However, the following limitations should be taken into account prior to the applications of the model :

- The hydrologic simulations are limited to single storm due to the fact that provision is not made for soil moisture recovery during periods of no precipitation.
- Stream flow routings are performed by hydrologic routing methods and do not reflect the full St. Venant equations which are required for flat wadi slopes.
- The stepped boundary condition used in the subsurface flow model with the fine grid to represent a curved boundary seeks fairly good approximation. However, this might cause problems in matching the geometrical irregularities, which would be better represented by

using the practice of mixed elements as in the finite element method which is not possible under the present discretization scheme.

Problems involving ground water flow and solute transport in variably saturated porous media are of a great interest for environmental engineers. For instance, the use of agricultural fertilizers, pesticides, and the reuse of upgraded effluents of waste water for agricultural practices as well as for recharge, have large effects on ground water quality and supply. To predict the extent of the hazards posed by pollutants carried by infiltrated waters, it is necessary to investigate the processes that control the movement of these waters. Accurate prediction of the transient water flow in variably saturated soil is essential to the control of ground water contamination. The present formulations of the control volume simulation component at the present time do not address this problem. Therefore, it is recomended to extend the its formulations to account for contaminant transport in porous media.

Incremental dynamic programming was shown to acheive acurate results for the problem at hand where a maximum of five reservoirs has been optimized. However, for a system consisting more than five reservoirs, incremental dynamic programming would not achive the optimal solution due to DP dimensionality problem. Therefore, optimization techniques based on the optimal control theory would be an excelent alternative.

BIBLIOGRAPHY

1. Agar-Hydrotechnik, "Hydrogeology of Azraq Aquifer", Internal Report, Jordan Ministry of Water Supply and Irrigation, Amman, Jordan, 1977.

2. Al-Harithi, T., "Overpopulation and Water Demand in Jordan", First Conference of The Arab Scientists and Technologists Abroad, (ASTA), Amman, Jordan, 1992.

3. Ahlfeld, D. P., "Two-stage Ground Water Remediation Design", J. Water Resour. Plann. Manage., 116(4), 517-529, 1990.

4. Bellman R., "Dynamic Programming", Princeton University Press, Princeton NJ. U.S.A, 1957.

5. Brimberg, J., Oron, G., and Mehrez, A., "A Model for The Development of Marginal Water Sources in Arid Zones: The Case of the Negev Desert, Israel", J. Water Reseour. Res., 29(9) 3059-3067, 1993.

6. Brooks, R. H., and Cory, A. T., "Hydraulic Properties of Porous Media", Hydrol. Pap. 3, 27 pp., Color. Stat Univ., Fort Collins, 1964.

7. Buckingham, E., "Studies on The Movement of Soil Moisture", Bull. No. 38, U. S. Dept. Agriculture, 1907.

8. Carrigan, P.H. "Calibration of U.S. Geological Survey Rainfall-Runoff Model for Peak-Flow Synthesis-Natural Basins", U.S. Geological Survy Computer Report, U.S. Department of Commerce National Technical Information Service,1992.

9. Cellia, M. A., and Pinder, G. F., "Orthogonal Colloction and Alternating-Direction Procedures For Unsaturated Problems", Adv. Water Resour. Res., 10, 178-187, 1987.

10. Cellia, M. A., Bouloutas, E. T., and Zarba, R., "A General Mass-Conservative Numerical Solution for the Unsaturated Flow Equation", J. Water Reseour. Res., 26(7) 1483-1496, 1990.

11. Chang, L. C., Shoemaker, C., A., and Lui, P. L. F., "Optimal Time-varying Pumping Rates For Ground Water Remediation: Application of a Constrained Optimal Control Algorithm, J. Water Reseour. Res., 28(12) 3157-3174, 1992.

12. Cheng-Kang T., Toth, G., Oswald, G. E., and Mays, L., "Austin Detention Basin Optimization Model", J. Hydraulic Engineering, ASCE, 113(7), 1987.

13. Cooley, R. L., and Westphal, J. A., "An Evaluation of The Theory of Groundwater and River-Water Interchange, Winnemucca Reach of The Humboldt River", Nevada, Hydrologic Water Resources Publication, 19, 74 pp., Center For Water Resources Research, University of Nebraska, Reno, 1974.

14. Culver, T., B., and Shoemaker, C., A., "Optimal Control for Ground Water Remediation by Differential Dynamic Programming With Quasi-Newton Approximations", J. Water Reseour. Res., 29(4) 823-831, 1993.

15. Culver, T., B., and Shoemaker, C., A., " Dynamic Optimal Control of Ground Water Remediation With Flexible Management Periods", J. Water Reseour. Res., 28(3) 629-641, 1992.

16. Davis, L. A., and G. Segol, "Documentation and User's Guide: GS2 &GS3-Variably Saturated Flow and Mass Transport Models", Rep. NUREG/CR-3901, U.S. Nucl. Regul. Comm., Washington, D. C., 1985.

17. David, P., Smith, Jr., and Bedient, P. B., "Detention Storage For Urban Flood Control", J. Water Resou. Plann. and Manag. ASCE., 1980.

18. Doorenbos J, and W. O. Pruitt, "Guidelines For Predicting Crop Water Requirements" Food and Agriculture Organization of The United Nations, Rome, Italy, 1984.

19. Duan, Q., Sorooshian, S., and Gupta, V., "Effective and Efficient Global Optimization For Conceptual Rainfall-Runoff Models", J. Water Reseour. Res., 28(4), 1015-1031, 1992.

20. El-Kadi, A. I., and Ling, GE., "The Courant Peclet Number Criteria For the Numerical Solution of The Richards Equations", J. Water Resour. Res., 29(10) 3485-3494, 1993.

21. Elzeftawy, A. and Cartwright, K., "Undisturbed Core Method For Determining And Evaluating The Hydraulic Conductivity of Unsaturated Sediments", Rep. UILU-WRC-83-0177, 49 PP., Ill. State Geol. Surv., Springfield, 1983.

22. Friedrich Ebert Stiftung, "Jordan Water Resources and Their Future Potential", Proceedings of The Symposium, Amman, Jordan, 1991.

23. Frind, E. O., and M. J. Verge, "Three-Dimensional Modelling of Groundwater Flow Systems", Water Resour. Res., 14(5), 844-856, 1978.

24. Fontane D. G.," Comprehensive Reservoirs Sitting And Sizing Optimization Model, Program Screen", Presented at The Computer Assisted River Basin With Water Management Seminar And Work Shop, Department of Civil Engineering, Colorado State University Fort Collins, Colorado, U.S.A., 1982.

25. Freeze, R. A., "The Mechanism of Natural Groundwater Recharge and Discharge", 1. One-dimensional, Vertical, Unsteady, Unsaturated Flow Above a Recharging or Discharging Ground Water Flow System", Water Resour. Res., 5(1), 153-171, 1969.

26. Freeze, R. A., "Three-dimensional Transient Saturated-Unsaturated Flow in a Groundwater basin", Water Resour. Res., 7(2), 347-366, 1971.

27. Fujioka, Y., and T. Kitamura, "Approximate Solution to a Vertical Drainage Problem", J. Geophys. Res., 69(24), 5249-5255, 1964.

28. Gottardi, G., Venutelli, M., "Moving Finite Element Model For One-Dimensional Infiltration in Unsaturated Soil", Water Resour. Res., 28(12), 3259-3267, 1992.

29. Hall, W. A., Tauxe, G. W., and Yeh, W-G.," An Alternative Procedure For The Optimization of Operations For Planning Multiple-River, Multiple Purpose Systems," Water Resour. Res., 20(8), 1099-1115, 1984.

30. Hanks, R. J., Klute, A., and Bresler, E., "A Numeric Method For Estimating Infiltration, Redistribution, Drainge and Evaporation of Water From Soil". Water Resources Res., 5: 1064-1069, 1969.

31. Haverkamp, R., Vauclin, M., Touma, J., Wierenga, P., and Vachaud, G. "Comparison of Numerical Simulation Models For One-Dimensional Infiltration", Soil Sci. Soc. Am. J., 41, 285-294, 1977.

32. Heidari, M., Chow, P. V., Kokotovic, and Meredith, D. D., "Discrete Differential Dynamic Programming Approach to Water Resources Systems Optimization", Water Resour. Res., 7(2), 273-282, 1971.

33. Hornberger, G. M., "Irwin Remson, Numeric Studies of Composit Soil Moisture Groundwater System", Water Resour. Res., 5(4), 797-802, 1970

34. Hubbert, M.K., "The Theory Of Groundwater Motion", Jour. Geol., 48, part 1, 785-944, 1940.

35. Huyakorn, P. S., and Thomas, S. D., "Techniques For Making Finite-Elements Competitive in Modelling Flow in Variably Saturated Porous Media", Water Resour. Res., 20(8), 1099-1115, 1984.

36. Huyakorn, P. S., and Springer, E, "A Three-Dimensional Finite Element Model For Simulating Water Flow in Variably Saturated Porous Media", Water Resour. Res., 5(6), 1367-1372, 1969.

37. Huisman, B., and T. N. Olsthroon, "Artificial Groundwater Recharge", Pitman books Limited, London, 1983.

38. Jacoby and Lanucks, "Combined Use of Optimization and Simulation Models in River Basin Planning", Water Resources Research, Vol. 8, No. 6, Pages 1401-1414, 1972.

39. Karatzas, G. P., and Pinder, G. F.," Ground Water Management Using Numerical Simulation and Outer Approximation Method For Global Optimization", J. Water Reseour. Res., 29(10) 3371-3378, 1993.

40. Kirkland, M. R., Hills, R. G., and Wierenga, P. J., "Algorithms For Solving Richards Equation For Variably Saturated Soils", Water Resour. Res., 28(8), 2049-2058, 1992.

41. Kincaid, C. T., and Morey, J. R., "Geohydrochemical Models For Solute Migration, Preliminary Evaluation Of Selected Computer Codes", Tech. Rep. EPRIEA-3417, Electr. Power Res. Inst., Palo Alto, Calif., 1984.

42. Lareson, R. E., "State Incremental Dynamic Programming", Elsevier, New York, 1968.

43. Labadie, J., "Dynamic Programming With the Microcomputer, Program CSUDP", Water Resources Planning And Management Program, Department of Civil Engineering, Colorado State University Fort Collins, Colorado, U.S.A., 1990.

44. Labadie , J. W., Hiew, K., Vitasovic, Z., Swarner, and E. Seeper,"Optimal Use of In-System Storage For Real-Time Urban Storm water Control." Proceedings of the U.S. -Italy Bilateral Seminar on Urban Storm Drainage, National Science Foundation and Consiglio Nazionale Delle Richerche, Cagliari, Italy, 1988.

45. Linsley "Applied Hydrology", McGraw-Hill, New York, N.Y., 1975.

46. Loing, S. Y., Chan, W. T., and Lum, L. H., "Knowledge Based System For SWMM Runoff Component Calibration", J. Water Resour. Plann. Manage. Div. Am. Soc. Civ. Eng., 117(5), 507-524, 1991.

47. Milly, P. C. D., "Advances in Modelling of Water in The Unsaturated Zone", Trans. Porous Media, 3, 491-514, 1988.

48. Morel-Seytoux, H. J.,"A Simple Case of Conjunctive Surface-Ground Water Management", Ground Water, 13(4), 505-515, 1975a.

49. Morel-Seytoux, H. J., and Daly, C. J., " A Discrete Kernal Generator For Stream-Aquifer Studies", Water Resou. Res., 11(2), 253-260, 1975.

50. Morel-Seytoux, H. J., and Illangaserkare, T. H.,"Alternative Strategies of Surface and Ground Water Development for Wadi Aquifer Systems of South Tihama Region in Saudi Arabia: A Case Study for Wadi Jizan", HYDROWAR Program Report, 72 pp., Colo. State Univ., Fort Collins, 1982.

51. Morel-Seytoux, H. J., Miracapillo, C., and Abdulrazzak, M. J.,"A Reductionist Physical Approach to Unsaturated Aquifer Recharge From a Circular Spreading Basin", J. Water Reseour. Res., 26(4) 771-777, 1990.

52. Narasimhan, T. N., and P. A. Witherspoon, "An Integrated finite Difference Method for Analyzing Fluid Flow in Porous Media", Water Resour. Res., 12(2), 57-64, 1976.

53. Neuman, S. P., and Davis L. A. "Documentation And User's Guide: UNSAT2-Variably Saturated Flow Model", Rep. NUREG/CR-3390, U. S. Nucl. Regul. Comm. Rep., Washington, D. C.,1983.

54. Neuman, S. P., "Saturated-Unsaturated Seepage By Finit Elements", Jour. Hydr. Div., ASCE, 99 (HY 12), 2233-2250, 1973.

55. Patankar, S. V., "Numerical Heat Transfer And Fluid Flow", Hemisphere Publishing Corporation, 1980.

56. Philip, J. R., "The Theory Of Infiltration, Effect of Water depth Over Soil", Soil Sci., 85, 278-286, 1969.

57. Philip, J. R., "Numerical Solution of Equations of The Diffusion Type With Diffusivity Concentration-Dependent, Trans. Faraday Soc., 51, 885-892, 1955.

58. Reisenauer, A. E., et al., TRUST: "A Computer Program For Variably Saturated Flow in Multi-Dimensional, Deformable Media", Rep. NUREG/CR-2360, U.S. Nuucl. Regul. Comm., Washington, D. C., 1982.

59. Richards, L. A., "Capillary Conduction of Liquids Through Porous Mediums", Physics, 1, 318-333, 1931.

60. Ross, P. J., and Bristow, K. L.,''Simulating Water Movement in Layered And Gradational Soils Using The Kirchhoff Transfor", Soil Sci. Soc. Am. J., 54, 1519-1524, 1990.

61. Saleh, W., and Sarraf, S., "2-D Control-Volume Model For Subsurface Flow", Accepted in The Journal of Ground Water, 1994.

62. Saleh, W., Sarraf, S., and Taimeh, A., "Application of a Single-Event Hydrological Model to The Arid Watershed of Wadi El-Maghayer, Jordan"., Journal of Water Resources Development, Vol. 9, No. 4, 1993.

63. Salameh E., and K. Wirth, "Short Floods in Wadis and Their Possible Utilization for Ground-Water Recharge in Central Jordan", a Case Study, Internal Report, Water Research and Study Center, University of Jordan, Amman, Jordan, 1989.

64. Segol, G., "A Three-Dimensional Galerkin Finite-Element Model For The Analysis of Contaminant Transport in Saturated Unsaturated Porous Media", in Finite-Element in Water Resources, edited by W. G. Gray, G. F. Pinder, and C. A. Brebbia, pp. 2.123 2.144, Pentech, London, 1977.

65. Supangat N.,"Development of Methodologies For Determining Hydropower Water Storage Strategies" Ph.D. Thesis, Department of Civil Engineering, Colorado State University Fort Collins, Colorado, U.S.A, 1985.

66. "SWMM", Volume No. 1, Final Report for U.S. Environmental Protection Agency, Water Resources Engineers, and Metcalf and Eddy Inc., 1971.

67. Taylor, O. J., "Optimization of Conjunctive Use of Water in a Stream-Aquifer System Using Linear Programming", U.S. Geological Survey Professional Paper 700-C., C218-C221, 1970.

68. Taimeh, A., "Agricultural Production in Semi-Arid to Arid Land and Areas Suffering From Desertification", Annual report, University of Jordan, 1988.

69. Taimeh, A., "Agricultural Production in Semi-Arid to Arid Land and Areas Suffering From Desertification", Internal Report, Soils and Irrigation Dept., University of Jordan, Amman, Jordan, 1989.

70. Taimeh, A., "Soils of Muwaqar", Internal Report, Soils and Irrigation Dept., University of Jordan, Amman, Jordan, 1989.

71. Tsakiris, G. P., "2-D Unsaturated Flow in Irregularly Shaped Regions", Transport in Porous Media 6, 1991.

72. Williams J. R. and R. W. Hann,"HYMO: Problem-Oriented Computer Language for Hydrologic Modeling", U.S. Department of Agriculture, Agriculture Research Service, 1973.

73. U.S. Army Corps of Engineers HEC-1, "Flood Hydrograph Package Users Manual", The Hydrologic Engineering Center, Davis, Cal., U.S.A, 1985.

74. Van Genuchten, M.Th., "A Closed-Form Equation For Predicting The Hydraulic Conductivity of Unsaturated Soils", Soil Sci. Soc. Am. J., 44, 892-898, 1982.

75. Warren V., "Introduction To Hydrology", Third Edition, Harper Row, Publishers, Inc., 1989.

76. Yeh. W. W-G., and J. B. Franzini, "Moisture Movement in a Horizontal Soil Column Under The Influence Of An Applied Pressure", J. Geophys. Res., 73(16), 5151-5157, 1968.

77. Yazicigil H., and M. Rasheeduddin, "Optimization Model For Ground Water Management in Multi-Aquifer Systems", Water Res. Manage. Plann, Am. Society of Civ. Eng., (1987).

78. Zaidel, J., and Russo, D.,"Estimation of Finite Difference Interblock Conductivities For Simulation of Infiltration into Initially Dry Soils", Water Resour. Res., 28(9), 2285-2295, 1992.

APPENDIX A

Results Of The Subsurface Flow Simulation of Theoretical Case Problems

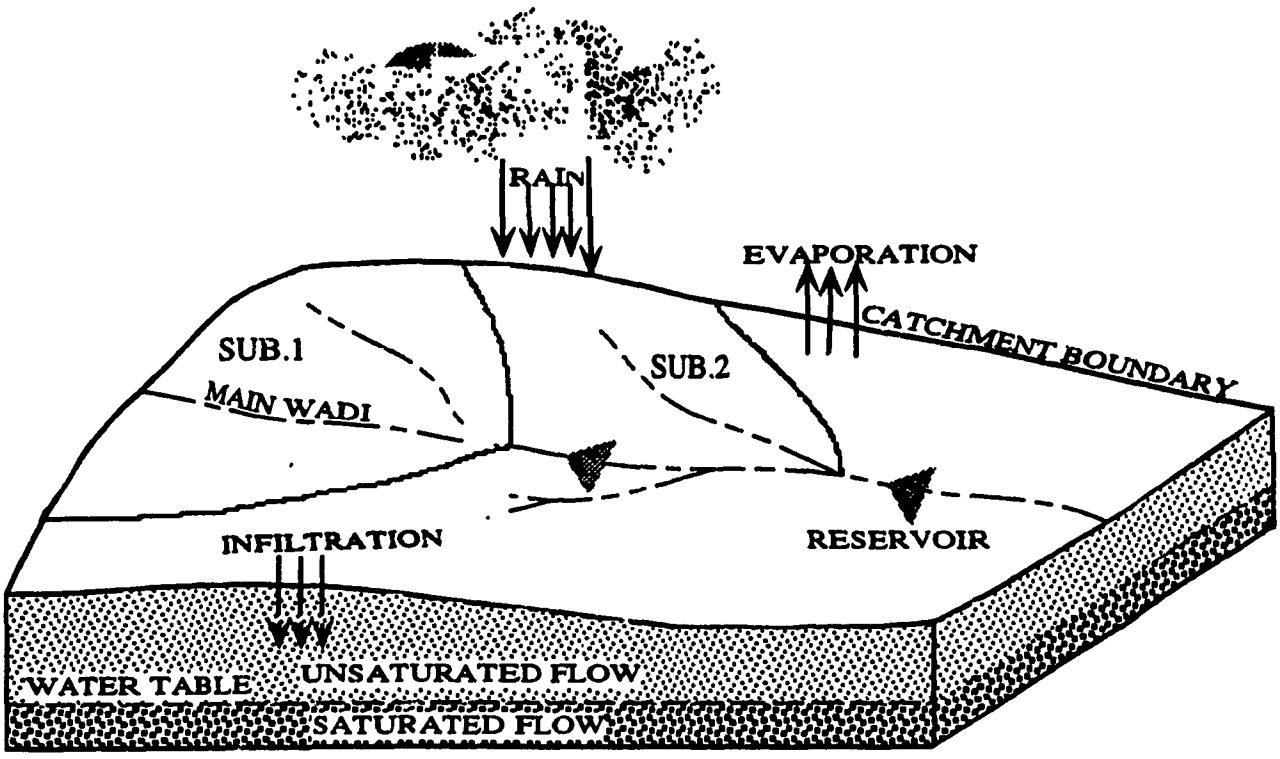

Fig.(2.1): A Typical Surface/Subsurface Flow System.

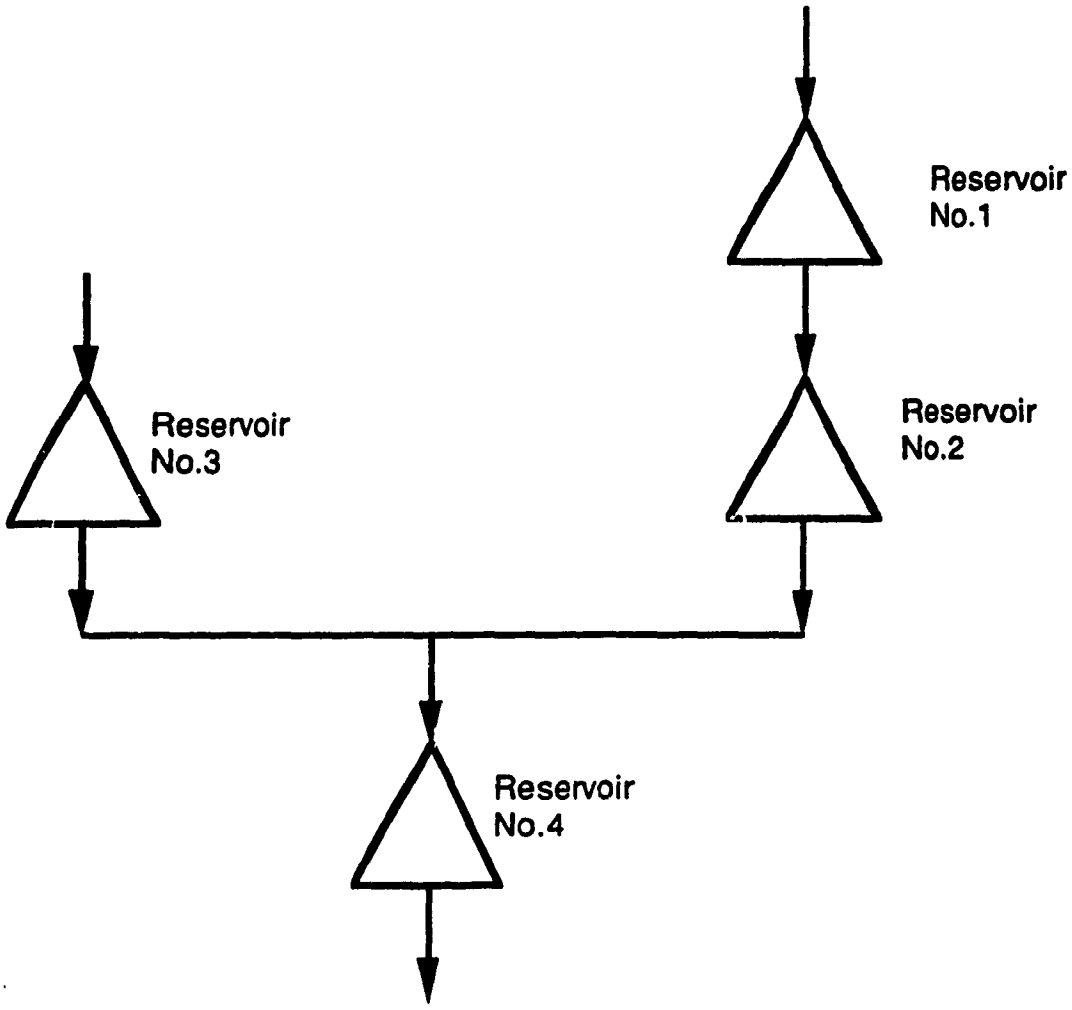

Fig.(2.2): A Typical Reservoir System Representation.

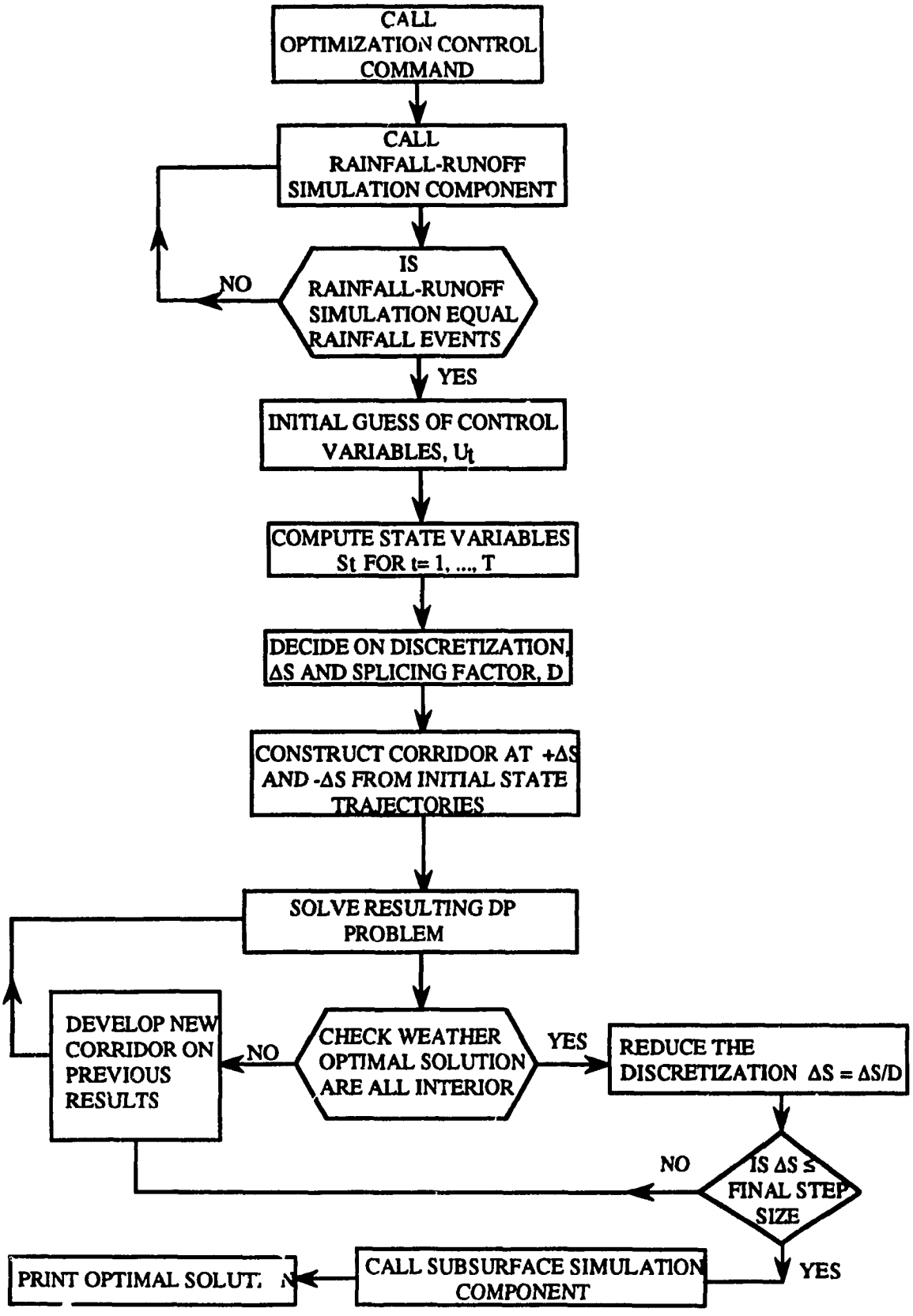

Fig.(3.1): Flow Chart of the Optimal Control Model.

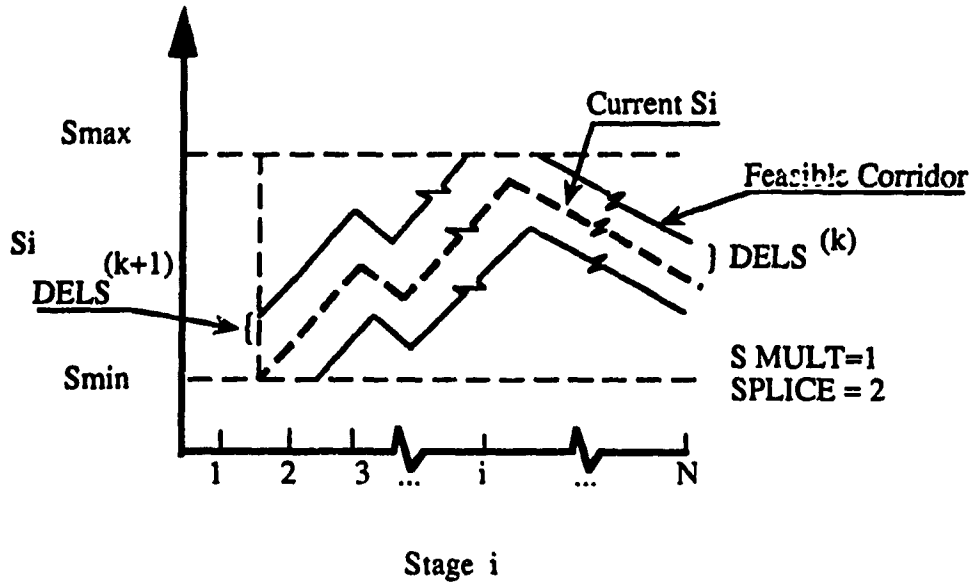

Fig.(3.2): Illustration of Reservoir Storage Increment Splicing Option

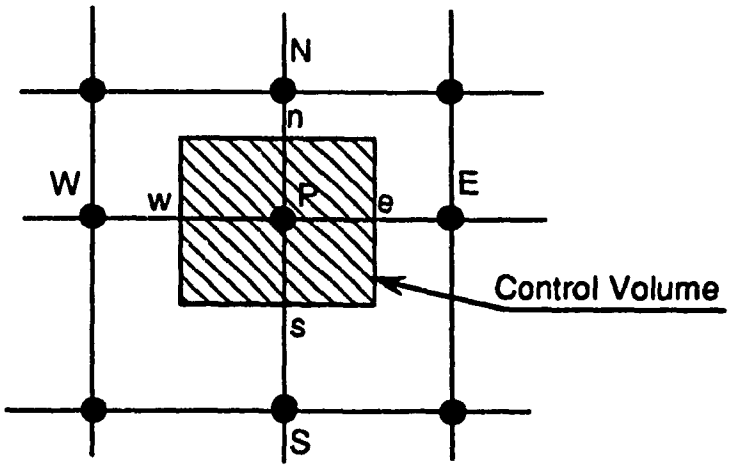

Fig. (3.3a): Typical Control Volume.

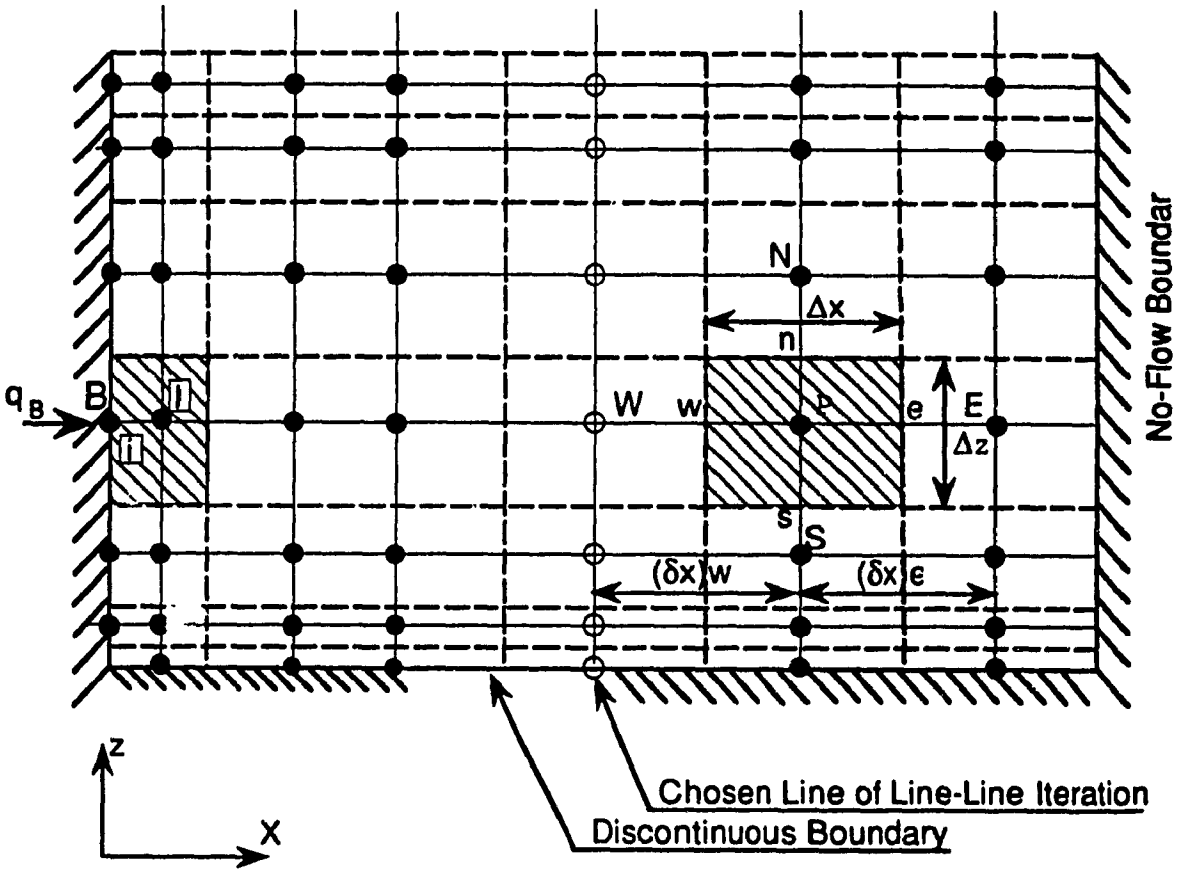

Fig. (3.3b): Discretization Scheme And The Overall Mesh.

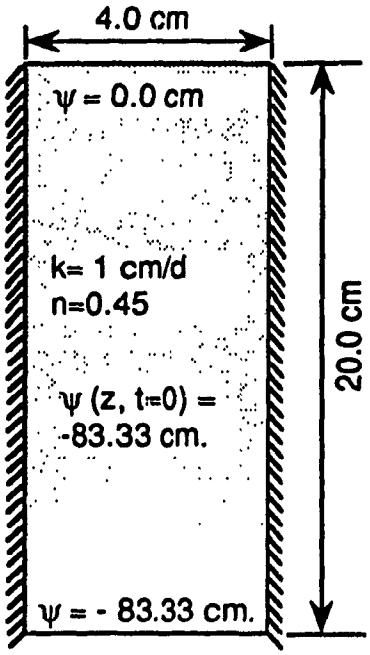

Fig. (4.1): Schematic Description For 1-D Test Case I.

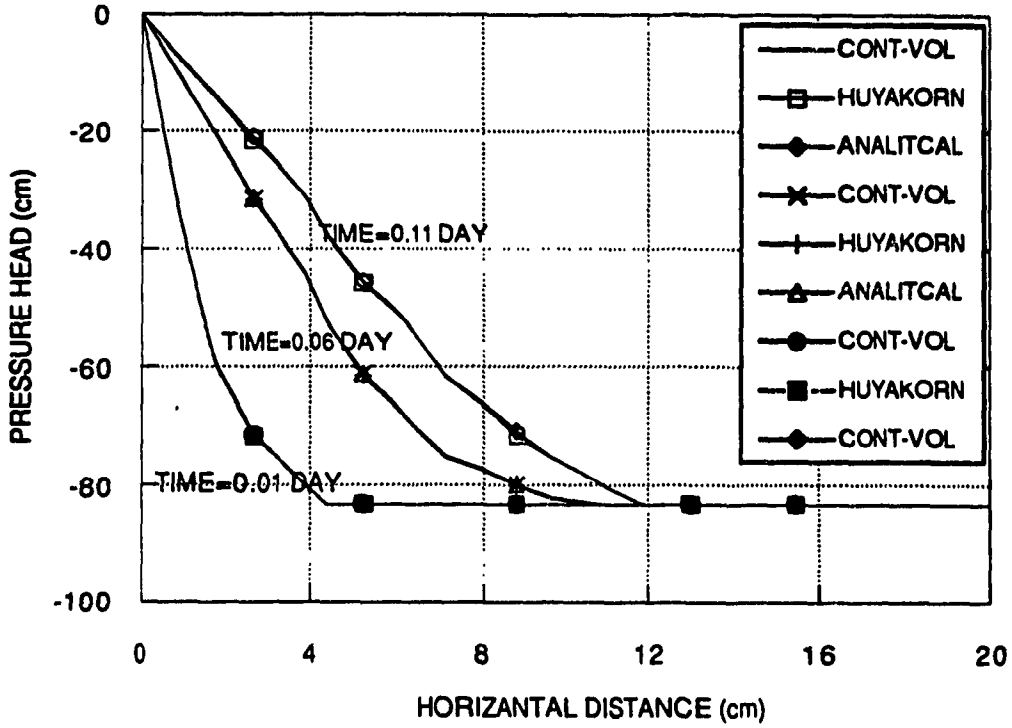

Fig.(4.2): Comparision Of Pressure Head Profiles At Typical Times.

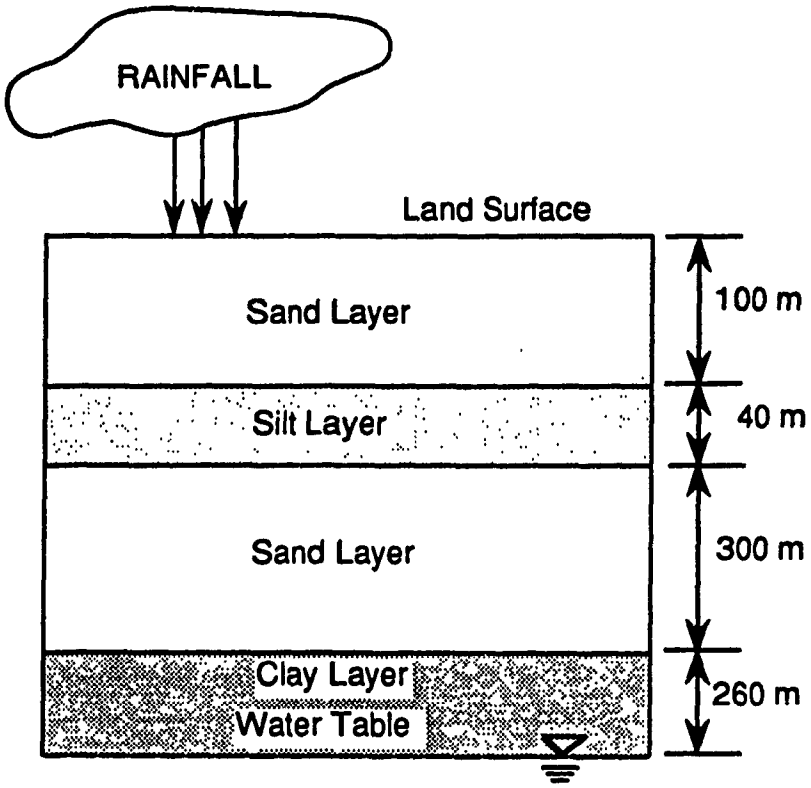

Fig. (4.3): Schematic Description For 1-D Test Case II

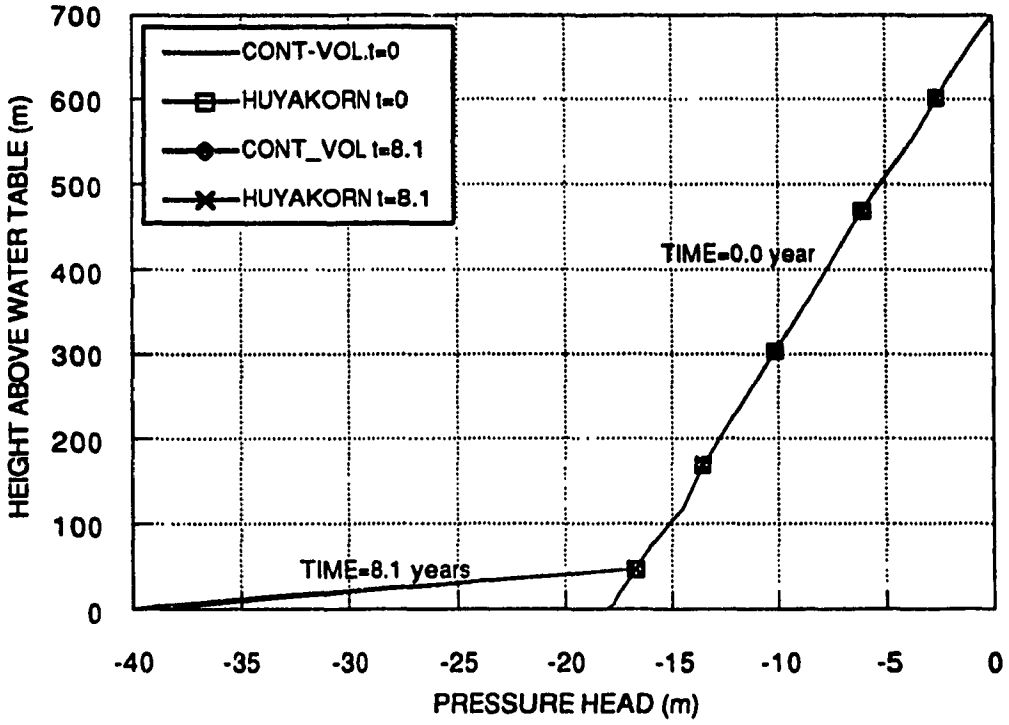

Fig.(4.4): Pressure Head Profiles At Typical time Values.

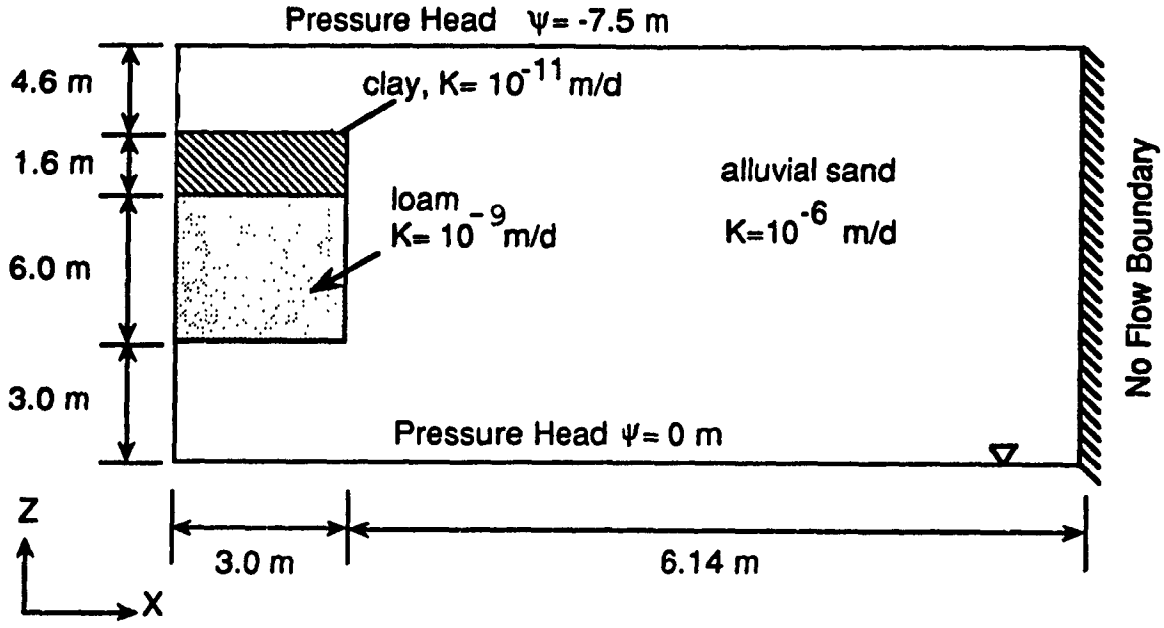

Fig. (4.5): Schematic Description For 2-D Test Case I .

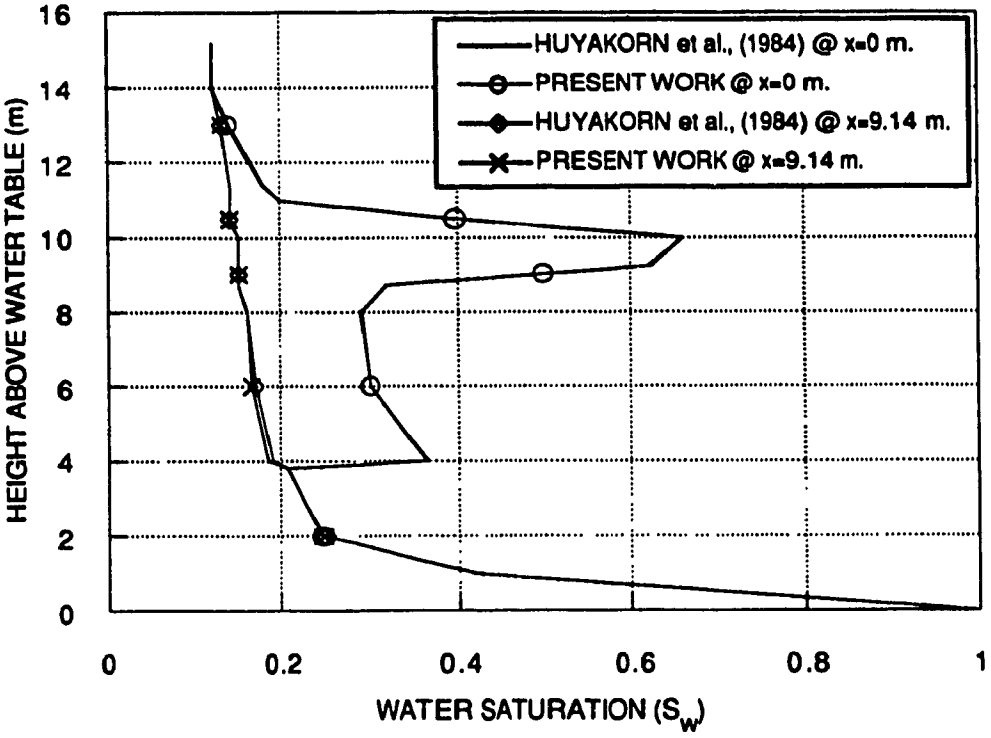

Fig.(4.6): Comparision Of Water Saturation Profiles.

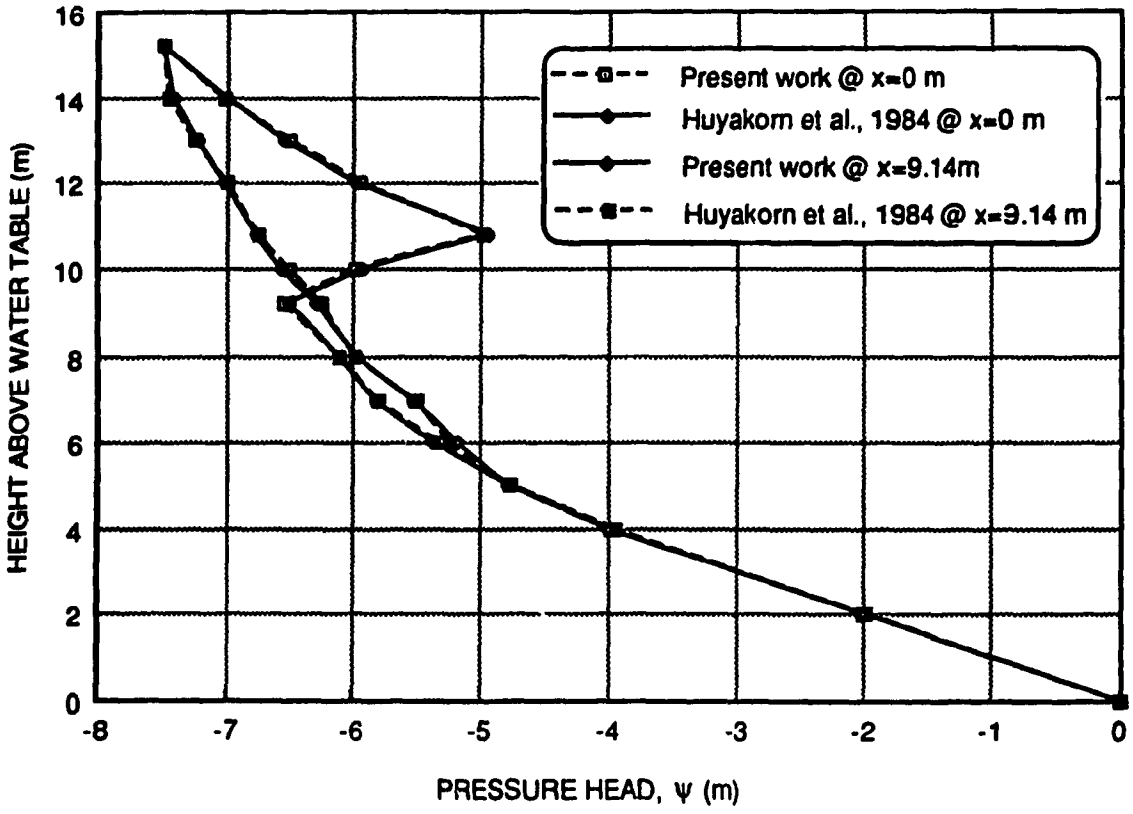

Fig. (4.7): Comparision Of The Pressure Head profiles.

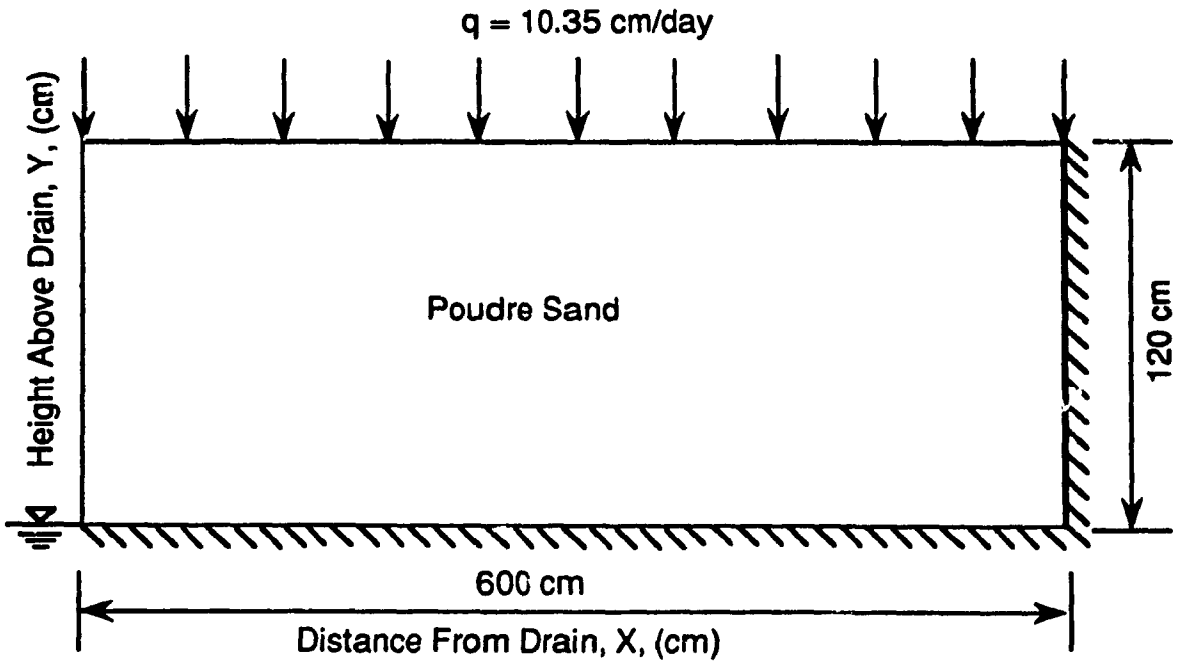

Fig. (4.8): Schematic Description For 2-D Test Case II.

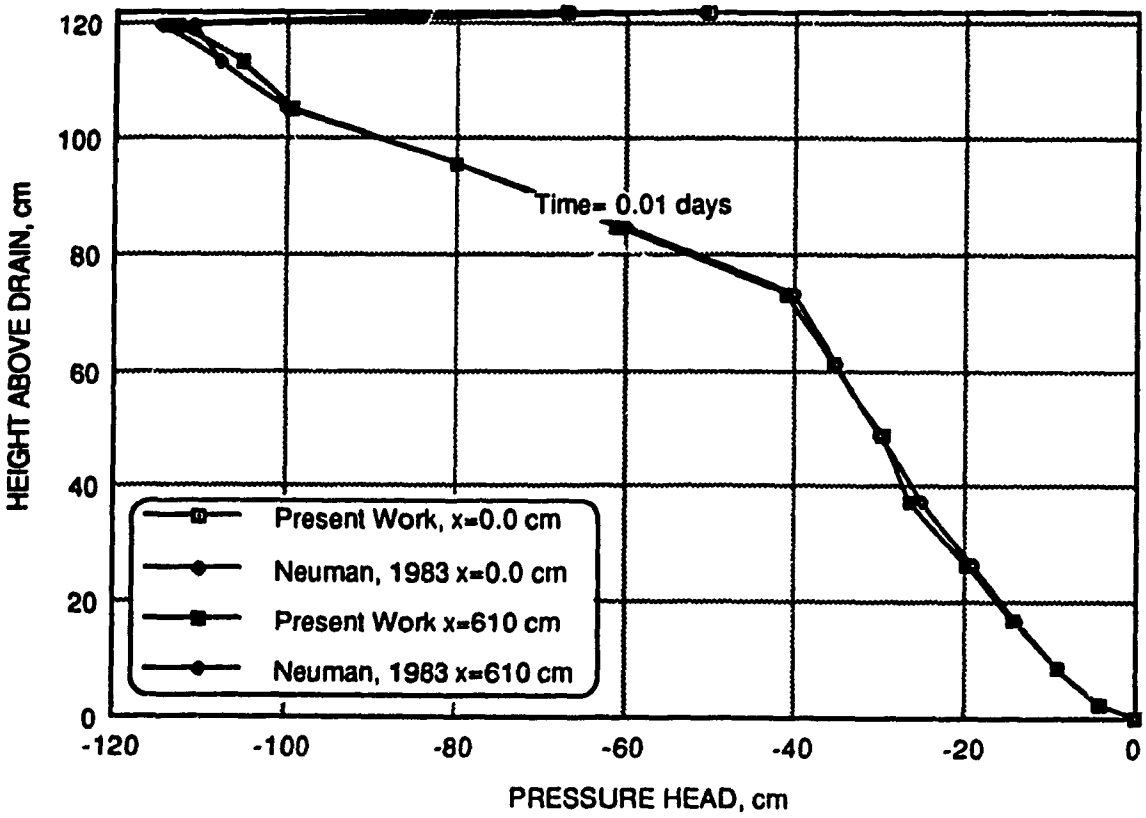

Fig. (4.9): Comparision Of Pressure Head At Typical Time Value.

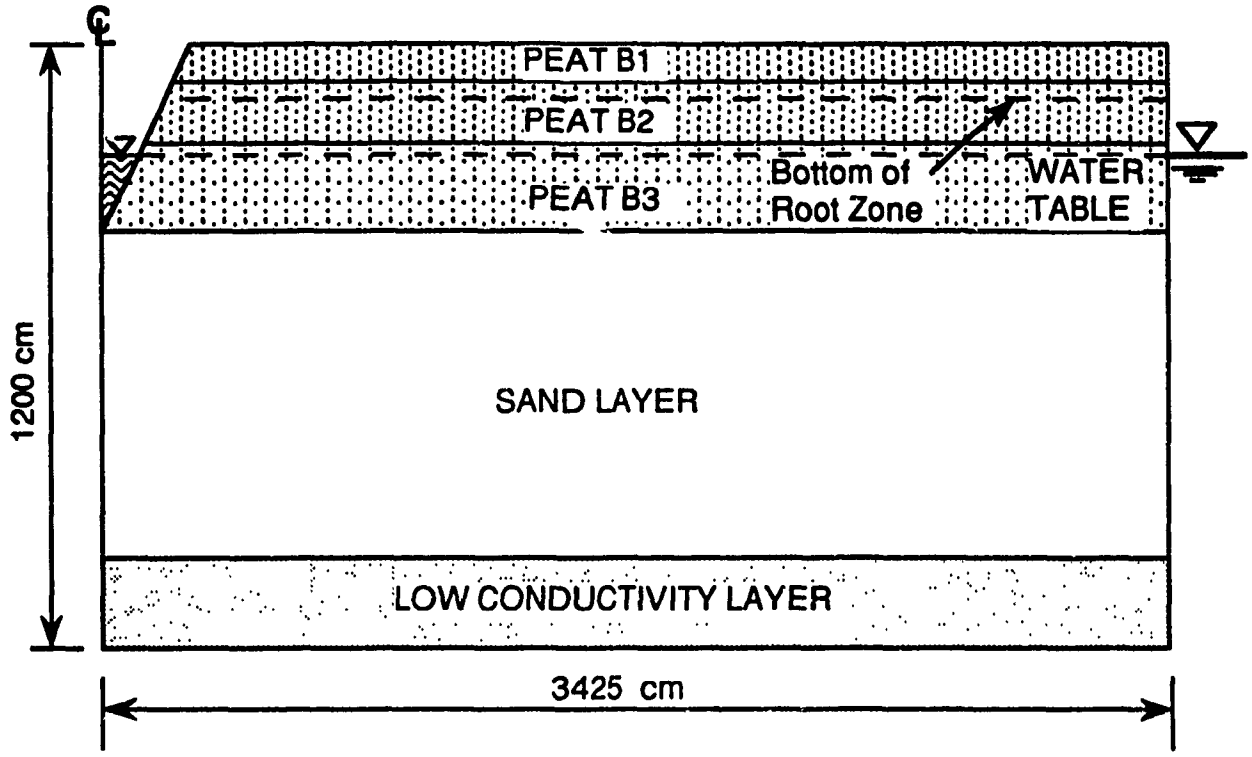

Fig. (4.10) Vertical Cross Section For 2-D Test Case III.

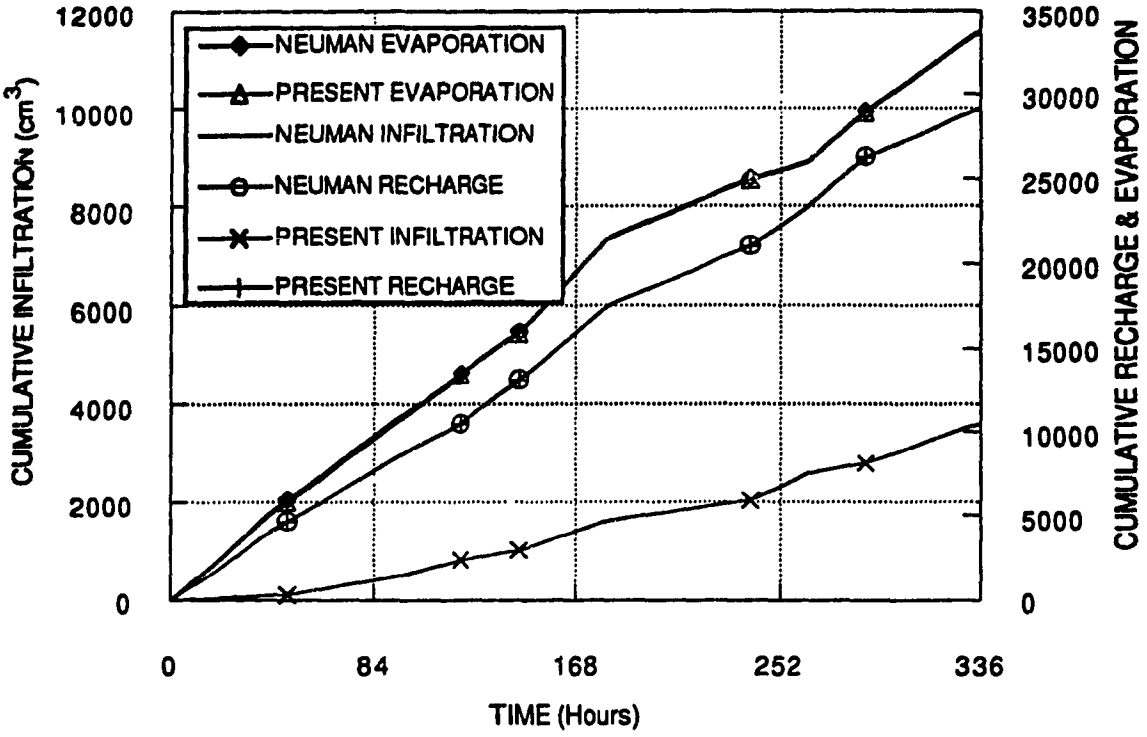

Fig.(4.11): Comparision Of The Cumulative Fluxes.

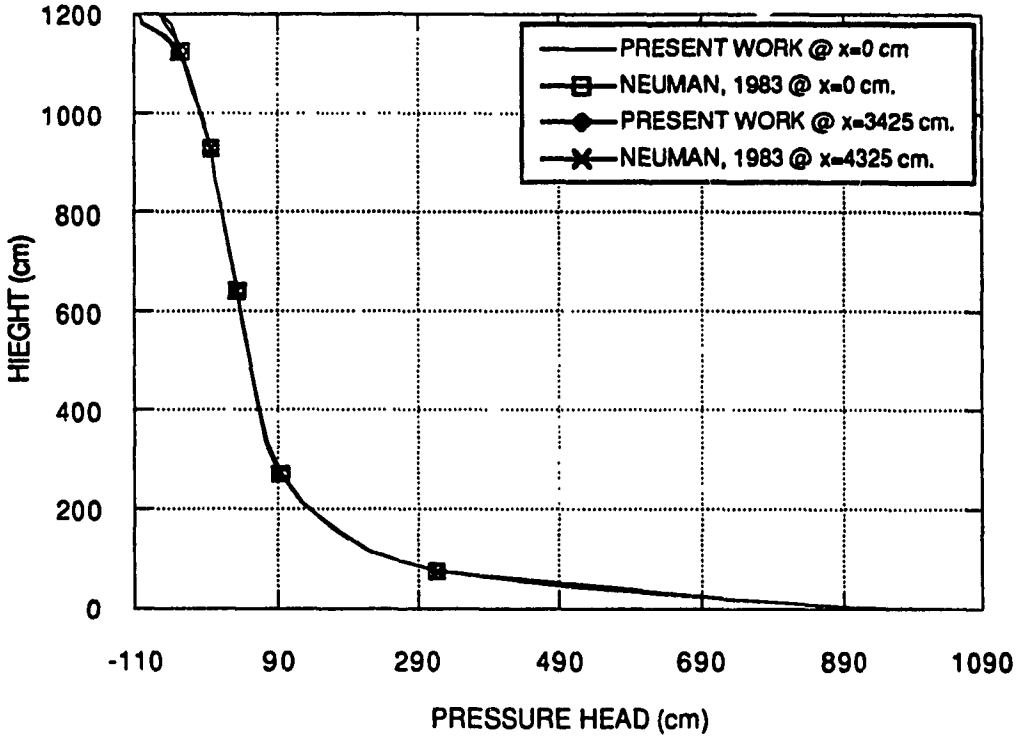

Fig.(4.12): Comparision Of Pressure Head Profiles At 24 hrs.

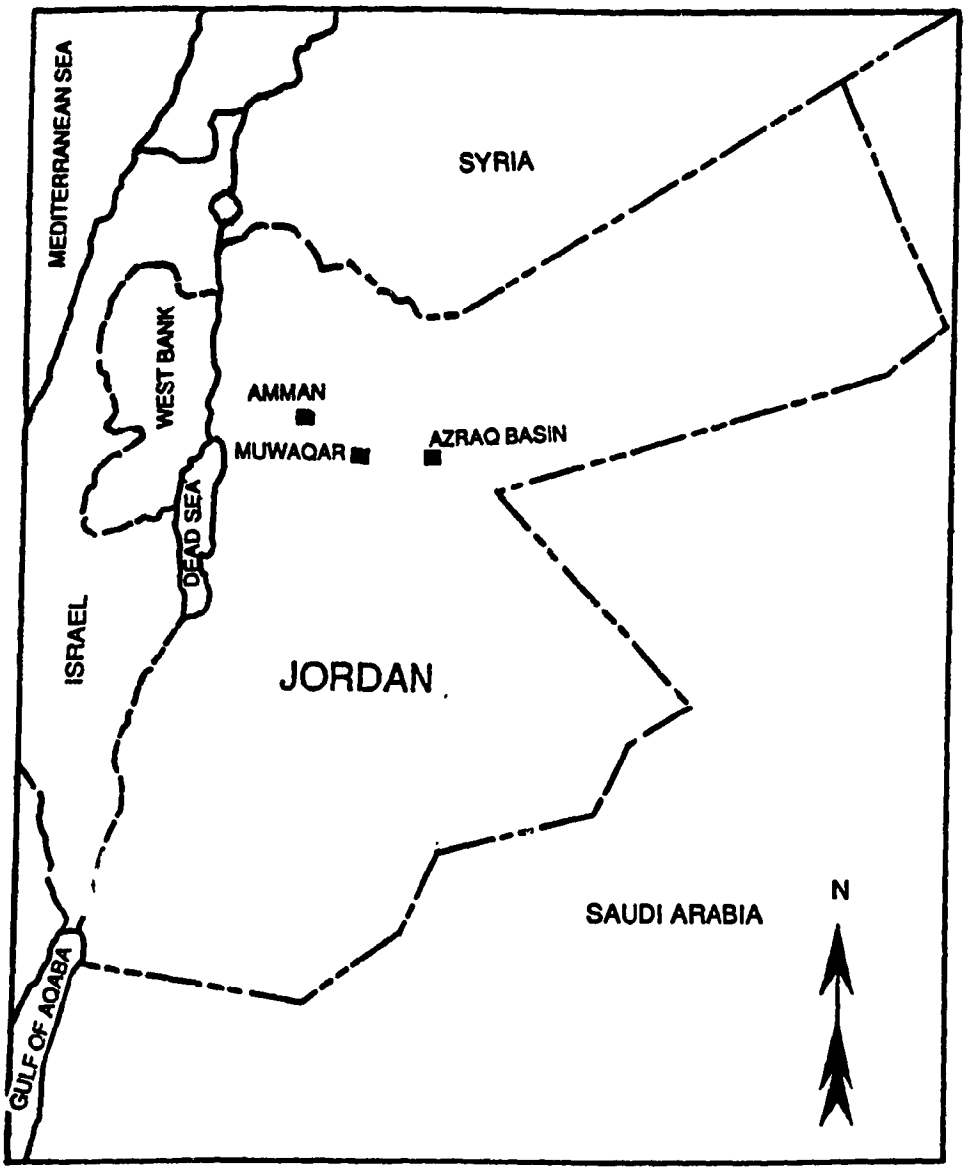

Fig.(5.1): Muwaqar Project Location.

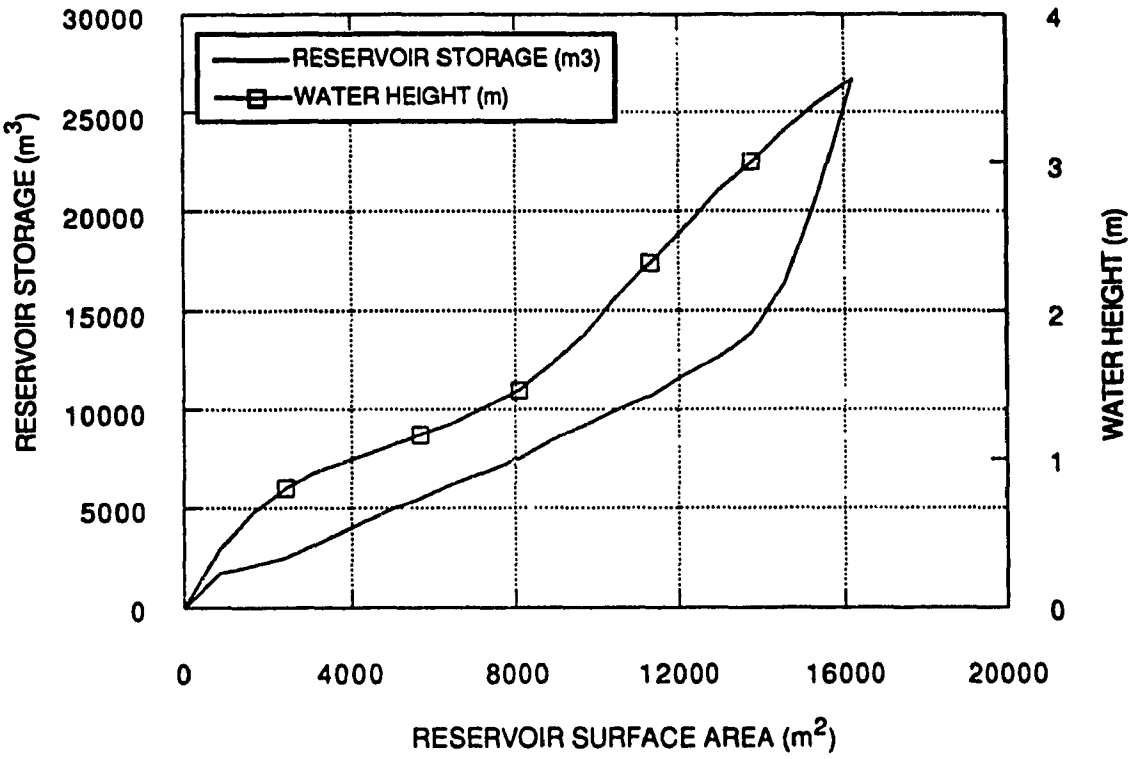

Fig.(5.2): Storage-Area-Height Of Reservoir No.1

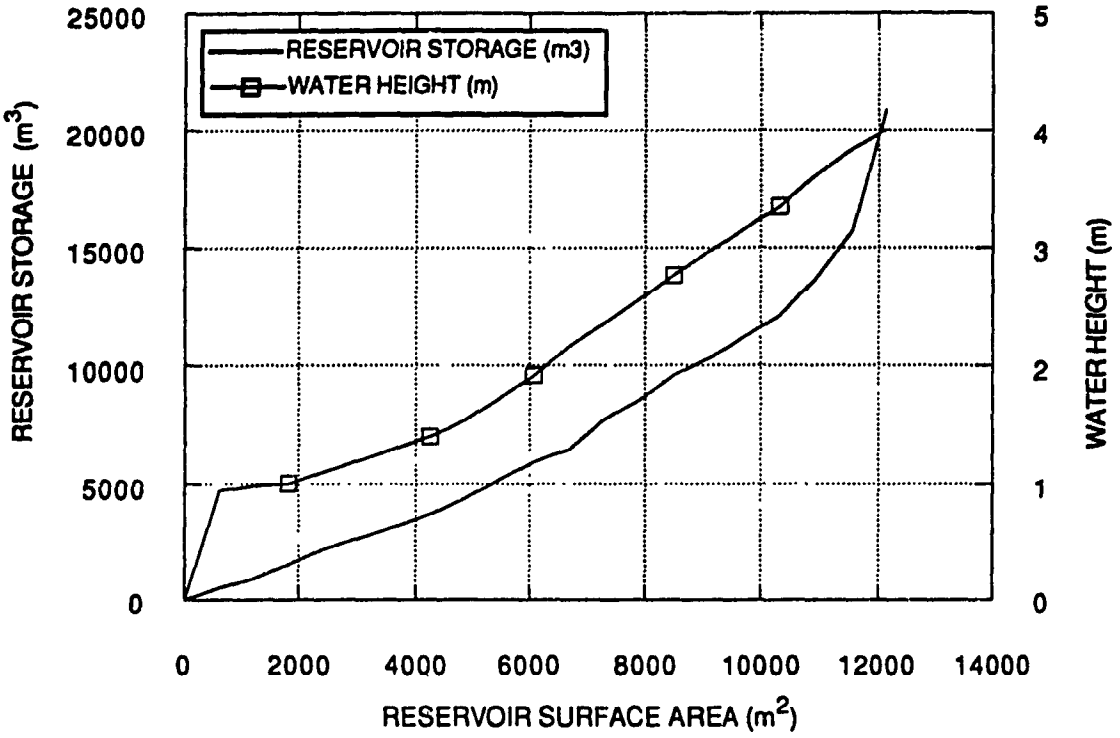

Fig.(5.3): Storage -Area-Height Of Reservoir NO.2

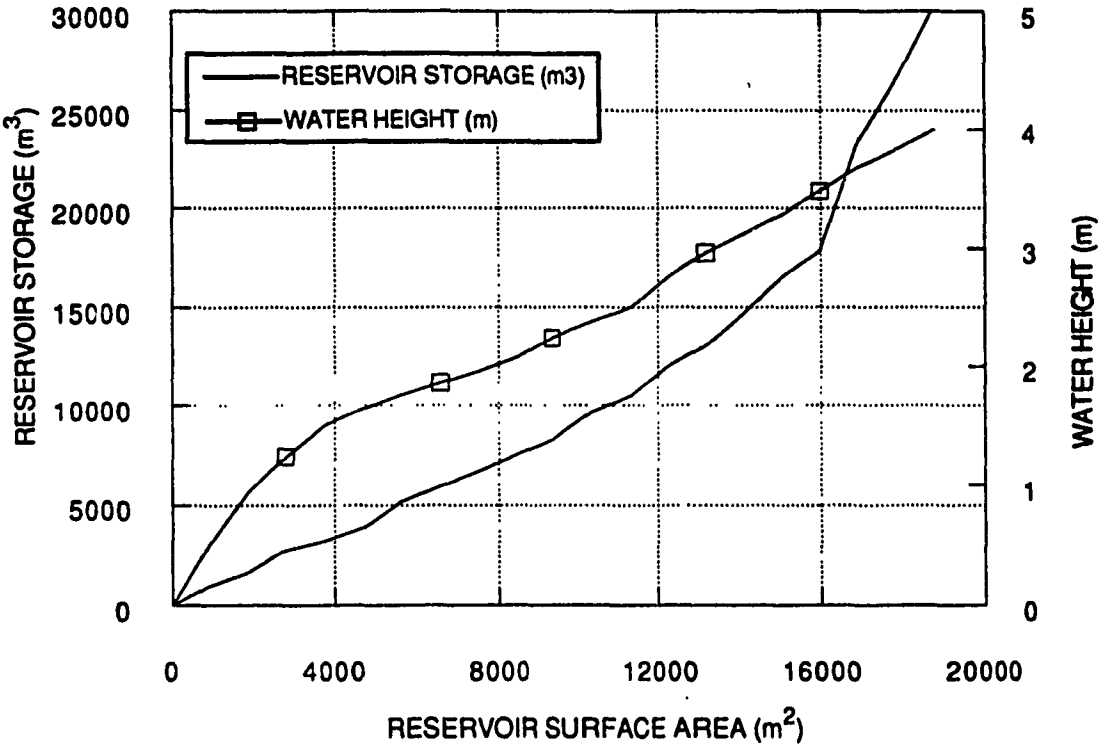

Fig.(5.4): Storage -Area-Height Of Reservoir NO.3

APPENDIX B

Results Of The Subsurface Flow Simulation of Field Case Problems

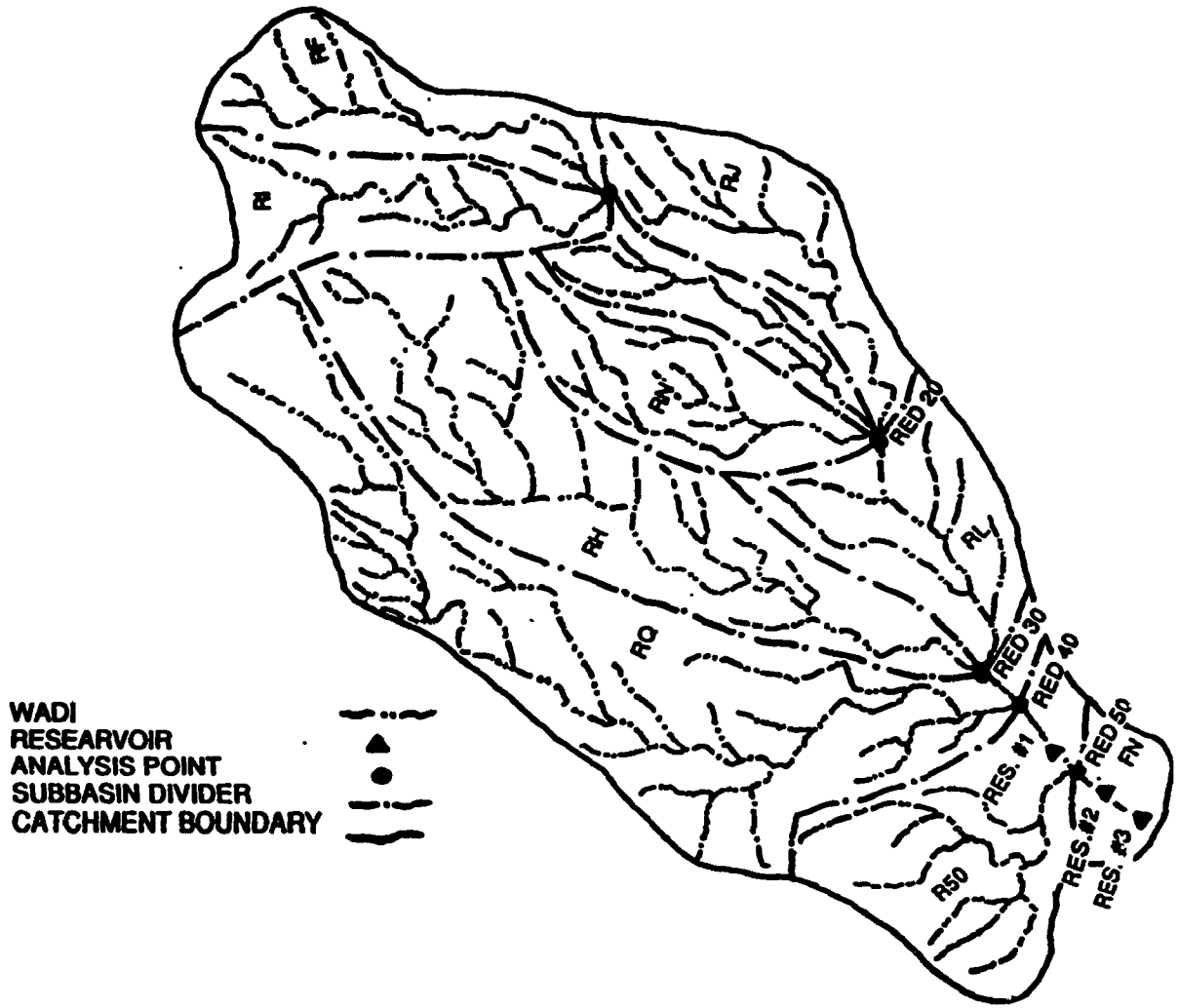

Fig.(6.1): Muwaqar Watershed and Reservoirs Locations

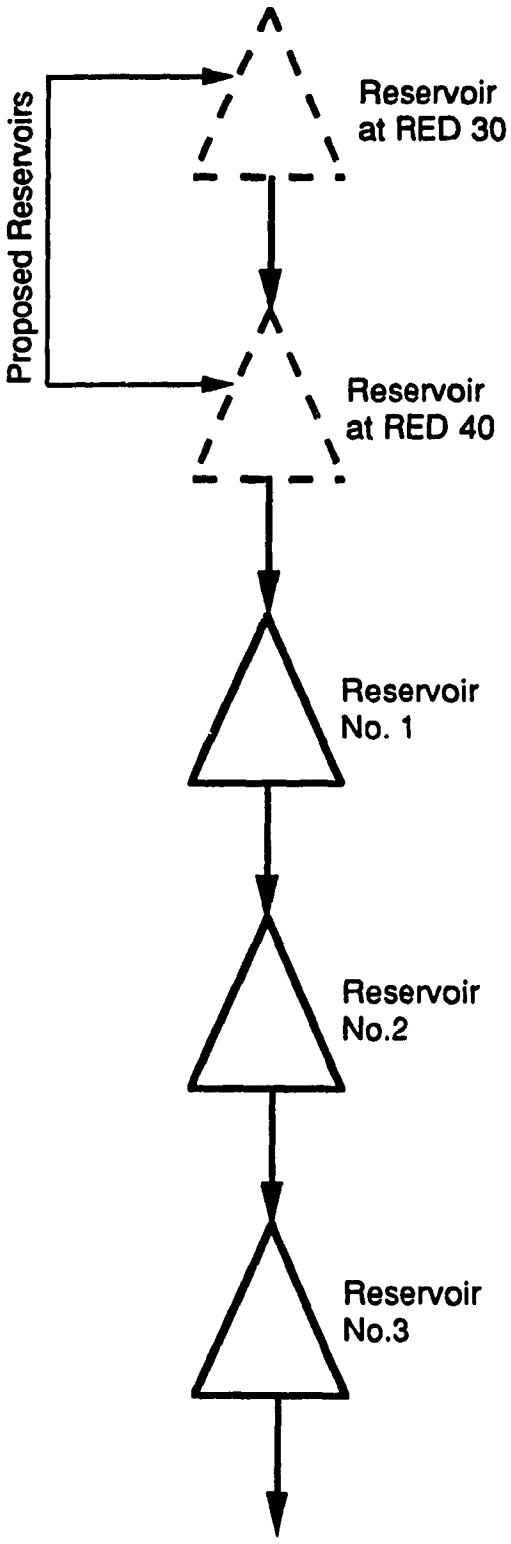

Fig.(6.2): Schematic Representation of Muwaqar Reservoir System.

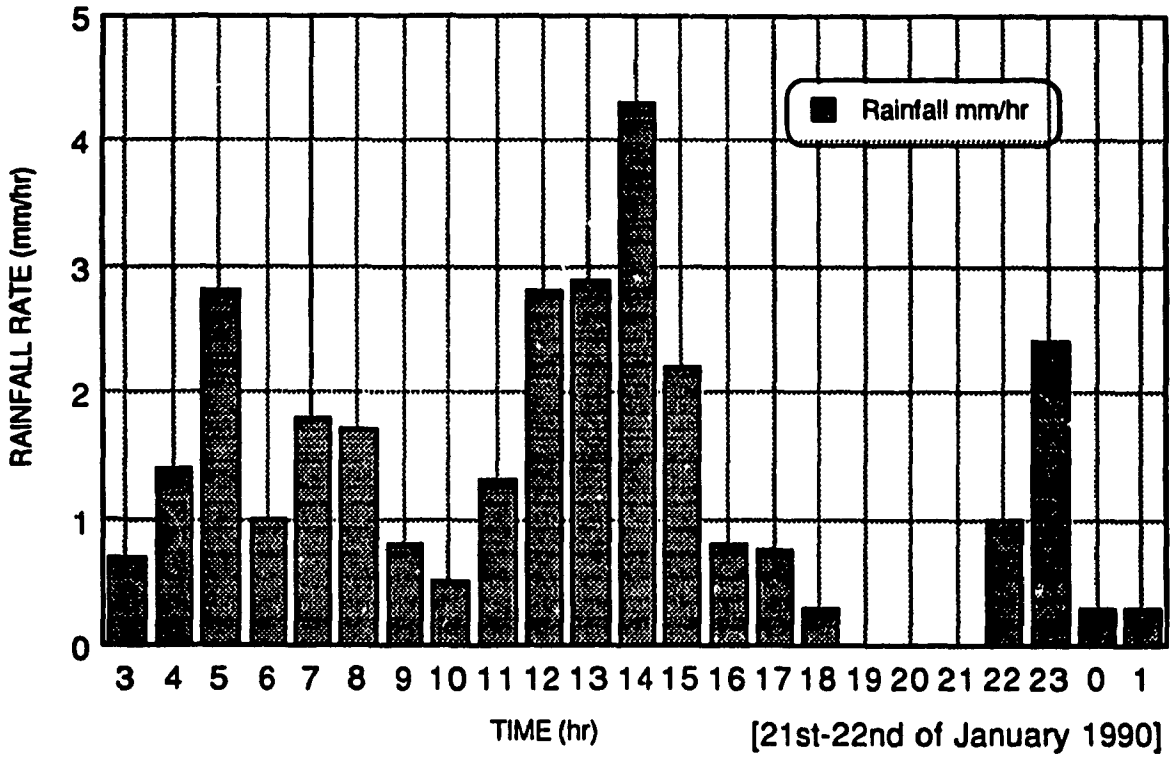

Fig. (6.3): Precipitation Heytograph For The First Simulation Run.

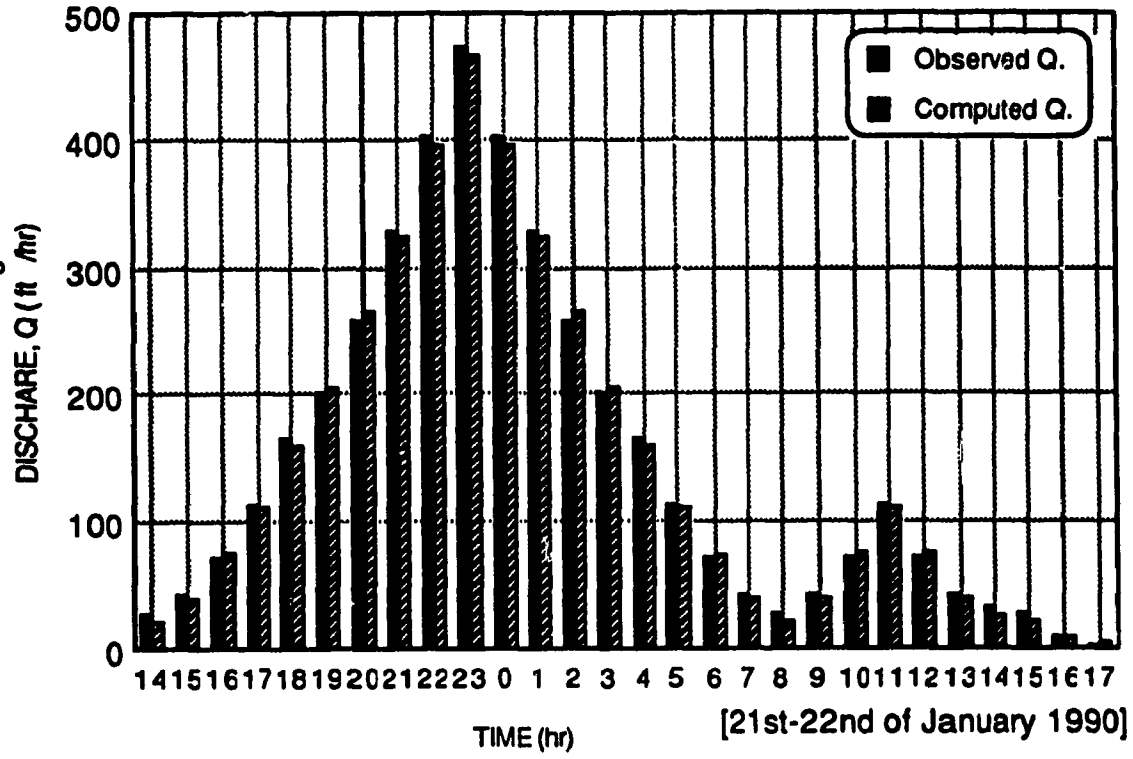

Fig. (6.4): Comparision Of Discharges At Reservoir No. 1.

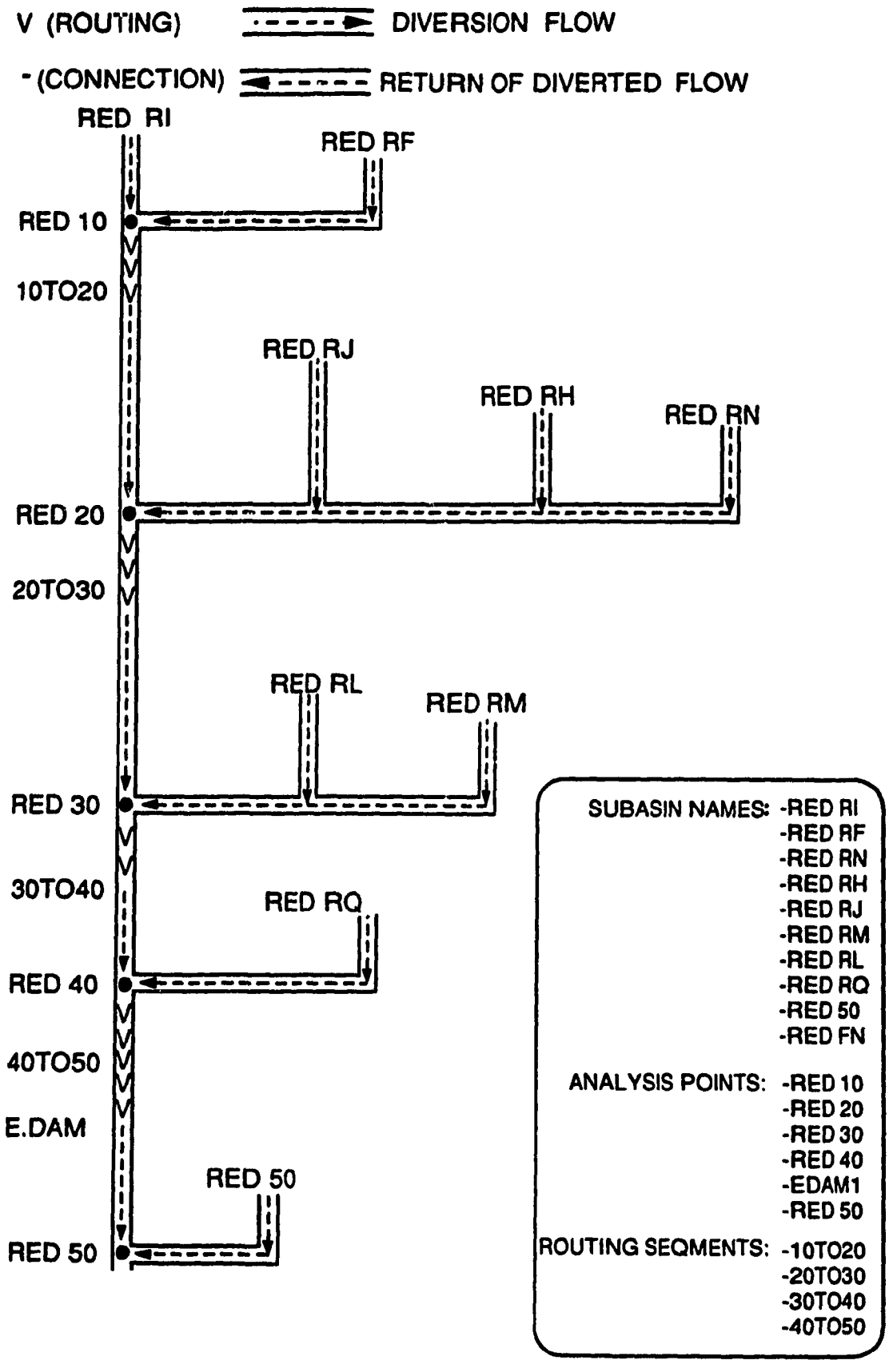

Fig. (6.5): Schematic Diagram Of Muwaqar Wadi For The First Run.

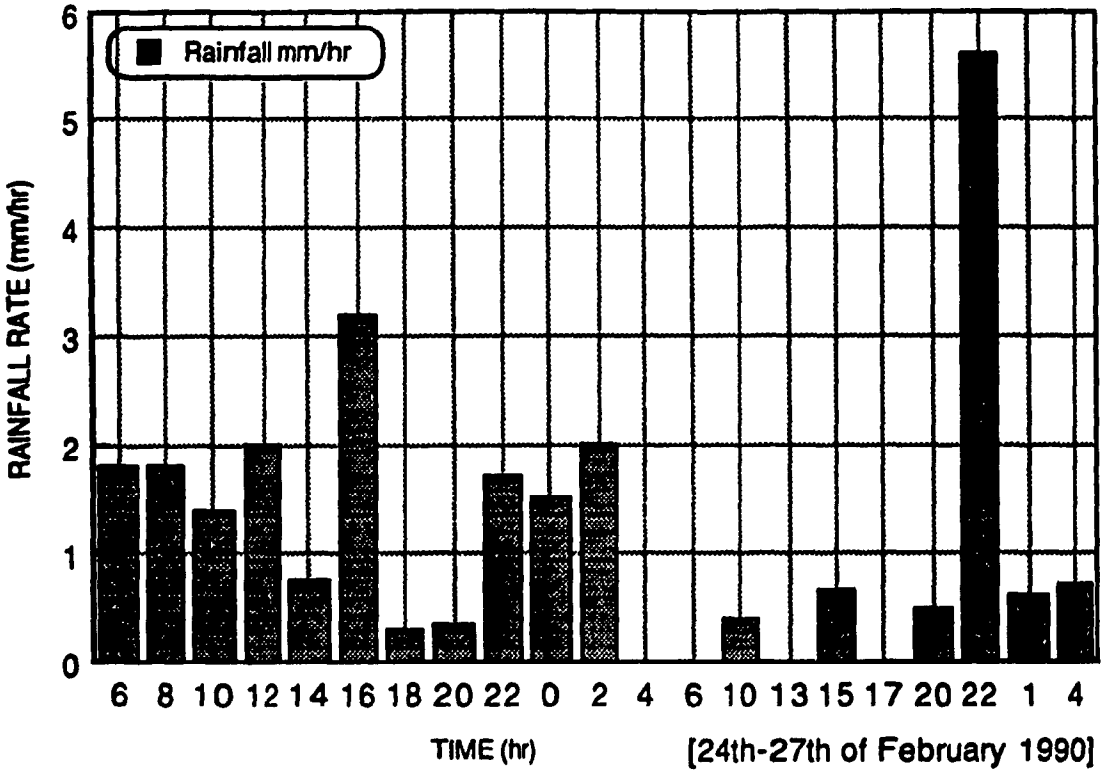

Fig. (6.6): Precipitation Hyetograph For The Second Simulation.

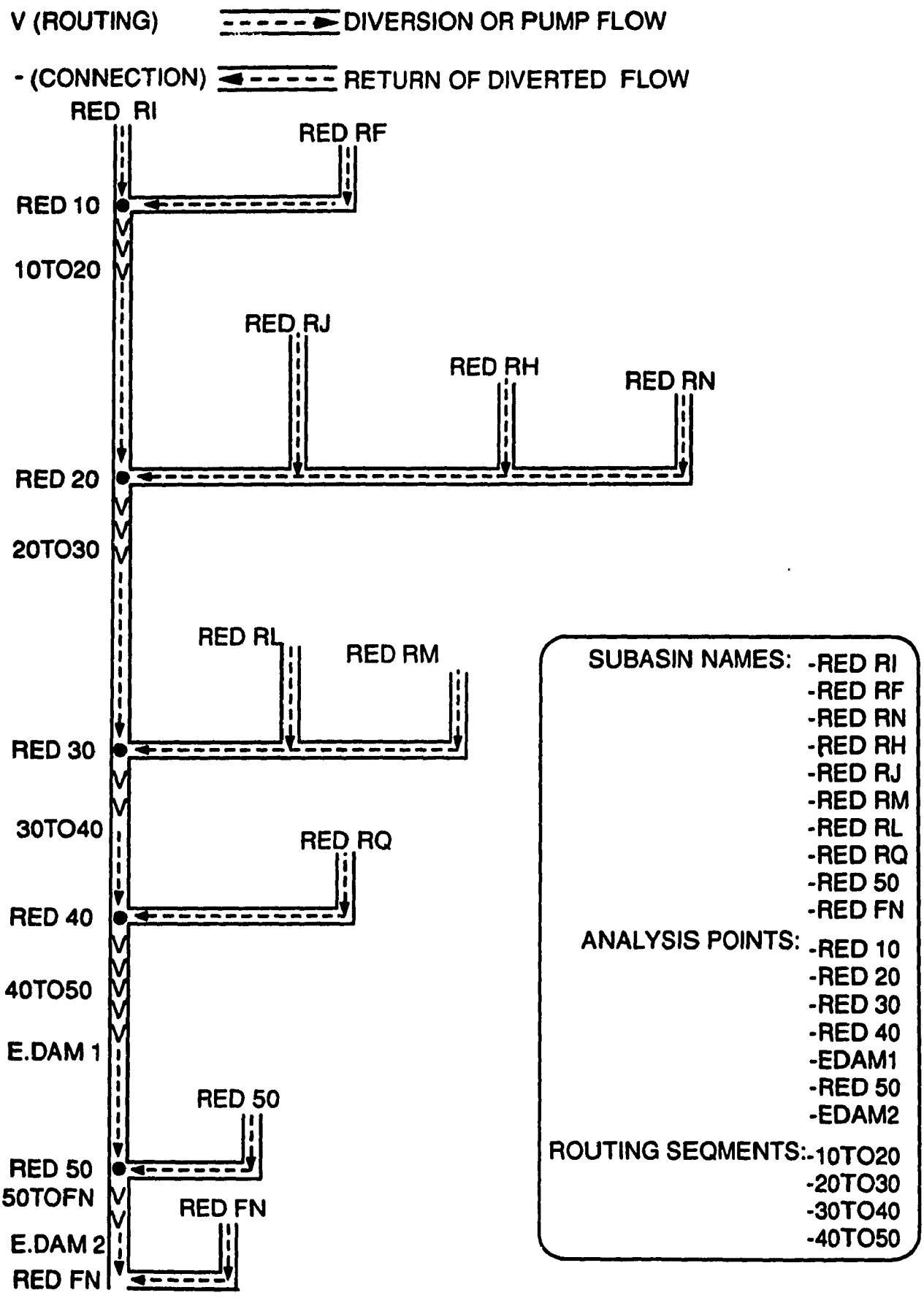

Fig. (6.7): Schematic Diagram Of Muwaqar Wadi For The Second Run.

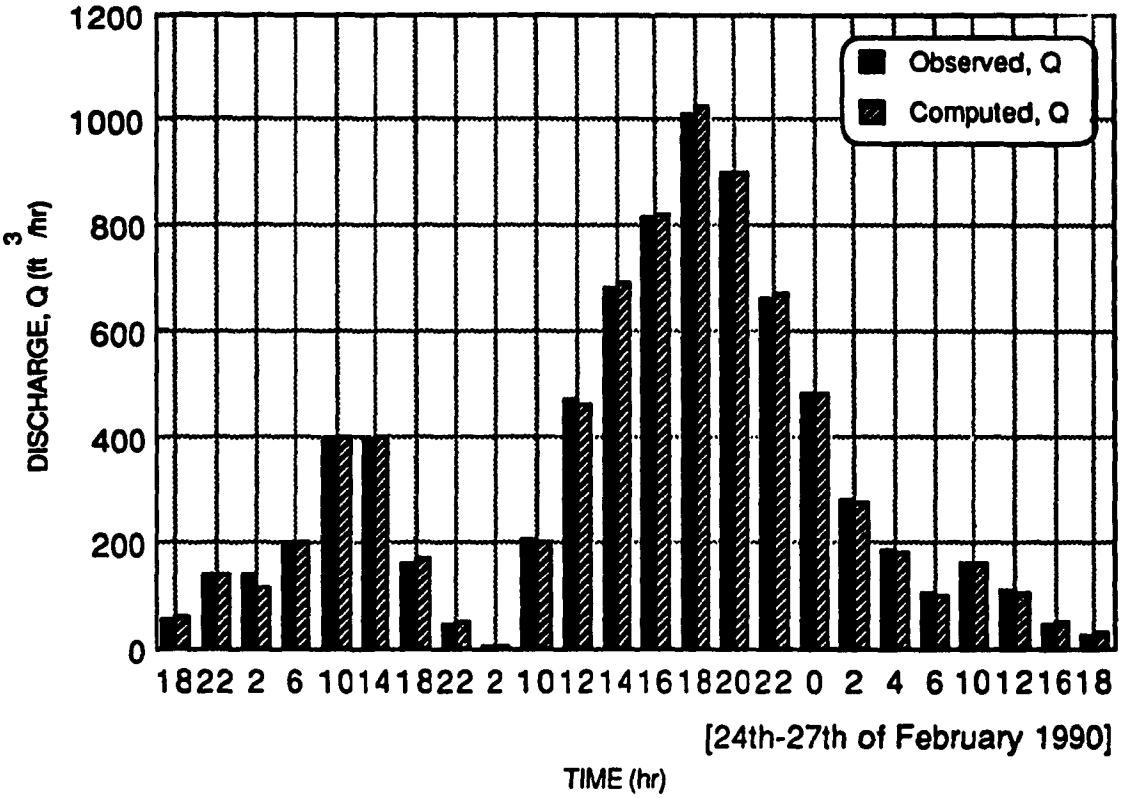

Fig. (6.8): Comparision Of Discharges At Reservoir No. 2.

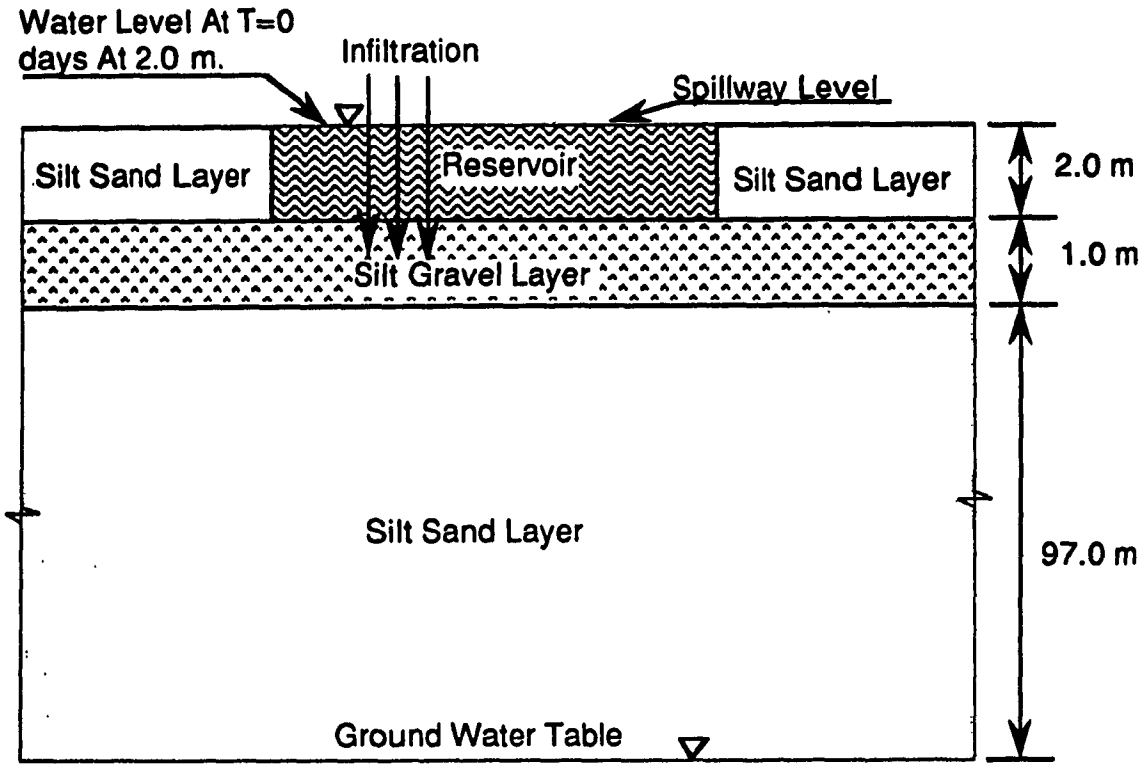

Fig. (6.9): Schematic Description Of Muwaqar Case Study I

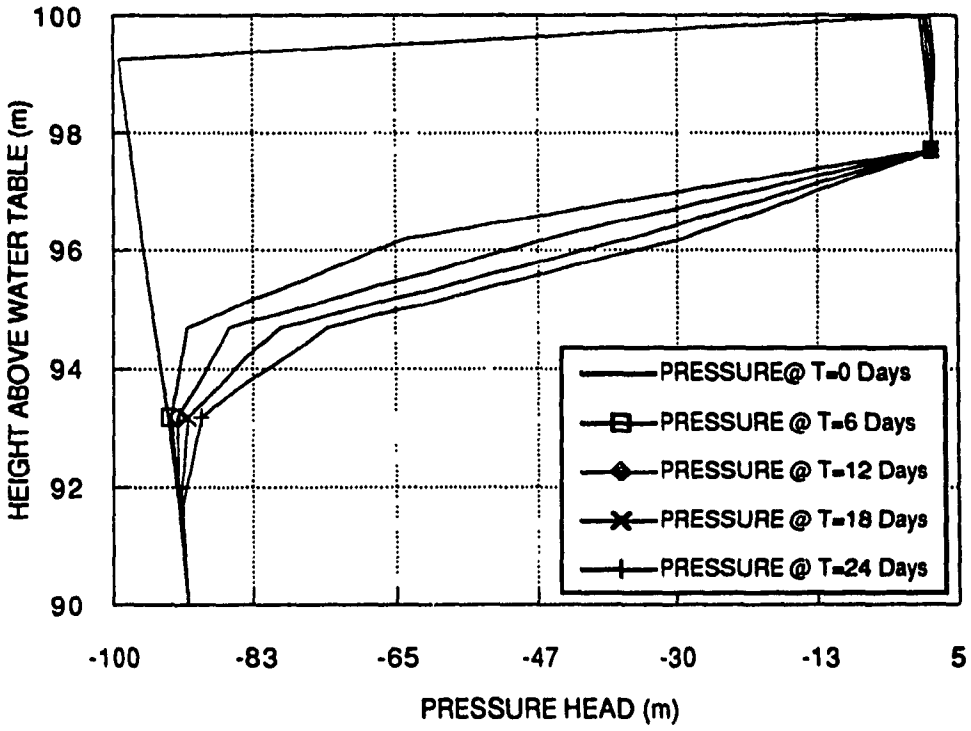

Fig.(6.10): Pressure Head Profiles At Typical Time Values.

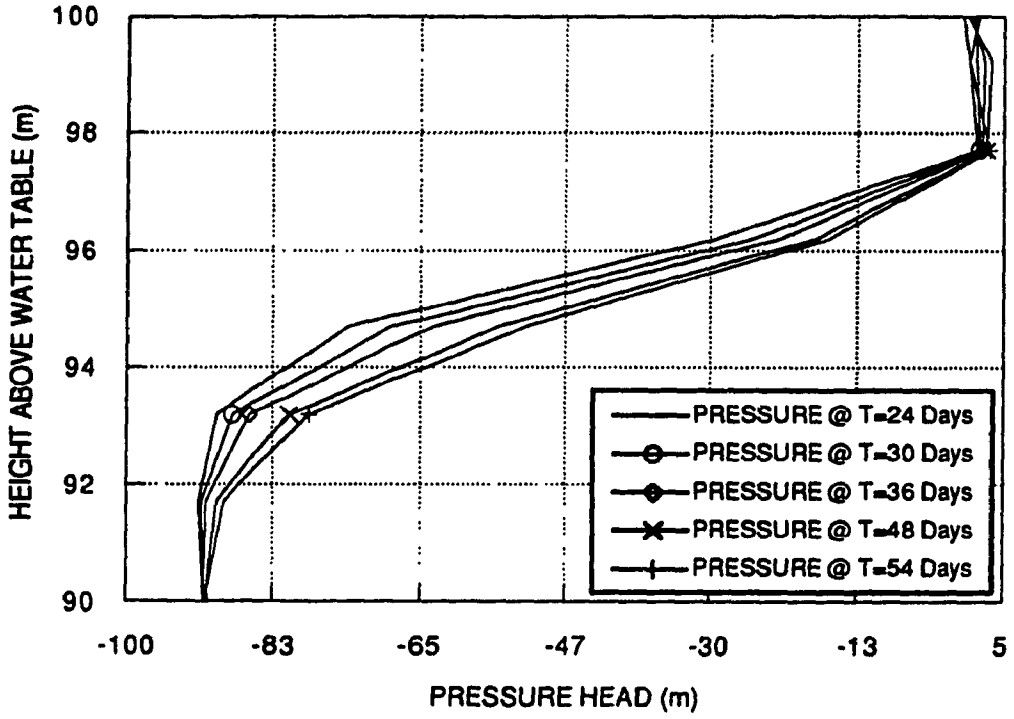

Fig.(6.11): Pressure Head Profiles At Typical Time Values.

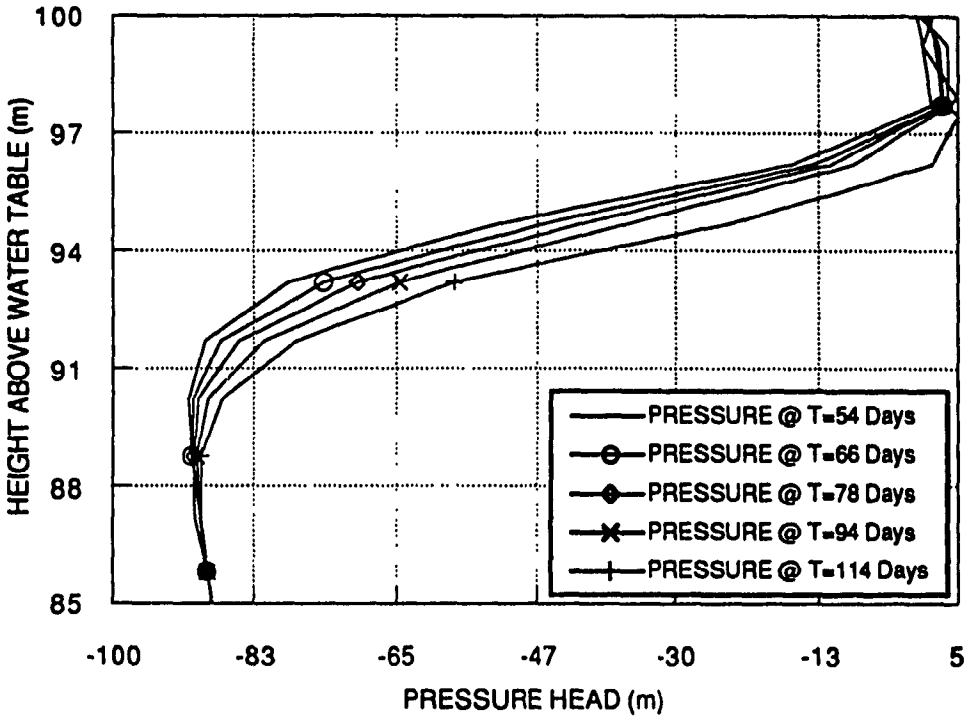

Fig.(6.12): Pressure Head Profiles At Typical Time Values.

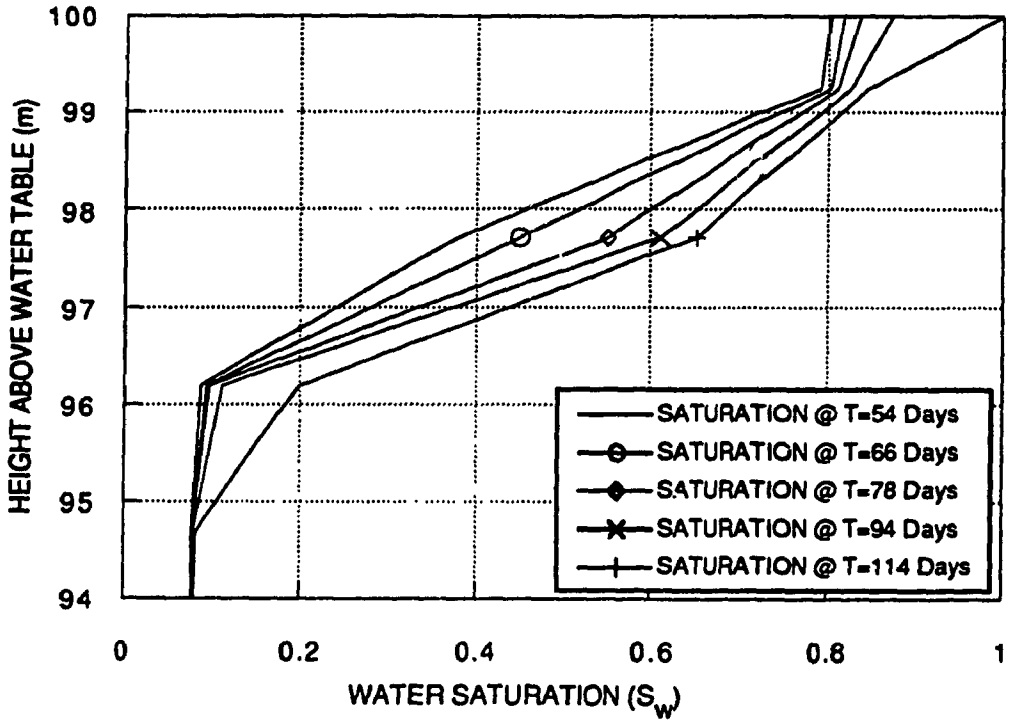

Fig.(6.13): Water Saturation Profiles At Typical Time Values.

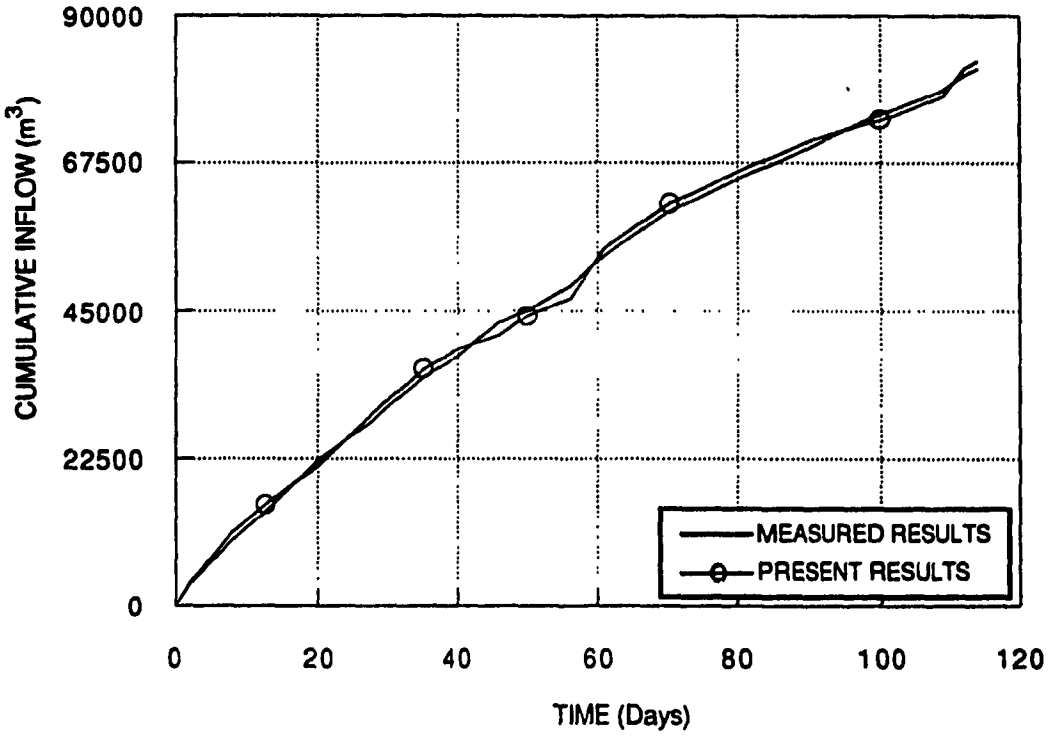

Fig.(6.14): Comparision Of The Cumulative Inflow At Muwaqar.

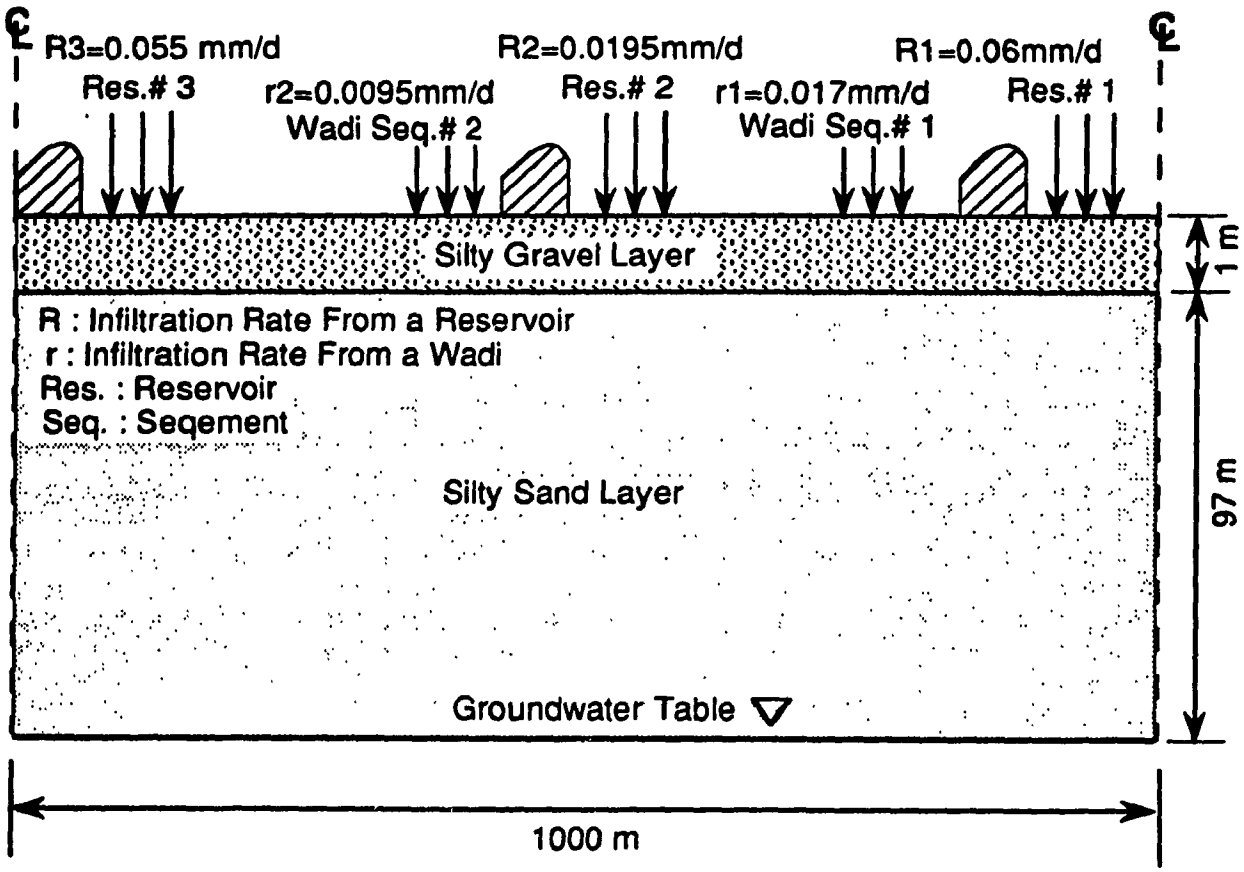

Fig. (6.15): Schematic Description of Muwaqar Case Study II

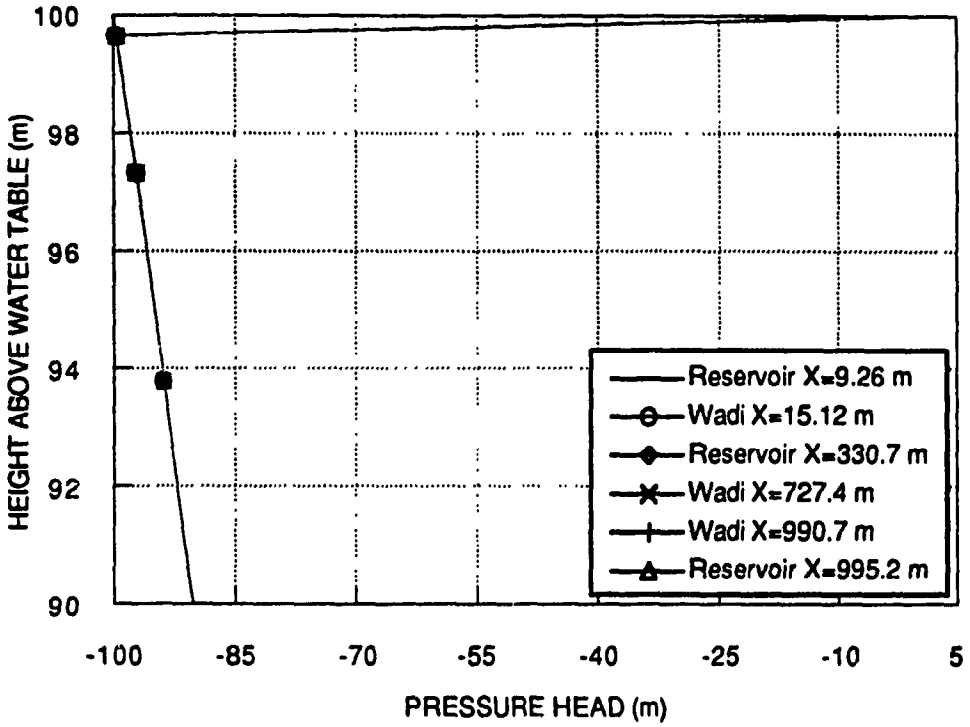

Fig.(6.16): Pressure Head Profile After 0 Days Of Simulation.

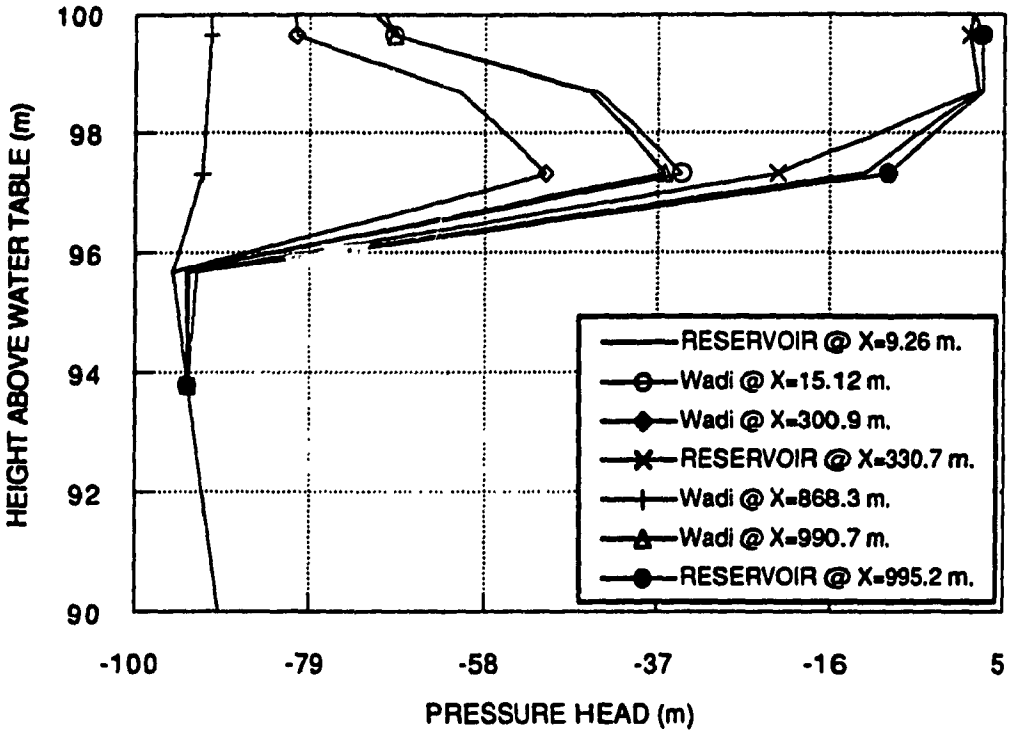

Fig.(6.17): Pressure Head Profile After 8 Days Of Simulation.

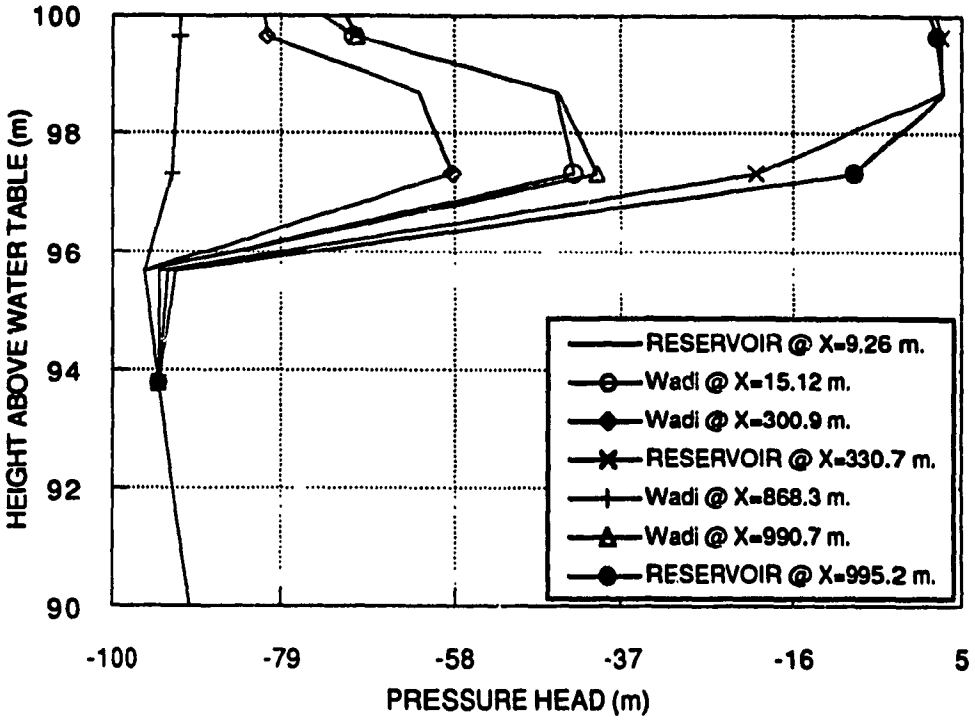

Fig.(6.18): Pressure Head Profile After 10 Days Of Simulation.

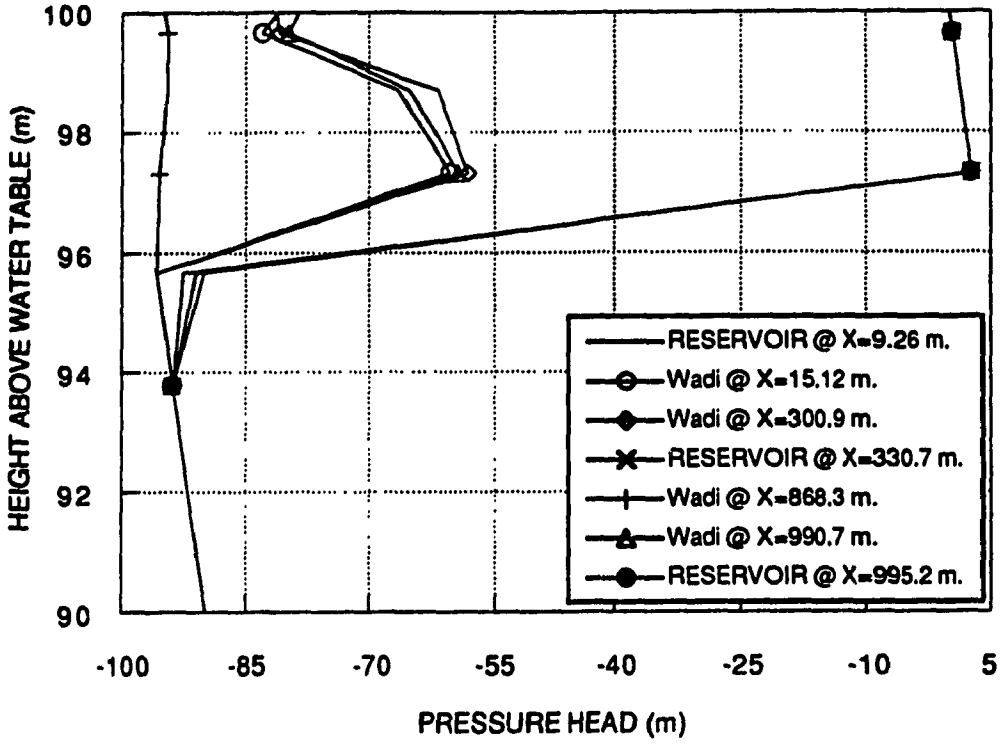

Fig.(6.19): Pressure Head Profile After 24 Days Of Simulation.

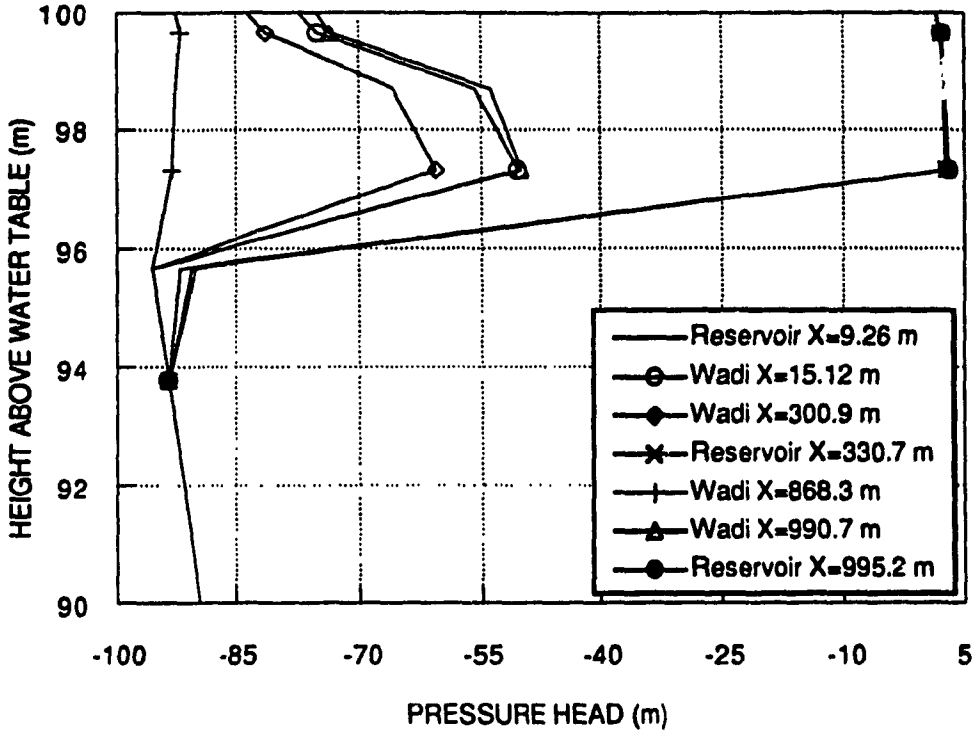

Fig.(6.20): Pressure Head Profile After 26 Days Of Simulation.

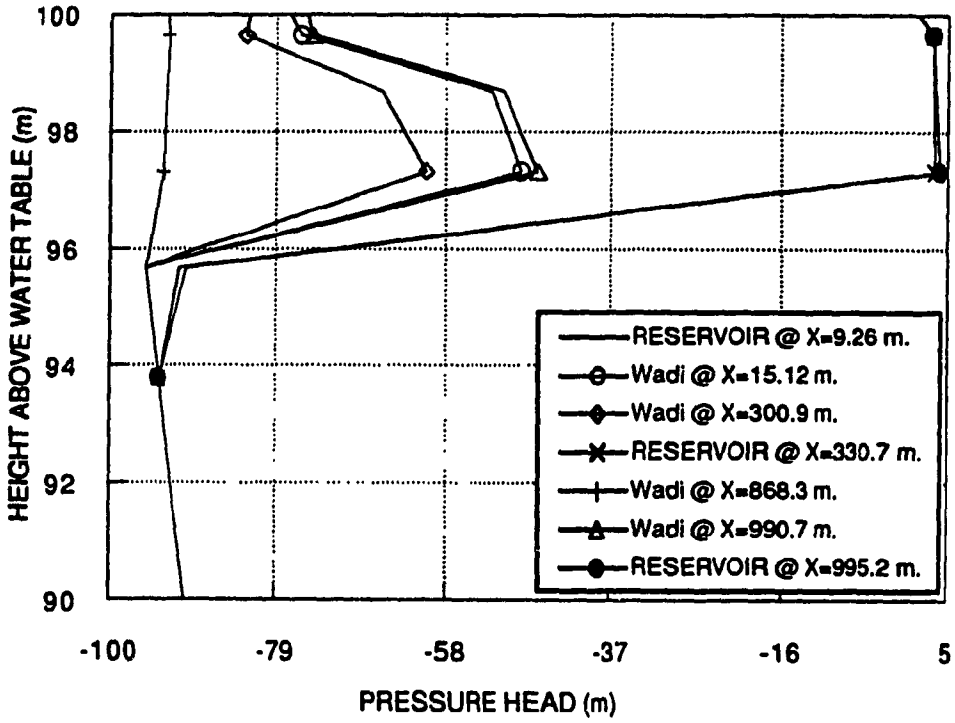

Fig.(6.21): Pressure Head Profile After 32 Days Of Simulation.

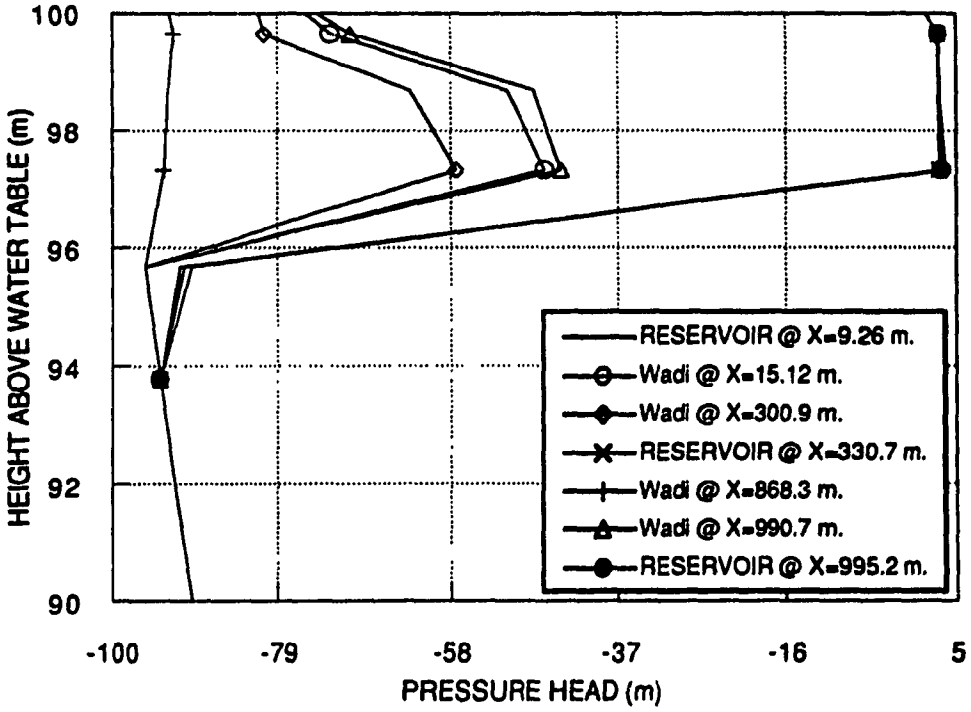

Fig.(6.22): Pressure Head Profile After 34 Days Of Simulation.

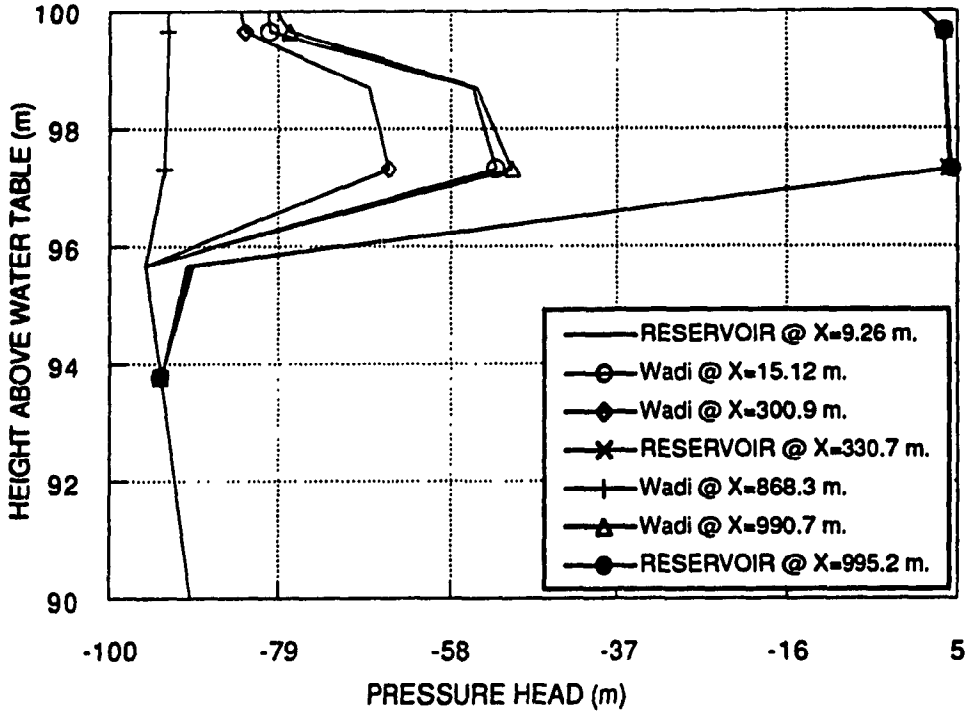

FIG.(6.23): Pressure Head Profile After 44 Days Of Simulation.

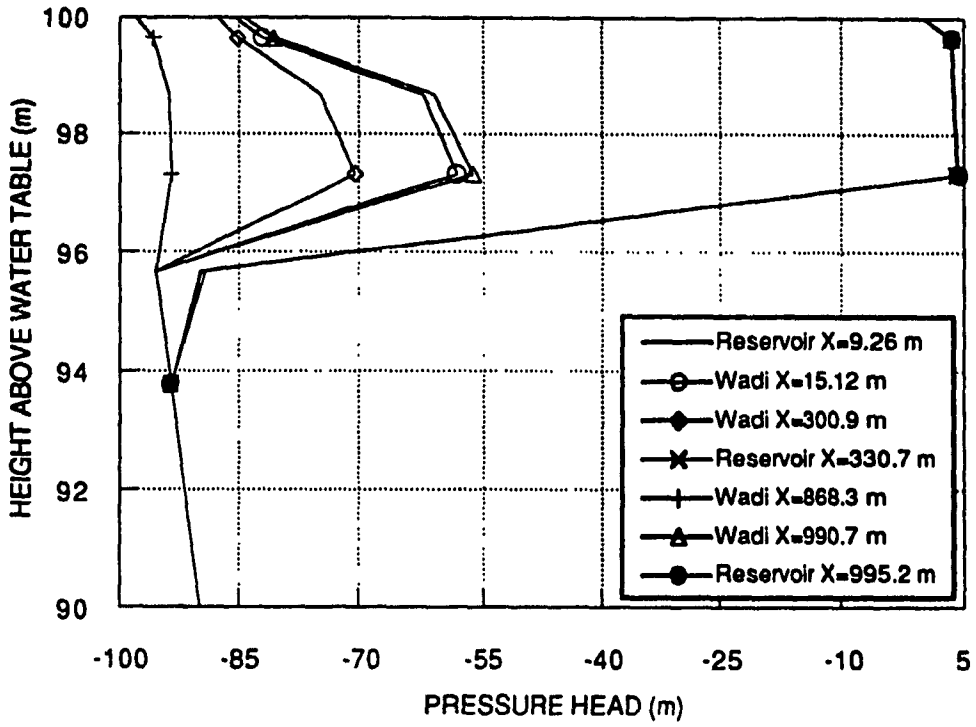

Fig.(6.24):Pressure Head Profile After 54 Days Of Simulation.

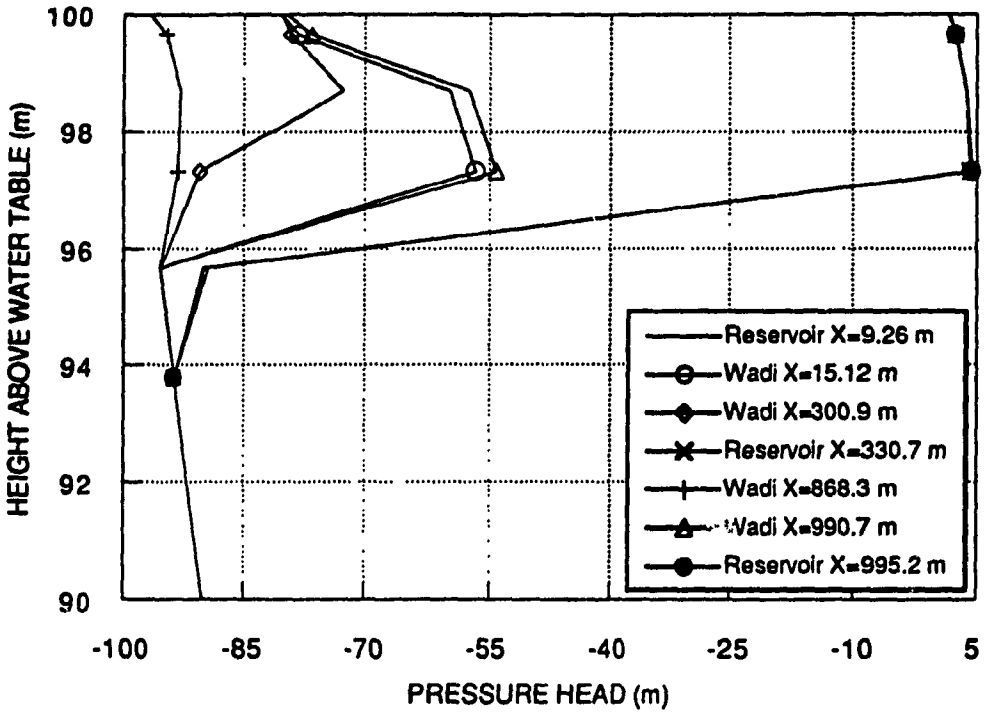

Fig.(6.25): Pressure Head Profile After 62 Days Of Simulation.

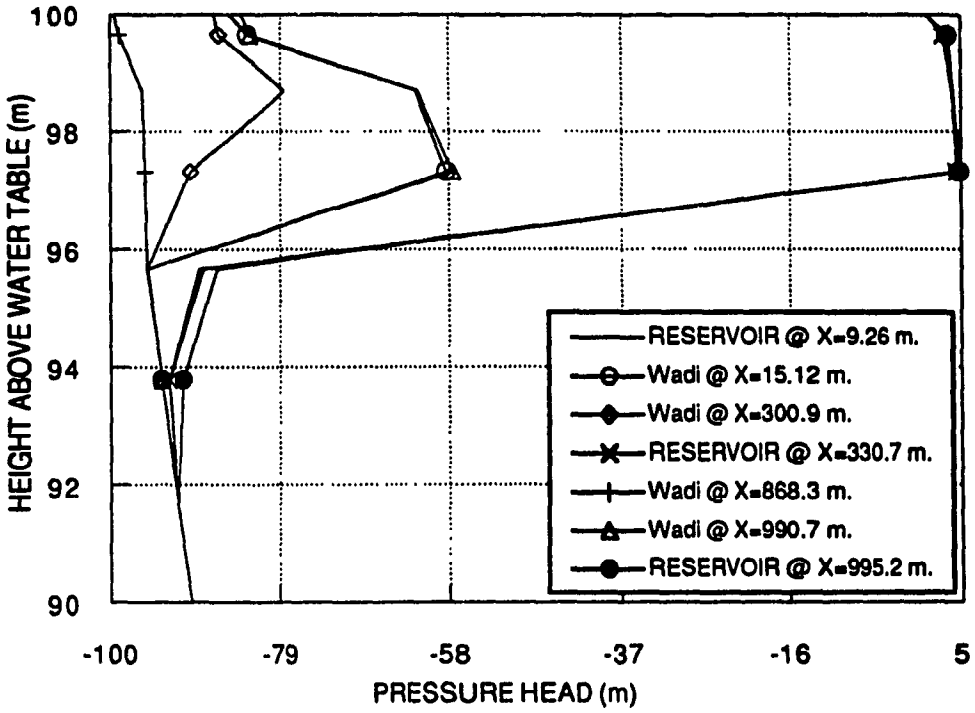

Fig.(6.26):Pressure Head Profile After 74 Days Of Simulation.

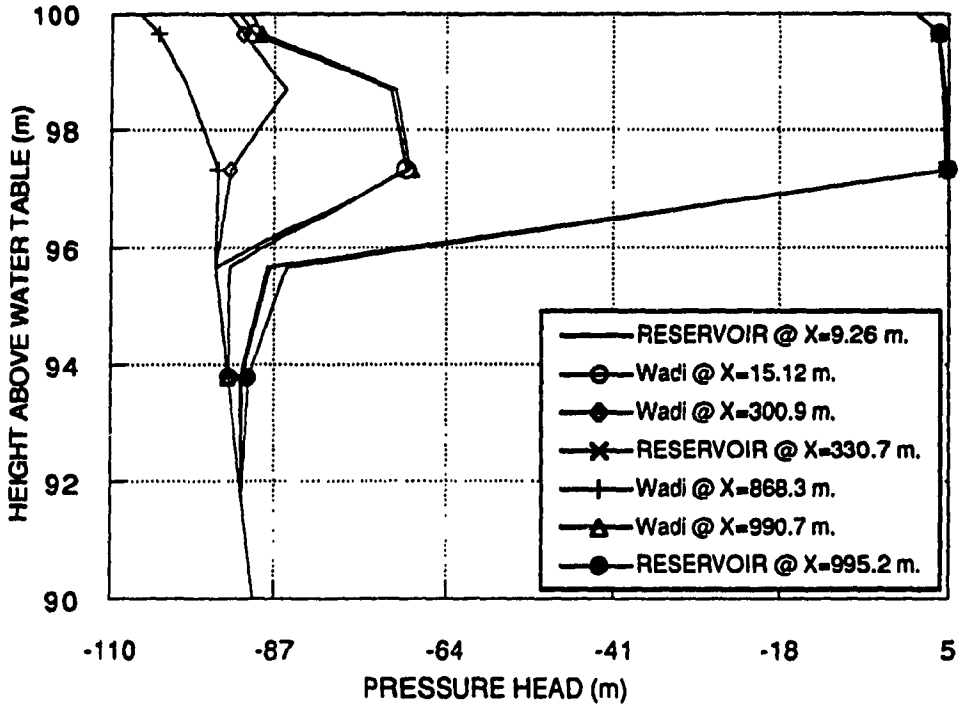

Fig.(6.27): Pressure Head Profile After 94 Days Of Simulation.

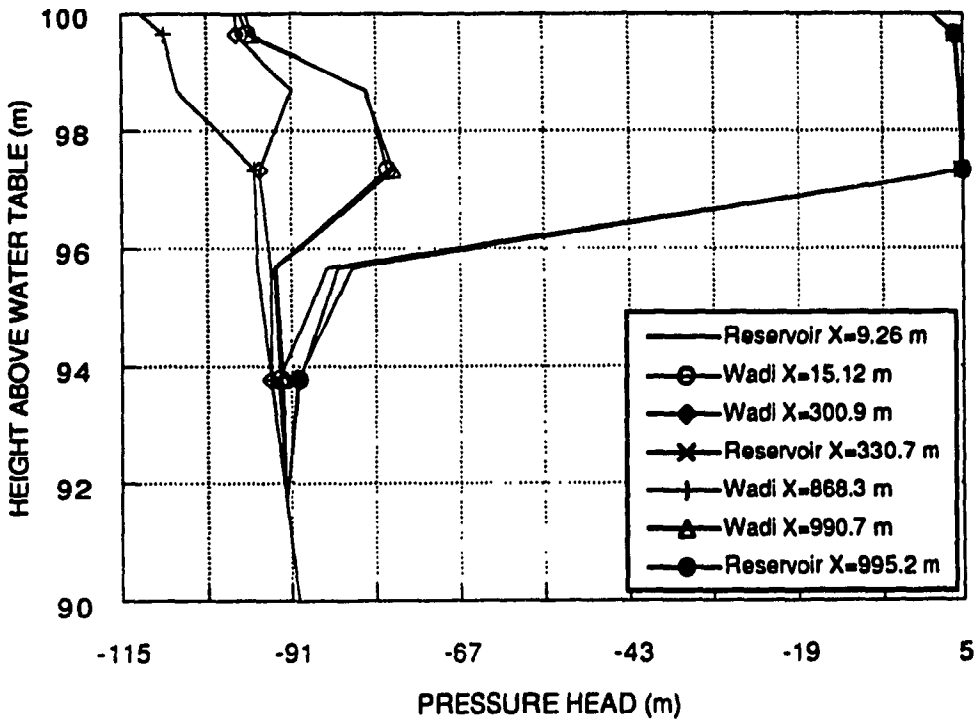

Fig.(6.28): Pressure Head Profile After 114 Days Of Simulation.

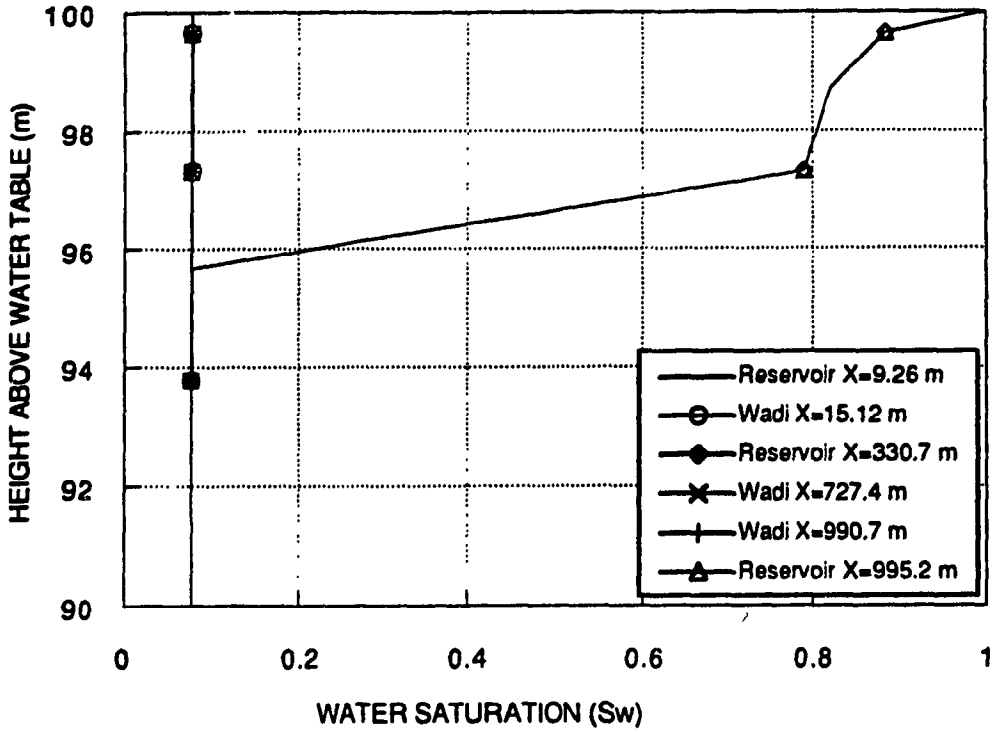

Fig.(6.29): Water Saturation Profile After 54 Days Of Simulation.

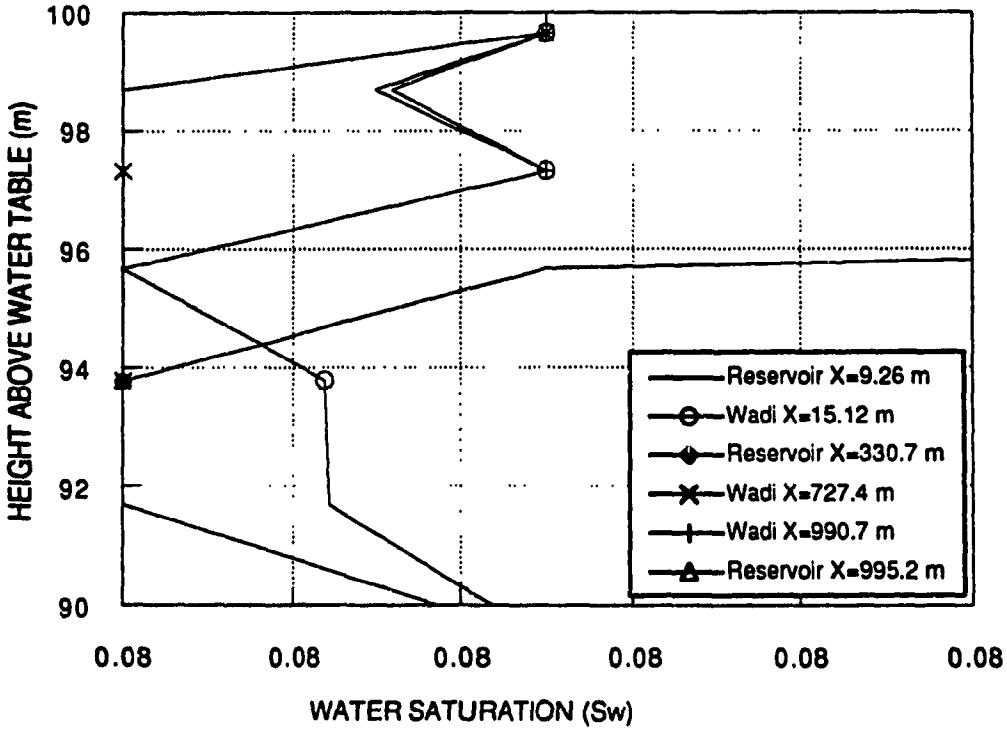

Fig.(6.29): DetailL Of Water Saturation Profile After 54 Days Of Simulation.

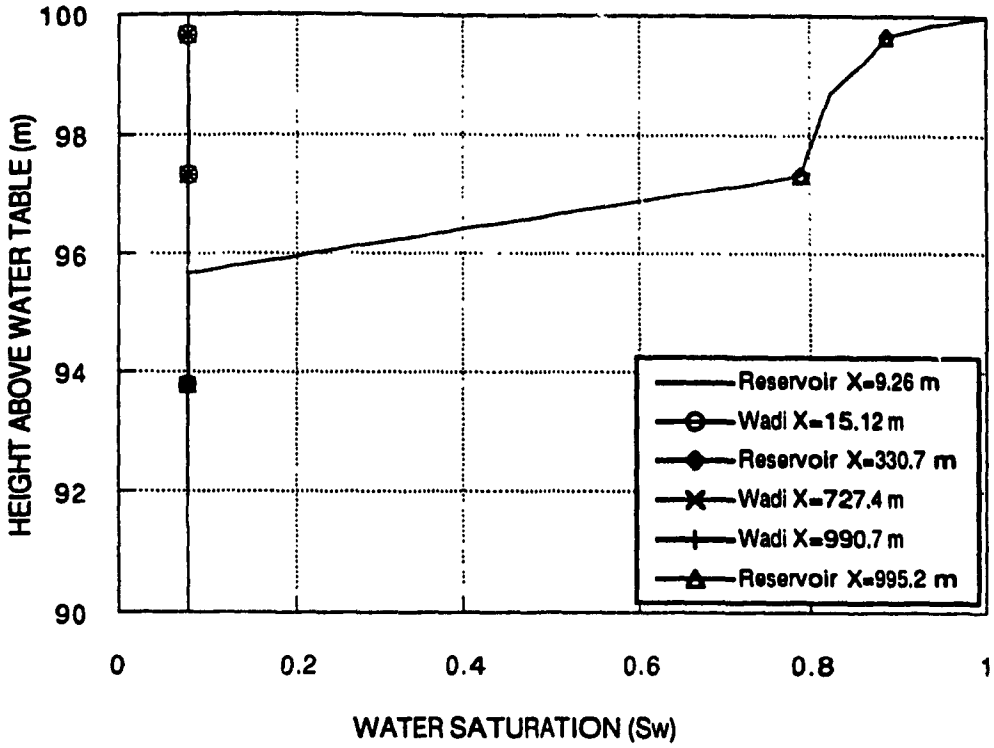

Fig.(6.30): Water Saturation Profile After 114 Days Of Simulation.

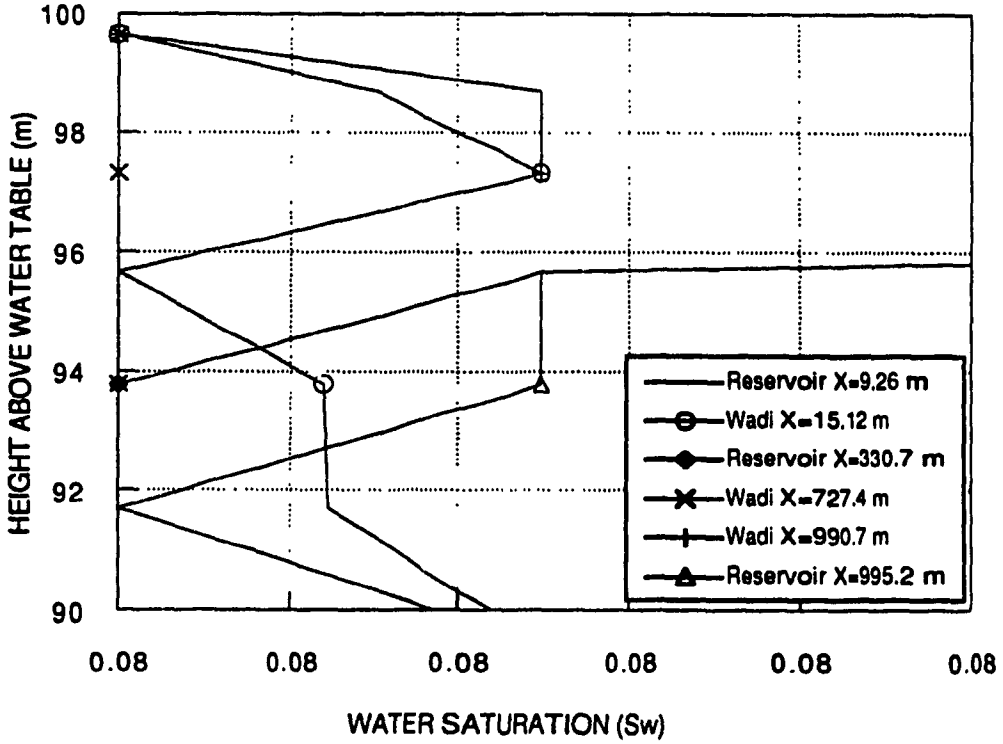

Fig.(6.30): Detail Of water Saturation Profile After 114 Days Of Simulation.

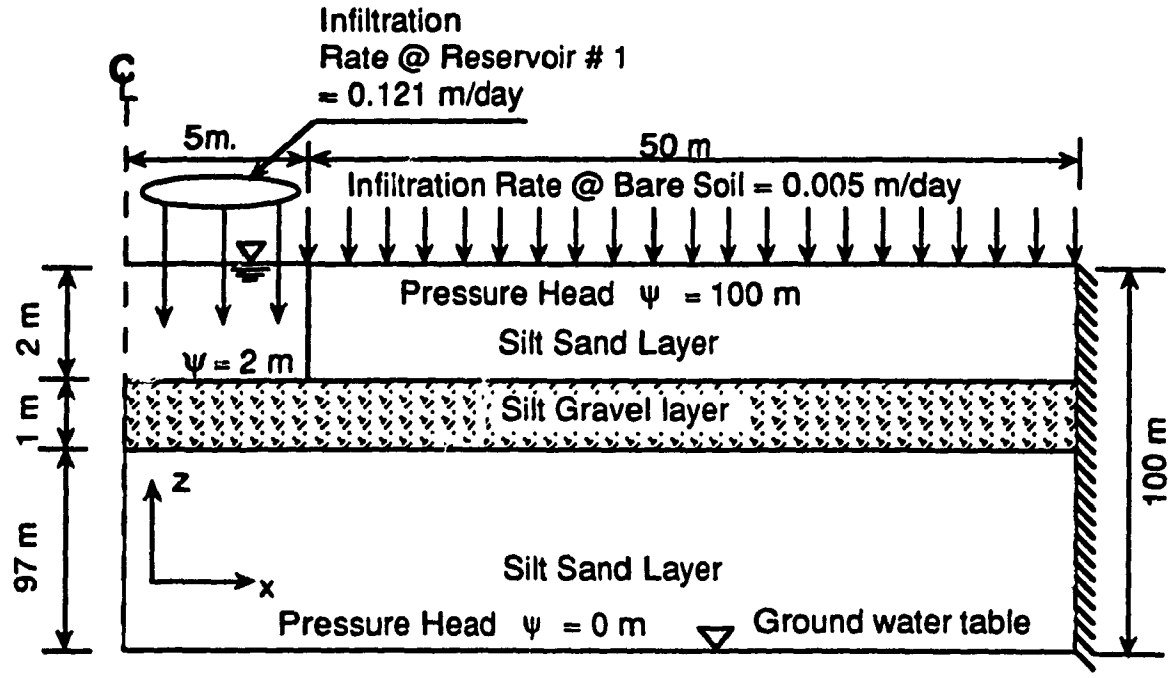

Fig.(6.31): Schematic Description of Muwaqar Case Study II

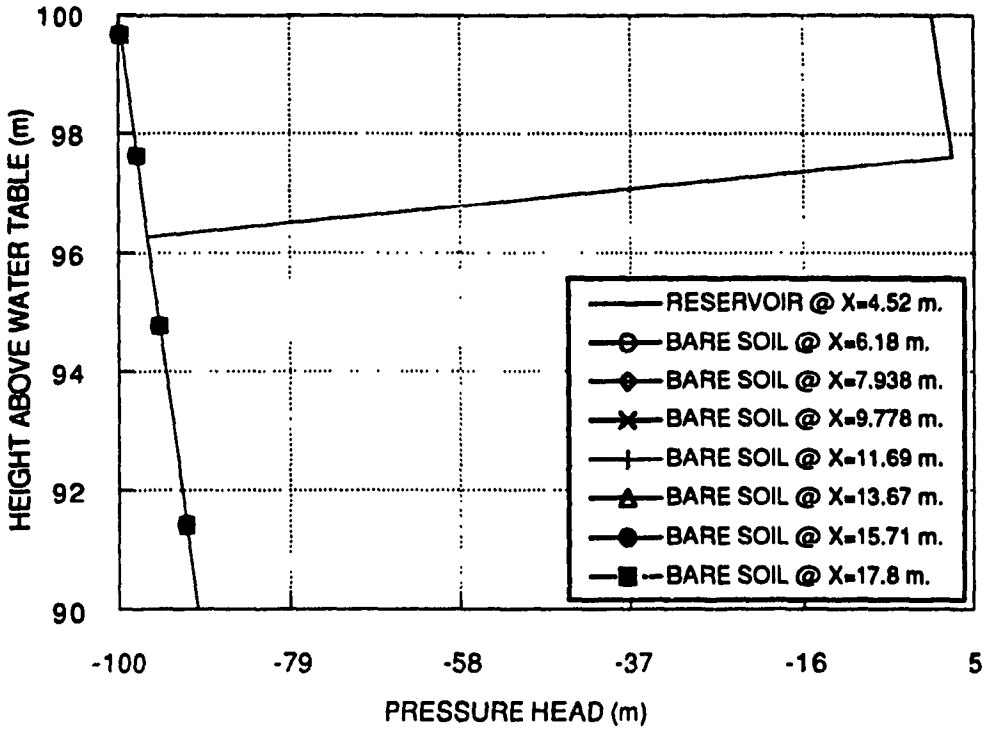

Fig.(6.32): Pressure Head Profile After 0 Days Of Simulation.

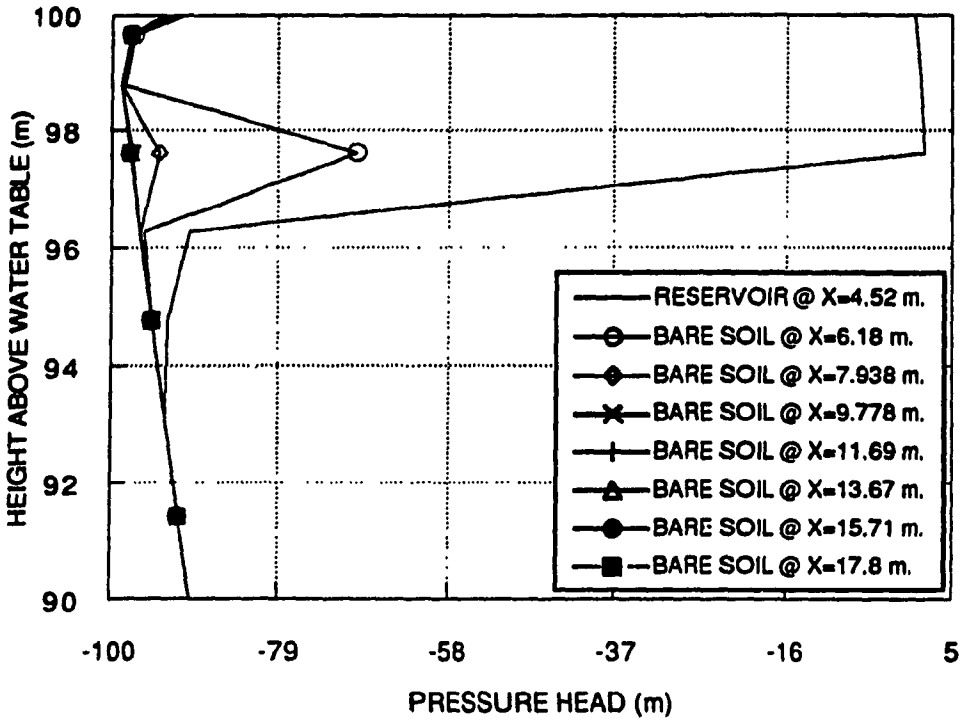

Fig.(6.33): Pressure Head Profile After 2 Days Of Simulation.

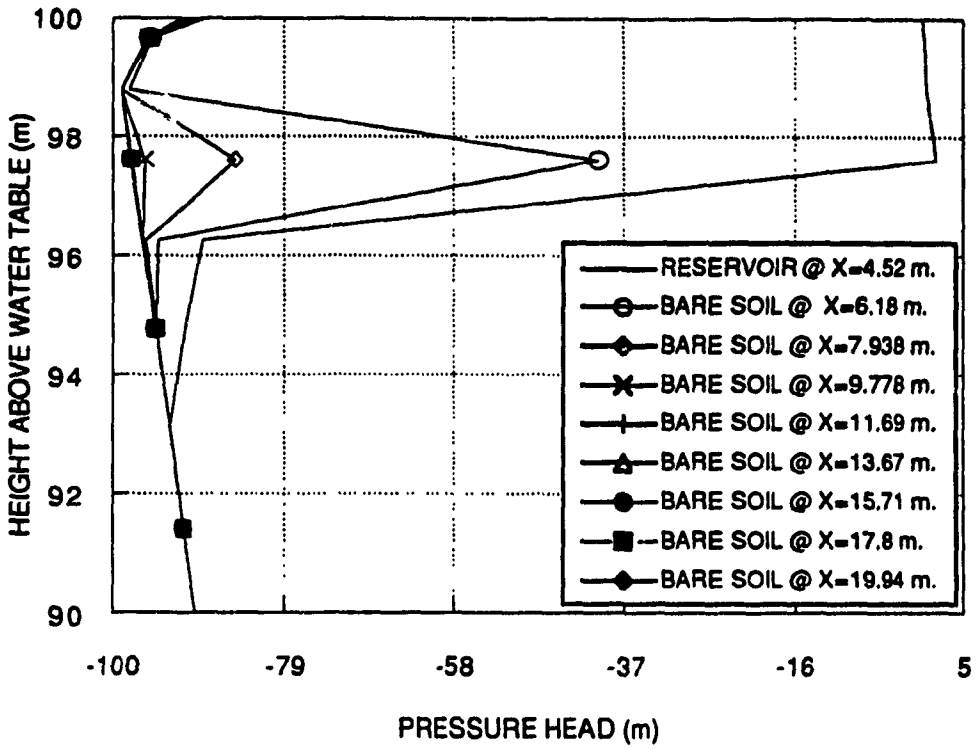

Fig.(6.34): Pressure Head Profile After 10 Days Of Simulation.

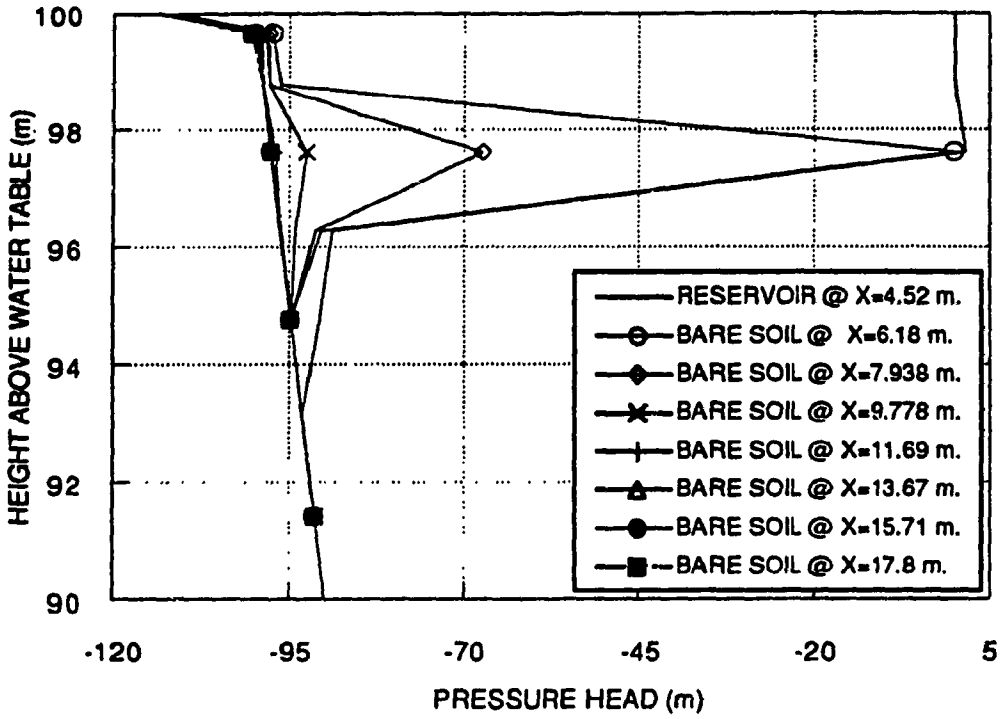

Fig.(6.35): Pressure Head Profile After 24 Days Of Simulation.

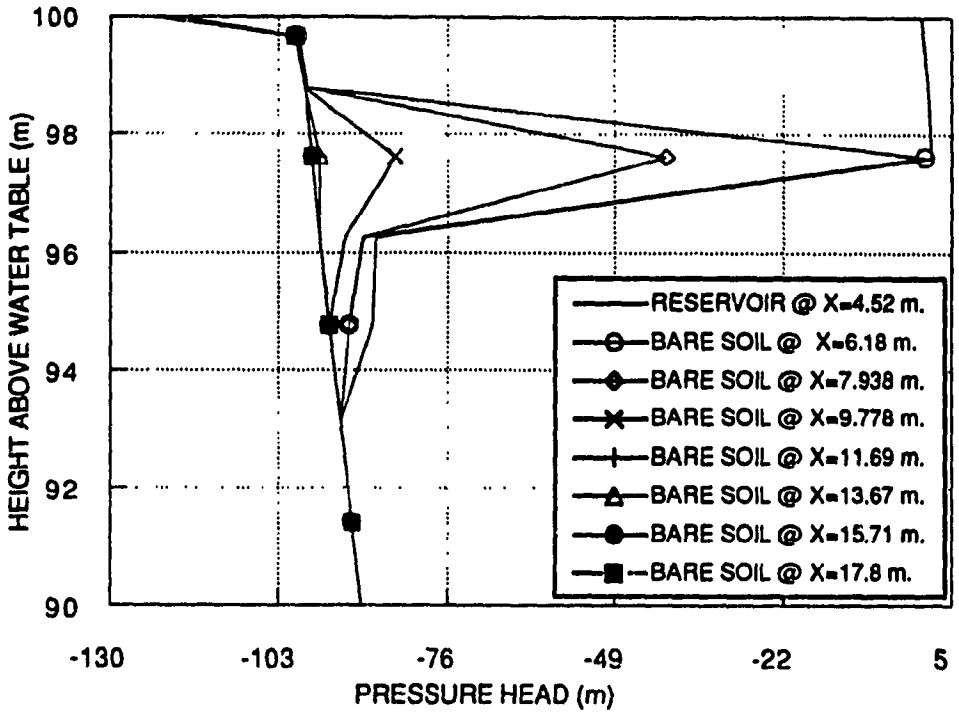

Fig.(6.36): Pressure Head Profile After 26 Days Of Simulation.

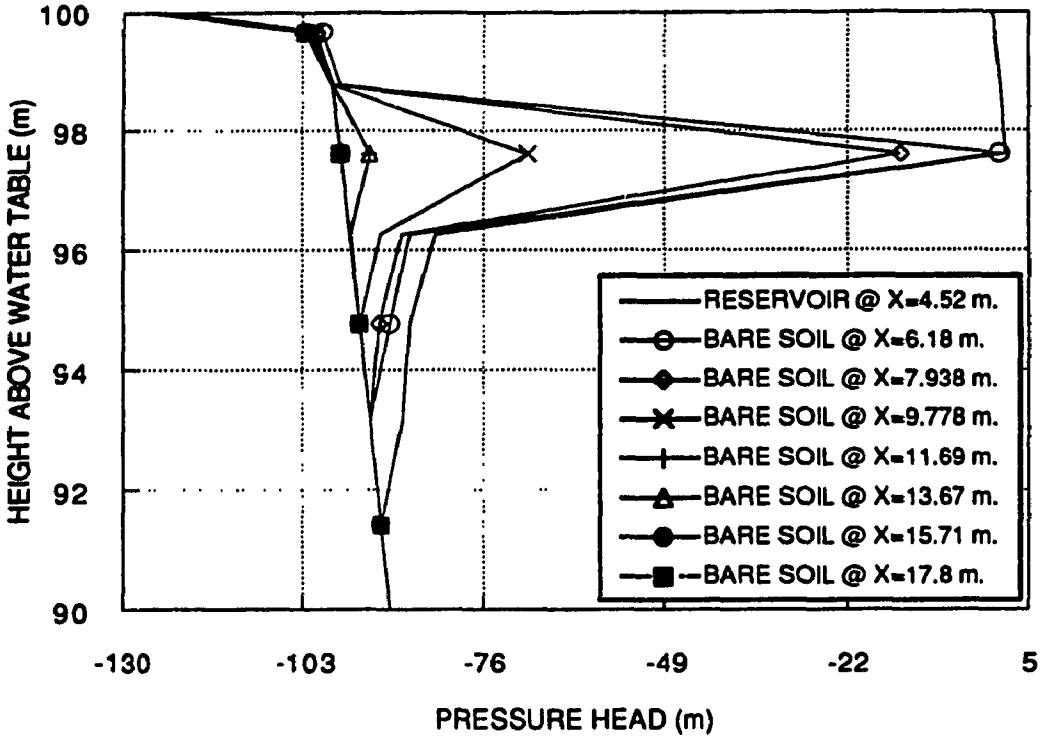

Fig.(6.37): Pressure Head Profile After 36 Days Of Simulation.

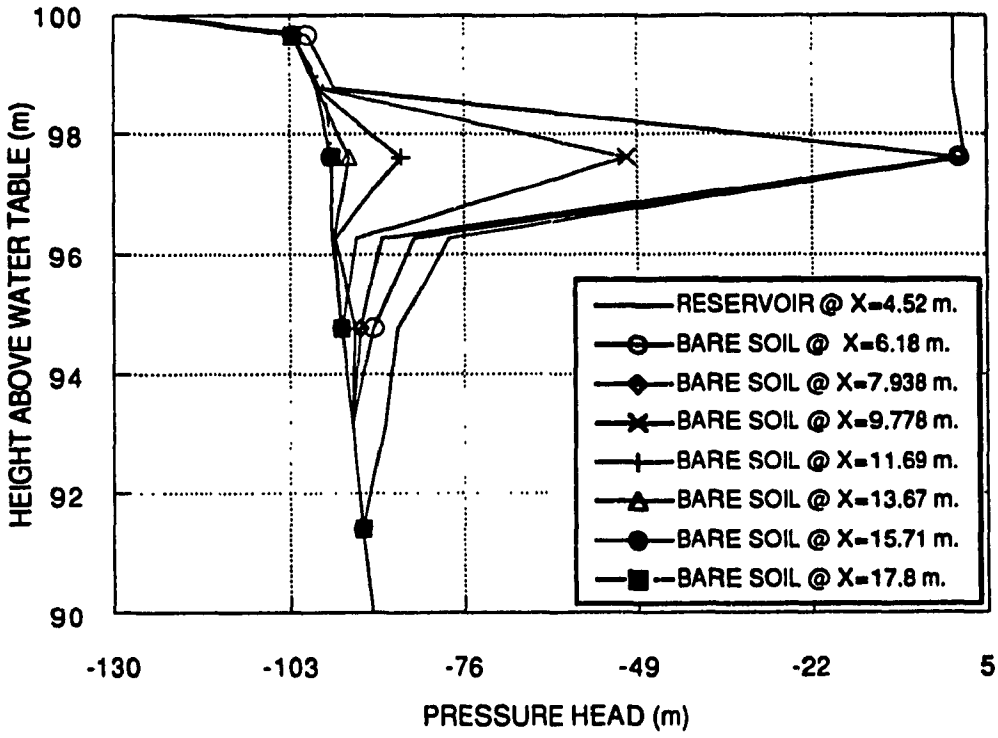

Fig.(6.38): Pressure Head Profile After 54 Days Of Simulation.

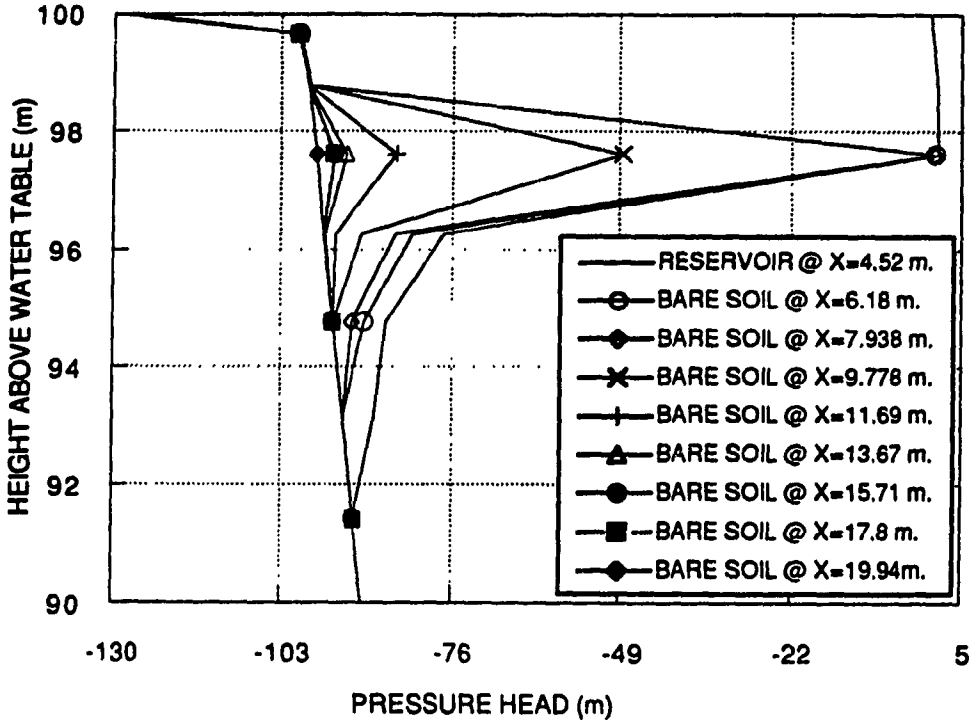

Fig.(6.39): Pressure Head Profile After 56 Days Of Simulation.

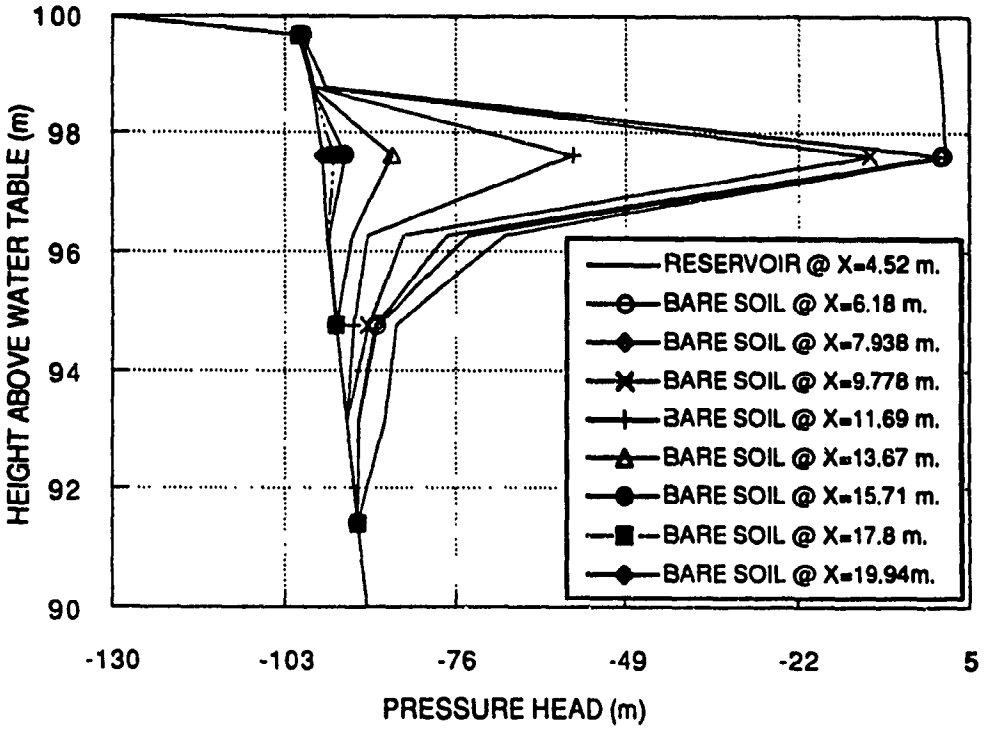

Fig.(6.40): Pressure Head Profile After 64 Days Of Simulation.

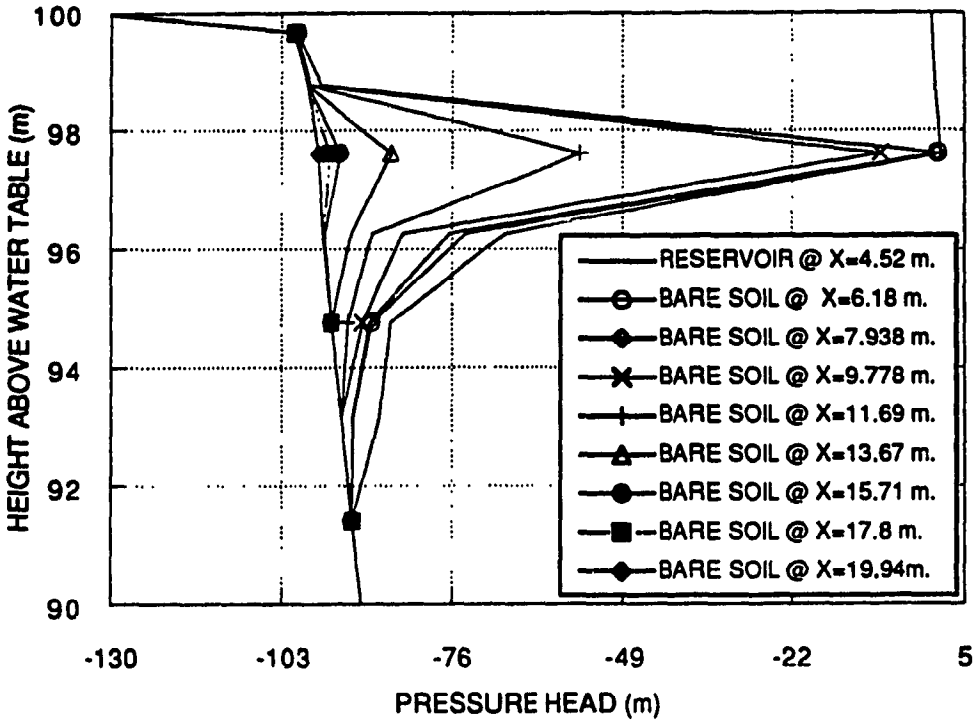

Fig.(6.41): Pressure Head Profile After 74 Days Of Simulation.

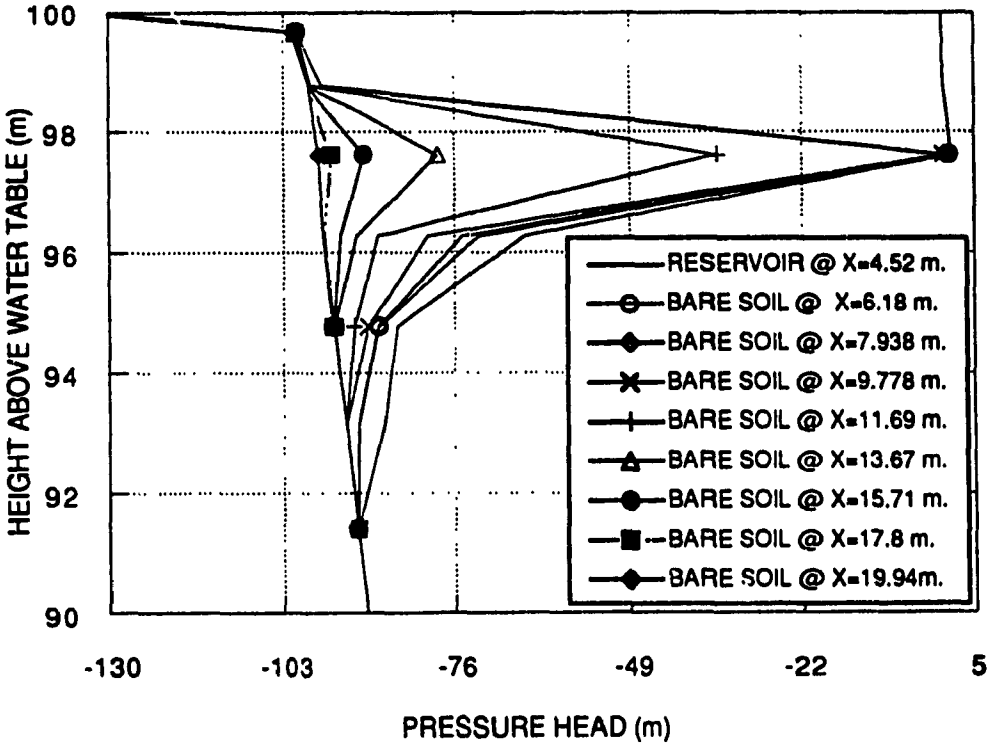

Fig.(6.42): Pressure Head Profile After 94 Days Of Simulation.

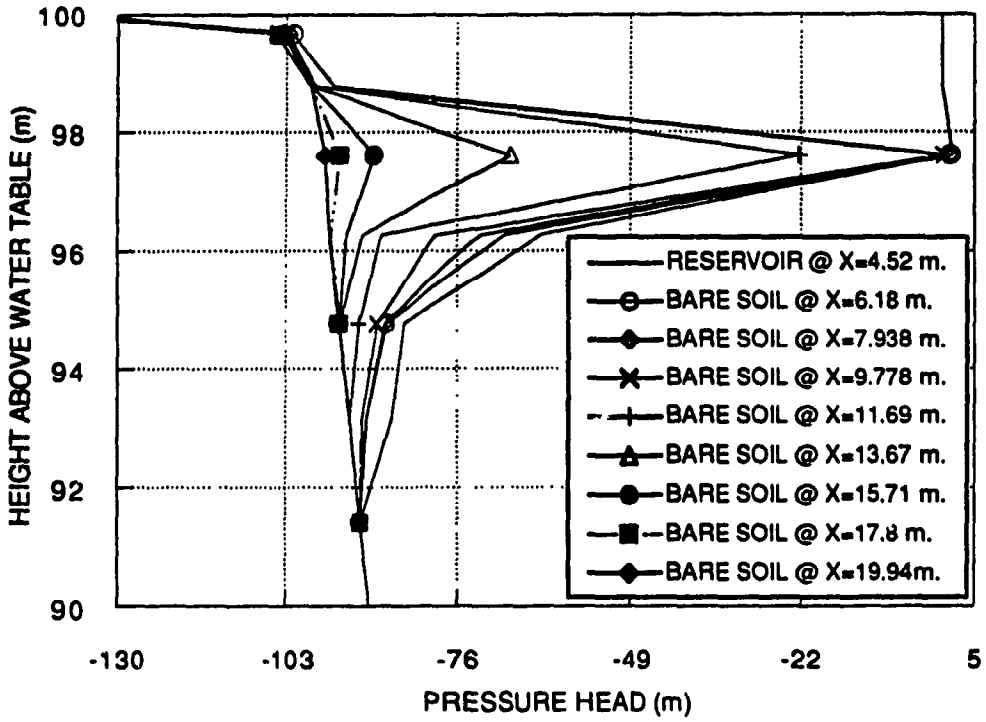

Fig.(6.43): Pressure Head Profile After 114 Days Of Simulation.

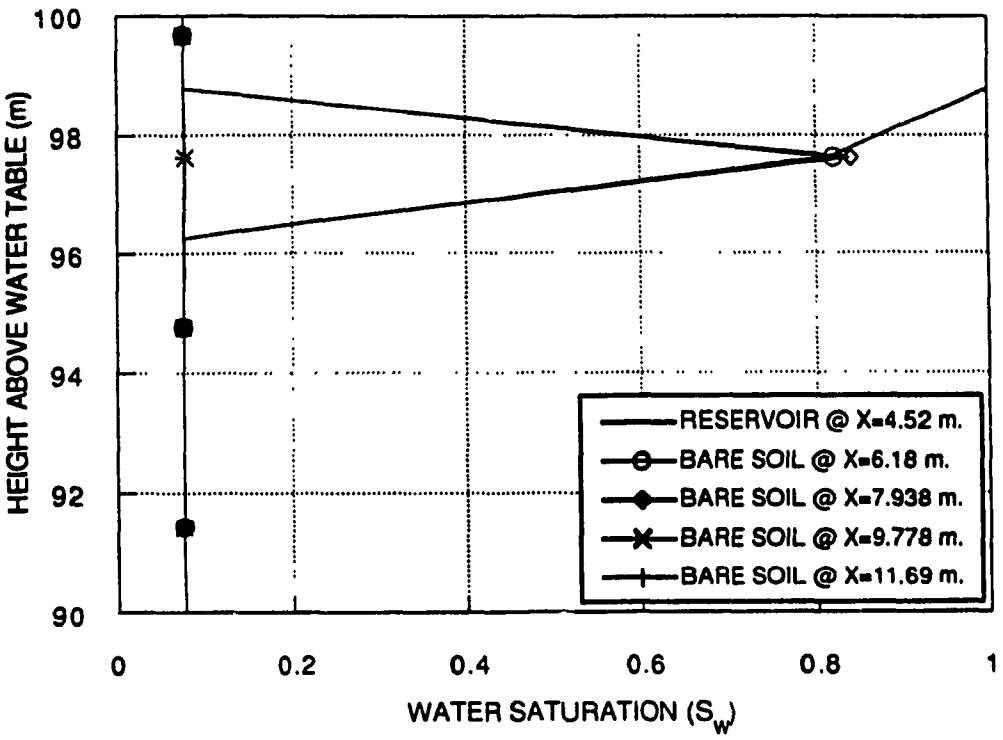

Fig.(6.44): Water Saturation Profile After 54 Days Of Simulation.

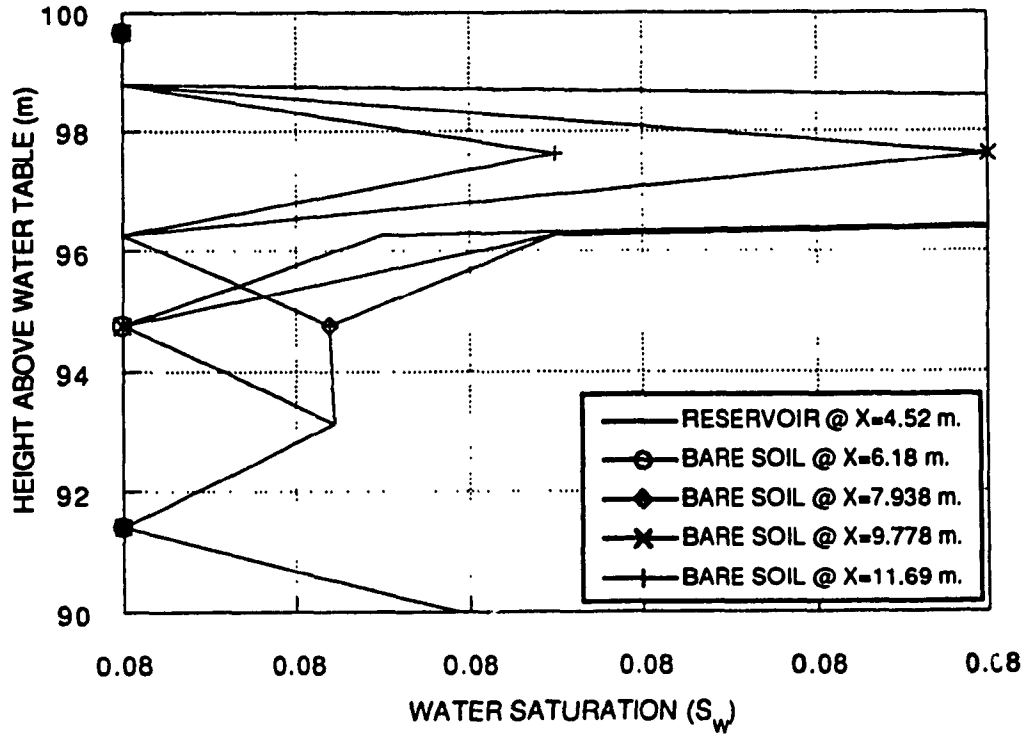

Fig.(6.44): Detail Of Water Saturation Profile After 54 Days Of Simulation.

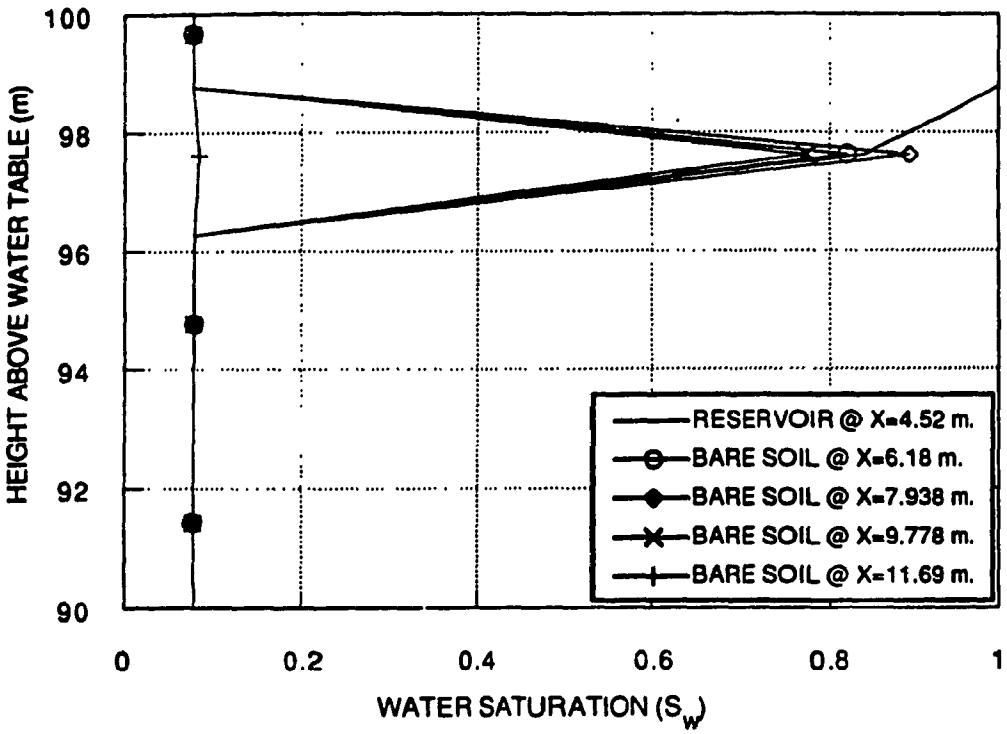

Fig.(6.45): Water Saturation Profile After 114 Days Of Simulation.

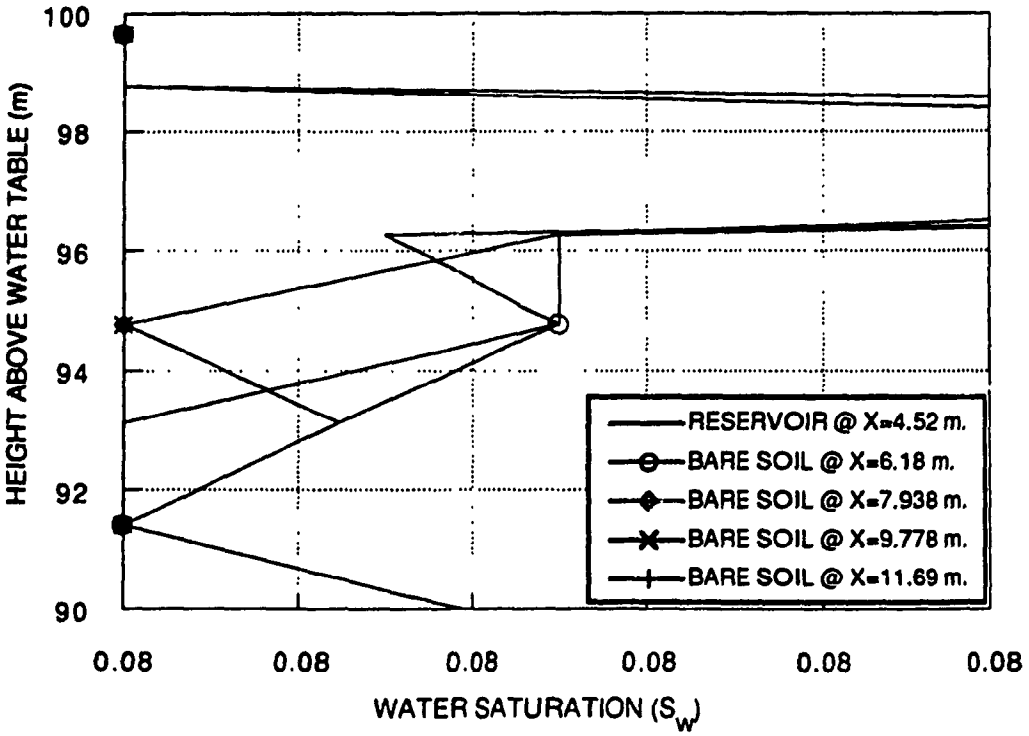

Fig.(6.45): Detail Of Water Saturation Profile After 114 Days Of Simulation.

APPENDIX C

Results Of The Optimization Simulation

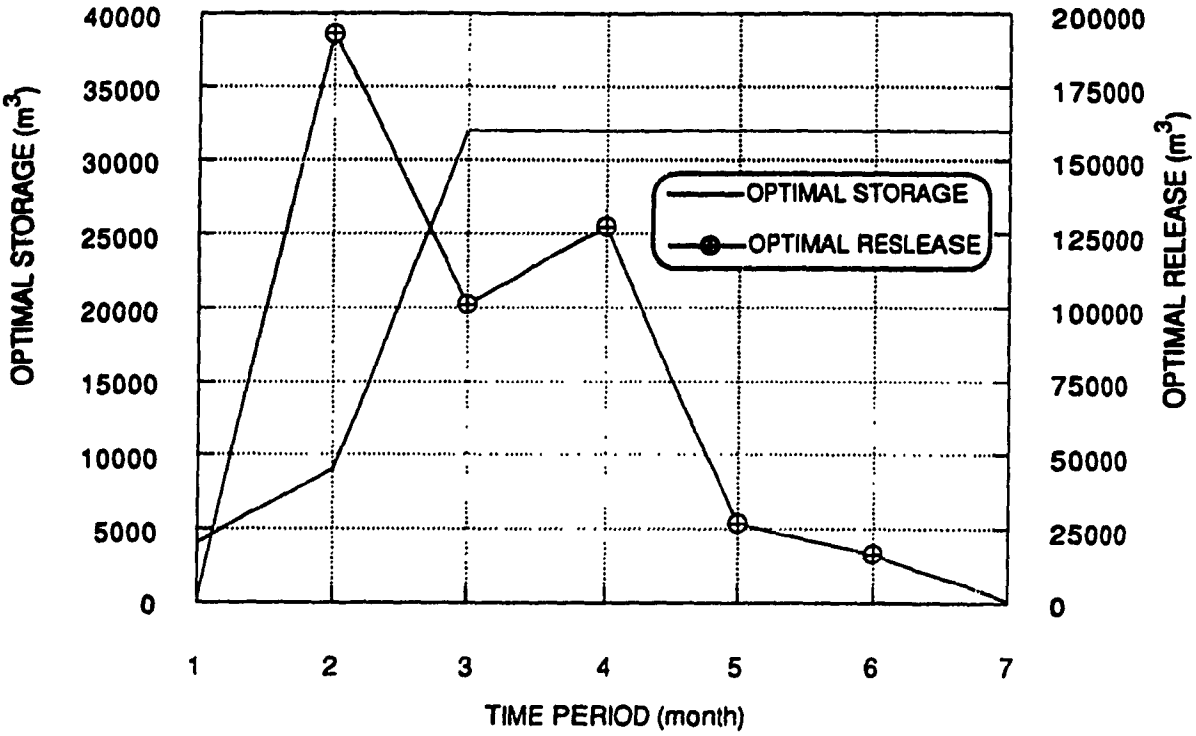

Fig.(6.46): Optimum Monthly Storage &Release Trajectories Of Reservoir No.1

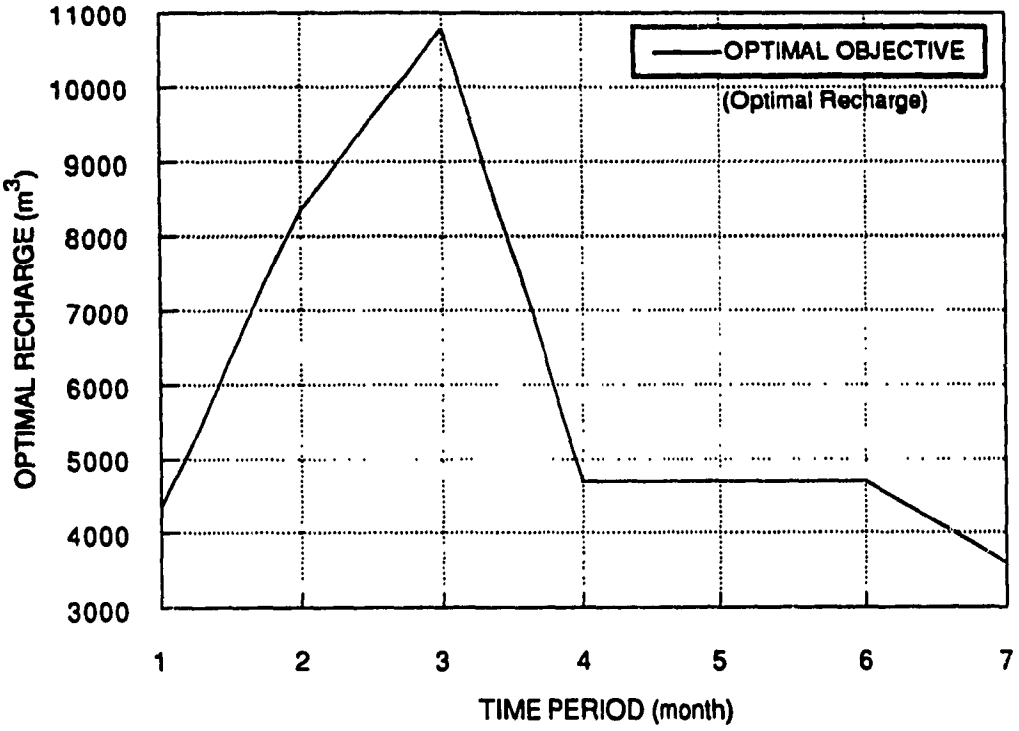

Fig.(6.47): Optimum Monthly Recharge Function Of Reservoir No.1

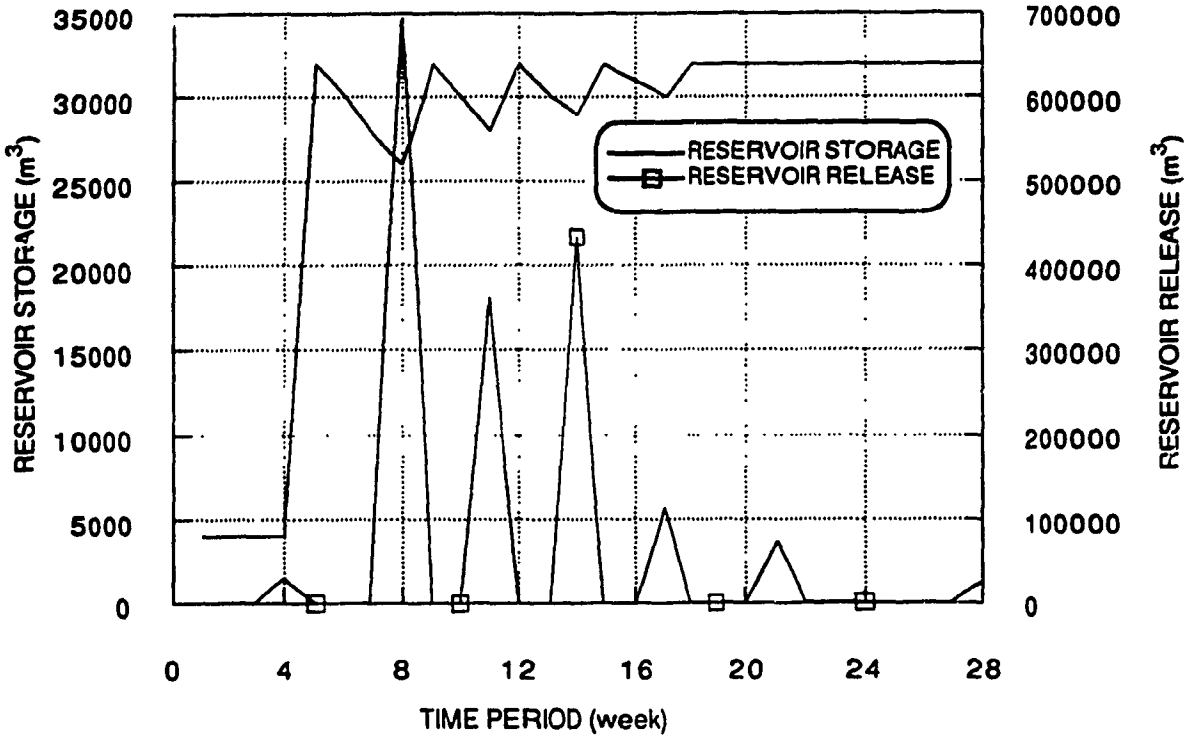

Fig.(6.48): Optimum Weekly Storage &Release Trejectories Of Reservoir No. 1.

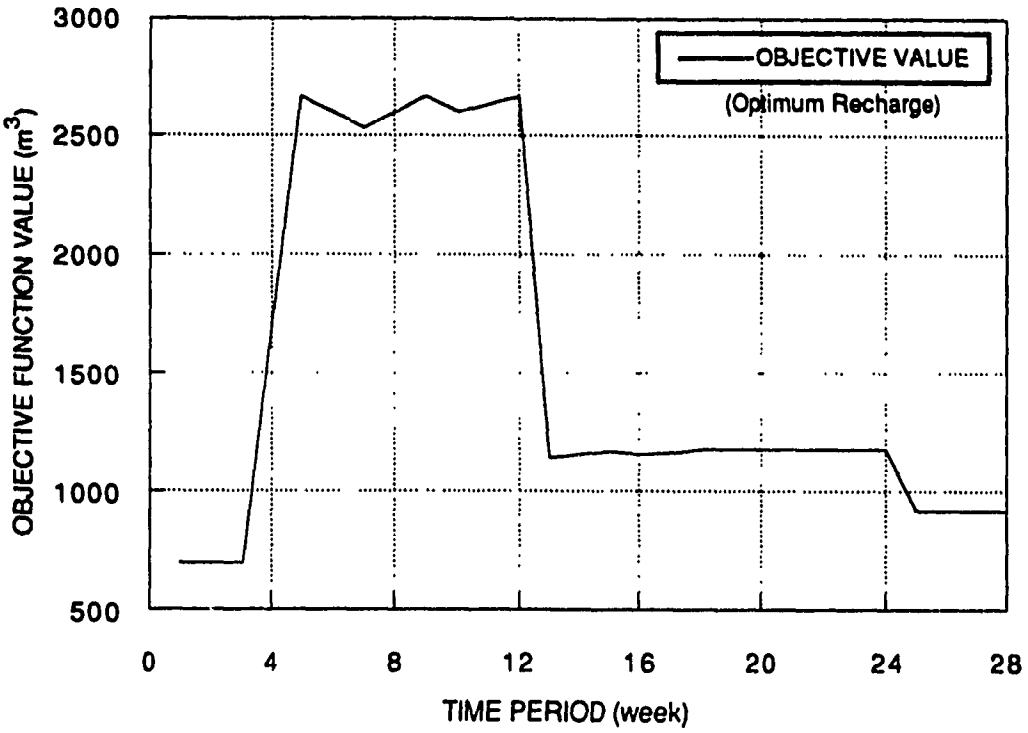

Fig.(6.49): Optimum Weekly Recharge Function Of Reservoir No.1

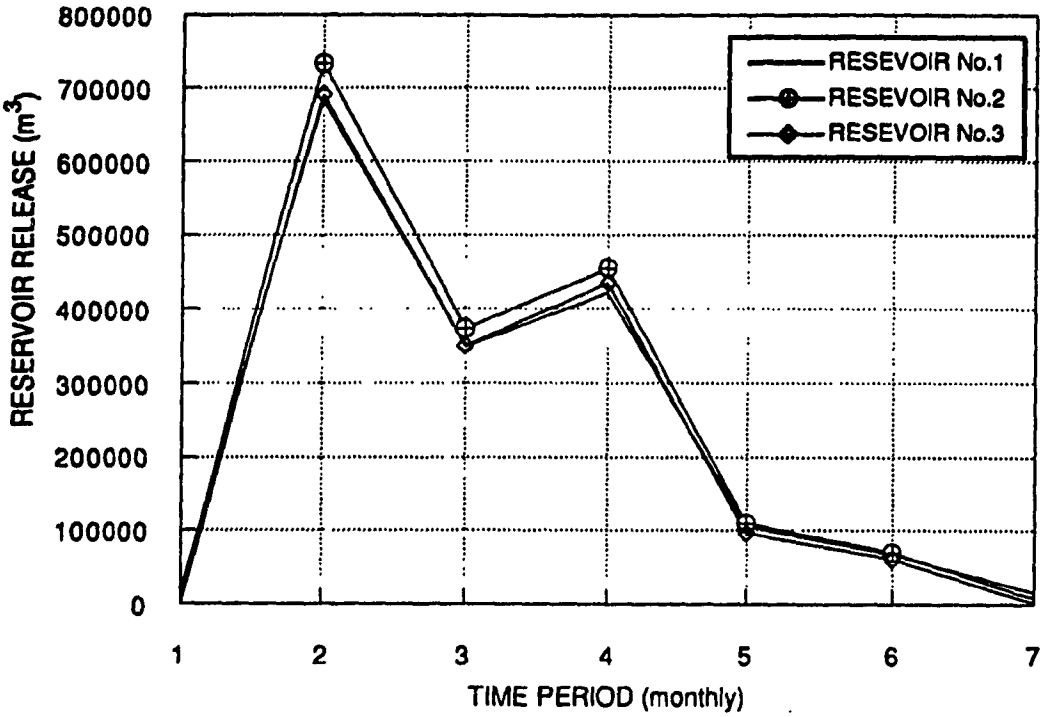

Fig.(6.50): Optimum Release Trajectories Of The Three Reservoirs.

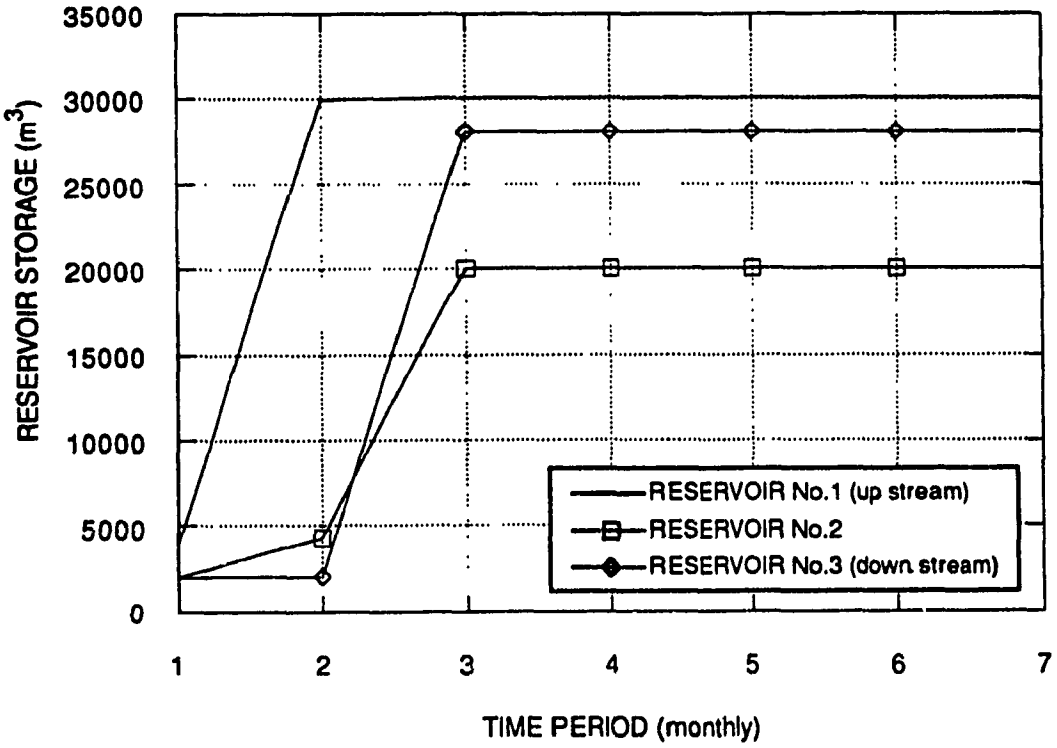

Fig.(6.51): Optimum Monthly Storage Trajectories Of The Three Reservoirs.

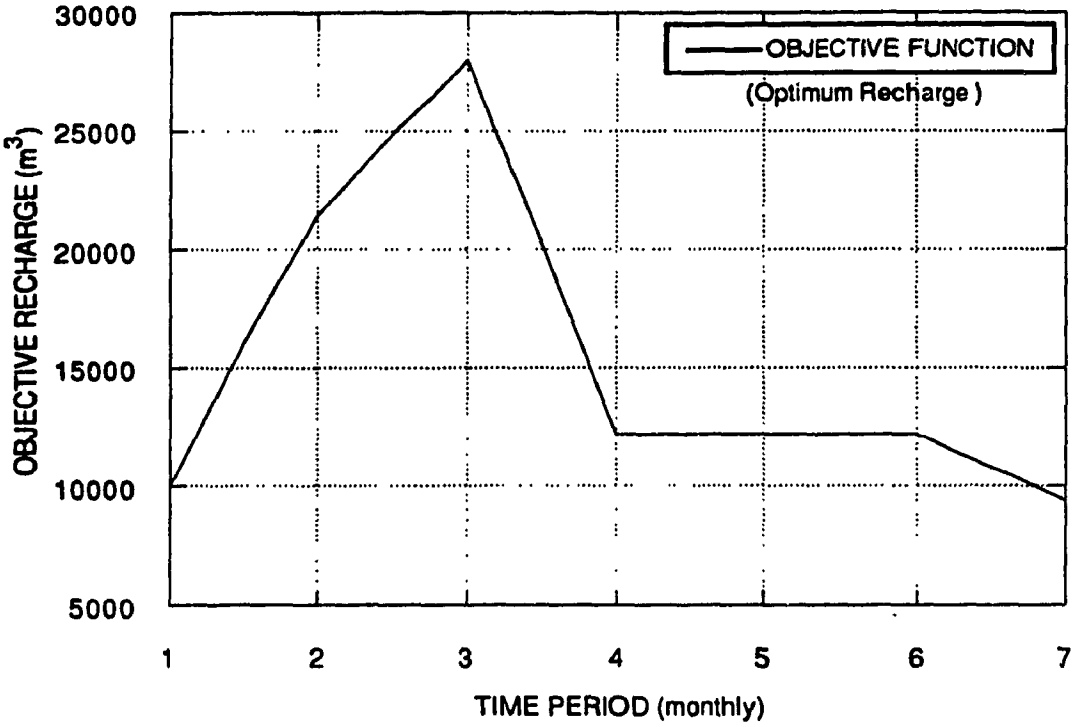

Fig.(6.52): Optimum Monthly Recharge Of The Three Reservoirs.

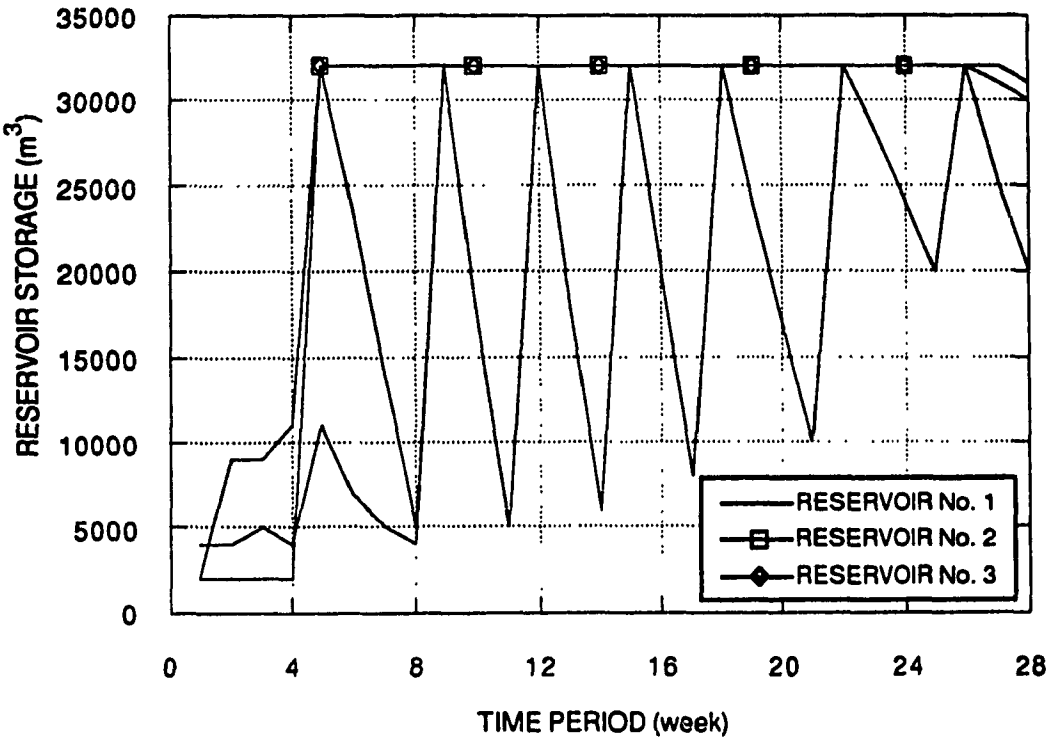

Fig.(6.53): Optimum Weekly Storage Trajectories Of The Three Reservoirs.

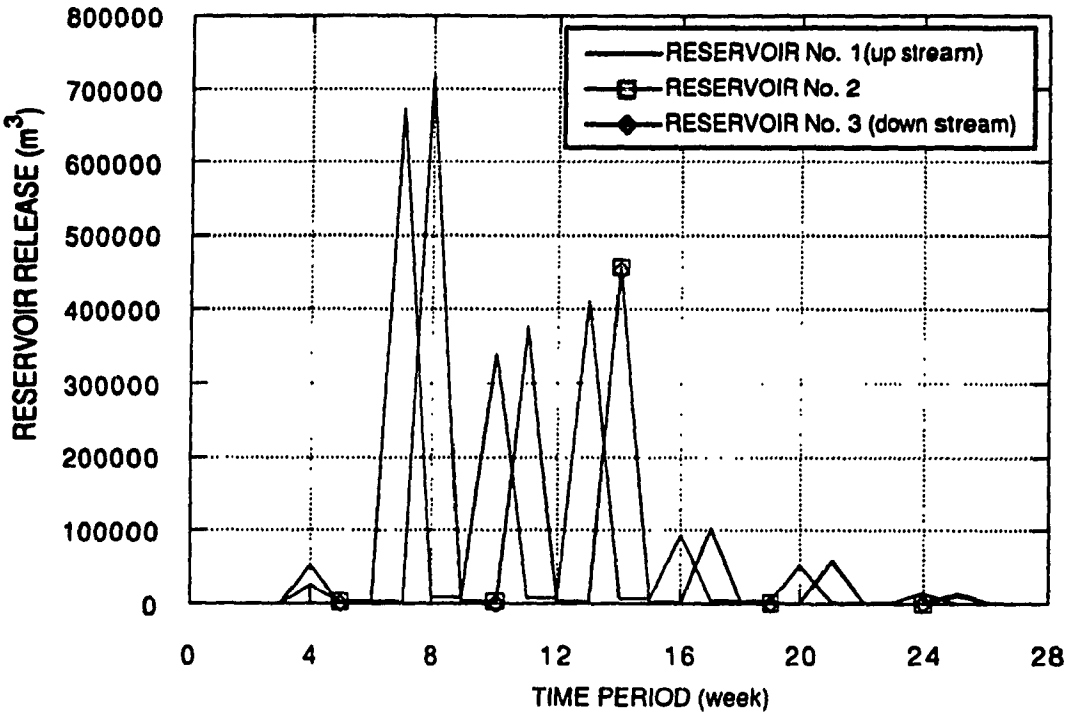

Fig.(6.54): Optimum Weekly release Trajectories Of The Three Reservoirs.

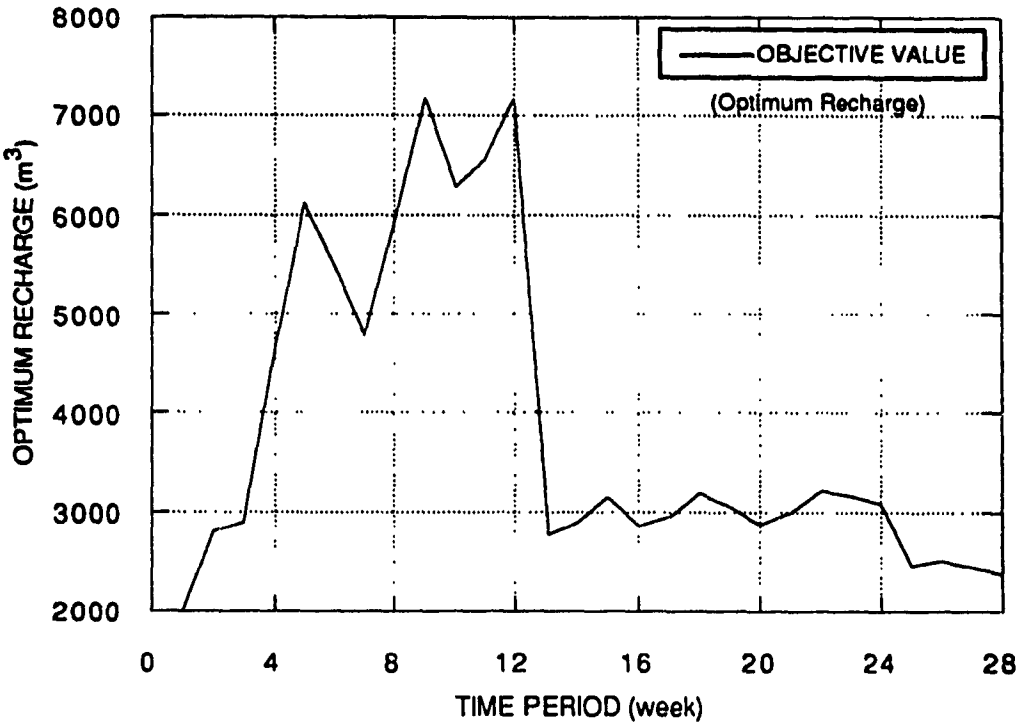

Fig.(6.55): Optimum Weekly Recharge Of The Three Reservoirs.

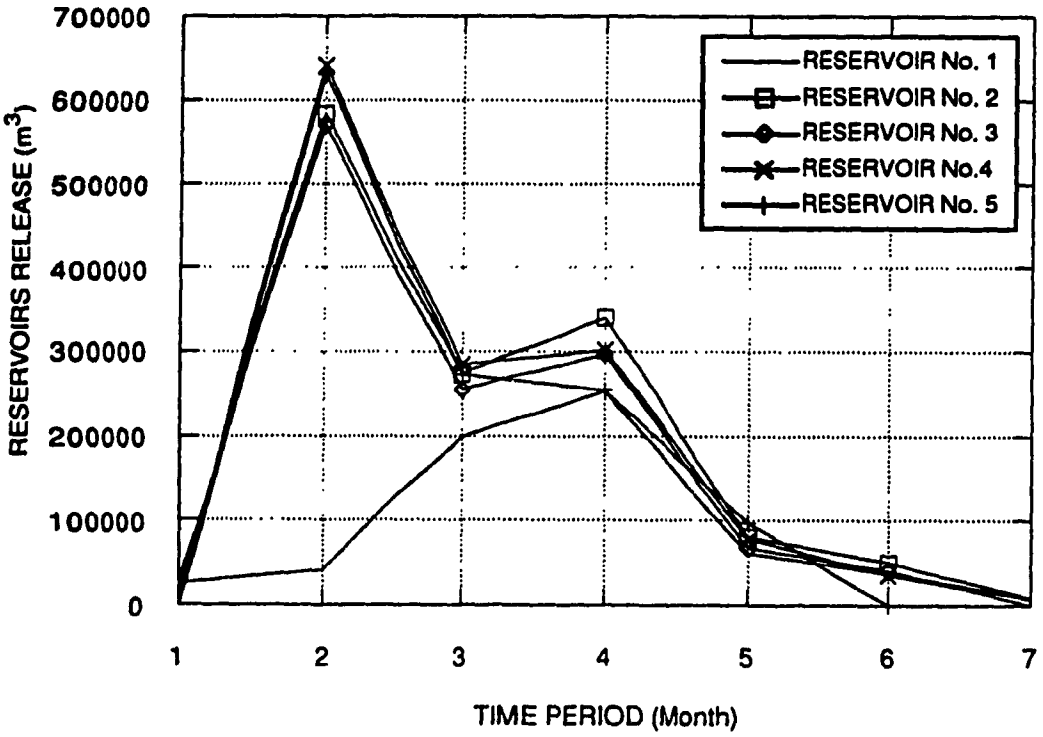

Fig.(6.56): Optimum Monthly Release Trajectories Of The Five Reservoirs.

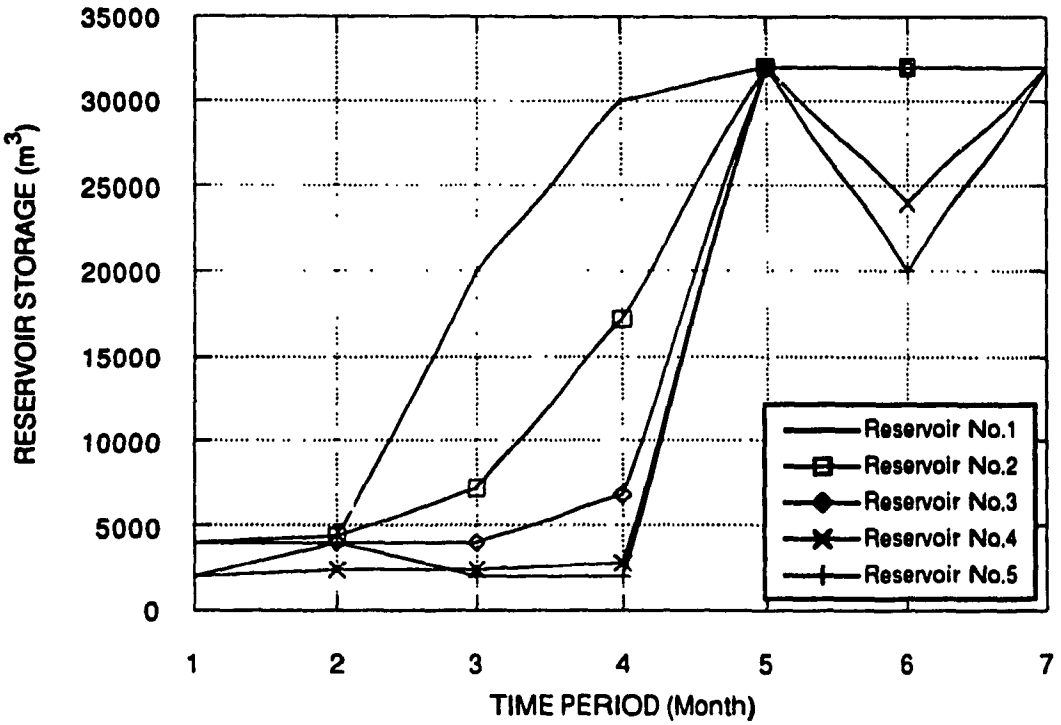

Fig.(6.57): Optimum Monthly Storage Trajectories Of The Five Reservoirs.

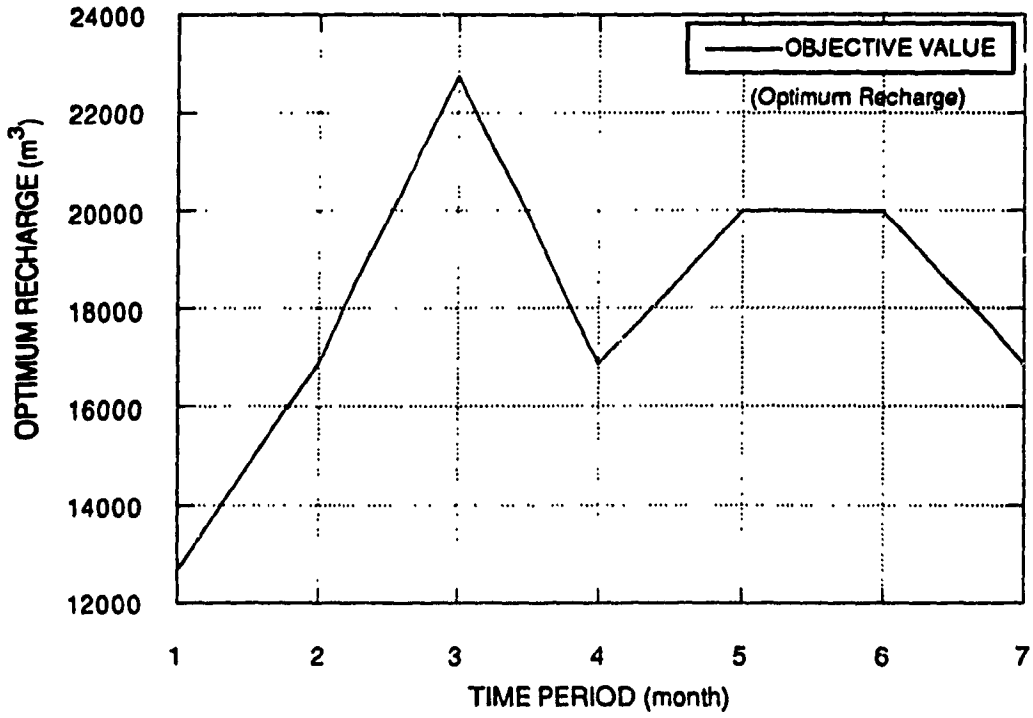

Fig.(6.58): Optimum Monthly Recharge Function For The Five Reservoirs.

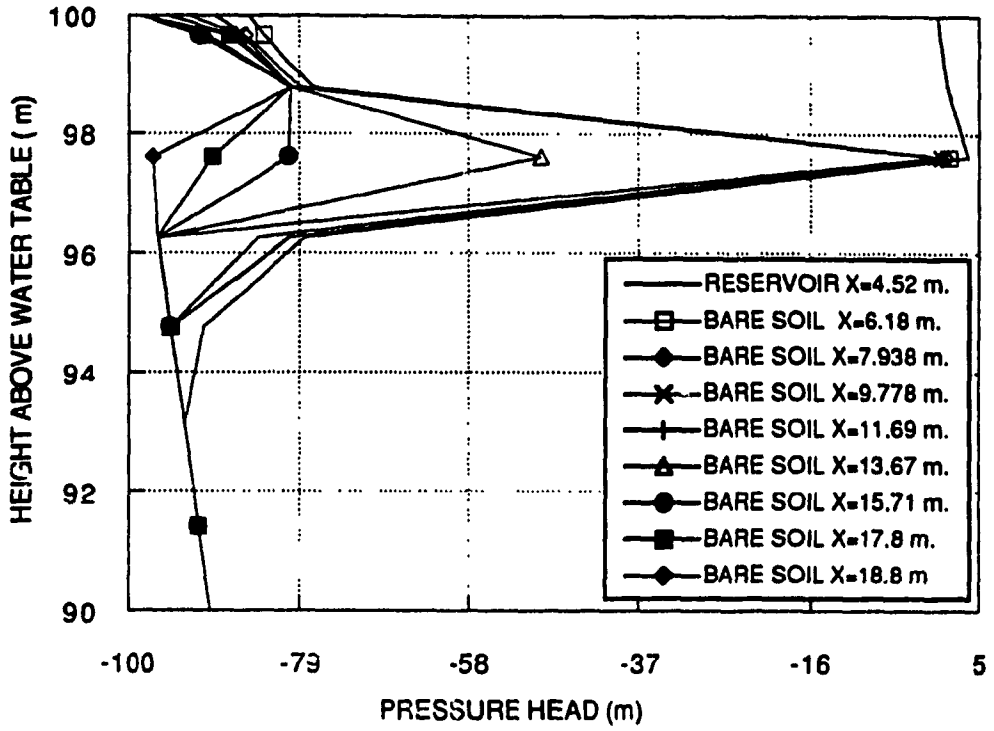

Fig.(6.59): Optimal Pressure Head Profile After 24 days Of Simulation.

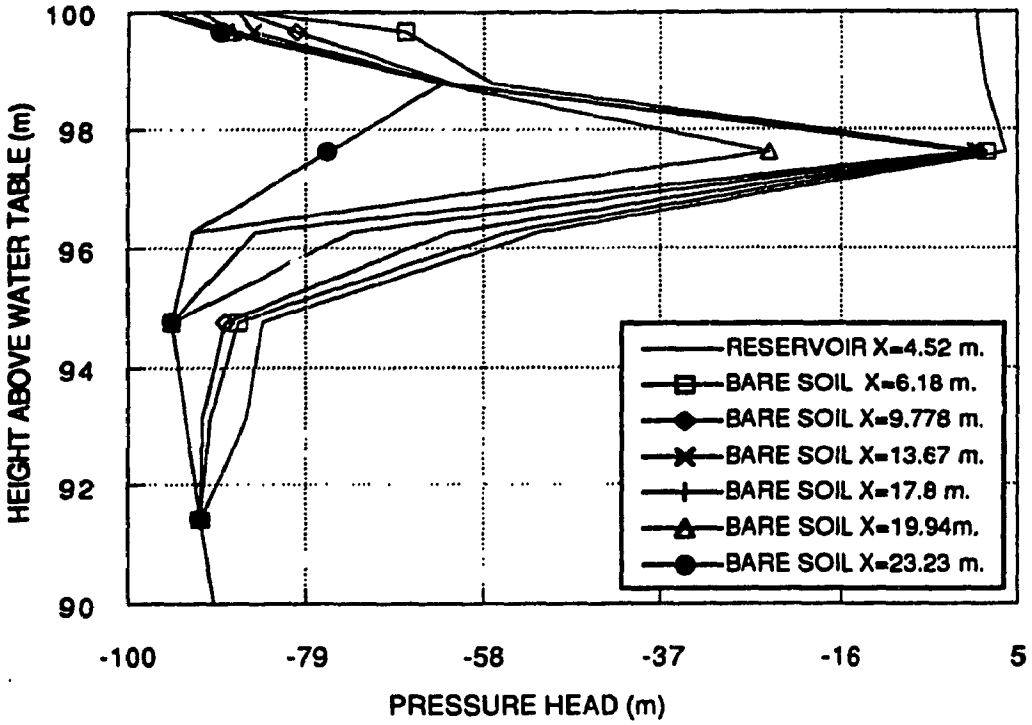

Fig.(6.60): Optimal Pressure Head Profile After 54 Days Of Simulation.

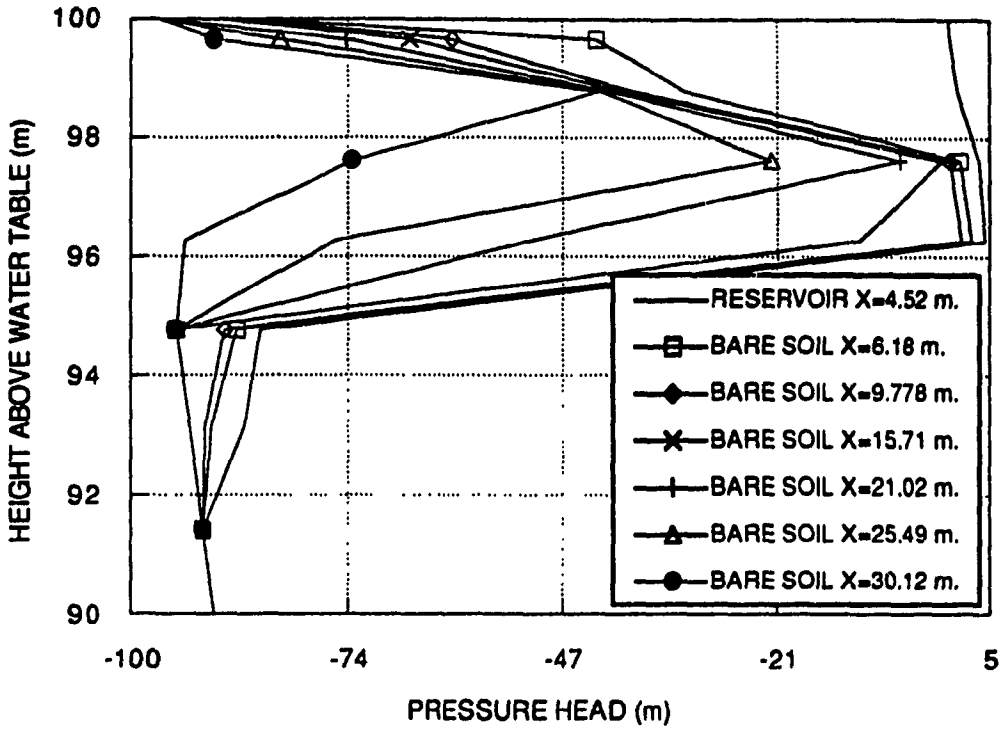

Fig.(6.61): Optimal Pressure Head Profile After 114 Days Of Simulation.

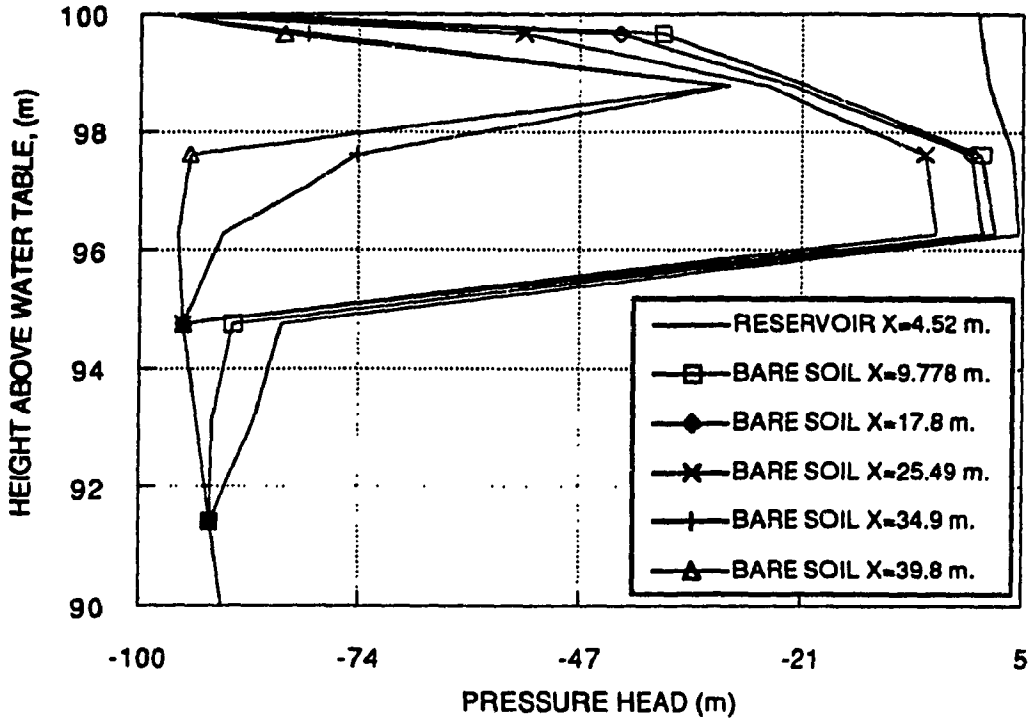

Fig.(6.62): Optimal Pressure Head Profile After 210 Days Of Simulation.

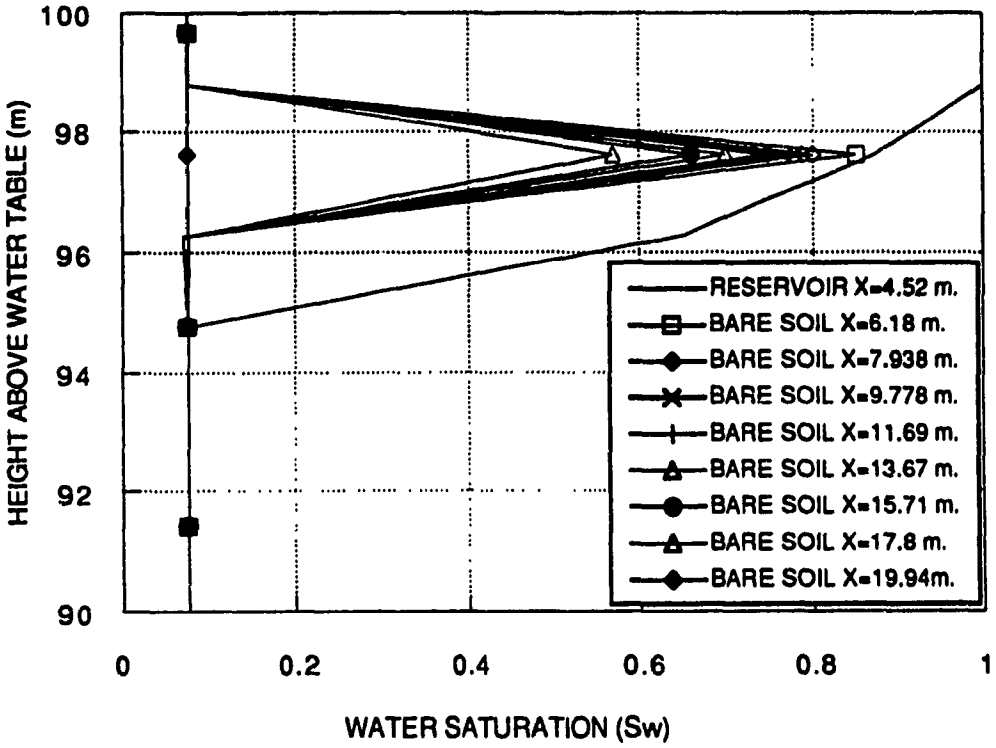

Fig.(6.63): Optimal Water Saturation Profile After 54 Days Of Simulation.

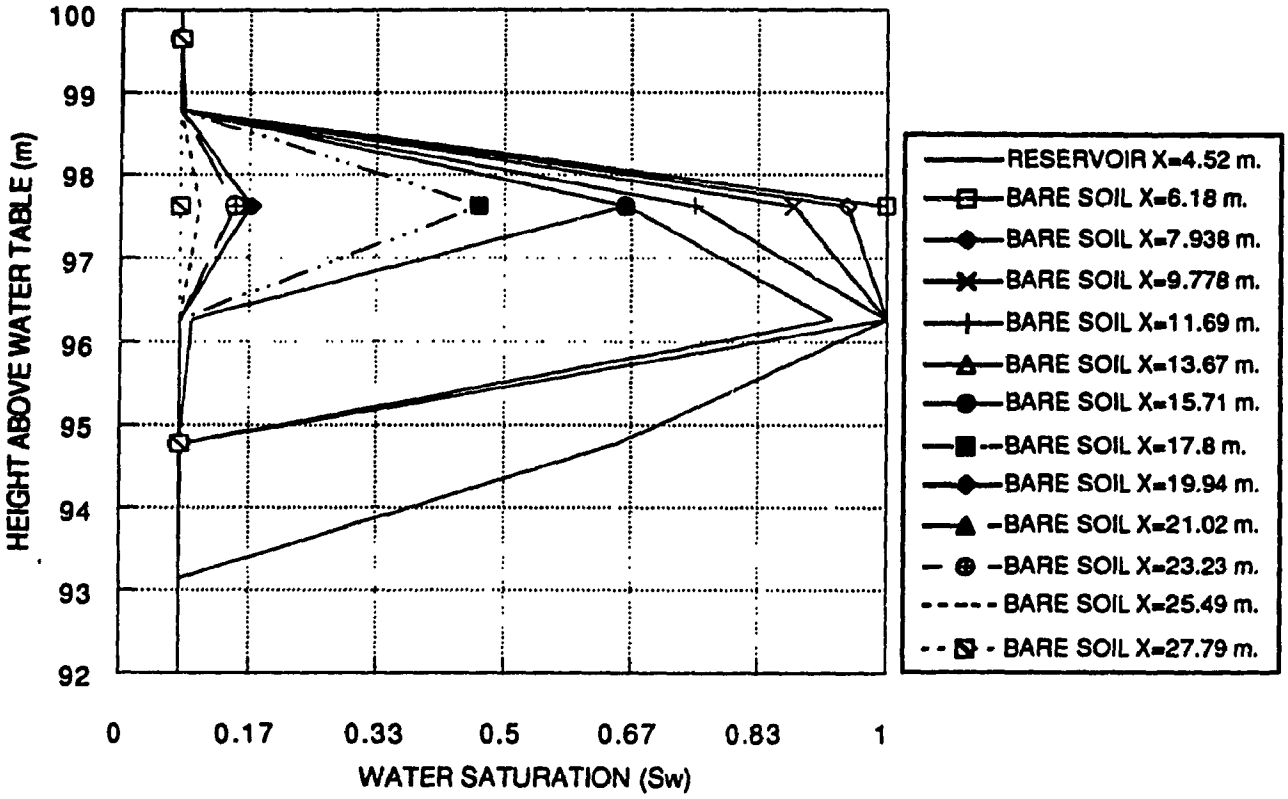

Fig.(6.64): Optimal Water Saturation Profile After 114 Days Of Simulation.

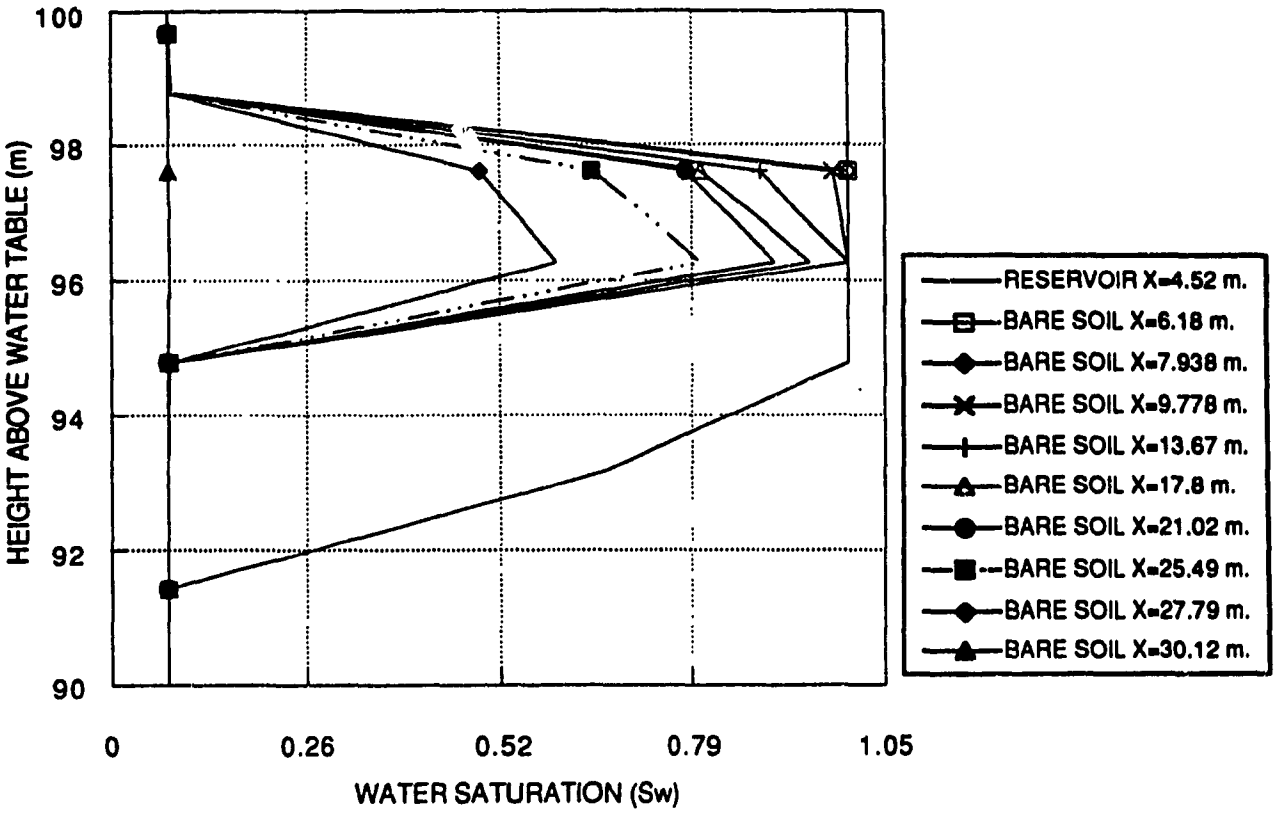

Fig.(6.65): Optimal Water Saturation Profile After 210 Days Of Simulation.